Université de Sherbrooke

Effect of multiple ionization on the radiolysis of liquid water irradiated with heavy ions: A theoretical study using Monte-Carlo simulations

by

Jintana MEESUNGNOEN

Département de médecine nucléaire et de radiobiologie
Faculté de médecine et des sciences de la santé, Université de Sherbrooke
Sherbrooke (Québec) J1H 5N4, Canada

Thesis Submitted to the Faculty of Medicine and Health Sciences
for the Degree of Philosophiae Doctor (Ph.D.) in Radiobiology

September 2007

Your file Votre référence
ISBN: 978-0-494-37986-8
Our file Notre référence
ISBN: 978-0-494-37986-8

Table of contents

List of illustrations (Tables and Figures)

CHAPTER III – Article No. 2

Acronyms, abbreviations and symbols

σ	Cross section
σ_{si}	Single ionization cross section
σ_{di}	Double ionization cross section
σ_{ti}	Triple ionization cross section
σ_{qi}	Quadruple ionization cross section
D	Diffusion coefficient
DEA	Dissociative electron attachment
DNA	Deoxyribonucleic acid
e^-_{aq}	Hydrated electron
eV	Electronvolts
G_x	Primary yield of radiolytic species X
G(X)	Experimental 100-eV yield of the final product X
Hole	Electron-loss center
IRT	Independent reaction times
k	Reaction rate constant
keV	Kilo-electronvolts
LET	Linear energy transfer
MC	Monte Carlo
MeV	Mega-electronvolts
MI	Multiple ionization
molec./100 eV	Molecule/100 eV
OER	Oxygen enhancement ratio
RBE	Relative biological effectiveness
Z	Projectile charge number

Abstract

Water makes up a predominant part of the milieu of living tissue, and, not surprisingly, plays a central role for understanding the interaction of ionizing radiation with biological systems. Most aqueous radiation chemistry studies have involved low-linear energy transfer (LET) radiation, such as ^{60}Co γ-rays or fast electrons. A survey of the literature shows that the radiolysis of liquid water at low LET is generally well understood. However, at high LET, several reported data have not hitherto been quantitatively explained:

(1) The primary yield of hydroperoxyl/superoxide anion ($HO_2^{\bullet}/O_2^{\bullet-}$, $pK_a = 4.8$) radicals increases with increasing LET, a behavior that is contrary to the other radical yields. As yet, the origin of these $HO_2^{\bullet}/O_2^{\bullet-}$ radicals is not clearly established, even though they are the major radical species produced at high LET;

(2) The primary yield of hydrogen peroxide rises with increasing LET to a maximum, after which it falls. No suitable explanation for the presence of such a decrease in H_2O_2 yields at high LET has been offered;

(3) The exact details of the mechanism by which high-LET radiations are very efficient for the inactivation of tumoral hypoxic cells, are still not well known. One possible explanation for the decreased radiobiological oxygen enhancement ratio (OER) at high LET is offered by the generation *in situ* of an oxygenated microenvironment around the tracks of more densely ionizing radiations (the so-called "oxygen-in-the-track" hypothesis).

This work has been originally motivated by the hypothesis proposed by FERRADINI and JAY-GERIN (1998) that multiple ionization (MI) of water would be responsible for the large $HO_2^{\bullet}/O_2^{\bullet-}$ yield produced in liquid water subject to heavy-ion irradiation. The purpose of this study is to test the validity of this hypothesis. To this

aim, Monte Carlo track structure simulations are used to calculate the *G*-values of the various radiolytic species, including O_2, generated in the radiolysis of deaerated liquid water by several different types of radiation ($^{1}H^{+}$, $^{4}He^{2+}$, $^{12}C^{6+}$, and $^{20}Ne^{9+}$ ions) over a wide range of LET up to ~900 keV/μm, at neutral pH and in 0.4 *M* H_2SO_4 (pH 0.46) solutions at 25 °C. It is found that, upon incorporating the mechanisms of double, triple, and quadruple ionizations of water in the calculations, a quantitative agreement between theory and experiment can be obtained. In particular, in neutral (pH 7) solutions, our results reproduce very well the large increase observed in $G_{HO_2^{\bullet}/O_2^{\bullet-}}$ at high LET. Under the conditions of this study, the mechanisms of triple and quadruple ionizations make only a minor contribution to the yield of $HO_2^{\bullet}/O_2^{\bullet-}$. With the exception of protons, our calculations also simultaneously predict a maximum in $G_{H_2O_2}$ around 100–200 keV/μm in accord with experiment. For each irradiating ion considered, this maximum occurs precisely at the point where $G_{HO_2^{\bullet}/O_2^{\bullet-}}$ begins to rise sharply, suggesting, in agreement with experiments, that the yields of $HO_2^{\bullet}/O_2^{\bullet-}$ and H_2O_2 are closely linked. Moreover, the incorporation of MI in our simulations has only little effect on the variation of the computed $G_{e_{aq}^-}$, $G_{H^{\bullet}}$, G_{H_2}, and $G_{^{\bullet}OH}$ values as a function of LET. In the case of acidic solutions irradiated by $^{12}C^{6+}$ and $^{20}Ne^{9+}$ ions, our results also predict a well-defined maximum in the curve of $G_{H_2O_2}$ as a function of LET of ~1.4 molec./100 eV (~45% greater in magnitude than that found in neutral water) around 180–200 keV/μm, in good agreement with experiment. Finally, our simulation results show a steep increase in the initial and primary yields of O_2 with increasing LET. For example, for 24-MeV $^{12}C^{6+}$ ions (LET ~ 500 keV/μm), the initial *in situ* track concentration of oxygen is estimated to be about 3 orders of magnitude higher than the concentration of O_2 found in typical human cells. Such results, which largely plead in favor of the "oxygen in the heavy-ion track" hypothesis, could have profound consequences in

radiobiology and in particular explain the observed reduction in the oxygen enhancement ratio (OER) with increasing LET.

In conclusion, our results strongly support the importance of the role of MI in the heavy-ion radiolysis of water at high LET. They suggest that MI, although infrequent relative to single ionization events, is very efficient chemically.

Résumé

L'eau est un constituant majeur de la plupart des organismes vivants. Elle joue, à ce titre, un rôle central en radiobiologie, en introduisant une part d'effet indirect et/ou quasi direct résultant de sa radiolyse. Une large majorité d'études de chimie sous rayonnement des solutions aqueuses concernent les rayonnements à faible transfert d'énergie linéique (TEL) tels que les rayons γ de ^{60}Co ou les électrons accélérés. Bien qu'elle soit encore incomplète à certains points de vue, un panorama de la radiolyse de l'eau pure ou contenant divers solutés à faible TEL peut être obtenu dans la plupart des cas. Il n'en est cependant pas ainsi pour les rayonnements à grand TEL où plusieurs aspects de cette radiolyse n'ont pas jusqu'ici été pleinement résolus. Parmi les points d'interrogation qui demeurent, citons :

(1) le rendement primaire des radicaux hydroperoxyle/anion superoxyde (pK_a = 4,8) augmente en fonction du TEL, et ceci même en l'absence d'oxygène. Un tel comportement est contraire à ce que l'on observe pour les autres rendements radicalaires. L'origine de ces radicaux n'est pas clairement établie, même s'ils constituent l'espèce radicalaire principale à haut TEL;

(2) le rendement primaire en H_2O_2 croît avec le TEL jusqu'à un maximum, après lequel il décroît; aucune explication satisfaisante n'a été offerte quant à la présence d'une telle décroissance de ce produit moléculaire à haut TEL;

(3) les détails précis du mécanisme par lequel les rayonnements à grand TEL sont très efficaces pour inactiver les cellules tumorales hypoxiques sont encore mal connus. Une interprétation possible de la réduction du facteur d'amplification de l'oxygène (FAO) à haut TEL est donnée par la génération *in situ* d'un microenvironnement oxygéné autour des trajectoires à grande densité d'ionisation (hypothèse de l'"oxygène à l'intérieur même des trajectoires").

Le présent travail a été motivé, à l'origine, par l'hypothèse avancée par FERRADINI et JAY-GERIN (1998) que l'intervention d'ions de l'eau multichargés pourrait être responsable de l'augmentation du rendement $G_{HO_2^{\cdot}/O_2^{\cdot-}}$ observée dans les radiolyses à grand TEL. Dans le but de tester la validité de cette hypothèse, nous avons utilisé des calculs de simulation Monte Carlo afin d'étudier l'influence de différents types de rayonnement (protons et les ions $^4He^{2+}$, $^{12}C^{6+}$ et $^{20}Ne^{9+}$) sur les rendements des diverses espèces radiolytiques, incluant O_2, produites lors de la radiolyse de l'eau liquide désaérée à pH neutre et pour des solutions acides 0,4 *M* en H_2SO_4 (pH 0,46) à 25 °C, pour des valeurs de TEL allant jusqu'à ~900 keV/μm. Les résultats obtenus montrent que, dans ces conditions d'irradiation, la prise en compte des mécanismes de double, triple et quadruple ionisations de l'eau permet de décrire quantitativement les rendements expérimentaux. En milieu neutre, notamment, nos calculs reproduisent très bien l'augmentation marquée de $G_{HO_2^{\cdot}/O_2^{\cdot-}}$ observée à haut TEL. Ils montrent également que les ionisations triples et quadruples, au moins pour la gamme de TEL considérée ici, contribuent très minoritairement à la production des radicaux $HO_2^{\bullet}/O_2^{\bullet-}$. À l'exception des protons, nos calculs prédisent de plus un maximum du rendement $G_{H_2O_2}$ autour de 100–200 keV/μm, en accord avec l'expérience. Pour chaque ion incident considéré, ce maximum apparaît précisément au point où $G_{HO_2^{\cdot}/O_2^{\cdot-}}$ commence à croître rapidement, suggérant ainsi, en accord avec les expériences, que les rendements de $HO_2^{\bullet}/O_2^{\bullet-}$ et H_2O_2 sont étroitement inter reliés. Par ailleurs, l'incorporation des ionisations multiples dans les simulations ne conduit qu'à un effet très limité sur la variation des valeurs de $G_{e_{aq}^-}$, $G_{H\cdot}$, G_{H_2} et $G_{\cdot OH}$ calculées en fonction du TEL. Dans le cas des solutions H_2SO_4 0,4 *M* irradiées par les ions $^{12}C^{6+}$ et $^{20}Ne^{9+}$, nos calculs prédisent également un maximum bien défini de $G_{H_2O_2}$ en fonction du TEL de ~1,4 moléc./100 eV (~45% plus élevé en amplitude que celui trouvé en milieu neutre) autour de 180–200 keV/μm, en bon accord avec l'expérience. Nos simulations montrent enfin une augmentation

substantielle des rendements initial et primaire de O_2 en fonction du TEL. Par exemple, pour des ions $^{12}C^{6+}$ de 24 MeV (TEL ~ 500 keV/μm), la concentration intratrajectoire *in situ* initiale d'oxygène est trouvée environ 3 ordres de grandeur plus élevée que la concentration de O_2 présente dans des cellules humaines types. De tels résultats, qui plaident largement en faveur de l'hypothèse de la production d"oxygène à l'intérieur même des trajectoires", pourraient avoir de profondes conséquences en radiobiologie et en particulier expliquer la réduction de facteur d'amplification de l'oxygène (FAO) avec l'augmentation du TEL.

En conclusion, nos résultats supportent fortement l'importance du rôle des ionisations multiples dans la radiolyse de l'eau par ions lourds accélérés à haut TEL. Ils suggèrent que l'ionisation multiple, quoique peu fréquente par rapport aux ionisations simples à un seul électron, est très efficace chimiquement.

I. Introduction

I.1. Importance of aqueous radiation chemistry in fundamental radiobiology

A large fraction of radiation chemistry has been concerned with studies of water and aqueous solutions, to a large extent because of the unique importance of water, particularly in biological systems, but also in various area of nuclear science and technology such as, for example, water-cooled nuclear power reactors, where the radiolytic processes need to be carefully controlled to avoid deleterious effects (e.g., corrosion and build-up of flammable quantities of hydrogen), and the environmental management of radioactive waste materials. Water also serves as the standard reference material for clinical radiation therapy because its absorption properties for ionizing radiation are similar to those of biological tissue (MEDIN et al., 2006). The study of the radiolysis of water has been actively examined for more than a century. In fact, CURIE and DEBIERNE (1901), GIESEL (1902, 1903), and RAMSAY and SODDY (1903) (very shortly after the discoveries of X rays by Wilhelm Conrad Roentgen in 1895, natural radioactivity of uranium compounds by Henri Becquerel in 1896, and the radioactive element radium by Pierre and Marie Curie and Gustave Bémont in 1898) were the first to observe that dissolved radium salts decompose aqueous solutions by liberating hydrogen and oxygen gases continuously (due principally to the release of α-particles from the radium). Excellent accounts of the history of aqueous radiation chemistry have been given by KROH (1989), JONAH (1995), FERRADINI and JAY-GERIN (1999), and ZIMBRICK (2002).

All biological systems are damaged by ionizing radiation. Since living cells consist mainly of water, which ranges by weight from about 70% in skin to 85% in muscle (SELMAN, 1983), one must understand the radiation chemistry of aqueous

solutions to understand the early stages in the complicated chain of radiobiological events which follows the passage of radiation and ultimately leads to the observation of a biological response. In this context, reactive species produced by water radiolysis in the cellular environment are likely to be major contributors to the induction of chemical modifications and changes in cells that may subsequently act as triggers of biological damage or signaling effects (MUROYA et al., 2006). Reference is made here to the so-called radiation-induced "bystander" effects (see, for example: NAGASAWA and LITTLE, 1992; AZZAM et al., 2003; MOTHERSILL and SEYMOUR, 2004). These effects, which have been observed in cells of varying genetic background, lineage, and organ origin, are initiated, presumably, by damage to a cellular molecule which then gives rise to a toxic chemical signal exported to neighboring cells not directly hit by radiation. Their widespread occurrence is likely to have important consequences for radiation risk assessment (including the long-term biological effects due to the space radiation risk that astronauts encounter) or regulation of exposure levels, radiotherapy and diagnostic radiology. Moreover, cellular radiobiological phenomena depend not only on the absorbed dose but also on the quality of radiation employed (a measure of which is given by the "linear energy transfer" or LET, which represents, to a first approximation, the nonhomogeneity of the energy deposition on a submicroscopic scale). For example, similar absorbed doses of different types of radiation lead to biological changes with varying effectiveness (BARENDSEN, 1968; TSURUOKA et al., 2005), where a more nonuniform geometric distribution of absorbed energy is biologically more efficient. In order to describe these differences, the "relative biological effectiveness" (RBE) of a test radiation Y has been defined as: RBE(Y) = dose of "standard radiation" required to produce a specific biological effect/dose of radiation Y required to produce the same effect (HALL and GIACCIA, 2006). In comparing different radiations, it has become customary to use 250-kV X-

rays as the standard reference. The RBE depends on several factors such as the biological system studied, the absorbed dose, the irradiation parameters (e.g., dose rate), and the environmental conditions (e.g., the level of oxygenation). The finding of a relationship between RBE and radiation quality (LET) emphasizes the importance of the initial spatial distribution of reactants (commonly referred to as the "track structure") in the response of irradiated cells. Successful description of the effects of radiation type and energy in cells also requires an accurate knowledge of the temporal, three-dimensional development of the track, in which the various radiolytic species are specified and allowed to diffuse and react with one another or with the milieu (MUROYA et al., 2006).

Therefore, it is critical to understand how the beam quality and the irradiation conditions affect the subsequent water decomposition products and their space distribution. Finally, it is also important to know how the initial nonhomogeneous distribution of reactive species relaxes in time toward a homogeneous distribution.

I.2. Direct and indirect modes of radiobiological action

When cells are exposed to ionizing radiation, the biological effects of radiation result mainly from damage to the DNA, which is considered to be the most critical target molecule within a cell. The most frequent types of DNA damage produced are base and sugar modifications, single- and double-strand breaks, sites of base loss, tandem lesions, DNA-DNA and DNA-protein crosslinks, and various clustered lesions. The so-called "locally multiply damaged sites" (also termed "clusters of damaged sites" or more conveniently "clustered lesions") refer to the formation of two or more lesions in close proximity along the DNA (including different combinations of all possible singly damaged sites produced in opposite strands or in the same strand within

about 10-20 base pairs separation) by a single radiation track (WARD, 1988; GOODHEAD, 1994; BOUDAÏFFA et al., 2000*a*). These clustered types of lesions, whose complexity depends on the LET of the radiation, result from the spatial heterogeneity of the energy deposition events that follow the passage of radiation through matter. Their cytotoxic effects are likely to be more severe than simple double-stranded discontinuities because they are probably repaired more slowly, if at all. Interestingly, it is the spatial distribution of the DNA lesions rather than their number that is biologically relevant. Such damage, if unrepaired or misrepaired, may contribute to mutagenesis, genome instability, carcinogenesis, aging, inherited disease, and cell death (see, for example: BECKER and SEVILLA, 1993; BREEN and MURPHY, 1995; CADET et al., 1997, 2005; WALLACE, 1998; SUTHERLAND et al., 2000; O'NEILL, 2001; NIKJOO et al., 2001; VON SONNTAG, 2006). In the interaction of ionizing radiation with DNA one generally distinguishes between the "direct" and "indirect" modes of action (Fig. 1).

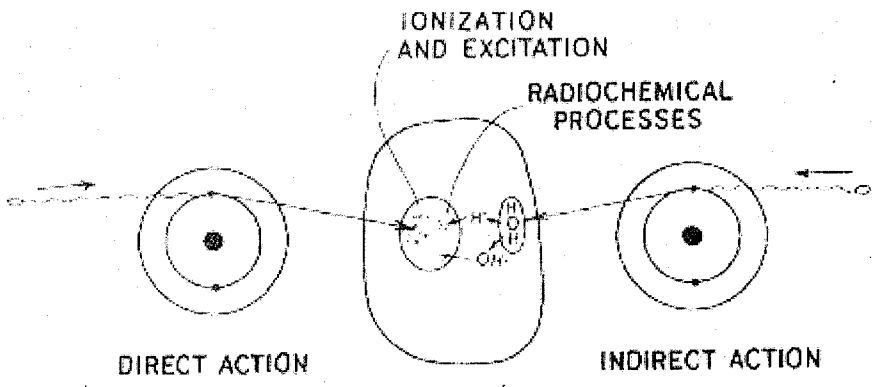

Figure 1. Mode of action of radiation on a cell. In direct (and quasi-direct) action (shown on the left), an electron resulting from absorption of an incident photon enters the nucleus and ionizes or excites the DNA. In indirect action (shown on the right), the ejected electron interacts with water to produce an $^{\bullet}OH$ radical, which diffuses to and reacts with the DNA. From SELMAN (1983).

In the *direct action*, the radiation interacts directly with the DNA itself resulting in the formation of a DNA radical cation ($DNA^{\bullet+}$) and an electron ejected during the ionization process. It has been demonstrated that the vast majority of these electrons (~90%) are created with initial kinetic energies below ~20 eV (LAVERNE and PIMBLOTT, 1995; COBUT et al., 1998; AUTSAVAPROMPORN, 2006). In addition, electronically excited DNA (DNA^*) may also be formed (directly or via ion recombination). There may be additional effects when the ionizing radiation is absorbed in a resonant transition such as the formation of DNA strand breaks by the K-shell X-ray excitation of the phosphorus atoms (Auger electron cascade) (BAVERSTOCK and CHARLTON, 1988; LE SECH et al., 1996). The $DNA^{\bullet+}$ may undergo rapid "hole" (i.e., electron-loss center) transfer to sites located predominantly on guanine (G), while secondary electrons, in competition with other reactions,[1] migrate, once thermalized, to cytosine (C) and thymine (T), the bases with the highest reduction potentials (see, for example: BECKER and SEVILLA, 1993; O'NEILL and FIELDEN, 1993; FARAGGI et al., 1995; FUCIARELLI and ZIMBRICK, 1995; FALCONE et al., 2005; VON SONNTAG, 2006). Subsequent interaction of these initially formed ion radicals (mainly $G^{\bullet+}$, $C^{\bullet-}$, and $T^{\bullet-}$) with their molecular environment can lead to various types of DNA damage in cells, including strand breakage and chemical modifications of its components, via complex reaction sequences. Ionizing radiation may also interact with water molecules that are closely associated with the DNA, within the primary hydration layer (about 12–15 water molecules per nucleotide

[1] Much attention has recently been given to the direct effects of low-energy secondary electrons (in particular, electrons below ionization or electronic excitation thresholds) and their capacity to induce complex DNA damage through the formation of dissociative anion states (resonances), i.e., dissociative electron attachment (DEA), in DNA or its individual basic components (BOUDAÏFFA et al., 2000*b*; SANCHE, 2002; HUELS et al., 2003).

in the B-form of DNA, on average) (SAENGER, 1984). The term "quasi-direct" effect has been introduced by BECKER and SEVILLA (1993) to specifically refer to these processes in which the direct ionization of the adjacent, tightly bound hydration waters is rapidly followed by the transfer of holes and electrons to the DNA, as described by the following reactions:

$$H_2O \rightsquigarrow H_2O^{\bullet+} + e^-$$

$$H_2O^{\bullet+} + DNA \rightarrow H_2O + DNA^{\bullet+}$$

$$e^- + DNA \rightarrow DNA^{\bullet-} (C^{\bullet-}, T^{\bullet-}) \qquad (1)$$

$$DNA^{\bullet+} + e^- \rightarrow DNA^* \text{ (ion recombination).}$$

Clearly, the quasi-direct and direct effects result in chemically indistinguishable radical species trapped on DNA and, therefore, induce similar cellular damage. In the current terminology, these two reaction pathways have been collectively called "direct-type" effects (MROCZKA et al., 1997; BERNHARD and CLOSE, 2004).

In the *indirect action*, DNA reacts with the diffusible products that result from the radiolysis of the water (see below) in the surrounding of the DNA [mostly the secondary and subsequent hydration layers, which act as "bulk" water (SAENGER, 1984)] and in particular the hydroxyl radical ($^{\bullet}OH$). Indeed, $^{\bullet}OH$ is the most reactive oxygen radical known, with a highly positive reduction potential (HALLIWELL and GUTTERIDGE, 1999); it readily attacks almost every type of molecule found in living cells, with equally high rate constants (BUXTON et al., 1988; VON SONNTAG, 2006, 2007). Due to this high reactivity, only those $^{\bullet}OH$ that are created within about 3-4 nm of the DNA (O'NEILL et al., 1991) contribute predominantly in chemical modification of the DNA. The two other main free-radical species formed by the irradiation of water, i.e., e^-_{aq} (hydrated electron) and $H^{\bullet}$ (hydrogen atom), do not cause as much

damage as $^{\bullet}OH$ due to their lower reactivities with most cellular molecules, including DNA (BUXTON et al., 1988). As for the molecular product H_2O_2 (hydrogen peroxide), which is also formed in liquid water radiolysis, it does not appear, by itself, to damage DNA. However, cells contain low concentrations of transition-metal ions, notably Fe^{2+} or Cu^{+} ions, which may convert H_2O_2 into $^{\bullet}OH$ "site specifically" (Fenton-type reactions), when the transition-metal ion is bound to DNA (HALLIWELL and GUTTERIDGE, 1999; VON SONNTAG, 2006). From consideration of a variety of results, it is estimated that about two-thirds of the overall X-ray or cobalt-60 γ-ray DNA damage in mammalian cells is caused by the indirect effect. By contrast, the direct-type effects predominate as the ionization density (LET) is increased (e.g., protons, α-particles or heavier charged particles).

I.3. Energy deposition events and creation of tracks by charged particles

I.3.1. Interaction of ionizing radiation with matter

Ionizing radiations are defined as those types of energetic particle and electromagnetic radiations that, either directly or indirectly, cause ionization of a medium, that is, the removal of a bound orbital electron from an atom or a molecule and, thereby, the production of a residual positive ion. Some molecules, instead of being ionized, may also be excited to upper electronic states (see, for example: EVANS, 1955; ANDERSON, 1984; IAEA-TECDOC-799, 1995; MOZUMDER, 1999; TOBUREN, 2004). Directly ionizing radiations are fast moving charged particles (e.g., electrons, protons, α-particles, stripped nuclei, or fission fragments) that produce ionizations through direct Coulomb interactions. In this case, note that particle-particle contact is not necessary since the Coulomb force acts at a distance. Indirectly ionizing radiations are energetic electromagnetic radiations (like X- or γ-ray photons) or

neutrons that can also liberate bound orbital electrons, but secondarily to a preliminary interaction. For photons, this interaction is predominantly via production of Compton electrons and photoelectrons (and, if the incident photon energy is greater than 1.02 MeV, the production of electron-positron pairs). Neutrons interact with matter through elastic nuclear scattering resulting in the production of energetic recoil protons or other positively charged nuclei (ions), characteristic of the irradiated medium, which can go on to generate ionized and excited molecules along their paths. Regardless of the type of ionizing radiation, the final common result in all modes of absorption of ionizing radiation is thus the formation of tracks of physical energy-loss events in the form of ionization and excitation processes and in a geometrical pattern that depends on the type of radiation involved.

Generally, the electrons ejected in the ionization events may themselves have sufficient energy to ionize one or more other molecules of the medium. In this way, the primary high-energy electron can produce a large number ($\sim 4 \times 10^4$ by a 1 MeV particle) of secondary or higher-order generation electrons (it is customary to refer to all electrons that are not primary as "secondary") along its track as it gradually slows down (ICRU REPORT 31, 1979). From atomic physics it is known that most energy-loss events by fast electrons involve small transfers of energy. In fact, the probability of a given energy transfer Q varies inversely with the square of that energy loss (EVANS, 1955). "Distant" or "soft" collisions, in which the energy loss is small, are therefore strongly favored over "close" or "hard" collisions, in which the energy loss is large (MOZUMDER, 1999). The vast majority of these secondary electrons have low initial kinetic energies with a distribution that lies essentially below 100 eV, and a most probable energy below 10 eV (LAVERNE and PIMBLOTT, 1995; SANCHE, 2002; AUTSAVAPROMPORN, 2006). In most cases, they lose all their excess energy by multiple quasi-elastic (i.e., elastic plus phonon excitations) and inelastic

interactions with their environment, including ionizations and/or excitations of electronic, intramolecular vibrational or rotational modes of the target molecules (MICHAUD et al., 2003), and quickly reach thermal equilibrium (i.e., they are "thermalized"). Determining exactly which of these competing interaction types will take place is a complex function of the target medium and the energy range of the incident electron. By definition, a measure of the probability that any particular one of these interactions will occur is called the "cross section" (expressed in units of area) for that particular interaction type (see, for example: JOACHAIN, 1975). The total interaction cross section σ, summed over all considered individual processes i, is used to determine the distance to the next interaction, and the relative contributions σ_i to σ are used to determine the type of interaction. Actually, the mean distance between two consecutive interactions or "mean free path" λ is defined by

$$\lambda = \frac{1}{N\sigma}, \tag{2}$$

where N is the number of atoms or molecules per unit volume, and

$$\sigma = \sum_i \sigma_i . \tag{3}$$

In a dilute aqueous environment, thermalized electrons undergo trapping and hydration in quick succession (within ~10^{-12} s) as a result of the water electric dipoles rotating under the influence of the negative charge (BERNAS et al., 1996). Some electrons that have kinetic energies lower than the first electronic excitation threshold of the medium, the so-called "subexcitation" electrons (PLATZMAN, 1955), may also undergo, prior to thermalization, prompt geminate ion recombination (FREEMAN, 1987) or induce the production of energetic (~1–5 eV) anion fragments via formation of dissociative negative ion states (resonances) (i.e., dissociative electron attachment, or DEA) (CHRISTOPHOROU et al., 1984; BASS and SANCHE, 2003). As a conse-

quence of the energy gained by the medium, a sequence of very fast reactions and molecular rearrangements lead to the formation of new, highly nonhomogeneously distributed chemical species in the system, such as charged and/or neutral molecular fragments, reactive free radicals, and other excited chemical intermediates. The trail of the initial physical events, along with the chemical species, is generally referred to as the track of a charged particle, and its overall detailed spatial distribution, including contributions from secondary electrons, is commonly known as "track structure" (see, for example: PARETZKE, 1987; MAGEE and CHATTERJEE, 1987; KRAFT and KRÄMER, 1993; PARETZKE et al., 1995; MOZUMDER, 1999; LAVERNE, 2000, 2004).

A charged particle is called "heavy" if its rest mass is large compared with that of an electron. Thus, protons ($^{1}H^{+}$), α-particles ($^{4}He^{2+}$), and their near relatives ($^{2}H^{+}$, $^{3}H^{+}$, $^{3}He^{2+}$), higher charged particles (i.e., $^{12}C^{6+}$, $^{7}Li^{3+}$, $^{20}Ne^{10+}$, $^{56}Fe^{26+}$, etc.), and fission fragments are all heavy charged particles. As most radiation chemical studies involve ions with initial energy of a few MeV per nucleon or more depending on the source, the main interaction responsible for energy loss at these energies is the Coulomb force between the charge of the incident heavy ion and that of the bound electrons of the medium. The tracks of heavy ions can thus be explained in basically the same manner as that for fast electrons. A heavy charged particle traversing matter loses energy primarily through the ionization and excitation of target atoms or molecules. This proceeds until the ions are so much slowed down that they may be neutralized by reaction with electrons, whereby their travel is stopped. For sufficiently fast ions and electrons, there are, however, some obvious differences due almost entirely to the small mass of the electron. For example, a (nonrelativistic) heavy ion (which has mass M, velocity v_i, and kinetic energy $E_i = M v_i^2/2$) is restricted to a

maximum allowed energy loss (Q_{max}) to an initially free stationary atomic electron (which has mass m_0) given by (EVANS, 1955; ANDERSON, 1984)

$$Q_{max} \approx E_i \left[\frac{4 M m_0}{(M + m_0)^2} \right] \approx 4 E_i \left(\frac{m_0}{M} \right) = 2 m_0 v_i^2 \quad (M >> m_0) , \tag{4}$$

whereas a fast incident electron can transfer all its initial kinetic energy in a single collision with a bound electron. As seen in Eq. (4), the energy that a heavy charged particle loses in each event and the corresponding change in its momentum amount to only a small fraction (proportional to m_0/M) of its total energy and momentum. Therefore, because the heavier mass of fast ions prevents them from being scattered as much as electrons, heavy ions move in a relatively straight line (their deflections in collisions are negligible) until very near the end of their range. By contrast, electrons can undergo large angle scattering in collisions with medium electrons, leading to extremely torturous paths.

I.3.2. Linear energy transfer (LET) and interaction cross sections for heavy charged particles

The earliest experiments on the radiation-chemical effects in liquid water showed that there were differences in the yields of radiolytic products for various types of radiation (KERNBAUM, 1910; USHER, 1911; DUANE and SCHEUER, 1913; DEBIERNE, 1914). The amount of changes observed in the quantities and proportions of the chemical species produced depends both on the total energy deposition and the spatial distribution of this energy. The "linear energy transfer" (LET), first introduced by ZIRKLE et al. (1952), is a measure of the rate of energy deposition along and within the track of a penetrating charged particle. This quantity is especially important in evaluating the overall chemical effect and in applications of radiation to biological

systems because concentration of the deposited energy is significant in those cases. It is defined as

$$\mathrm{LET} = -\frac{\mathrm{d}E}{\mathrm{d}x}, \tag{5}$$

where dE is the average energy locally (i.e., in the vicinity of the particle track) imparted to the medium by the particle in traversing a distance dx (ICRU REPORT 16, 1970). In this way, the (sometimes termed "energy-unrestricted", i.e., when all permissible energy transfers are included) LET is equivalent to the "stopping power" (which is commonly used in the domain of radiation physics) of the medium traversed (ANDERSON, 1984; ICRU REPORT 60, 1998; MOZUMDER, 1999). Usually, LET values are in units of keV per micron (the conversion to SI units is: 1 keV/μm ≈ 1.602 × 10^{-19} J/nm).

The Bethe theory of stopping power describes the average energy loss due to the electromagnetic interactions between fast charged particles and the electrons in absorber atoms (see, for example: FANO, 1963). For kinetic energies of ions that are small compared to their rest-mass energy, the nonrelativistic stopping power formula of Bethe (BETHE, 1930; BETHE and ASHKIN, 1953) is given by (in SI units):

$$-\frac{\mathrm{d}E}{\mathrm{d}x} = \left(\frac{1}{4\pi\varepsilon_0}\right)^2 \frac{4\pi Z^2 e^4}{m_0 V^2} N \ln\left(\frac{2m_0 V^2}{I}\right), \tag{6}$$

where Ze is the charge on the incident ion, V is the ion velocity, m_0 is the mass of an electron, N is the number of electrons per cubic meter of the absorbing medium, and I is the mean of all the ionization and excitation potentials of the bound electrons in the absorber. In most cases, I is determined by fitting the theory to experimental results related to the stopping power. For liquid water, I = 79.7 ± 0.5 eV (BICHSEL and HIRAOKA, 1992). Based on the lowest-order (or first "Born") approximation in the

electromagnetic interaction between the incident particle and the atomic electrons, the Bethe equation has a wide range of validity except for slow, highly charged heavy particles such as fission fragments.

As we can see from Eq. (6), for any incident particle, the LET depends on the particle's kinetic energy only through its velocity. It is approximately inversely proportional to V^2, but the mass of the fast moving particle does not appear. Hence there are really no isotope effects, provided the ions have the same velocity. For example, protons ($^1H^+$) and deuterons ($^2H^+$) of equal velocity give similar radiation chemical yields (ANDERSON and HART, 1961). Moreover, the velocity term in the numerator of the logarithm term and in the denominator of the pre-logarithmic term gives rise to the familiar Bragg peak, i.e., with decreasing velocity of the incident particle the LET increases to a maximum and then decreases at lower velocities (LAVERNE, 2000, 2004). Specifically, the Bragg peak refers to the increase in the density of ionizations as the incident heavy ion approaches the end of its track (range) and slows down (the slower the speed the more time the particle spends in the vicinity of an atom and therefore the greater the probability of interaction and resulting ionization and excitation). In Fig. 2, we show the LET as a function of incident energy for electrons and four different ions in liquid water. We see the large difference between the LET of electrons and heavy particles of the same energy (due to the difference in the velocity).

As Eq. (6) also shows, the LET is proportional to the square of the projectile charge number Z^2. An important implication of this result is the following. For example, a 1-MeV proton and a 26-MeV He^{2+} ion have approximately the same (instantaneous) LET in water (~26.4 and 26.7 keV/μm, respectively). In order for them to have the same LET, the He^{2+} ion has thus to have a velocity twice that of the proton. Hence, the heavier particle (helium in this case) will produce higher energy δ-rays (secondary electrons that have sufficient energy to form tracks of their own, branching from the

primary track). This results in the formation of a broader track structure for the He^{2+} ion.

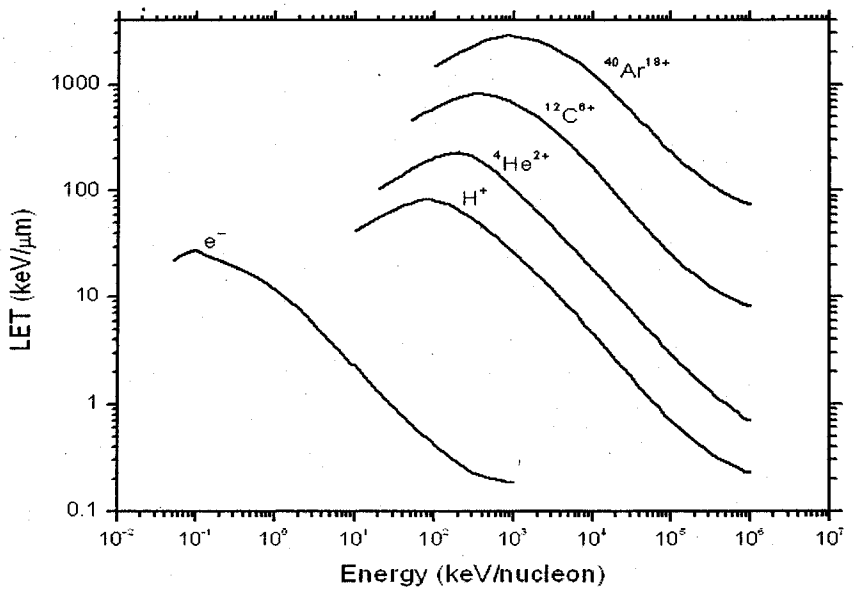

Figure 2. LET ($-dE/dx$) of some heavy ions and electrons in liquid water as a function of energy (WATT, 1996). The LET plotted here is the average energy dissipated per unit track length by the charged particles having the energy shown (and not the energy loss averaged over the whole track length). For the sake of reference, note that the value of LET for ^{60}Co γ-rays (photon energies of 1.17 and 1.33 MeV) is ~0.3 keV/μm; this value applies also to hard X-rays and fast electrons of the same energies.

An important feature of the first Born approximation is that it also provides a convenient framework to obtain the interaction cross sections of different, sufficiently fast projectile ions from one another by a simple Z^2 scaling operation. This follows from the similarity between the theoretical formulation of the stopping power and of the total cross section for inelastic scattering. In fact, within this theory, the cross section for the collision of a charged projectile with a single electron (assumed initially at rest) in an atom (known as the "Rutherford" cross section) behaves essentially as

$(Z/V)^2$, where Z is the projectile charge number and V is the impact speed, and does not depend upon the mass of the particle (INOKUTI, 1971; McDANIEL et al., 1993; ICRU REPORT 55, 1996; BICHSEL, 2006). This Z^2 scaling is particularly useful for providing cross sections for inelastic scattering by "bare" (i.e., fully ionized or stripped) ion projectiles, especially as there are only limited experimental data available involving ions heavier than proton or helium in collision with molecular targets of biological interest (e.g., H_2O). The "reference" cross-section data generally used in this context are those for proton impact, owing to the fact that protons represent, by far, the most comprehensive data base of collision cross sections for bare ions (RUDD, 1990; RUDD et al., 1992; IAEA-TECDOC-799, 1995; COBUT et al., 1998; DINGFELDER et al., 2000; TOBUREN, 2004). In other words, the cross sections for ionization or excitation by heavy charged particles of charge number Z are approximately Z^2 times the cross sections for proton impact *at the same velocity*. This simple scaling procedure holds only at sufficiently high energies. Deviations from that rule occur at lower energies (below approximately 1 MeV/nucleon), where the first Born approximation – which rests on the assumption that the projectile velocity is large compared to the orbital speeds of the valence electrons in the target – is no longer satisfied. Such slow ions are usually incompletely stripped and can undergo successive electron capture and loss events contributing to a changing equilibrium charge state that depends on the velocity (IAEA-TECDOC-799, 1995; ICRU REPORT 55, 1996; LAVERNE, 2004). On the average, the net positive (or "effective") charge on an incident ion decreases when the speed decreases. This charge exchange also complicates the derivation of relevant cross sections for heavy charged, partially "dressed" particles in the low-velocity regime.

I.4. Structure of charged-particle tracks in liquid water

I.4.1. Track structure in radiation chemistry and radiobiology

A great many experimental and theoretical studies have shown that the quantities and proportions of the chemical products formed in the radiolysis of water are highly dependent on the distances separating the primary radiolytic species from each other along the track of the ionization radiation. The distribution of separations, referred to as the "track structure" (see above), is determined to a large extent by the distribution of the physical energy deposition events and their geometrical dispositions, or, in other words, by the quality of the radiation. In fact, track-structure effects are also usually called "LET effects" as most of the early studies used this parameter to characterize the different radiation chemical yields (or "*G*-values") for various irradiating ions in liquid water. The radiation track structure is of crucial importance in specifying the precise spatial location and identity of all the radiolytic species and free-radical intermediates generated in the tracks, and their subsequent radiobiological action at the molecular and cellular levels. Track structure, coupled with a reaction scheme and yields of primary species, forms the basis of radiation-chemical theory (MOZUMDER, 1999). It is now well accepted by the scientific community that differences in the biochemical and biological effects (e.g., damage to DNA, changes in cell signaling, etc.) of different qualities of radiation must be analyzed in terms of track structure (CHATTERJEE and HOLLEY, 1993; MUROYA et al., 2006).

I.4.2. Spatial aspects of track structures

I.4.2.1. Low-LET radiation and track entities

The average LET of a 1-MeV electron in water is ~0.3 keV/μm. The track-averaged mean energy loss per collision event by such a fast electron is in the region

~48–65 eV (LAVERNE and PIMBLOTT, 1995; MOZUMDER, 1999; AUTSAVAPROMPORN, 2006). This means that the energy-loss events are, on the average, separated by distances of about 2000 Å. This nonhomogeneous distribution of energy deposition events in space gives rise to the "spur" theory for low-LET track structure (KARA-MICHAILOVA and LEA, 1940; ALLEN, 1948; SAMUEL and MAGEE, 1953; MAGEE, 1953; GANGULY and MAGEE, 1956), according to which the entire track is to be viewed as a random succession of (more or less spherical) spurs (sometimes called the "string-of-beads" model of a track), or *spatially localized* energy-loss events (it is assumed that irradiating particles are isolated from each other, an assumption not necessarily correct at very high dose rates or with very short pulses of intense beams). The few tens of electronvolts deposited in a spur cause a secondary electron to be ejected from a molecule. As the ejected electron moves away, it undergoes collisions with surrounding water molecules, loses its excess energy, and becomes thermalized (~0.025 eV) within about 80–120 Å of its geminate positive ion (GOULET and JAY-GERIN, 1988; MUROYA et al., 2002; MEESUNGNOEN et al., 2002*a*; PIMBLOTT and MOZUMDER, 2004). This electron thermalization distance or "penetration range" can be viewed as an estimate of the average radius of the spurs in the first stages of their development. Thus, the individual spurs produced by a radiation of low LET (so-called "sparsely" ionizing radiation) are so far apart along the track that they are not initially overlapping (but they will overlap somewhat later as they develop in time).

In their pioneering work to model the radiation chemical consequences of the different energy-loss processes, MOZUMDER and MAGEE (1966*a*, *b*) considered, somewhat arbitrarily, a low-LET track as composed of a random sequence of three types of essentially nonoverlapping entities: "spurs, blobs, and short tracks" (Fig. 3).

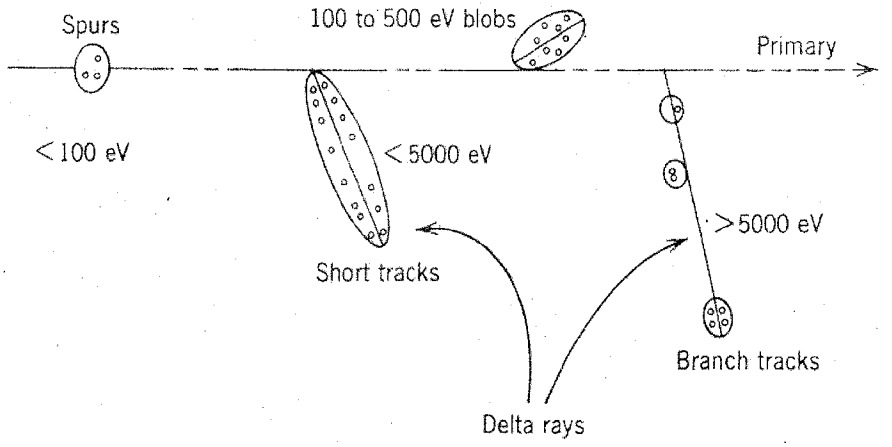

Figure 3. Track structure classification by track entities so-called spurs (spherical entities, up to 100 eV), blobs (spherical or ellipsoidal, 100–500 eV), and short tracks (cylindrical, 500 eV–5 keV) for a primary high-energy electron (not to scale; BURTON, 1969). The energy partition between the three track entities strongly depends on the incident particle energy, dividing approximately as the ratio of 0.75:0.12:0.13 between the spur, blob, and short track fractions for a 1-MeV electron in liquid water (PIMBLOTT et al., 1990).

The spur category contains all track entities created by the energy losses between the lowest excitation energy of water and 100 eV; in most cases, there are one to three ion pairs in such isolated spatial areas and about the same number of excited molecules (PIMBLOTT and MOZUMDER, 1991). Blobs are defined as track entities with energy transfers between 100 and 500 eV, and short tracks as those with energy transfers between 500 eV and 5 keV. Secondary electrons produced in energy transfers above 5 keV are considered as "branch tracks". Short and branch tracks are, collectively, described as δ-rays. This old concept of track entities proved to be very helpful in greatly facilitating the visualization of track processes and in modeling radiation-chemical kinetics. It is still a useful approach for the classification of track structures,

since it takes into account the spatial arrangements of initial species, which affect their subsequent reactions.

For the sake of illustration of low-LET tracks, Fig. 4 shows an example of the complete tracks of six 800-keV electrons and the secondary electrons they produce in water, calculated by a Monte Carlo simulation program, OREC (HAMM et al., 1985).

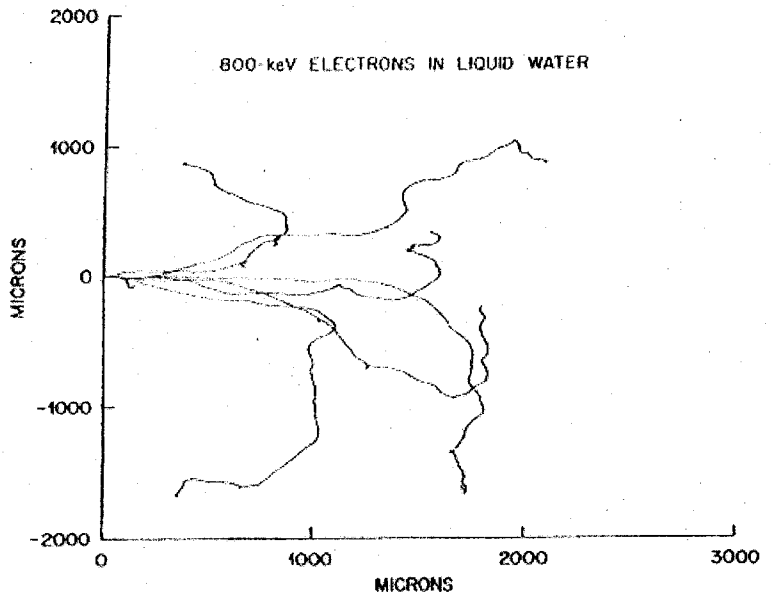

Figure 4. Simulated tracks (projected into the *XY* plane of figure) of six 800-keV electrons in water, showing the stochastic nature of paths. Each electron is generated at the origin on the *Y* axis and starts moving horizontally toward the right. From TURNER et al. (1988*a*).

I.4.2.2. Structure of high-LET radiation tracks

With increasing LET, the distantly-spaced, nearly spherical spurs are formed increasingly closer together and eventually overlap (for LET greater than ~10–20 keV/μm) to form dense continuous columns of species consisting initially of a cylindrical "core" of high LET produced by the heavy-particle track itself and a surrounding region traversed by the emergent, comparatively low-LET secondary electrons (δ-rays)

called the "penumbra" (MOZUMDER et al., 1968; CHATTERJEE and SCHAEFER, 1976; FERRADINI, 1979; MAGEE and CHATTERJEE, 1980, 1987; MOZUMDER, 1999; LAVERNE, 2000, 2004). Figure 5 illustrates typical two-dimensional representations of short (1–5 μm) track segments of $^{1}H^{+}$, $^{4}He^{2+}$, $^{12}C^{6+}$, and $^{20}Ne^{10+}$ ions

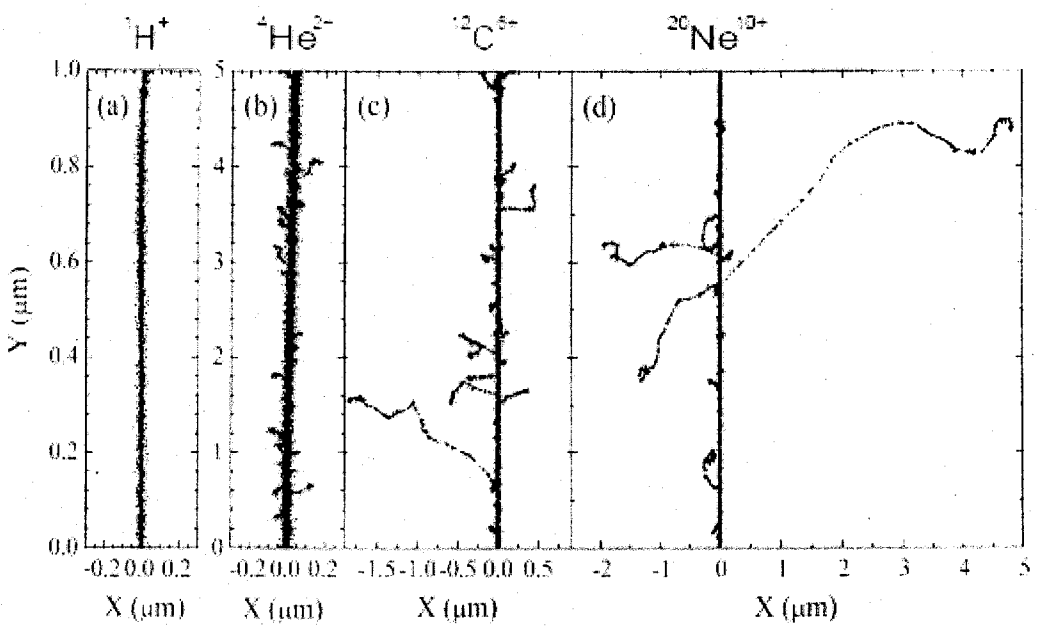

Figure 5. Projections over the *XY* plane of track segments calculated (at ~10^{-13} s) for (a) $^{1}H^{+}$ (0.15 MeV), (b) $^{4}He^{2+}$ (1.75 MeV/nucleon), (c) $^{12}C^{6+}$ (25.5 MeV/nucleon), and (d) $^{20}Ne^{10+}$ (97.5 MeV/nucleon) impacting ions. Ions are generated at the origin and along the *Y* axis in liquid water under identical LET conditions (~70 keV/μm). The track segments for the different ions have been chosen equal to 5 μm, except for $^{1}H^{+}$, for which we have adopted a track length of 1 μm. This reduction in the track length for $^{1}H^{+}$ was dictated by the fact that the penetration range of this ion in liquid water, at the considered energy of 0.15 MeV, amounts to only ~2.3 μm. For the case of a 1-μm segment of 0.15 MeV proton track, the LET is nearly constant (~70 keV/μm) along the trajectory. Dots represent the energy deposited at points where an interaction occurred. From MUROYA et al. (2006).

calculated with our own Monte Carlo simulation code called IONLYS (see below) under the same LET conditions (~70 keV/μm). As one can see, these tracks can be

considered as straight lines (see above). It is also seen that the ejected high-energy secondary electrons travel to a greater average distance away from the track core as the velocity of the incident ion increases, from protons to neon ions. In other words, even though all those particles are depositing the same amount of energy per unit path length, that energy is lost in a volume that increases in the order $^{1}H^{+} < {}^{4}He^{2+} < C^{6+} < {}^{20}Ne^{10+}$, indicating that the higher-Z particle has the lower mean density of reactive species. This irradiating-ion dependence of the track structure at a given LET (i.e., tracks of different ions with the same LET have different radial profiles) is in accord with Bethe's theory of stopping power[2] and indicates, as it has been frequently noted (see, for example: SCHULER and ALLEN, 1957; MILLER, 1958; SAUER et al., 1977; LAVERNE and SCHULER, 1987*a*; KAPLAN and MITEREV, 1987; FERRADINI, 1990; FERRADINI and JAY-GERIN, 1999; PIMBLOTT and LAVERNE, 2002; LAVERNE, 2000, 2004), that LET is not a unique descriptor of the radiation chemical effects within heavy charged particle tracks. Attempts have been made to introduce in place of LET other comparative characteristics of radiation, like for instance the factor Z^2/β^2 (where Z is the charge number of the ion and β is the ratio of its velocity to that of light) (KATZ, 1970) or, equivalently, the parameter MZ^2/E (where M is the heavy ion mass and $E = \frac{1}{2} MV^2$ its kinetic energy) (PIMBLOTT and LAVERNE, 2002; LAVERNE, 2004). If several sets of radiation chemical data appear to be better unified using these parameters (instead of LET), some others do not. Following PIMBLOTT and LAVERNE (2002), it should be recognized, however, that no deterministic parametrization can realistically represent a phenomenon (namely, the effect of radiation quality on early radiation chemistry) that is stochastic in nature. KATZ (1978) also indicated that no fewer than two parameters are needed in order to

[2] It follows from Eq. (6) that for two different ions of equal LET, the one with the higher charge will have the higher velocity.

speak of a track structure and that single parameter reductions do not fully describe observed effects. Nevertheless, despite its limitations, LET still continues to be a dominant parameter in the radiation chemistry of heavy ions.

I.5. Radiolysis of liquid water and aqueous solutions

I.5.1. The radiolysis of water at low LET

The complex succession of events that follow the irradiation of water is usually divided into three, more or less distinct, consecutive stages (PLATZMAN, 1958): (1) deposition of radiant energy and formation of initial products in a specific, highly non-homogeneous track structure geometry ("physical" stage), (2) establishment of thermal equilibrium in the bulk medium with reactions and reorganization of initial products to give stable molecules and chemically reactive species such as free atoms and radicals ("physicochemical" stage), and (3) thermal chemistry during which the various reactive species diffuse and react with one another (or with the environment) ("chemical" stage). The radiolysis of water by low-LET, sparsely ionizing radiation (for example, energetic photons, such as γ-rays from ^{60}Co or ^{137}Cs or hard X-rays, or high-energy charged particles, such as fast electrons or protons generated by a particle accelerator) is generally well understood. It leads to the formation of the free radicals and molecular products e^-_{aq}, H^+, OH^-, $H^\bullet$, H_2, $^\bullet OH$, H_2O_2, $HO_2^\bullet/O_2^{\bullet-}$ (hydroperoxyl/superoxide anion radicals, $pK_a = 4.8$), etc.[3] (see, for example: DRAGANIĆ and DRAGANIĆ, 1971; SPINKS and WOODS, 1990; FERRADINI and JAY-GERIN, 1999; BUXTON, 2004). Under ordinary irradiation conditions (i.e., at modest dose

[3] Several other chemical species are also formed in the low-LET radiolysis of water, such as O^-, HO_2^-, O_3^-, etc. However, for both neutral water and acidic solutions at room temperature, these species are normally ignored as their yields are extremely small.

rates), these products are generated nonhomogeneously on subpicosecond time scales in spurs along the track of the incident radiation (see, for example: PLANTE et al., 2005; PLANTE, 2005). Owing to diffusion from their initial positions, the radiolytic products then either react within the spurs as they develop in time or escape into the bulk solution. At ambient temperature and pressure, the so-called "spur expansion" is essentially complete by about 10^{-6} s after the initial energy deposition. At this time, the species that have escaped from spur reactions become homogeneously distributed throughout the bulk of the solution (also referred to as the "background") and the track of the radiation no longer exists. The radical and molecular products, considered as additions to the background, are then available to react with solutes (treated as spatially homogeneous) present in moderate concentrations.

For low-LET radiation, the radiolysis of pure, deaerated (air-free) liquid water can be adequately described by the following *global* equation, written for an absorbed energy of 100 eV (FERRADINI and JAY-GERIN, 1999):

$$G_{\text{-H}_2\text{O}}\ \text{H}_2\text{O} \rightsquigarrow G_{e^-_{aq}}\ e^-_{aq} + G_{\text{H}\cdot}\ \text{H}^\bullet + G_{\cdot\text{OH}}\ {}^\bullet\text{OH} + G_{\text{H}^+}\ \text{H}^+ + G_{\text{OH}^-}\ \text{OH}^- + G_{\text{H}_2}\ \text{H}_2 + G_{\text{H}_2\text{O}_2}\ \text{H}_2\text{O}_2 + \ldots , \quad (7)$$

where the coefficients G_X (symbol G with the formula of the species as subscript) are the so-called "primary" free-radical and molecular yields ("long-time" or "escape" yields) representing the numbers of the various radiolytic species X that remain throughout the bulk of the solution at the end of the nonhomogeneous chemical stage (i.e., after spur expansion). At this stage, $G_{\text{-H}_2\text{O}}$ denotes the corresponding yield for net water decomposition. For ^{60}Co γ-radiation and neutral water at room temperature (LET ~ 0.3 keV/μm, pH 7), the most recently reported values of the primary yields (expressed in units of molecules/100 eV) are (LAVERNE, 2004):

$$G_{e^-_{aq}} = 2.50 \qquad G_{H\cdot} = 0.56 \qquad G_{H_2} = 0.45$$

$$G_{\cdot OH} = 2.50 \qquad G_{H_2O_2} = 0.70\,. \tag{8}$$

These primary yield values [note that, for low-LET radiolysis, $HO_2^{\bullet}/O_2^{\bullet-}$ has a very small yield in comparison to the other radiolytic species and can normally be neglected (BJERGBAKKE and HART, 1971)], are connected by the following equations:

$$G_{e^-_{aq}} + G_{OH^-} = G_{H^+} \tag{9}$$

$$G_{-H_2O} = G_{e^-_{aq}} + G_{H\cdot} + 2G_{H_2} \tag{10}$$

$$= G_{\cdot OH} + 2G_{H_2O_2}\,, \tag{11}$$

expressing the charge conservation (electroneutrality) and material balance of Eq. (7), respectively. Note that Eqs. (9)–(11) can readily be derived by writing that, at any time, the total (algebraic) charge of the transient species and stable products formed in the decomposition of water should be zero and the total number of $H^{\bullet}$ atoms in the transients and products considered should be equal to twice the number of O atoms.

I.5.2. Time scale of events and formation of primary free-radical and molecular products in neutral water radiolysis

The overall process of producing chemical changes by ionizing radiation starts with the bombardment of water by the high-energy radiation and terminates with the re-establishment of chemical equilibrium. As mentioned above, this process can be divided into three temporal stages (the time scale of events that occur in the radiolysis of water is shown in Fig. 6) that we briefly describe below.

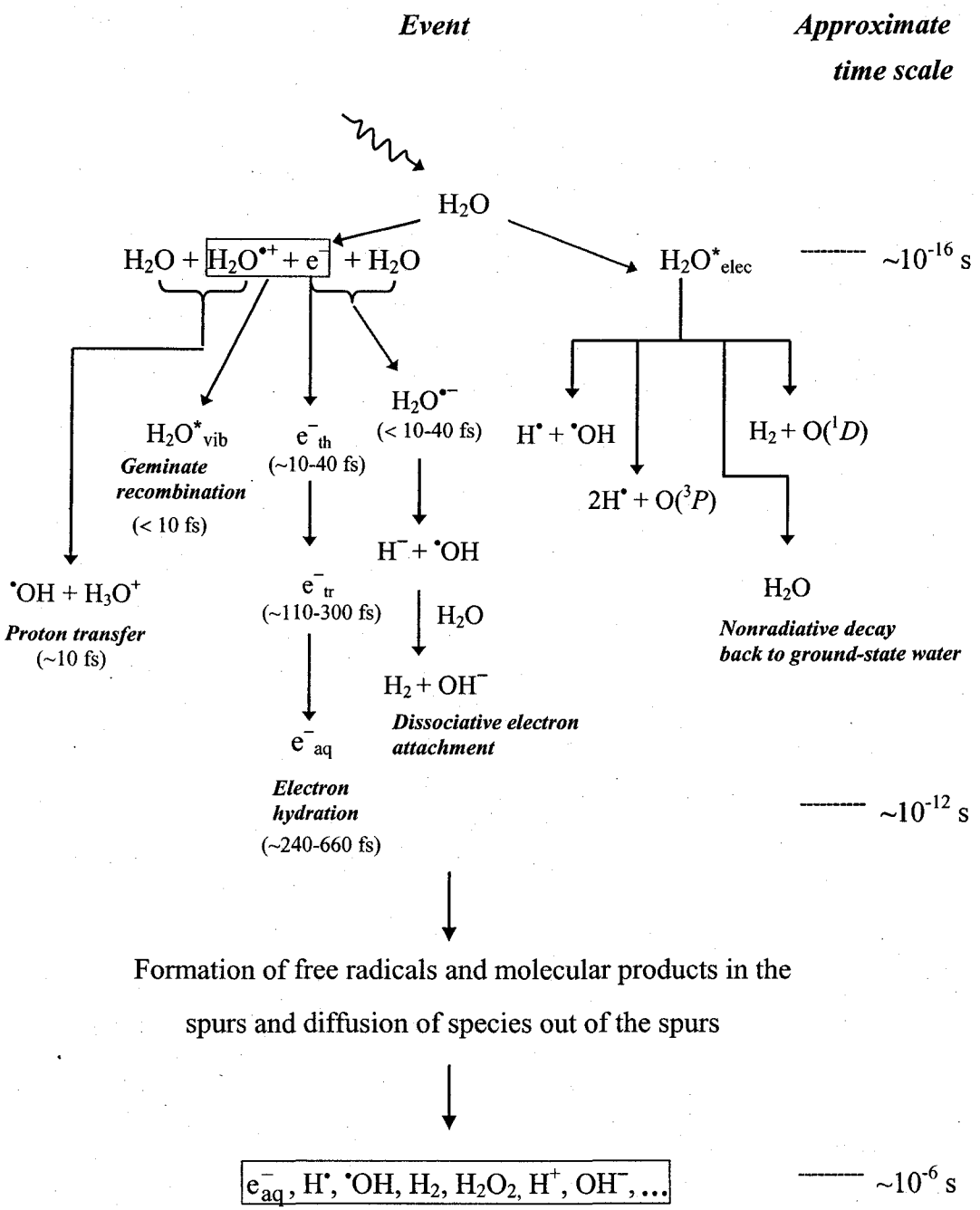

Figure 6. Time scale of events in the low-LET radiolysis of deaerated water.

(1) The "physical" stage consists of the phenomena by which energy is transferred from the incident ionizing radiation to the system. It lasts not more than $\sim 10^{-16}$ s. This time is too short for molecular motions of any kind, and only electronic processes

are possible. The result of this energy absorption is the production, along the path of the radiation, of a large number of ionized and electronically excited water molecules (noted $H_2O^{\bullet+}$ and $H_2O^*_{elec}$, respectively). Note that $H_2O^*_{elec}$ represents here the many excited states, including the so-called superexcitation states (PLATZMAN, 1962*a*) and the excitations of collective electronic oscillations of the "plasmon" type (HELLER et al., 1974; BEDNÁŘ, 1985; KAPLAN and MITEREV, 1987; ZAIDER et al., 1990; LAVERNE and MOZUMDER, 1993; WILSON et al., 2001). The earliest processes in the radiolysis of water are:

$$H_2O \rightsquigarrow H_2O^{\bullet+} + e^- \qquad (12)$$

$$H_2O \rightsquigarrow H_2O^*_{elec} \qquad (13)$$

Generally, the electron ejected in the ionization event has sufficient energy to ionize or excite one or more other water molecules in the vicinity, and this leads, as mentioned above, to the formation of track entities that contain the products of the events and that have been called "spurs".

(2) The "physicochemical" stage consists of the processes which lead to the establishment of thermal equilibrium in the system. Its duration is about 10^{-12} s. During this stage, the ions and excited-state water molecules dissipate their excess energy by bond rupture, luminescence, energy transfer to neighboring molecules, etc.

The secondary electron ejected from an ionized water molecule undergoes scattering as it moves away from its parent ion. It transfers energy to the molecules with which it collides and eventually reaches thermal equilibrium with the liquid. Once it has slowed down to thermal energy (e^-_{th}), it can be localized or trapped (e^-_{tr}) in a preformed potential energy well of appropriate depth in the liquid, before it reaches a fully relaxed, hydrated state (e^-_{aq}) as the dipoles of the surrounding molecules orient in

response to the negative charge of the electron. Thermalization, trapping, and hydration can then follow in quick succession (less than ~10^{-12} s) (MOZUMDER, 1999):

$$e^- \rightarrow e^-_{th} \rightarrow e^-_{tr} \rightarrow e^-_{aq} . \qquad (14)$$

The ejected electron that escapes process (14), after reaching the final stages of energy degradation, can also be temporarily captured resonantly by a water molecule to form a transient molecular anion. This anion then undergoes dissociation mainly into H^- and $^{\bullet}OH$ according to

$$e^- + H_2O \rightarrow H_2O^{\bullet -} \rightarrow H^- + {}^{\bullet}OH , \qquad (15)$$

followed by the reaction of the hydride anion with another water molecule through a fast proton transfer

$$H^- + H_2O \rightarrow H_2 + OH^- . \qquad (16)$$

This "dissociative electron attachment" or DEA process (see above) has been observed in amorphous solid water at ~20 K for electron energies between about 5 and 12 eV (ROWNTREE et al., 1991). DEA to water is considered to be responsible, at least in part, for the yield of the (apparently) "nonscavengeable" molecular hydrogen observed experimentally in the radiolysis of liquid water at very early times (PLATZMAN, 1962*b*; FARAGGI and DÉSALOS, 1969; GOULET and JAY-GERIN, 1989; KIMMEL et al., 1994; COBUT et al., 1996, 1998; MEESUNGNOEN and JAY-GERIN, 2005*a*).

At the end of the physical stage, a substantial yield of $H_2O^{\bullet +}$ radical ions is formed within Coulomb interaction distance of the slowing-down ("dry") electron (prior to its thermalization). This Coulomb attraction between the sibling ion and electron tends to draw them back together to undergo electron-cation "geminate" recombination:

$$e^- + H_2O^{\bullet+} \rightarrow H_2O^*_{vib}\,. \qquad (17)$$

As the electron is recaptured, the parent ion is transformed into a (vibrationally) excited neutral molecule.

In the time scale of $\sim 10^{-14}$ s (time required for a single vibration of a water molecule) (MOZUMDER and MAGEE, 1975), the positive ions $H_2O^{\bullet+}$ undergo a proton transfer reaction with neighboring H_2O molecules:

$$H_2O^{\bullet+} + H_2O \rightarrow H_3O^+ + {}^{\bullet}OH\,, \qquad (18)$$

where H_3O^+ (or equivalently, H^+_{aq}) represents the hydrated proton. However, OGURA and HAMILL (1973) pointed out that $H_2O^{\bullet+}$ may migrate (randomly) during its very short lifetime (<10 fs) by means of a sequence of resonant electron transfers from neighboring water molecules to the $H_2O^{\bullet+}$ hole. In fact, the results found by these authors suggest that the positive hole jumps on the average about twenty times before reaction (18) occurs. Estimates of the jump time are 10^{-15} s (MOZUMDER and MAGEE, 1975) and the ranges of a migrating hole are a few molecular diameters (COBUT et al., 1998).

Excited molecules may be produced directly in an initial act [reaction (13)] or by neutralization of an ion [reaction (17)]. We have little knowledge, from both a theoretical and an experimental point of view, about the decay channels for excited water molecules in the liquid phase and the branching ratios associated with each of them. Fortunately, the contribution of the water excited states to the primary free radical and molecular products in water radiolysis is of relatively minor importance in comparison with that of the ionization processes, so that the lack of information about their decomposition has only limited consequences. Consequently, the competing deexcitation mechanisms of H_2O^* are generally assumed to be essentially the same as those reported

for an isolated water molecule (note that the same decay processes have been reported to occur for the electronically and vibrationally excited H_2O molecules in the gas phase), namely (see, for example: SWIATLA-WOJCIK and BUXTON, 1995; COBUT et al., 1998; MEESUNGNOEN and JAY-GERIN, 2005*a*):

$$H_2O^* \rightarrow H^\bullet + {}^\bullet OH \qquad (19)$$

$$H_2O^* \rightarrow H_2 + O(^1D) \qquad (20)$$

$$H_2O^* \rightarrow 2\,H^\bullet + O(^3P) \qquad (21)$$

$$H_2O^* \rightarrow H_2O + \text{release of thermal energy}, \qquad (22)$$

where $O(^1D)$ and $O(^3P)$ represent oxygen atoms produced in their singlet ^1D excited state and triplet ^3P ground state, respectively (see Fig. 6). Note that the dissociation of excited water molecules via reaction (19) is the main source of the initial yield of hydrogen atoms. As for the different branching ratios (or decay probabilities) associated with reactions (19)–(22), they are chosen in order to consistently match the observed picosecond *G*-values of the various spur species (MUROYA et al., 2002; MEESUNGNOEN and JAY-GERIN, 2005*a*). It should be recalled here that the $O(^1D)$ atoms produced in reaction (20) react very efficiently with water to form H_2O_2 or possibly also $2\,{}^\bullet OH$ (TAUBE, 1957; BIEDENKAPP et al., 1970). In contrast, ground-state oxygen atoms $O(^3P)$ in aqueous solution are rather inert to water but react with most additives (AMICHAI and TREININ, 1969).

(3) The "nonhomogeneous chemical" stage consists of diffusion and chemical reactions of the reactive species leading to the re-establishment of chemical equilibrium. As stated above, the various "initial" decomposition products (e^-_{aq}, ${}^\bullet OH$, $H^\bullet$, H_2, H_3O^+, OH^-, ${}^\bullet O^\bullet$,...) present at $\sim 10^{-12}$ s following the passage of the ionizing radiation are distributed nonhomogeneously with high concentrations in the center of spurs or

along the axis of tracks. They then proceed to diffuse away from the site where they were originally produced according to macroscopic diffusion laws and to react with themselves or with dissolved solutes (if any) present at the time of irradiation, until all spur or track reactions are complete. A number of like radicals will combine to form the molecular products H_2 and H_2O_2; a number will combine to re-form H_2O, while the remainder will diffuse out into the bulk of the solution. Table 1 gives the main reaction set used to model the reactions that are likely to occur while the spurs expand. The time for completion of spur processes is generally taken to be $\sim 10^{-6}$ s. By this time, the spatially nonhomogeneous distribution of reactive species has relaxed. Basically, it is the competition between reaction and escape which determines the "primary" or "escape" yields of the radical and molecular products (see above).

Finally, we should note that, in the time domain beyond a few microseconds, the reactions which occur in the bulk solution can usually be well described with conventional homogeneous chemistry methods (PASTINA and LAVERNE, 2001).

I.6. Controversial issues on the primary yields of $HO_2^{\bullet}/O_2^{\bullet-}$ and H_2O_2 versus LET in the heavy-ion radiolysis of water at high LET

Under heavy-ion irradiation conditions, the general trends on increasing LET of the radiation are to give lower free-radical (e.g., e_{aq}^-, $^{\bullet}OH$, and $H^{\bullet}$) and higher molecular (e.g., H_2) primary yields (see, for example: ALLEN, 1961; ANDERSON and HART, 1961; PUCHEAULT, 1961; BURNS and SIMS, 1981; APPLEBY, 1989; ELLIOT et al., 1996; McCRACKEN et al., 1998; LAVERNE, 2000, 2004). This behavior is explained by the increased intervention of radical-radical reactions as the local concentration of radicals along the track of the impacting ion is high and many radical interactions occur before the products can escape into the bulk solution (see above). This should permit fewer radicals to escape combination and recombination

Table 1. Main reaction scheme and rate constants (k) used in our simulations of the nonhomogeneous chemical stage in the radiolysis of pure liquid water at 25 °C.[4]

Reaction	k (M^{-1} s^{-1})	Reaction	k (M^{-1} s^{-1})
$H^{\bullet} + H^{\bullet} \rightarrow H_2$	5.03×10^9	$e^-_{aq} + e^-_{aq} \rightarrow H_2 + 2\ OH^-$	5.0×10^9
$H^{\bullet} + {}^{\bullet}OH \rightarrow H_2O$	1.55×10^{10}	$e^-_{aq} + O_2^{\bullet-} \rightarrow H_2O_2 + 2\ OH^-$	1.3×10^{10}
$H^{\bullet} + H_2O_2 \rightarrow H_2O + {}^{\bullet}OH$	3.5×10^7	$e^-_{aq} + HO_2^- \rightarrow O^{\bullet-} + OH^-$	3.51×10^9
$H^{\bullet} + e^-_{aq} \rightarrow H_2 + OH^-$	2.5×10^{10}	$e^-_{aq} + O^{\bullet-} \rightarrow 2\ OH^-$	2.31×10^{10}
$H^{\bullet} + OH^- \rightarrow H_2O + e^-_{aq}$	2.51×10^7	$e^-_{aq} + H_2O \rightarrow H^{\bullet} + OH^-$	15.8
$H^{\bullet} + O_2 \rightarrow HO_2^{\bullet}$	2.1×10^{10}	$e^-_{aq} + O_2 \rightarrow O_2^{\bullet-}$	1.74×10^{10}
$H^{\bullet} + HO_2^{\bullet} \rightarrow H_2O_2$	1.0×10^{10}	$e^-_{aq} + HO_2^{\bullet} \rightarrow HO_2^-$	1.28×10^{10}
$H^{\bullet} + O_2^{\bullet-} \rightarrow HO_2^-$	1.0×10^{10}	$e^-_{aq} + O(^3P) \rightarrow O^{\bullet-}$	2.0×10^{10}
$H^{\bullet} + HO_2^- \rightarrow {}^{\bullet}OH + OH^-$	1.46×10^9	$e^-_{aq} + O_3 \rightarrow O_3^{\bullet-}$	3.6×10^{10}
$H^{\bullet} + O(^3P) \rightarrow {}^{\bullet}OH$	2.02×10^{10}	$e^-_{aq} + H^+ \rightarrow H^{\bullet}$ ($pK_a = 9.6$)	2.11×10^{10}
$H^{\bullet} + O^{\bullet-} \rightarrow OH^-$	2.0×10^{10}	$H^+ + O^{\bullet-} \rightarrow {}^{\bullet}OH$ ($pK_a = 11.9$)	4.78×10^{10}
$H^{\bullet} + H_2O \rightarrow H_2 + {}^{\bullet}OH$	0.086	$H^+ + O_2^{\bullet-} \rightarrow HO_2^{\bullet}$ ($pK_a = 4.8$)	4.78×10^{10}
${}^{\bullet}OH + {}^{\bullet}OH \rightarrow H_2O_2$	5.5×10^9	$H^+ + OH^- \rightarrow H_2O$ ($pK_w = 14$)	1.12×10^{11}
${}^{\bullet}OH + H_2O_2 \rightarrow HO_2^{\bullet} + H_2O$	2.87×10^7	$H^+ + HO_2^- \rightarrow H_2O_2$ ($pK_a = 11.7$)	5.0×10^{10}
${}^{\bullet}OH + H_2 \rightarrow H^{\bullet} + H_2O$	3.28×10^7	$H^+ + O_3^{\bullet-} \rightarrow {}^{\bullet}OH + O_2$	9.0×10^{10}
${}^{\bullet}OH + e^-_{aq} \rightarrow OH^-$	2.95×10^{10}	$OH^- + O(^3P) \rightarrow HO_2^-$	4.2×10^8
${}^{\bullet}OH + OH^- \rightarrow O^{\bullet-} + H_2O$	6.3×10^9	$OH^- + HO_2^{\bullet} \rightarrow O_2^{\bullet-} + H_2O$	6.3×10^9
${}^{\bullet}OH + HO_2^{\bullet} \rightarrow O_2 + H_2O$	7.9×10^9	$O_2 + O(^3P) \rightarrow O_3$	4.0×10^9
${}^{\bullet}OH + HO_2^- \rightarrow HO_2^{\bullet} + OH^-$	8.32×10^9	$HO_2^{\bullet} + O_2^{\bullet-} \rightarrow HO_2^- + O_2$	9.7×10^7
${}^{\bullet}OH + O(^3P) \rightarrow HO_2^{\bullet}$	2.02×10^{10}	$HO_2^{\bullet} + HO_2^{\bullet} \rightarrow H_2O_2 + O_2$	8.3×10^5
${}^{\bullet}OH + O^{\bullet-} \rightarrow HO_2^-$	1.0×10^9	$HO_2^{\bullet} + O(^3P) \rightarrow O_2 + {}^{\bullet}OH$	2.02×10^{10}
${}^{\bullet}OH + O_3 \rightarrow O_2 + HO_2^{\bullet}$	1.11×10^8	$O_2^{\bullet-} + O^{\bullet-} \rightarrow O_2 + 2\ OH^-$	6.0×10^8
$H_2O_2 + e^-_{aq} \rightarrow OH^- + {}^{\bullet}OH$	1.1×10^{10}	$O_2^{\bullet-} + O_3 \rightarrow O_3^{\bullet-} + O_2$	1.5×10^9
$H_2O_2 + O(^3P) \rightarrow HO_2^{\bullet} + {}^{\bullet}OH$	1.6×10^9	$HO_2^- + O^{\bullet-} \rightarrow O_2^{\bullet-} + OH^-$	3.5×10^8
$H_2 + O(^3P) \rightarrow H^{\bullet} + {}^{\bullet}OH$	4.77×10^3	$HO_2^- + O(^3P) \rightarrow O_2^{\bullet-} + {}^{\bullet}OH$	5.3×10^9
$H_2 + O^{\bullet-} \rightarrow H^{\bullet} + OH^-$	1.21×10^8	$O^{\bullet-} + O^{\bullet-} \rightarrow H_2O_2 + 2\ OH^-$	1.0×10^8
$O(^3P) + O(^3P) \rightarrow O_2$	2.2×10^{10}	$O^{\bullet-} + O_3^{\bullet-} \rightarrow 2\ O_2^{\bullet-}$	7.0×10^8
$O(^3P) + H_2O \rightarrow 2\ {}^{\bullet}OH$	1.9×10^3	$O^{\bullet-} + H_2O \rightarrow {}^{\bullet}OH + OH^-$	1.02×10^6

[4] Note that, in contrast to the ground-state $O(^3P)$ oxygen atom, singlet oxygen, $O(^1D)$, does not appear in the reaction mechanism of the chemical stage as it is assumed to react very rapidly with a water molecule in the physicochemical stage to form H_2O_2 or possibly also $2\ {}^{\bullet}OH$ (see text).

reactions during the expansion of the tracks, and in turn the formation of more molecular products. However, there are two important exceptions to this rule:

(1) Unlike the behavior of other radicals, the primary yield of $HO_2^{\bullet}/O_2^{\bullet-}$ radicals rises sharply with LET (DONALDSON and MILLER, 1956; LEFORT and TARRAGO, 1959; APPLEBY and SCHWARZ, 1969; BIBLER, 1975; BAVERSTOCK and BURNS, 1976; SIMS, 1978; BURNS and SIMS, 1981; LAVERNE et al. 1986; LAVERNE and SCHULER, 1987*b*; BALDACCHINO et al., 1998*a*, *b*; McCRACKEN et al., 1998; WASSELIN-TRUPIN et al., 2000; TAGUCHI et al., 2005). As mentioned earlier, with fast electrons and γ-rays, the production of $HO_2^{\bullet}/O_2^{\bullet-}$ is normally neglected because its very small yield of ~0.02 molec./100 eV accounts for less than 1% of the other primary radiolytic species. However, with high-LET heavy ions, it is the major radical product. The origin of these $HO_2^{\bullet}/O_2^{\bullet-}$ radicals is as yet not clearly established, even though there are a number of suggested (but not completely adequate) mechanisms to account for their formation and their increase with increasing LET (for reviews, see: SIMS, 1978; LAVERNE, 1989; FERRADINI and JAY-GERIN, 1998). The most recent mechanism is that proposed by FERRADINI and JAY-GERIN (1998) who suggest, as an alternative, that multiple ionization (MI) of water is responsible for the large yields of $HO_2^{\bullet}/O_2^{\bullet-}$ produced in the heavy-ion radiolysis of water at high LET. This will be discussed more thoroughly below.

(2) A second peculiar feature is that the primary yield of H_2O_2 rises with increasing LET to a maximum, after which it falls (SIMS, 1978; BURNS and SIMS, 1981; PASTINA and LAVERNE, 1999; WASSELIN-TRUPIN et al., 2002). It has been shown, in particular, that the maximum in the value of $G_{H_2O_2}$ occurs precisely at the point where $G_{HO_2^{\bullet}/O_2^{\bullet-}}$ begins to rise sharply, suggesting that the yields of $HO_2^{\bullet}/O_2^{\bullet-}$ and H_2O_2 are closely linked (SIMS, 1978). Apart from calculations using

the Schwarz diffusion model (SCHWARZ, 1968; BURNS and SIMS, 1981, and references therein), which predict a slight maximum in the H_2O_2 yield but at lower LET than is found experimentally,[5] there is hitherto no suitable explanation for the presence of such a maximum in $G_{H_2O_2}$ as a function of LET.

I.7. The "oxygen-in-the-track" hypothesis

Oxygen is a powerful radiation sensitizer; increasing the concentration of molecular oxygen during irradiation has the remarkable property of enhancing the likelihood that a cell exposed to a given dose of X or γ radiation will die. The oxygen's ability to sensitize cells to damage from ionizing radiation has been known for many years (see, for example: FERRADINI and JAY-GERIN, 1999; HALL and GIACCIA, 2006; for an account of the historical development of the subject, see: GRAY et al., 1953; PATT, 1953; HOWARD-FLANDERS, 1958). The degree of sensitization can be quantified by the "oxygen enhancement ratio" (OER), the ratio of doses without and with oxygen needed to produce the *same* biological effect (fraction of cells surviving the irradiation). The OER is recognized as a dose-modifying factor of fundamental importance in radiobiology as well as of great practical relevance in radiotherapy. For low-LET radiations with conventional dose rates, the OER values are generally found between 2 and 3. For most cellular organisms, the oxygen effect shows a strong dependence on radiation quality; the value of OER decreases progressively with increasing LET of the radiation (see, for example: BARENDSEN et al., 1966; BARENDSEN, 1968; ALPER and BRYANT, 1974). This is illustrated in Fig. 7 for cultured cells of human origin. As we can see from the figure, the OER falls rela-

[5] In addition, the Schwarz model cannot account for the $HO_2^{\bullet}/O_2^{\bullet-}$ yield at high LET, suggesting that at high LET additional mechanisms become important which are not included in the model.

tively slowly at first, from ~2.6 to 2.05 between ~5.6 and 61 keV/μm, after which it decreases more rapidly and approaches unity at an LET value of ~165 keV/μm. To account for this experimental finding, SCHOLES and WEISS (1959), SWALLOW and VELANDIA (1962), and NEARY (1965) invoked the "oxygen-in-the-track" hypothesis, suggesting that molecular oxygen generated in the tracks of densely ionizing particles as they traverse the biological material is responsible for the decrease

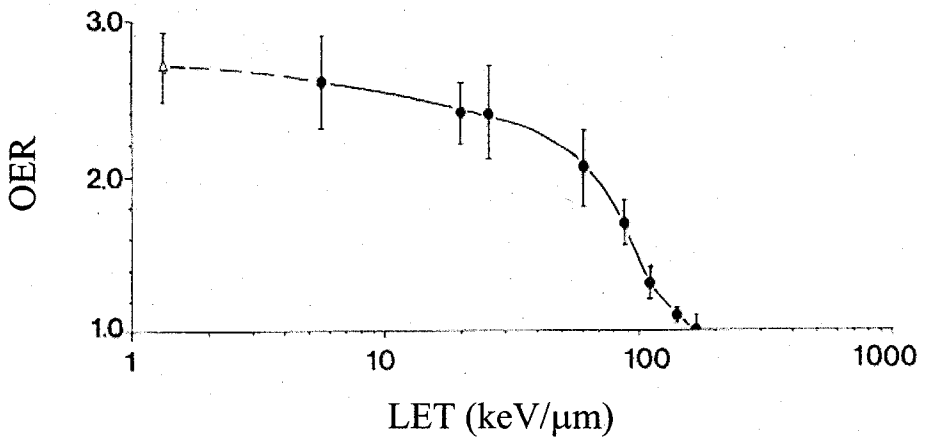

Figure 7. Oxygen enhancement ratio (OER) as a function of LET obtained with monoenergetic ions for impairment of the proliferative capacity of cultured human cells (solid circles). Triangle: 250-kVp X-rays, for which a track-average LET of 1.3 keV/μm has been assumed (BARENDSEN et al., 1966).

of OER with LET. In other words, cells exposed to high-LET radiation exhibit an oxygenated microenvironment around the particle track, even when they are irradiated under anoxic (i.e., no oxygen) conditions (BAVERSTOCK and BURNS, 1976, 1981). This hypothesis of the generation of molecular oxygen in heavy-ion tracks, which presupposes that O_2 is a product of the radiolysis of water at high LET, has often been invoked for a variety of aqueous biological systems. However, different conclusions

have been drawn (STUGLIK, 1995; see also, for example: ALPER, 1956; HOWARD-FLANDERS, 1958; ALPER and BRYANT, 1974; SAUER et al., 1978; JONAH, 1985; KIEFER, 1975, 1990; FRANKENBERG-SCHWAGER et al., 1994; MICHAEL and PRISE, 1996; BARILLA and LOKAJÍČEK, 2000) and an internally consistent picture supporting this hypothesis has not yet been forthcoming.

I.8. Multiple ionization of water in single collisions under heavy-ion bombardment

When an impacting heavy charged particle (particularly a multiply-charged heavy ion) collides violently with a multielectron target molecule, some of the translational kinetic energy of the ion is deposited in the electronic degrees of freedom of the target, with the result that the target emerges with an electronic ionization or excitation. Collisions at sufficiently large impact parameters will produce only singly ionized and excited molecules. As the impact parameter becomes smaller, multiple ionization (MI) of the target outer (loosely bound) electron shells in a "single act" occurs with appreciable probabilities. For small impact parameters, inner-shell electrons can be ejected along with the multiple ionization of the outer shells (for reviews, see: DUBOIS and MANSON, 1987; COCKE and OLSON, 1991; McDANIEL et al., 1993; ICRU REPORT 55, 1996; TOBUREN, 2004). Although inner-shell ionization (followed by Auger relaxation) effects are well known,[6] the consequences of direct multiple outer-

[6] Creation of an initial inner-shell vacancy (hole) by a swift charged particle is followed by the emission of one (or several) Auger electrons (commonly called an Auger cascade) in the ensuing "rearrangement" of the electron cloud as the excited atom/molecule relaxes to the ground state. Typically, the energy transferred in such a process amounts to some hundreds of electronvolts (i.e., the *K*-shell ionization energies of a C, N, and O atom are 283.8, 401.6, and 532 eV, respectively). Auger relaxation

shell ionization with two (or more) outgoing electrons in the final state have not often been considered in models of radiation chemistry and biology. In fact, more than fifty years ago, PLATZMAN (1952) concluded, in a discussion of the possible role of direct multiple target ionization in radiation action, that these processes, although infrequent relative to single ionization events, should be "extremely effective chemically" owing to the high instability of the multiply ionized molecules produced.[7] In this same radiation-chemical context, the hypothesis of "multiple ionization of a single or of near neighbors" was also proposed by GÄUMANN and SCHULER (1961) and SCHULER (1965) as a possible explanation for the large increase in the yield of H_2 in the radiolysis of benzene by densely ionizing radiations (relative to that produced by fast electrons). Recently, FERRADINI and JAY-GERIN (1998) re-considered this earlier hypothesis and suggested that MI could play a significant role in the heavy-ion radiolysis of liquid water at high LET. In particular, they proposed that MI would be responsible for the large yields of $HO_2^{\bullet}/O_2^{\bullet-}$ observed experimentally in high-LET water radiolysis (see above). A similar proposition was also published in a preliminary report by some members of the FERRADINI's group at the "Université René-Descartes" in Paris (GARDÈS-ALBERT et al., 1996) and later by OLIVERA et al. (1998).

---

can produce doubly (or multiply) charged target ions (see, for example: DURUP and PLATZMAN, 1975; CHATTORJI, 1976).

[7] PLATZMAN (1952) also pointed out the possibility of formation by the incident particle, in single collisions, of multiply "excited" atoms or molecules. By multiple excitation is meant the *simultaneous* excitation, by a passing charged particle, of several electrons in a single atom or in atoms closely coupled together in a molecule. According to this author, this process should be less likely to have a significant influence on chemical or biological effects than does multiple ionization. Multiple excitation has been ignored in the present work.

Multiple ionization has long been recognized as an important process in atomic physics and experimental data have accumulated for many years. Most experiments have been performed with light ions in the gas phase. The importance of the direct outer-shell ionization in fast ion-atom collisions was first clearly demonstrated by the measurements of MANSON et al. (1983), who studied 0.5 to 4-MeV protons incident on neon. They showed, at least for that target, that direct double ionization was the dominant Ne^{2+} production process, far more probable than inner-shell ionization (the Auger channel). In fact, inner-shell ionization cross sections are generally several orders of magnitude smaller than direct outer-shell ionization, that is, inner-shell ionization is a "rare" event (TOBUREN, 2004). The multiple ionization and the possible avenues of fragmentation (following MI) of polyatomic molecular targets induced by the interaction with heavy ions have been investigated intensively only recently (mainly in the last decade). For water vapor, experimental studies have been reported so far by several groups (JARDIN et al., 1994; WERNER et al., 1995*a*, *b*; OLIVERA et al., 1998; SIEGMANN et al., 1999; PEŠIĆ et al., 2004; LEGENDRE et al., 2005; MONTENEGRO and LUNA, 2005; ALVARADO et al., 2005; for a recent review, see: STOLTERFOHT et al., 2007). Specifically, it is found that the cross section for double ionization is usually more than an order of magnitude less than for single ionization. Triple ionization is usually more than an order of magnitude less than double ionization. Similar ionization of higher multiplicity is much less probable (LAVERNE, 2000; CHAMPION, 2003; CHAMPION et al., 2005; GERVAIS et al., 2005, 2006). To our best knowledge, only limited data exist for studies of MI under highly charged ion impact for molecular systems of chemical or biological importance in the "condensed" phase. This is explained by the fact that such experiments are extremely difficult and in general further complicated by the occurrence of many possible molecular break-up channels following ionization. Theoretically, a detailed

description of MI is also a difficult task due to the complex, quantum-mechanical many-body nature of the scattering mechanisms involved. Nevertheless, a few attempts have been made recently to simulate the role of multiple ionization in *liquid* water with the aim of evaluating its consequences in the heavy-ion radiation chemistry of water (see Chapters II-IV; GERVAIS et al., 2005, 2006; GAIGEOT et al., 2007).

I.9. Monte Carlo simulations of high-LET water radiolysis

The complex sequence of events that follow absorption in liquid water of ionizing radiation can be modeled successfully by the use of Monte Carlo simulation techniques. Such a procedure is well adapted to account for the *stochastic* nature of the phenomena, provided that realistic probabilities and cross sections for all possible events are adequately known. The simulation then allows one to reconstruct the intricate action of the radiation. It also offers a powerful tool for appraising the validity of different assumptions, for making a critical examination of proposed reaction mechanisms, and for estimating some unknown parameters. The accuracy of these calculations is best determined by comparing their predictions with experimental data on well-characterized chemical systems that have been examined with a wide variety of incident radiation particles and energies.

TURNER and his collaborators at the Oak Ridge National Laboratory (Oak Ridge, Tennessee, U.S.A.) jointly with MAGEE and CHATTERJEE at Lawrence Berkeley Laboratory (Berkeley, California, U.S.A.) were the first to use Monte Carlo simulations to derive computer-plot representations of the chemical evolution of a few keV electron tracks in liquid water at times between ~10^{-12} and 10^{-7} s (TURNER et al., 1981, 1983, 1988*b*). Following this pioneering work, stochastic simulation codes employing Monte Carlo procedures were used with success by a number of investigators

to study the relationship between the initial track structure and the ensuing chemical processes that occur in the radiolysis of both pure water and water containing solutes (for a comprehensive list and reviews, see, for example: BALLARINI et al., 2000; UEHARA and NIKJOO, 2006). Two main approaches have been widely used: (1) the "step-by-step" (or random flights Monte Carlo simulation) method, in which the trajectories of the diffusing species of the system are modeled by time-discretized random flights and in which reaction occurs when reactants undergo pairwise encounters, and (2) the "independent reaction times" (IRT) method (CLIFFORD et al., 1986; PIMBLOTT et al., 1991; PIMBLOTT and GREEN, 1995), which allows the calculation of reaction times without having to follow the trajectories of the diffusing species. Among the stochastic approaches, the most reliable is certainly the full random flights simulation, which is generally considered as a measure of reality. However, this method can be exceedingly consuming in computer time when large systems (such as complete radiation tracks or track segments) are studied. The IRT method, a computer efficient stochastic simulation technique, has been devised to achieve much faster realisations than are possible with the full Monte Carlo model. In essence, it relies on the approximation that the distances between pairs of reactants evolve independently of each other, and therefore the reaction times of the various potentially reactive pairs are independent of the presence of other reactants in the system. For every pair, a reaction time is stochastically sampled according to the time-dependent survival function (GREEN et al., 1990; GOULET and JAY-GERIN, 1992; FRONGILLO et al., 1998) that is appropriate for the type of reaction considered. This function depends on the initial (or zero-time) distance separating the species, their diffusion coefficients, their Coulomb interaction, their reaction radius, and the probability of reaction during one of their encounters. The first reaction time is found by taking the minimum of the resulting ensemble of reaction times and allowing the corresponding pair of species to react

at this time. This procedure for modeling reaction is continued either until all reactions are completed or until a pre-defined cut-off time is reached. The IRT simulation technique also allows one to incorporate in a simple way pseudo first-order reactions of the radiolytic products with various scavengers that are homogeneously distributed in the medium (such as H^+, OH^-, and H_2O itself, or more generally any solutes for which the relevant reaction rates are known). The ability of the IRT method to give accurate time-dependent chemical yields has been well validated by comparison with full random flights Monte Carlo simulation, which does follow the reactant trajectories in detail (PIMBLOTT et al., 1991; GOULET et al., 1998).

In a program begun in the early 1990's, the Sherbrooke group has also developed and progressively refined with very high levels of detail several Monte Carlo codes that simulate the track structure of ionizing particles in water, the production of the various ionized and excited species, and the subsequent reactions of these species in time with one another or with available solutes (COBUT et al., 1994, 1998; FRONGILLO et al., 1998; HERVÉ DU PENHOAT et al., 2000; MEESUNGNOEN et al., 2001, 2003; MEESUNGNOEN and JAY-GERIN, 2005*a*, *b*; MUROYA et al., 2002, 2006; PLANTE et al., 2005; AUTSAVAPROMPORN et al., 2007). A most recent version of the Sherbrooke codes, called IONLYS-IRT (MEESUNGNOEN and JAY-GERIN, 2005*a*, *b*), has been used in the present work.

Briefly, the IONLYS step-by-step simulation program models all of the events of the physical and physicochemical stages in the track development. To take into account the effects of multiple ionizations under high-LET heavy-ion impact, the model incorporates double, triple, and quadruple ionization processes in single ion-water collisions (see above). Following the mechanism proposed by FERRADINI and JAY-

GERIN (1998), the double ionization of water is assumed to lead to the formation of $HO_2^{\bullet}/O_2^{\bullet-}$ through oxygen atoms produced in their ^3P ground state, according to[8]

$$H_2O^{++} + 2\,H_2O \rightarrow 2\,H_3O^{+} + O(^3P) \qquad (23)$$

at very short times, followed by

$$^{\bullet}OH + O(^3P) \rightarrow HO_2^{\bullet}\,. \qquad (24)$$

As for the triple and quadruple ionizations of water molecules, they are assumed to lead directly to the formation of $HO_2^{\bullet}/O_2^{\bullet-}$ and molecular oxygen, respectively, by acid-base re-equilibration, according to the *overall* reactions:

$$H_2O^{\bullet 3+} + 4\,H_2O \rightarrow 3\,H_3O^{+} + HO_2^{\bullet} \qquad (25)$$

and

$$H_2O^{4+} + 5\,H_2O \rightarrow 4\,H_3O^{+} + O_2\,. \qquad (26)$$

The complex spatial distribution of reactants at the end of the physicochemical stage, which is provided as an output of this program, is then used directly as the starting point for the nonhomogeneous chemical stage. This third and final stage is covered by the program IRT, which employs the IRT method to model the chemical development that occurs during this stage and to simulate the formation of measurable yields of chemical products. Its detailed implementation has been given previously (FRONGILLO et al., 1998). Only slight adjustments have been made in some reaction rate constants (see Table 1) and diffusion coefficients of reactive species to take

[8] A fragmentation mechanism, based on the "Coulomb explosion" of multiply ionized water molecules observed in the gas phase, has also been proposed recently to explain the formation of $HO_2^{\bullet}/O_2^{\bullet-}$ and O_2 in the heavy-ion radiolysis of liquid water at high LET (GERVAIS et al., 2005, 2006; GAIGEOT et al., 2007). This mechanism is discussed in Chapter V in relation with reactions (23)–(26).

account of the latest data available from the literature. The simulations of the radiolysis of (deaerated) water under acidic conditions (0.4 *M* H_2SO_4, pH 0.46) are described elsewhere (MEESUNGNOEN et al., 2001; AUTSAVAPROMPORN et al., 2007).

Finally, the influence of the LET on the yields of the various radiation-induced species produced in neutral water and in 0.4 *M* H_2SO_4 aqueous solutions at 25 °C has been investigated by varying the incident ion energy from ~300 to 0.15 MeV (~0.3–70 keV/μm) for protons, ~300 to 0.3 MeV/nucleon (~1.25–213 keV/μm) for $^4He^{2+}$, ~300 to 1.25 MeV/nucleon (~12–604 keV/μm) for $^{12}C^{6+}$, and ~300 to 3.2 MeV/nucleon (~25–938 keV/μm) for $^{20}Ne^{9+}$. The calculations are performed by simulating short (~1.5–100 μm) ion track segments, over which the energy and LET of the ion are well defined and remain nearly constant. Typically, ~5000 to 400 000 reactive chemical species are generated in those simulated track segments (depending on ion type and energy), thus ensuring only small statistical fluctuations in the determination of average yields.

I.10. Objectives of the research project

As seen earlier, the radiolysis of liquid water by low-LET radiation is generally well understood. However, under high-LET conditions and in the limit of very short times, several data given in the literature have not hitherto been quantitatively explained, namely:

(1) The primary yield of $HO_2^{\bullet}/O_2^{\bullet-}$ radicals ($G_{HO_2^{\bullet}/O_2^{\bullet-}}$) increases with increasing LET, a behavior that is akin to the molecular yields. The actual mechanism of formation of these radicals remains uncertain, even though at high LET they are the major radical species.

(2) The primary yield of H_2O_2 ($G_{H_2O_2}$) rises with increasing LET to a maximum around 100–200 keV/μm after which it falls. No suitable explanation for the presence of such a maximum in $G_{H_2O_2}$ as a function of LET has been offered.

(3) The hypothesis of the radiolytic formation of O_2 in the tracks of heavy charged particles has often been invoked for a variety of aqueous biological materials ("oxygen-in-the-track" hypothesis), but the conclusion is not clear yet.

The primary purpose of this study is to clarify the role and extent of the mechanism of multiple ionization of water in the radiolysis of liquid water under high-LET conditions, and to demonstrate that this mechanism can account satisfactorily for all recorded data. This innovative study has been motivated by the hypothesis put forward several years ago by FERRADINI and JAY-GERIN (1998) that multiple ionization would be responsible for the large $HO_2^{\bullet}/O_2^{\bullet-}$ yield produced in water subject to heavy-ion irradiation.

The complex sequence of events of liquid water radiolysis and theoretical descriptions of the radiation chemistry of water is well described using Monte Carlo techniques. So far, the application of those methods has been mainly limited to the case of low-LET radiations due to the scarcity of reliable scattering cross-sections at low heavy-ion energies which are necessary for a realistic description of the physical aspects of the radiation track structure.

In the present study, Monte Carlo track structure simulations are used to investigate the effects of multiple ionization of water molecules on the *G*-values of the radiolytic free radical and molecular species, including O_2, produced in the radiolysis of liquid water by several different types of radiation (including $^{1}H^{+}$, $^{4}He^{2+}$, $^{12}C^{6+}$, and $^{20}Ne^{9+}$ ions) over a wide range of LET up to ~900 keV/μm, at neutral pH (Chapters II and III) and in acidic (0.4 *M* H_2SO_4) solutions (Chapter IV) at 25 °C. Taking into account the double, triple, and quadruple ionizations of water molecules, the primary

yields $G_{e^-_{aq}}$, $G_{H\cdot}$, $G_{\cdot OH}$, G_{H_2}, $G_{HO_2\cdot/O_2\cdot^-}$, $G_{H_2O_2}$, and G_{O_2} are calculated as a function of LET for the four irradiating ions used and compared with available experimental data. A large part of this work is devoted specifically to the yields of $HO_2^{\bullet}/O_2^{\bullet-}$ and H_2O_2 in order to address the importance of the role of multiple ionization in the production of these species. Furthermore, the simultaneous formation of molecular oxygen within the tracks of densely ionizing radiations is examined in close relation with the "oxygen-in-the-track" hypothesis (Chapter III). Our results provide evidence which supports this hypothesis.

Throughout this work, radiation chemical yields (*G*-values) are expressed in the units of molecules per 100 eV. For conversion into SI units (mol/J): 1 molecule/100 eV $\approx$ 0.10364 μmol/J. Note also that this work deals only with 25 °C results.

II. Article No. 1

In this chapter, we report our first preliminary Monte Carlo track structure simulation study regarding the effects of multiple ionization of water molecules on the formation of $HO_2^{\bullet}/O_2^{\bullet-}$ and H_2O_2 in the radiolysis of pure, deaerated liquid water with high-LET $^{12}C^{6+}$ ions up to ~430 keV/μm, at 25 °C.

This work is presented in the following article, entitled: "**Multiple ionization effects on the yields of $HO_2^{\bullet}/O_2^{\bullet-}$ and H_2O_2 produced in the radiolysis of liquid water with high-LET $^{12}C^{6+}$ ions: A Monte Carlo simulation study**", by J. Meesungnoen, A. Filali-Mouhim, N. Snitwongse Na Ayudhya, S. Mankhetkorn, and J.-P. Jay-Gerin.

This article is published in *Chemical Physics Letters*, Vol. **377**, Issues 3-4, Pages 419–425 (15 August 2003).

Multiple ionization effects on the yields of $HO_2^{\bullet}/O_2^{\bullet-}$ and H_2O_2 produced in the radiolysis of liquid water with high-LET $^{12}C^{6+}$ ions: A Monte-Carlo simulation study

by

Jintana Meesungnoen [a,b], Abdelali Filali-Mouhim [a], Nitaya Snitwongse Na Ayudhya [a,b], Samlee Mankhetkorn [b], Jean-Paul Jay-Gerin [a,*]

[a] *Département de Médecine Nucléaire et de Radiobiologie, Faculté de Médecine, Université de Sherbrooke, Sherbrooke (Québec) J1H 5N4, Canada*

[b] *Laboratory of Physical Chemistry, Molecular and Cellular Biology, Faculty of Science, Burapha University, Bangsaen, Chonburi 20131, Thailand*

[*] *Corresponding author*:

Prof. Jean-Paul Jay-Gerin
Département de médecine nucléaire et de radiobiologie
Faculté de médecine
Université de Sherbrooke
Sherbrooke (Québec) J1H 5N4
Canada

Tel. (819) 346-1110, ext.
Fax: (819) 564-5442
E-mail address:

Chemical Physics Letters **377**, 419–425 (2003)

Abstract

Monte-Carlo simulations are used to investigate the effects of multiple ionization on the formation of $HO_2^{\bullet}/O_2^{\bullet-}$ and H_2O_2 in the radiolysis of water by $^{12}C^{6+}$ ions up to ~430 keV/μm, at neutral pH and 25 °C. Taking into account the double and triple ionizations of water molecules, the primary yields $G_{HO_2^{\bullet}/O_2^{\bullet-}}$ and $G_{H_2O_2}$ are calculated as a function of linear energy transfer (LET). Our results quantitatively reproduce the large increase observed in $G_{HO_2^{\bullet}/O_2^{\bullet-}}$ at high LET. They also simultaneously predict a slight maximum in $G_{H_2O_2}$ at ~180-200 keV/μm, in excellent agreement with experiment. Under the conditions of this study, triple ionization is found to contribute only negligibly to $G_{HO_2^{\bullet}/O_2^{\bullet-}}$.

Keywords: Liquid water, radiolysis, accelerated carbon ions, multiple ionization, cross-sections, linear energy transfer, hydroperoxyl/superoxide anion radicals, hydrogen peroxide, radiolytic yields, Monte-Carlo track-structure simulations.

1. Introduction

The radiolysis of pure deaerated liquid water by low linear energy transfer (LET) radiation (such as ^{60}Co γ-rays, hard X-rays, or fast electrons) is generally well understood and leads to the formation of the radicals and molecular products e^-_{aq}, $H^\bullet$, $^\bullet OH$, H_2, H_2O_2, H_3O^+, OH^-, etc. (for a review, see [1]). Under usual irradiation conditions, these species are generated nonhomogeneously in small regions of high ionization and excitation densities, commonly referred to as spurs, that are widely separated along the track of the radiation. The so-called primary radical and molecular yields (or "escape" yields) $G_{e^-_{aq}}$ (= $G_{H_3O^+} - G_{OH^-}$), $G_{H^\bullet}$, $G_{^\bullet OH}$, G_{H_2}, and $G_{H_2O_2}$ represent the numbers of species of each kind formed per 100 eV of absorbed energy that remain after spur expansion. At room temperature, this spur expansion is essentially complete on the time scale of ~10^{-6} s after the initial energy deposition. At this time, the species that have diffusively escaped from spur reactions become homogeneously distributed throughout the bulk of the solution and available to react with added solutes at moderate concentrations.

With increasing LET, the nearly "spherical" spurs are formed increasingly closer together and eventually overlap to form continuous columns of species consisting initially of a "cylindrical" track core surrounded by a region of radiation effects due to the ejected secondary electrons commonly referred to as the penumbra [2,3]. As the interspur distance decreases, more radicals are formed in close proximity with a correspondingly increased probability of reacting with one another to produce the molecular products or to reform water. Under these conditions, the radical yields are expected to diminish as the LET is increased, whereas the molecular yields increase and the net water decomposition yield decreases (for a review, see [4]). There are two important exceptions to this rule. First, the primary yield of hydroperoxyl/superoxide anion ($HO_2^\bullet$, or its deprotonated form $O_2^{\bullet-}$, pK_a = 4.8) radicals increases with increasing LET [5-11] (note that, for low-LET radiolysis, the production of $HO_2^\bullet/O_2^{\bullet-}$ is usually

neglected because its very small yield of ~0.02 molec./100 eV [12] accounts for less than 1% of the other primary radiolytic species). The increase in $G_{HO_2^{\bullet}/O_2^{\bullet-}}$ is gradual up to ~100-200 keV/μm, but at this point there is a sharp rise [7]. As yet, the origin of these $HO_2^{\bullet}/O_2^{\bullet-}$ radicals is not clearly established (for example, see [13,14]), even though at high LET they are the major radical species. A second peculiar feature is that $G_{H_2O_2}$ rises with increasing LET to a maximum around 100-200 keV/μm after which it falls [7,15]. As will be seen below, it is pertinent to note that this maximum in $G_{H_2O_2}$ occurs at the point where $G_{HO_2^{\bullet}/O_2^{\bullet-}}$ begins to rise sharply, suggesting that the yields of $HO_2^{\bullet}/O_2^{\bullet-}$ and H_2O_2 are closely linked [16]. Apart from calculations using the Schwarz diffusion model which predict a shallow maximum in the hydrogen peroxide yield but at lower LET than is found experimentally (note, in addition, that the Schwarz model cannot account for the $HO_2^{\bullet}/O_2^{\bullet-}$ yield at high LET) (see [7] and references cited therein), there is hitherto no suitable explanation for the presence of such a maximum in $G_{H_2O_2}$ as a function of LET (for example, see [15,17]).

The aim of the present work is to investigate the effects of multiple ionization of water molecules on the formation of both $HO_2^{\bullet}/O_2^{\bullet-}$ and H_2O_2 in the radiolysis of liquid water by $^{12}C^{6+}$ ions up to ~430 keV/μm, at neutral pH and 25 °C. This innovative study has been motivated by the hypothesis proposed recently [14] that multiple ionization could be responsible for the large $HO_2^{\bullet}/O_2^{\bullet-}$ yield produced in irradiated water under fast heavy-ion impact. Using Monte-Carlo track structure simulations that incorporate double and triple ionizations (higher-order ionizations being much less probable), we calculate the primary yields of $HO_2^{\bullet}/O_2^{\bullet-}$ and H_2O_2 at high LET. The main features of our approach are presented briefly in the next section.

2. Monte-Carlo simulations

The radiolysis of liquid water has been modeled by using an extended version of our previous Monte-Carlo simulation code [18-20]. In this version, several modifica-

tions have been made, mainly in the description of the physical and physicochemical stages of the code. In particular, our code now incorporates the newly reported elastic, phonon, and vibrational scattering cross sections of Michaud et al. [21], obtained from slow (~1-100 eV) electron-impact experiments on thin amorphous solid water films, and increased here by a factor of about 2 to account for differences between solid- and liquid-phase cross sections [18,22]. We have also re-examined certain adjustable parameters that enter our code in order to reconcile our calculations with the recently revised experimental hydrated electron (e^-_{aq}) yield data at early times [23-25]. These parameters comprise the thermalization distance of subexcitation electrons, the recombination cross section of the electrons with their water parent cations prior to thermalization, and the branching ratios used for the different competing mechanisms in the decay of vibrationally excited water molecules formed by electron-cation geminate recombination [18]. The values of these parameters have been obtained by using a global-fit procedure, which consists in simultaneously fitting our computed time-dependent yields of e^-_{aq} and of the other radiolytic species ($H^\bullet$, $^\bullet OH$, H_2, and H_2O_2) to experiment [25].

The energy deposition by the incident charged particle and by all the secondary electrons that it has generated occurs through the slowing down of those particles via a variety of inelastic scattering processes, including ionization, electronic and vibrational excitation of single water molecules, and excitation of plasmon-type collective modes ("physical stage"). To take into account the effects of multiple ionization under fast-heavy-ion impact, the model has been extended to incorporate double and triple ionization processes in single ion-water collisions [14]. Ionizations of higher multiplicity are neglected as their occurrence is much less probable in the range of LET of interest here. In the simulations, the double-ionization energy of water molecules (40 eV) is taken from gas-phase studies [26], whereas the value for the triple-ionization energy (chosen equal to 50 eV) is assumed to be near the energy needed for the triple ioniza-

tion of oxygen. Unfortunately, there is as yet little information on the values of the cross-sections for the double (σ_{di}) and triple (σ_{ti}) ionizations of water [4,27]. In this study, σ_{di} is deduced from Rudd's single ionization cross-sections (σ_{si}) for water vapor [28] (adapted here to the liquid phase as previously described [18]), assuming that the ratio σ_{di}/σ_{si} is known. In a first step, we have used for this ratio the recent data of Champion [27] who reported the values of σ_{di}/σ_{si} as a function of E_{ion}/Q_{ion}, where E_{ion} is the ion energy per nucleon and Q_{ion} is the projectile charge, for various ions at intermediate velocities and gaseous targets including water. In a second step, we have treated σ_{di}/σ_{si} in our simulations as an adjustable parameter chosen to reproduce the experimental values of ($G_{O_2} + G_{HO_2^\bullet}$) as a function of LET in the $^{12}C^{6+}$ radiolysis of liquid water under acidic conditions [8,9,13]. As will be seen below, this latter approach offers a powerful means to estimate the ratio σ_{di}/σ_{si} for heavy ion-water collisions in the liquid phase. As for the triple ionization, we assume that, for the collisions of ~4.5-15 MeV/nucleon carbon ions on H_2O, σ_{ti} is an order of magnitude less than σ_{di} [4,27].

The energy that has been so deposited in the medium is then used to produce the "initial" radical and molecular species of the radiolysis, distributed in a highly nonhomogeneous track structure ("physicochemical stage"). The production of $HO_2^\bullet/O_2^{\bullet-}$ via the double ionization of water is assumed to involve oxygen atoms [8,29,30] formed in their ^3P ground state [14], according to

$$H_2O^{2+} + 2\,H_2O \rightarrow 2\,H_3O^+ + O(^3P)\,, \qquad \text{(R1)}$$

followed by

$$O(^3P) + {}^\bullet OH \rightarrow HO_2^\bullet \qquad \text{(R2)}$$

at a very early stage in the expansion of the tracks. It should be recalled here that the O atoms produced in their singlet ^1D state react rapidly with water. In contrast, the ground-state $O(^3P)$ atoms are rather inert to water and will react with $^\bullet OH$ radicals in

the heavy particle track core because of the very high local concentrations of radicals [14]. As for the triple ionization of water molecules, we assume that it directly leads to the formation of $HO_2^{\bullet}/O_2^{\bullet-}$ radicals by an acid-base re-equilibration, according to the overall reaction [14]

$$H_2O^{\bullet 3+} + 4\,H_2O \rightarrow 3\,H_3O^{+} + HO_2^{\bullet}. \qquad \text{(R3)}$$

In our simulations, the H_3O^+ ions in reactions (R1) and (R3) are positioned at 0.3 nm from the $O(^3P)$ atom and the $HO_2^{\bullet}$ radical (which are left in place), respectively, assuming the same relative position between H_3O^+ and the $^{\bullet}OH$ radical following the decomposition of $H_2O^{\bullet+}$ [18]. In addition, the emission angles for the secondary electrons ejected by the incident particle are separated by 180° and 120° when dealing with double and triple ionization, respectively, and the total energy deposited at each point of interaction (after subtraction of the ionization energy of the water molecule) is equally distributed between the ejected electrons.

The step-by-step simulation codes that we use to cover these two stages are TRACPRO and TRACELE [18-20] under their extended versions. The complex spatial distribution of reactants at $\sim 10^{-13}$ s, which is provided as an output of the program TRACELE, is then used directly as the starting point for the so-called "stage of nonhomogeneous chemistry". This third and final stage, during which the various radiolytic species diffuse and react with one another until all spur/track reactions are complete, is covered by our TRACIRT simulation code [18-20], using the independent reaction times (IRT) method [31] to model the nonhomogeneous reaction kinetics. In this study, the effect of LET on $G_{HO_2^{\bullet}/O_2^{\bullet-}}$ and $G_{H_2O_2}$ at neutral pH and 25 °C has been determined by varying the incident energy of the $^{12}C^{6+}$ ions from ~4.5 to 300 MeV/nucleon (~430-12 keV/μm). The calculations are performed by simulating short (1.5-50 μm) particle track segments, over which the LET remains essentially constant. It is worth noting that, typically, about 3×10^4 (~12 keV/μm) to 2×10^5 (~430

keV/μm) reactive chemical species are generated in those simulated track segments (depending on the LET), thus ensuring only small statistical fluctuations in the determination of average yields.

3. Results and discussion

Figures 1 and 2 display our calculated values of $G_{HO_2^{\bullet}/O_2^{\bullet-}}$ and $G_{H_2O_2}$ (obtained at homogeneity at 10^{-6} s) as a function of LET for pure, deaerated liquid water irradiated by $^{12}C^{6+}$ ions up to ~430 keV/μm, at 25 °C, respectively. Available experimental data are also included in the figures for the sake of comparison [5,10,15-17,32-34]. As we can see from Fig. 1, our curve of $G_{HO_2^{\bullet}/O_2^{\bullet-}}$ versus LET calculated without including the mechanism of multiple ionization of water discussed above cannot account quantitatively for the totality of the measured $HO_2^{\bullet}/O_2^{\bullet-}$ yield at high LET. The same conclusion also applies for the H_2O_2 yield; in fact, as seen in Fig. 2, our values of $G_{H_2O_2}$ calculated without multiple ionization of water molecules continuously increases as the LET increases [35], in disagreement with experiment which indicates a decrease in $G_{H_2O_2}$ above 100-200 keV/μm. However, when double and triple ionizations are incorporated in the simulations, we find that a remarkable agreement between theory and experiment can be obtained in both cases. To show this, we have used, in a first step, the values of the ratio σ_{di}/σ_{si} of the double to the single ionization cross-sections reported by Champion [27] for the case of carbon ions in the energy range ~4.2-12 MeV/nucleon (~430-170 keV/μm) and gaseous water (see Fig. 3). The corresponding computed $G_{HO_2^{\bullet}/O_2^{\bullet-}}$ and $G_{H_2O_2}$ values are shown by the dotted lines in Figs. 1 and 2, respectively. As can be seen in Fig. 1, the magnitude of the $HO_2^{\bullet}/O_2^{\bullet-}$ escape yield so obtained compares very well with experiment. However, $G_{HO_2^{\bullet}/O_2^{\bullet-}}$ is nearly invariant over the LET range considered, whereas a continuous decrease should obviously be expected as the LET decreases. Quite similarly, Fig. 2 shows that $G_{H_2O_2}$ computed using the σ_{di}/σ_{si} values of Champion [27] is almost constant as a function of

LET in this same LET range. But its magnitude is well inferior to our H_2O_2 yield values calculated for the same LET in the absence of the multiple ionization of water, which clearly indicates that, when the mechanism of multiple ionization is included in the calculations, a maximum in the $G_{H_2O_2}$ versus LET curve should be present around 100-200 keV/μm.

In a second step, we have treated the ratio σ_{di}/σ_{si} in our simulations as an adjustable parameter chosen to reproduce the available experimental data of ($G_{O_2} + G_{HO_2^\bullet}$) as a function of LET in the $^{12}C^{6+}$ radiolysis of liquid water under acidic conditions [8,9,13]. To this end, we have adapted our Monte-Carlo code to simulate these particular experimental conditions. A detailed description of the procedure used here will be reported elsewhere. Briefly, in those experiments [9], the production of $HO_2^\bullet$ is determined by measuring the yield of molecular oxygen formed in deaerated acidic (0.005 *M* H_2SO_4) solutions of $FeSO_4$ (1 m*M*)-$CuSO_4$ (10 m*M*) in which $HO_2^\bullet$ radicals are converted to O_2 by reaction with $^\bullet OH$ radicals and Cu^{++} (the measured O_2 yield value thus corresponds to the sum $G_{O_2} + G_{HO_2^\bullet}$). The values of σ_{di}/σ_{si} so obtained are plotted in Fig. 3 for the selected energy range ~4.5-15 MeV/nucleon (~430-125 keV/μm). As we can see, our values generally differ appreciably from those reported by Champion [27], except for energies around ~5 MeV/nucleon where the two sets of values become quite comparable. Using our σ_{di}/σ_{si} values in our simulation code of the $^{12}C^{6+}$ radiolysis of neutral water, we have then calculated $G_{HO_2^\bullet/O_2^{\bullet-}}$ and $G_{H_2O_2}$ as a function of LET. The results, shown by the solid lines in Figs. 1 and 2, respectively, are in very good agreement with experiment. In particular, we find a slight maximum in the variation of $G_{H_2O_2}$ with LET at ~180-200 keV/μm, which corroborates the recent measurements of Pastina and LaVerne [15] and the early observations of Burns and Sims [7]. Quite remarkably, extrapolation of our H_2O_2 yield values to higher LET also seems to reproduce very well the data of these authors obtained with carbon ions near ~600-800 keV/μm [15], and with 46-MeV $^{14}N^{4+}$ and 30-MeV $^{20}Ne^{9+}$ ions near

~650 and 1570 keV/μm [7], respectively. Moreover, Figs. 1 and 2 indicate that the maximum in the value of $G_{H_2O_2}$ occurs precisely where $G_{HO_2^{\bullet}/O_2^{\bullet-}}$ begins to rise sharply, in excellent accord with experiment [16] and clearly showing that the yields of $HO_2^{\bullet}/O_2^{\bullet-}$ and H_2O_2 are closely linked. In fact, hydrogen peroxide is formed within the spurs/tracks mainly by the combination reaction of two $^{\bullet}OH$ radicals produced in the decomposition of water

$$^{\bullet}OH + {}^{\bullet}OH \rightarrow H_2O_2 . \qquad \text{(R4)}$$

As $^{\bullet}OH$ reacts with $O(^3P)$ by reaction (R2), this reaction competes with reaction (R4) causing a decrease in the observed H_2O_2 yield at high LET. This very good agreement between theory and experiment supports *a posteriori* our assumption made in reaction (R1) that, for the high-LET range considered here, O atoms are primarily produced in their ^3P ground state (rather than in their singlet ^1D state).

Finally, we have found by independent simulations incorporating the sole mechanism of double ionization of water molecules that triply charged water ions make in fact a negligible contribution to $G_{HO_2^{\bullet}/O_2^{\bullet-}}$ under the condition $\sigma_{ti}/\sigma_{di} = 0.1$ adopted in this study. In addition, we have also found that the incorporation of multiple ionization in the simulations has only little effect on the variation of our computed $G_{e^-_{aq}}$, $G_{H^{\bullet}}$, $G_{^{\bullet}OH}$, and G_{H_2} values as a function of LET (data not shown).

4. Conclusion

In this study, we have investigated the effects of multiple ionization on the formation of $HO_2^{\bullet}/O_2^{\bullet-}$ and H_2O_2 in the radiolysis of liquid water by $^{12}C^{6+}$ ions up to ~430 keV/μm, at neutral pH and 25 °C. Using Monte-Carlo simulations that incorporate double and triple ionizations of water molecules, the primary yields of $HO_2^{\bullet}/O_2^{\bullet-}$ and H_2O_2 have been calculated at high LET. Our results quantitatively reproduce the large increase observed in the $HO_2^{\bullet}/O_2^{\bullet-}$ yield as the LET increases above 100-200 keV/μm. They also simultaneously predict a slight maximum in the yield of H_2O_2 as a

function of LET at ~180-200 keV/μm, in excellent agreement with experiment. In addition, in the range of LET considered in this work and under the condition σ_{ti}/σ_{di} = 0.1, it is found that the mechanism of triple ionization contributes only negligibly to the production of $HO_2^{\bullet}/O_2^{\bullet-}$ and that reactions (R1) and (R2) are responsible of most of the effects observed.

Overall, this study strongly supports the importance of the role of multiple ionization in the radiolysis of water under high-LET irradiation conditions.

Acknowledgements

We thank Professor Jay A. LaVerne for kindly sending us his experimental $HO_2^{\bullet}$ and H_2O_2 yield values for carbon ions as a function of LET, and Professor Hans Bichsel and Dr. John H. Miller for useful correspondence concerning the triple ionization of water. We would also like to thank the "Réseau québécois de calcul de haute performance" (RQCHP) for providing generous computing facilities. Financial support from the Canadian Institutes of Health Research (Grant No. MT-14617) is gratefully acknowledged.

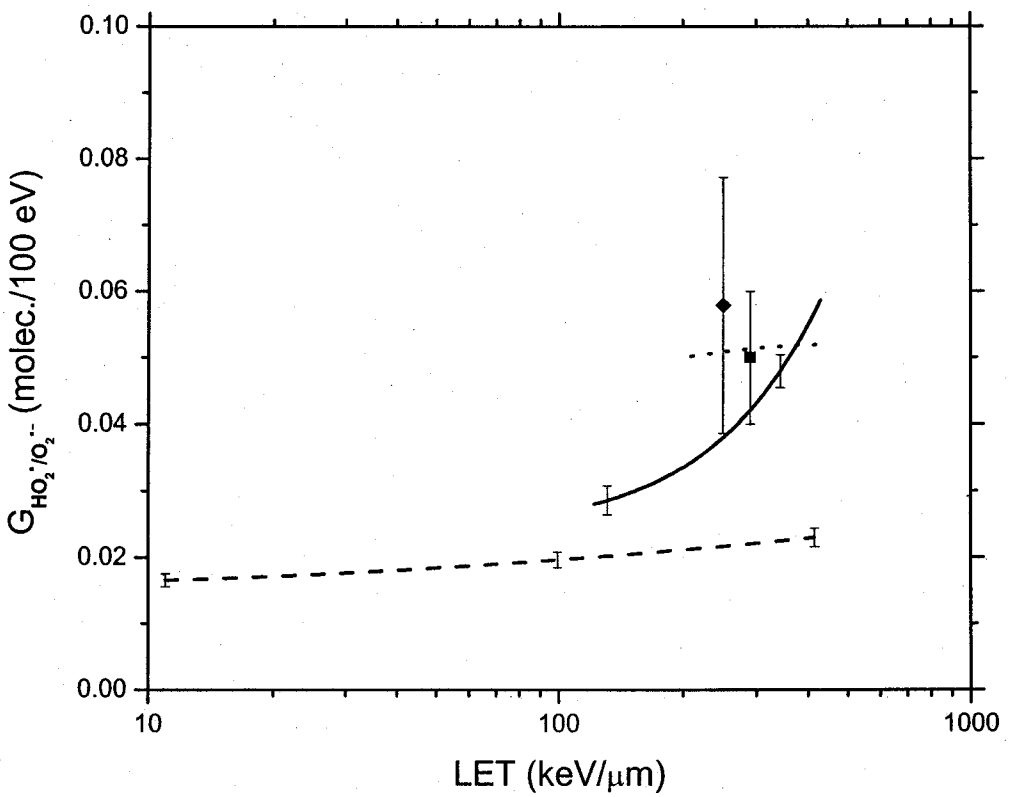

Figure 1: Variation of the primary $HO_2^{\bullet}/O_2^{\bullet-}$ yield ($G_{HO_2^{\bullet}/O_2^{\bullet-}}$) (in molecule/100 eV) of the radiolysis of liquid water by $^{12}C^{6+}$ ions as a function of LET over the range ~12-430 keV/μm, at neutral pH and 25 °C. The solid line represents the results of our Monte-Carlo simulations incorporating the double and triple ionizations of water molecules, obtained at homogeneity at 10^{-6} s (see text). The dotted line has been obtained by using the ratio σ_{di}/σ_{si} reported by Champion [27] for carbon ions and water in the vapor phase. The dashed line corresponds to our $G_{HO_2^{\bullet}/O_2^{\bullet-}}$ values calculated as a function of LET without including the mechanism of multiple ionization of water. The error bars show the 95% confidence intervals of the IRT simulation results. Experiments (at pH close to 7) are from [10]: (◆) $^{36}S^{16+}$ ions (77 MeV/nucleon, LET ~ 250 keV/μm) and [32]: (■) $^{40}Ar^{18+}$ ions (70 MeV/nucleon, LET ~ 290 keV/μm). For conversion of yield values into SI units: 1 molecule/100 eV ≈ 0.10364 μmol/J.

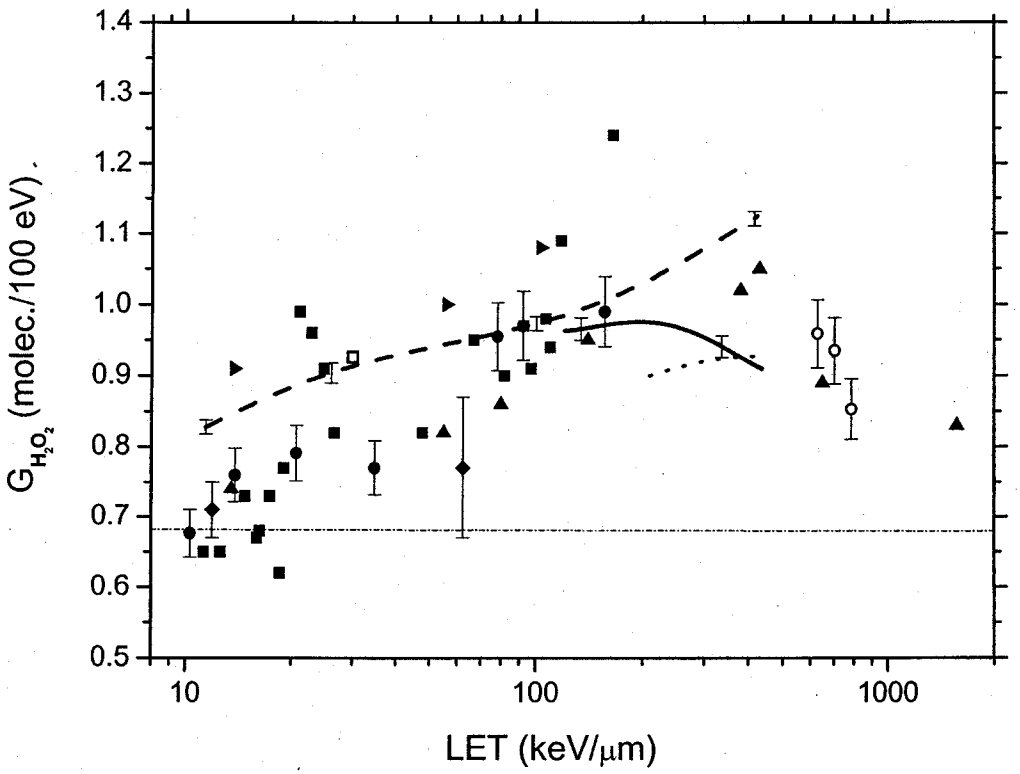

Figure 2: Variation of the primary H_2O_2 yield ($G_{H_2O_2}$) (in molecule/100 eV) of the radiolysis of liquid water by $^{12}C^{6+}$ ions as a function of LET over the range ~12-430 keV/μm, at neutral pH and 25 °C. The solid line represents the results of our Monte-Carlo simulations incorporating the double and triple ionizations of water molecules, obtained at homogeneity at 10^{-6} s (see text). The maximum of the curve is found at ~180-200 keV/μm. The dotted line has been obtained by using the ratio σ_{di}/σ_{si} reported by Champion [27] for carbon ions and water in the vapor phase. The dashed line corresponds to our $G_{H_2O_2}$ values calculated as a function of LET without including the mechanism of multiple ionization of water. The error bars show the 95% confidence intervals of the IRT simulation results. Experiments with carbon ions (open symbols) are from [15]: (○) 10-, 20-, and 30-MeV $^{12}C^{6+}$ ions (LET ~ 787, 703, and 629 keV/μm, respectively) and [17]: (□) 1140-MeV $^{12}C^{6+}$ ions (LET ~ 30 keV/μm). Experimental data with other ions (closed symbols) are also included in the figure for the sake of comparison: (▶) $^2H^+$ and $^4He^{2+}$ [5]; (▲) $^1H^+$, $^4He^{2+}$, $^{14}N^{5+}$, $^{14}N^{4+}$, and $^{20}Ne^{9+}$ [7,16]; (●) $^1H^+$ and $^4He^{2+}$ [15]; (■) $^1H^+$, $^2H^+$, and $^4He^{2+}$ [33]; and (◆)$^2H^+$ and $^7Li^{3+}$ [34]. The dot-dashed line represents the limiting primary H_2O_2 yield with ^{60}Co γ-rays or fast electrons (0.68 molec./100 eV [1]).

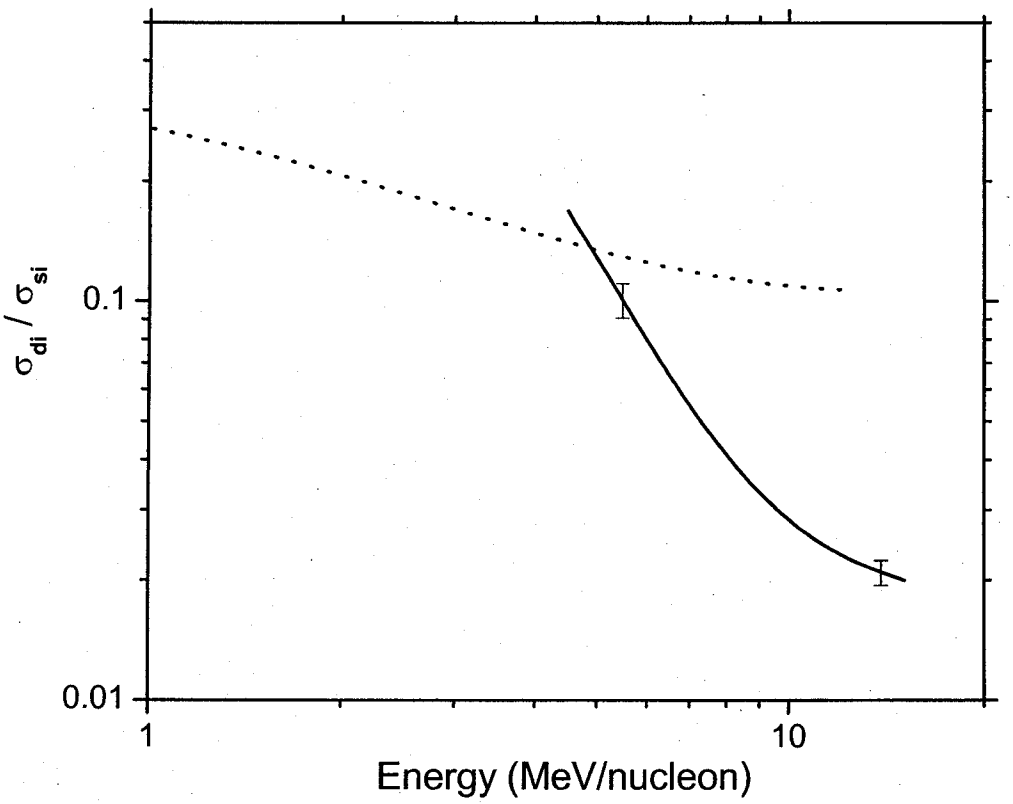

Figure 3: Ratio of the double-to-single ionization cross-sections (σ_{di}/σ_{si}) as a function of the $^{12}C^{6+}$ ion energy (in MeV/nucleon). The solid line represents the results of our Monte-Carlo simulations in which σ_{di}/σ_{si} is treated as an adjustable parameter chosen to reproduce the experimental data of LaVerne and Schuler [9] of ($G_{O_2} + G_{HO_2\cdot}$) as a function of LET (in the range ~125-430 keV/μm) in the $^{12}C^{6+}$ radiolysis of deaerated acidic solutions of $FeSO_4$-$CuSO_4$ (see text). The error bars represent the uncertainty obtained on σ_{di}/σ_{si} taking account of the experimental uncertainty on ($G_{O_2} + G_{HO_2\cdot}$) (± 5%) given by LaVerne and Schuler [9]. The values reported by Champion [27] for carbon ions and gaseous water are shown by the dotted line.

References

[1] C. Ferradini, J.-P. Jay-Gerin, Can. J. Chem. 77 (1999) 1542.

[2] J.L. Magee, A. Chatterjee, in: G.R. Freeman (Ed.), Kinetics of Nonhomogeneous Processes, Wiley, New York, 1987, p. 171.

[3] A. Mozumder, Fundamentals of Radiation Chemistry, Academic Press, San Diego, CA, 1999, p. 41.

[4] J.A. LaVerne, Radiat. Res. 153 (2000) 487.

[5] A. Appleby, H.A. Schwarz, J. Phys. Chem. 73 (1969) 1937.

[6] K.F. Baverstock, W.G. Burns, Nature 260 (1976) 316.

[7] W.G. Burns, H.E. Sims, J. Chem. Soc., Faraday Trans. 1, 77 (1981) 2803.

[8] J.A. LaVerne, R.H. Schuler, W.G. Burns, J. Phys. Chem. 90 (1986) 3238.

[9] J.A. LaVerne, R.H. Schuler, J. Phys. Chem. 91 (1987) 6560.

[10] G. Baldacchino, D. Le Parc, B. Hickel, M. Gardès-Albert, Z. Abedinzadeh, D. Jore, S. Deycard, S. Bouffard, V. Mouton, E. Balanzat, Radiat. Res. 149 (1998) 128.

[11] D.R. McCracken, K.T. Tsang, P.J. Laughton, Aspects of the physics and chemistry of water radiolysis by fast neutrons and fast electrons in nuclear reactors, Report AECL-11895, Atomic Energy of Canada Ltd., Chalk River, Ontario, 1998.

[12] E. Bjergbakke, E.J. Hart, Radiat. Res. 45 (1971) 261.

[13] J.A. LaVerne, Radiat. Phys. Chem. 34 (1989) 135.

[14] C. Ferradini, J.-P. Jay-Gerin, Radiat. Phys. Chem. 51 (1998) 263.

[15] B. Pastina, J.A. LaVerne, J. Phys. Chem. A 103 (1999) 1592.

[16] H.E. Sims, Ph.D. Thesis, University of Salford, Salford, U.K., 1978.

[17] V. Wasselin-Trupin, G. Baldacchino, S. Bouffard, B. Hickel, Radiat. Phys. Chem. 65 (2002) 53.

[18] V. Cobut, Y. Frongillo, J.P. Patau, T. Goulet, M.-J. Fraser, J.-P. Jay-Gerin, Radiat. Phys. Chem. 51 (1998) 229.

[19] Y. Frongillo, T. Goulet, M.-J. Fraser, V. Cobut, J.P. Patau, J.-P. Jay-Gerin, Radiat. Phys. Chem. 51 (1998) 245.

[20] M.-A. Hervé du Penhoat, T. Goulet, Y. Frongillo, M.-J. Fraser, Ph. Bernat, J.-P. Jay-Gerin, J. Phys. Chem. A 104 (2000) 11757.

[21] M. Michaud, A. Wen, L. Sanche, Radiat. Res. 159 (2003) 3.

[22] T. Goulet, J.-P. Jay-Gerin, Y. Frongillo, V. Cobut, M.-J. Fraser, J. Chim. Phys. 93 (1996) 111.

[23] D.M. Bartels, A.R. Cook, M. Mudaliar, C.D. Jonah, J. Phys. Chem. A 104 (2000) 1686.

[24] Y. Muroya, M. Lin, G. Wu, H. Iijima, K. Yoshii, T. Ueda, H. Kudo, Y. Katsumura, J. Meesungnoen, S. Mankhetkorn, A. Filali-Mouhim, T. Goulet, J.-P. Jay-Gerin, in: M. Tsuji (Ed.), Proceedings of the 45th Annual Meeting on Radiation Chemistry, Japan Society of Radiation Chemistry, Tokyo, 2002, p. 191.

[25] Y. Muroya, J. Meesungnoen, J.-P. Jay-Gerin, A. Filali-Mouhim, T. Goulet, Y. Katsumura, S. Mankhetkorn, Can. J. Chem. 80 (2002) 1367.

[26] J.C. Severs, F.M. Harris, S.R. Andrews, D.E. Parry, Chem. Phys. 175 (1993) 467.

[27] C. Champion, Nucl. Instr. Methods Phys. Res. B 205 (2003) 671.

[28] M.E. Rudd, Radiat. Prot. Dosim. 31 (1990) 17.

[29] M. Gardès-Albert, D. Jore, Z. Abedinzadeh, A. Rouscilles, S. Deycard, S. Bouffard, J. Chim. Phys. 93 (1996) 103.

[30] G.H. Olivera, C. Caraby, P. Jardin, A. Cassimi, L. Adoui, B. Gervais, Phys. Med. Biol. 43 (1998) 2347.

[31] S.M. Pimblott, M.J. Pilling, N.J.B. Green, Radiat. Phys. Chem. 37 (1991) 377.

[32] G. Baldacchino, S. Bouffard, E. Balanzat, M. Gardès-Albert, Z. Abedinzadeh, D. Jore, S. Deycard, B. Hickel, Nucl. Instr. Methods Phys. Res. B 146 (1998) 528.

[33] A.R. Anderson, E.J. Hart, Radiat. Res. 14 (1961) 689.

[34] A.J. Elliot, M.P. Chenier, D.C. Ouellette, V.T. Koslowsky, J. Phys. Chem. 100 (1996) 9014.

[35] J. Meesungnoen, J.-P. Jay-Gerin, A. Filali-Mouhim, S. Mankhetkorn, Can. J. Chem. 80 (2002) 68.

III. Article No. 2

To gain further insight into the effects of multiple ionization on the production of $HO_2^{\bullet}/O_2^{\bullet-}$ and H_2O_2 in the heavy-ion radiolysis of pure, deaerated liquid water at high LET, we extend here our study presented in Chapter II to several other types of irradiating ions ($^1H^+$, $^4He^{2+}$, $^{12}C^{6+}$, and $^{20}Ne^{9+}$) and to a wider range of LET up to ~900 keV/μm, at 25 °C. The yields of formation of the various radiolytic species (e_{aq}^-, $^{\bullet}OH$, $H^{\bullet}$, H_2, $HO_2^{\bullet}/O_2^{\bullet-}$, and H_2O_2), including molecular oxygen, are calculated as a function of LET with and without taking into account the mechanism of multiple ionization of water in our Monte Carlo simulations.

The complete work is reported in the following article, entitled: "**High-LET radiolysis of liquid water with $^1H^+$, $^4He^{2+}$, $^{12}C^{6+}$, and $^{20}Ne^{9+}$ ions: Effects of multiple ionization**", by J. Meesungnoen and J.-P. Jay-Gerin.

This article is published in *The Journal of Physical Chemistry A*, Vol. **109**, Issue 29, Pages 6406–6419 (July 28, 2005).

High-LET radiolysis of liquid water with $^{1}H^{+}$, $^{4}He^{2+}$, $^{12}C^{6+}$, and $^{20}Ne^{9+}$ ions: Effects of multiple ionization

by

Jintana Meesungnoen and Jean-Paul Jay-Gerin*

Département de Médecine Nucléaire et de Radiobiologie, Faculté de Médecine et des Sciences de la Santé, Université de Sherbrooke, 3001, 12e Avenue Nord, Sherbrooke (Québec) J1H 5N4, Canada

Number of Figures: 10

Number of Tables: 5

Number of References and Notes: 114

**Corresponding author*:

Prof. Jean-Paul Jay-Gerin
Département de médecine nucléaire et de radiobiologie
Faculté de médecine et des sciences de la santé
Université de Sherbrooke
3001, 12e Avenue Nord
Sherbrooke (Québec) J1H 5N4
Canada

Tel. (1-819) 346-1110, ext.
Fax: (1-819) 564-5442
E-mail address:

The Journal of Physical Chemistry A **109**, 6404-6419 (2005)

Abstract

Monte Carlo simulations are used to investigate the effects of multiple ionization of water molecules on the yields of formation of free radical and molecular species, including molecular oxygen, in the radiolysis of pure, deaerated liquid water by using different types of radiation ($^{1}H^{+}$, $^{4}He^{2+}$, $^{12}C^{6+}$, and $^{20}Ne^{9+}$ ions) up to ~900 keV/μm, at neutral pH and 25 °C. Taking into account the double, triple, and quadruple ionizations of water, the primary (or "escape") yields (at 10^{-6} s) of the various radiolytic species ($G_{e^-_{aq}}$, $G_{H^\bullet}$, G_{H_2}, $G_{^\bullet OH}$, $G_{HO_2^\bullet/O_2^{\bullet-}}$, $G_{H_2O_2}$, and G_{O_2}) are calculated as a function of the linear energy transfer (LET) of the radiation. Our results quantitatively reproduce the large increase observed in $G_{HO_2^\bullet/O_2^{\bullet-}}$ at high LET. Under the conditions of this study, the mechanisms of triple and quadruple ionizations contribute only weakly to the production of $HO_2^\bullet/O_2^{\bullet-}$. With the exception of protons, our calculations also simultaneously predict a maximum in $G_{H_2O_2}$ corresponding to the LET of ~4.5-MeV $^{4}He^{2+}$ ions (~100 keV/μm) and ~110-MeV $^{12}C^{6+}$ ions (~180 keV/μm). This maximum occurs where $G_{HO_2^\bullet/O_2^{\bullet-}}$ begins to rise sharply, suggesting, in agreement with previous experimental data, that the yields of $HO_2^\bullet/O_2^{\bullet-}$ and H_2O_2 are closely linked. Moreover, our results show a steep increase in the initial and primary yields of O_2 with increasing LET, giving support to the "oxygen in heavy-ion tracks" hypothesis. By contrast, it is found that, in the whole LET range considered, the incorporation of multiple ionization in the simulations has only little effect on the variation of our computed $G_{e^-_{aq}}$, $G_{H^\bullet}$, G_{H_2}, and $G_{^\bullet OH}$ values as a function of LET. As expected, $G_{e^-_{aq}}$ and $G_{^\bullet OH}$ decrease continuously with increasing LET. $G_{H^\bullet}$ at first increases and then decreases at high LET. Finally, G_{H_2} monotonically rises with increasing LET. Our calculated yield values compare generally very well with experiment.

Keywords: Liquid water, radiolysis, accelerated protons and heavy ions, linear energy transfer, multiple ionization, ionization cross-sections, radiolytic yields, hydroperoxyl/superoxide anion radicals, hydrogen peroxide, molecular oxygen, Monte Carlo track structure simulations.

1. Introduction

The radiolysis of pure, deaerated liquid water by low-LET (linear energy transfer, or energy loss per unit track length, -dE/dx) radiation such as ^{60}Co γ-rays, hard X-rays, fast electrons, or high-energy protons, at room temperature, is generally well understood. Briefly, it leads to the formation of the free radicals and molecular products e^-_{aq}, H$^\bullet$, $^\bullet$OH, H_2, H_2O_2, H^+, OH^-, etc.[1-3] Under ordinary irradiation conditions, these species are generated nonhomogeneously on subpicosecond time scales in small, widely separated regions of dense ionization and excitation events, commonly referred to as "spurs",[4] along the track of the ionizing radiation.[5] Owing to diffusion from their initial positions, the radiolytic products then either react within the spurs as they expand or escape into the bulk solution. The so-called "primary" radical and molecular yields (or "escape" yields) $G_{e^-_{aq}}$, $G_{H^\bullet}$, $G_{^\bullet OH}$, G_{H_2}, and $G_{H_2O_2}$ represent the numbers of species of each kind formed or destroyed per 100 eV of deposited energy that remain after spur expansion.[6] At room temperature, this spur expansion is essentially complete on the time scale of ~10^{-6} s after the initial energy deposition. At this time, the species that have escaped from spur reactions become homogeneously distributed throughout the bulk of the solution (or background) and the track of the radiation no longer exists. The radical and molecular products, considered as additions to the background, are then available for reaction with added solutes (treated as spatially homogeneous) at moderate concentrations.

With increasing LET, the nearly spherical spurs are formed increasingly closer together and eventually overlap to form dense continuous columns of species consisting initially of a cylindrical track "core" surrounded by a region of radiation effects due to the ejected secondary electrons, commonly referred to as the "penumbra".[7-11] As the interspur distance decreases, more radicals are formed in close proximity with a correspondingly increased probability of reacting with one another to produce the molecular products or to reform water. Under these conditions, the radical yields are expected to diminish as the LET is increased, whereas the molecular yields increase and the net

water decomposition yield decreases.[10,12] There are two important exceptions to this rule: (i) the primary yield of hydroperoxyl/superoxide anion ($HO_2^{\bullet}/O_2^{\bullet-}$, pK_a = 4.8) radicals increases with increasing LET, a behavior that is akin to the molecular yields,[13-22] and (ii) the primary yield of hydrogen peroxide (H_2O_2) rises with increasing LET to a maximum, after which it falls.[18,23]

We have recently carried out Monte Carlo track structure simulations to investigate the effects of multiple ionization of water molecules on the formation of $HO_2^{\bullet}/O_2^{\bullet-}$ and H_2O_2 in the radiolysis of liquid water with high-LET $^{12}C^{6+}$ ions up to ~430 keV/μm, at ambient temperature.[24] This innovative study was motivated by the hypothesis that multiple ionization could be responsible for the large $HO_2^{\bullet}/O_2^{\bullet-}$ yield produced in irradiated water under high-LET heavy-ion impact.[25] Indeed, incorporating the mechanisms of double and triple ionization in single ion–water collisions allowed us to quantitatively reproduce the large increase observed in $G_{HO_2^{\bullet}/O_2^{\bullet-}}$ as the LET increases above 100-200 keV/μm. The same calculations could also simultaneously predict a maximum in the variation of $G_{H_2O_2}$ with LET at ~180-200 keV/μm, in remarkable agreement with experiment. These results strongly support the importance of the role of multiple ionization in the radiolysis of water under high-LET irradiation conditions. They also suggest that multiple ionization, although infrequent relative to single ionization events, is very efficient chemically.[26]

Unfortunately, the available information on the cross-sections (probabilities) for the double (σ_{di}) and triple (σ_{ti}) ionizations of water is still quite limited.[10,27] However, using the recent *n*-fold ionization cross-section values reported by Champion[27] for the case of carbon ions in the energy range ~4.2-12 MeV/nucleon (~430-170 keV/μm) and gaseous water allowed us to obtain the good order of magnitude for both $G_{HO_2^{\bullet}/O_2^{\bullet-}}$ and $G_{H_2O_2}$, but the variation of these yields with LET was not correctly reproduced.[24] To overcome these difficulties and estimate in particular the values of the heavy ion–water cross-sections in the *liquid* phase, we used[24] an original approach that consisted of treating the ratio of double-to-single ionization cross-sections ($\alpha = \sigma_{di}/\sigma_{si}$, where σ_{si}

is known) in our simulations as an adjustable parameter chosen to reproduce the available experimental data of ($G_{HO_2^\bullet} + G_{O_2}$) as a function of LET in the $^{12}C^{6+}$ radiolysis of deaerated ferrous sulfate-cupric sulfate aqueous solutions under *acidic* conditions.[19,20] As for the triple ionization, σ_{ti} was assumed to be an order of magnitude less than σ_{di}.[10,27] Using the values of the double and triple ionization cross-sections so obtained in our simulation code of the radiolysis of *neutral* water, both the magnitude of the experimental primary $HO_2^\bullet/O_2^{\bullet-}$ and H_2O_2 yields and their variation with LET could then be reproduced very well by our simulations.[24]

To allow a more rigorous test of our previous findings and to gain further insights into the effects of multiple ionization on the production of $HO_2^\bullet/O_2^{\bullet-}$ and H_2O_2 in the heavy-ion radiolysis of water at high LET, it is important to extend our previous study to other types of irradiating particles and to a wider range of LET. In the present work, we perform Monte Carlo track structure simulations that incorporate double, triple, and quadruple ionizations of water molecules to calculate the yields of formation of the various radiolytic species, including molecular oxygen, in the radiolysis of pure, deaerated liquid water by several different types of radiation ($^1H^+$, $^4He^{2+}$, $^{12}C^{6+}$, and $^{20}Ne^{9+}$ ions) at high LET up to ~900 keV/μm. This paper deals only with results at 25 °C. The main features of our simulation approach are presented in the next section, followed by the results and their discussion. Conclusions are drawn in the final section.

2. Monte Carlo simulations

The radiolysis of liquid water has been modeled by using an updated and extended version of our originally developed Monte Carlo simulation codes TRACPRO, TRACELE, and TRACIRT.[24,28-32] In this new version, which we have renamed IONLYS-IRT, significant changes in certain parameters have been made, mainly in the description of the early physical and physicochemical stages of the code. In particular, our code now employs the newly reported elastic, phonon, and vibra-

tional electron scattering cross-sections of Michaud et al.,[33] obtained from ~1-100 eV electron-impact experiments on amorphous ice films, and increased here by a factor of about 2 to account for differences between solid- and liquid-phase cross-sections.[28,34] We have also modified certain adjustable parameters that enter our code in order to reconcile the results of our simulations with (i) the recently reevaluated "initial" e^-_{aq} yield data (4.0 ± 0.2 molec./100 eV at "time zero"[35] and 4.1 ± 0.2 molec./100 eV at 20 ps,[36] as compared to the hitherto accepted value of 4.8 molec./100 eV at 100 ps[37]);[32] (ii) the newly measured e^-_{aq} decay kinetic profile in the time range from 100 ps to 10 ns;[35] and (iii) the newly determined yield of "nonscavengeable" molecular hydrogen produced on a subpicosecond time scale (0.34 molec./100 eV or ~75% of the total H_2 formed,[38] instead of the previously accepted limiting yield of 0.15 molec./100 eV[39,40]). These parameters comprise (i) the thermalization distance of subexcitation electrons (e^-_{sub}),[41] (ii) the recombination cross section of the electrons with their water parent cations prior to thermalization,[42] (iii) the branching ratios used for the different competing mechanisms in the decay of "directly" excited electronic states ($\tilde{A}^1B_1$ and $\tilde{B}^1A_1$) of water molecules and of vibrationally excited water molecules ($H_2O^*_{vib}$) formed by electron-cation geminate recombination, and (iv) the dissociative capture of electrons by water molecules.[28] The values of these parameters have been obtained here by using a global-fit procedure, which consists of *simultaneously* fitting our computed time-dependent yields of e^-_{aq} and of the other radiolytic species ($H^\bullet$, H_2, $^\bullet OH$, and H_2O_2) to experiment.[32] Using this procedure, the average electron thermalization distance calculated from our simulations is ~11.7 nm (with the corresponding average electron thermalization time of ~56 fs), a value that is somewhat larger than the typical range (or "spur" radius) of ~6.4-8.3 nm commonly used to describe the chemical evolution of the hydrated electrons in current deterministic "average" models of "spur" chemistry for low-LET radiation.[10,43-45] As for the geminate electron-cation recombination probability, 25.5% of the subexcitation electrons are found to initially recombine with their water parent cations (on the average, this recombination occurs in the

first steps of the e^-_{sub} random walk, that is, in times as short as a few femtoseconds)[42] to form $H_2O^*_{vib}$. This latter value is consistent with the prompt electron-cation recombination (≥15%) in water radiolysis reported recently by Bartels et al.[46] The revised values of the branching ratios used for the different dissociative decay channels of $H_2O^*_{vib}$ are shown in Table 1A. We should note here that the various decay channels of directly excited electronic states of water molecules have little effect in the yield calculations. Nevertheless, those branching ratios have been slightly modified with respect to those previously published[28] (see Table 1B). Finally, the maximum value of the dissociative electron attachment cross section has been adjusted to ~4.5×10^{-18} cm^2 at ~8.6 eV in order to reproduce the prompt "nonscavengeable" yield of H_2 observed experimentally.[28,47] This value compares well with that determined recently in amorphous ice (2.7×10^{-18} cm^2)[33] and with the corresponding gas-phase value (6.7×10^{-18} cm^2).[48]

During the physical stage, the energy deposition by the incident charged particle and by all the secondary electrons that it has generated occurs through the slowing down of those particles via a variety of elastic and inelastic scattering processes, including ionization, electronic and vibrational excitation of single water molecules, and excitation of plasmon-type collective modes. The details of our track structure simulation modeling and the scattering cross-sections used are described in our earlier publications.[24,28-32] To take into account the effects of multiple ionization under high-LET heavy-ion impact, the model has been extended to incorporate double, triple, and quadruple ionization processes in single ion–water collisions.[24,25] Ionizations of higher multiplicity are neglected as their occurrence is much less probable in the range of LET of interest here. In the simulations, a value of 40 eV is accepted for the total energy needed to eject two electrons from a water molecule (double-ionization energy) as taken from gas-phase studies,[49] whereas the values for the triple- and quadruple-ionization energies (chosen equal to 65 and 88 eV, respectively) are assumed to be near the energies needed for the triple and quadruple ionizations of oxygen.[50] Unfortunately,

little is known yet about the values of the cross sections for the double (σ_{di}), triple (σ_{ti}), and quadruple (σ_{qi}) ionizations of water.[10,27] In this study, σ_{di} is deduced from the knowledge of the ratio $\alpha = \sigma_{di}/\sigma_{si}$ and Rudd's semi-empirical single ionization cross sections (σ_{si}) for proton impact on water vapor[51] (adapted here to the liquid phase as previously described[28] and extended to collisions by any other ion projectile of the same velocity according to a Z^2 scaling law, where Z is the charge state of the ion[52]). Following the approach used previously,[24] we have treated α in our simulations as an adjustable parameter chosen to get the best fit of the experimental values of ($G_{HO_2^\bullet} + G_{O_2}$) as a function of LET in the radiolysis of air-free aqueous $FeSO_4$ (1 m*M*)–$CuSO_4$ (10 m*M*) solutions with $^1H^+$, $^4He^{2+}$, $^{12}C^{6+}$, and $^{20}Ne^{9+}$ ions under acidic (0.005 *M* H_2SO_4) conditions.[19,20,53,54] As shown in our previous paper,[24] this approach offers an original tool to estimate the ratio σ_{di}/σ_{si} for heavy ion–water collisions in the *liquid* phase. As for the triple and quadruple ionizations, we assume that, for the range of impacting ion energies considered in this work, $\sigma_{ti} = \alpha^2\,\sigma_{si}$ and $\sigma_{qi} = \alpha^3\,\sigma_{si}$, where $\alpha < 0.5$.[27] We have also multiplied the total cross-sections for all interaction processes induced by ions by an energy-dependent factor that constrains the LET of the irradiating ions to conform with the recommended values of Watt.[55] Finally, at the incident ion energies of interest here, interactions involving electron capture and loss by the moving ion (charge-changing collisions) have been neglected.[56]

The energy that has been so deposited in the medium is then used to produce the "initial" radical and molecular species of the radiolysis, distributed in a specific, highly nonhomogeneous track structure which depends on the primary ion type and energy. The physicochemical stage consists of the processes that lead to the establishment of thermal equilibrium in the system. Its duration is of the order of 10^{-12} s for aqueous solutions. Among those processes, the production of $HO_2^\bullet/O_2^{\bullet-}$ via the double ionization of water is assumed to involve oxygen atoms[19,57-59] formed in their ^3P ground state,[25] according to

$$H_2O^{2+} + 2\,H_2O \rightarrow 2\,H_3O^+ + O(^3P) \qquad \text{(R1)}$$

at very short times, followed by

$$^{\bullet}OH + O(^3P) \rightarrow HO_2^{\bullet} . \quad (R2)$$

It should be recalled here that the O atoms produced in their singlet ^1D state react rapidly with water.[60,61] In contrast, the ground-state $O(^3P)$ atoms are rather inert to water[60,62] and will then react efficiently with $^{\bullet}OH$ radicals in the heavy particle track core because of the very high local concentration of radicals.[25] For the triple and quadruple ionizations of water molecules, we assume that they directly lead to the formation of $HO_2^{\bullet}/O_2^{\bullet-}$ and molecular oxygen by acid-base re-equilibrations, respectively, according to the following overall reactions:[25]

$$H_2O^{\bullet 3+} + 4\,H_2O \rightarrow 3\,H_3O^+ + HO_2^{\bullet} \quad (R3)$$

and

$$H_2O^{4+} + 5\,H_2O \rightarrow 4\,H_3O^+ + O_2 . \quad (R4)$$

The H_3O^+ ions formed in reactions (R1), (R3), and (R4) are positioned at 0.3 nm from their respective co-products $O(^3P)$, $HO_2^{\bullet}$, and O_2, which are held in place. This is the same separation as that used between H_3O^+ and the $^{\bullet}OH$ radical in our simulation of events following the dissociation of $H_2O^{\bullet+}$.[28] In addition, the emission angles for the secondary electrons ejected from the target by the impacting ion are separated by 180°, 120°, and 90° when dealing with double, triple, and quadruple ionization, respectively, and the total incident energy deposited at each point of interaction (after subtraction of the required ionization energy of the water molecule) is equally distributed between the ejected electrons.

All of the events of the physical and physicochemical stages are handled by our revised step-by-step simulation program IONLYS (which replaces TRACPRO and TRACELE)[24,28-32] extended here to incorporate multiple ionization of water molecules as described above. The complex spatial distribution of reactants at $\sim 10^{-13}$ s, which is provided as an output of this program, is then used directly as the starting point for the

subsequent nonhomogeneous chemical stage. This third and final stage, during which the various radiolytic species diffuse and react with one another (or with the environment) until all spur or track reactions are complete (~10^{-6} s), is covered by our IRT program.[24,28-32] This program employs the independent reaction times (IRT) method[63] to model the chemical development that occurs during this stage and to simulate the formation of measurable product yields. Its implementation has been described in detail,[29] and its validity has been established through a comparison with a full step-by-step Monte Carlo simulation.[64]

The reaction scheme and reaction parameters, as well as the diffusion coefficients of reactive species used in our IRT program for pure liquid water, are given in Tables 1 and 2 of ref 29. Only slight adjustments were made in some reaction rate constants and diffusion coefficients to take account of the latest data available from the literature. To simulate the radiolysis of the Fe^{2+}/Cu^{2+} system in deaerated 0.005 *M* H_2SO_4 aqueous solutions (pH ≈ 2.1), we have supplemented the pure-water reaction scheme to include the 31 reactions listed in Table 2. In addition, we have introduced the effects due to the ionic strength of the solutions[78] for the two reactions[31]

$$H^+ + e^-_{aq} \rightarrow H^\bullet$$

and

$$H^+ + OH^- \rightarrow H_2O\,,$$

as well as for all reactions between ions given in Table 2. The rate constants for those various reactions, corrected for these ionic-strength effects, have been used in the present study.[79]

Finally, the influence of the LET on the yields of the various radiation-induced species in neutral water at ambient temperature has been investigated by varying the incident ion energy from ~300 to 0.15 MeV (~0.3-70 keV/μm) for $^1H^+$, ~300 to 0.3 MeV/nucleon (~1.25-213 keV/μm) for $^4He^{2+}$, ~300 to 1.25 MeV/nucleon (~12-604 keV/μm) for $^{12}C^{6+}$, and ~300 to 3.2 MeV/nucleon (~25-938 keV/μm) for $^{20}Ne^{9+}$. The

calculations are performed by simulating short (~1.5-100 μm) ion track segments, over which the energy and LET of the ion are well defined and remain nearly constant. Typically, ~5×10^3 to 4×10^5 reactive chemical species are generated in those simulated track segments (depending on the irradiating-ion type and energy), thus ensuring only small statistical fluctuations in the determination of average yields.

3. Results and discussion

As described above, the ratio of double-to-single ionization cross sections $\alpha = \sigma_{di}/\sigma_{si}$ is treated as an adjustable parameter and obtained from our simulations by fitting the available data[19,20] of ($G_{HO_2\cdot} + G_{O_2}$) in the $^1H^+$, $^4He^{2+}$, $^{12}C^{6+}$, and $^{20}Ne^{9+}$ radiolysis of deaerated aqueous $FeSO_4$–$CuSO_4$ solutions under acidic conditions over the range of ion energies studied experimentally. The values of α so obtained are shown in Figure 1 for the four ion types used as a function of the ion energy per nucleon divided by the projectile charge state (E_{ion}/Z). The corresponding σ_{di}/σ_{si} values reported by Champion[27] for various ions and *gaseous* targets, extrapolated to the case of any heavy ion and to water molecules, are also included in Figure 1 for the sake of comparison. It is seen that, in contrast to Champion's values,[27] our values of α do not follow a unique law, independent of the projectile ion. In fact, the present data show that the ratio σ_{di}/σ_{si} depends on the type of the impacting ion and, for a given value of E_{ion}/Z, increases from protons ($Z = 1$) to neon ions ($Z = 9$). Moreover, even if our σ_{di}/σ_{si} values bear some qualitative resemblance in trends with those of Champion,[27] they generally differ appreciably in absolute value from the latter, except for $^{12}C^{6+}$ ions around 2.5–5 MeV/nucleon (~440–280 keV/μm) where the two sets of values are quite comparable. The source of these differences in the σ_{di}/σ_{si} values is not obvious, although they are undoubtedly a manifestation of a subtle interplay during the collision between the ion-target interaction and the effects of electron-electron correlations.[51,80] This is an area where very little is known and where more experimental and theoretical work is required. In this respect, the σ_{di}/σ_{si} values reported here could

provide a useful test for theories calculating many-electron emission cross sections in single ionizing collisions.

Using these values of σ_{di}/σ_{si} in our simulation code of the radiolysis of pure, deaerated, *neutral* water with $^{1}H^{+}$, $^{4}He^{2+}$, $^{12}C^{6+}$, and $^{20}Ne^{9+}$ ions, we have then calculated $G_{HO_2^{\bullet}/O_2^{\bullet-}}$ and $G_{H_2O_2}$ (at 10^{-6} s) as a function of LET up to ~900 keV/μm, at 25 °C. The results are shown in Figures 2 and 3, respectively, along with experimentally determined yields from the literature.[15,21,23,81-84] As can be seen in Figure 2, our curves of $G_{HO_2^{\bullet}/O_2^{\bullet-}}$ versus LET calculated without including the mechanism of multiple ionization of water cannot account quantitatively for the totality of the measured $HO_2^{\bullet}/O_2^{\bullet-}$ yield[21,81] at high LET. However, when the double, triple, and quadruple ionizations are incorporated in the simulations for the four irradiating ions studied, the magnitude of the $HO_2^{\bullet}/O_2^{\bullet-}$ escape yields so obtained compares well with experiment. Figure 2 also shows that, for different incident ions of equal LET but different velocities, $G_{HO_2^{\bullet}/O_2^{\bullet-}}$ decreases as the ion velocity increases.[85] This irradiating-ion dependence of the yields at a given LET indicates, as it has been frequently noted,[2,10-12,56,86-90] that LET is not a unique parameter to correctly describe the radiation chemical effects within heavy ion tracks. This is explained by the greater mean energy of ejected electrons (the so-called low-LET "short" and "branch" tracks in the terminology of Mozumder and Magee,[9,91] or "δ-rays") from the higher velocity ion, which will travel to a greater average distance away from the track core, and so lead to a greater dispersion of the initial radical positions around the track. In other words, the actual mean initial volume density of free radicals formed in the track will be lower. Under these conditions, a greater fraction of those radicals will be allowed to escape recombination as they subsequently diffuse with consequent tendency for increase in the radical yields measured after track expansion, along with decreased molecular product yields. However, the decrease observed in our simulated $G_{HO_2^{\bullet}/O_2^{\bullet-}}$ values with increasing ion velocity at the same LET (the production of $HO_2^{\bullet}/O_2^{\bullet-}$ is lower for the heavier ions) supports our assumption made in reaction (R2) that $HO_2^{\bullet}$ is formed by radical combination processes within the

track,[92] in quite the same fashion as the general formation of molecular species.[10,11] LaVerne and co-workers[19] also concluded that the yield of ($HO_2^{\bullet}$ + O_2) is significant only at high LET and that it is produced mainly in the heavy-particle track core at high radical concentration. It is finally worth noting that independent simulations incorporating the sole mechanism of double ionization of water molecules have shown that triply and quadruply charged water ions make in fact only a minor contribution to $G_{HO_2^{\bullet}/O_2^{\bullet-}}$ and $G_{H_2O_2}$ (~15% and 2% for ~555-keV/μm $^{12}C^{6+}$ ions, respectively) under the conditions $\sigma_{ti} = \alpha^2 \sigma_{si}$ and $\sigma_{qi} = \alpha^3 \sigma_{si}$ ($\alpha < 0.5$) adopted in this study (data not shown).

Quite similarly, Figure 3 shows that our values of $G_{H_2O_2}$ calculated without multiple ionization of water continuously increase with increasing LET. However, when the double, triple, and quadruple ionizations are incorporated in the simulations, the curves of $G_{H_2O_2}$ versus LET first rise, then bend downward ($^1H^+$) and, at higher LET, reach a maximum ($^4He^{2+}$ and $^{12}C^{6+}$) after which they fall. This maximum is relatively shallow for $^4He^{2+}$ ions but more pronounced for $^{12}C^{6+}$ ions. Its position also slightly shifts to higher LET as the ion charge increases, going from ~100 keV/μm for ~4.5-MeV $^4He^{2+}$ ions to ~180 keV/μm for ~110-MeV $^{12}C^{6+}$ ions. For $^{20}Ne^{9+}$ ions, it is apparent from Figure 3 that a maximum should also exist, perhaps near ~200 keV/μm, even if we could not have a better definition of our curve of $G_{H_2O_2}$ below ~700 keV/μm due to a lack of experimental data of ($G_{HO_2^{\bullet}}$ + G_{O_2}) in the radiolysis of the Fe^{2+}/Cu^{2+} system with high-energy $^{20}Ne^{9+}$ ions under acidic conditions.[19,20] These results are in good agreement with experiment, especially with the recent measurements of Pastina and LaVerne[23] for $^4He^{2+}$ and $^{12}C^{6+}$ ions and of Wasselin-Trupin et al.[82] for $^{12}C^{6+}$ ions. Moreover, if we consider the curve of $G_{H_2O_2}$ as a function of LET that includes the ensemble of our four calculated $G_{H_2O_2}$(LET) curves for the different ions studied, we can estimate an overall maximum around 100-200 keV/μm, which is in remarkable agreement with the early observations of Bibler[16] and of Burns and Sims.[18] As observed with $HO_2^{\bullet}/O_2^{\bullet-}$, the H_2O_2 yields are also both LET and irradiat-

ing-ion dependent. For different impacting ions of equal LET but different velocities, Figure 3 shows that $G_{H_2O_2}$ decreases as the ion velocity increases,[85] from protons to neon ions. As discussed above, this result conforms well to the general model of formation of molecular species. Finally, Figures 2 and 3 also indicate that, for each ion investigated, the maximum in the value of $G_{H_2O_2}$ occurs precisely where $G_{HO_2^{\bullet}/O_2^{\bullet-}}$ begins to rise sharply. This is in excellent accord with experiment and clearly shows that the yields of $HO_2^{\bullet}/O_2^{\bullet-}$ and H_2O_2 are closely linked.[18,24] In fact, hydrogen peroxide is formed within the tracks mainly by the combination reaction of two $^{\bullet}OH$ radicals produced in the decomposition of water:

$$^{\bullet}OH + {}^{\bullet}OH \rightarrow H_2O_2 . \qquad \text{(R5)}$$

As $^{\bullet}OH$ reacts with $O(^3P)$ by reaction (R2), this reaction competes with reaction (R5) causing a decrease in the observed H_2O_2 yield at high LET. This very good agreement between theory and experiment supports *a posteriori* our assumption[25] made in reaction (R1) that, for the high-LET range considered here, O atoms are primarily produced in their ^3P ground state (rather than in their singlet ^1D state).

To gain further insights into the effects of multiple ionization of water on $G_{HO_2^{\bullet}/O_2^{\bullet-}}$ and $G_{H_2O_2}$ in the high-LET heavy-ion water radiolysis, it is of interest to examine the unfolding of the various reactions that contribute to the formation or decay of $HO_2^{\bullet}/O_2^{\bullet-}$ and H_2O_2 in the ion tracks as they expand by diffusion. This can readily be done with our Monte Carlo simulations, which enable us to determine quantitatively the time dependence of each reaction. The main reactions that are involved in the primary yields of $HO_2^{\bullet}/O_2^{\bullet-}$ and H_2O_2 in the case of pure, deaerated liquid water irradiated by 24-MeV $^{12}C^{6+}$ ions (~500 keV/μm) at 25 °C are listed in Tables 3 and 4, respectively. The importance of these reactions can be quantified by the yield variations $\Delta G(HO_2^{\bullet}/O_2^{\bullet-})$ and $\Delta G(H_2O_2)$ that they cause over the time interval of nonhomogeneous track chemistry (~10^{-12}-10^{-6} s). Figures 4 and 5 compare, with and without multiple ionization of water, the time profiles of $\Delta G(HO_2^{\bullet}/O_2^{\bullet-})$ and $\Delta G(H_2O_2)$ of each

of these reactions, respectively. As we can see in Figure 4, when the double, triple, and quadruple ionizations of water molecules are included in the simulations, $HO_2^{\bullet}/O_2^{\bullet-}$ is formed mainly by reactions (R2), (R10), (R11), and (R15), whereas its decay is dominated by reactions (R6), (R8), (R12), and (R14). The large increase in the fractions of $HO_2^{\bullet}/O_2^{\bullet-}$ formed by reactions (R2), (R10), and especially (R11) compared to their corresponding values in the absence of multiple ionization, is a reflection of the large increase in the yields of $O(^3P)$ and O_2 at high LET (see below). As regards to H_2O_2, Figure 5 clearly demonstrates that H_2O_2 is formed within the tracks almost entirely by the reaction (R5) of the $^{\bullet}OH$ radical with itself, with or without multiple ionization of water. However, our simulation results show that, upon incorporation of the multiple-ionization mechanism, the formation of H_2O_2 due to reaction (R5) decreases. As noted above, this is explained by the fact that, in ~500-keV/μm $^{12}C^{6+}$ tracks, reactions (R2), (R6), and (R7) compete with reaction (R5) causing a decrease in the observed H_2O_2 yield (see Figure 3). Another reason for such a decrease in $G_{H_2O_2}$ arises from the decrease in the initial yield of $^{\bullet}OH$ (at 10^{-13} s) due to the occurrence of reactions (R1), (R3), and (R4) – which do not produce $^{\bullet}OH$ radicals – at the expense of the proton-transfer reaction $H_2O^{\bullet+} + H_2O \rightarrow H_3O^+ + {}^{\bullet}OH$ which occurs following the formation of singly ionized water molecules. The contributions of the reactions (R17) and (R19) to the removal of H_2O_2 also decrease with including the multiple ionization of water as a result of the decrease in the H_2O_2 yield. As for the fractions of hydrogen peroxide formed by reactions (R12) and (R18), they are very small at the LET of ~500 keV/μm considered here and show only little increases when multiple ionizations of water molecules are incorporated in the simulations, due to the increase in $HO_2^{\bullet}/O_2^{\bullet-}$ yields (see Figure 2). The net effects of multiple ionization of water on $G_{HO_2^{\bullet}/O_2^{\bullet-}}$ and $G_{H_2O_2}$ with increasing LET are shown in Figures 2 and 3, respectively.

The variations of $G_{e_{aq}^-}$ and $G_{^{\bullet}OH}$ (obtained at 10^{-6} s) as a function of LET for pure, deaerated liquid water irradiated by $^1H^+$, $^4He^{2+}$, $^{12}C^{6+}$, and $^{20}Ne^{9+}$ ions up to ~900 keV/μm, at 25 °C, are shown in parts (a) and (b) of Figure 6, respectively. As can be

seen, the primary yields of the hydrated electron and the hydroxyl radical diminish steeply as the LET is increased, and for the highest LET studied, there is almost no e^-_{aq} and $^{\bullet}OH$ surviving at the microsecond time scale. Also, for incident ions of equal LET, $G_{e^-_{aq}}$ and $G_{^{\bullet}OH}$ increase as the ion velocity increases, from protons to neon ions. This is as expected.[85] Figure 6 also shows that, for the range of LET considered here, the incorporation of multiple ionization of water in our simulations has almost no effect on $G_{e^-_{aq}}$ and $G_{^{\bullet}OH}$. In fact, our calculated yield values are nearly identical to those obtained without multiple ionization of water. Over the whole LET range, the simulations for the four ions are in quite good agreement with available experimental data.[15,18,84,88,93,94]

The effect of LET on $G_{H^{\bullet}}$ and G_{H_2} (obtained at 10^{-6} s) for pure, deaerated liquid water irradiated by $^1H^+$, $^4He^{2+}$, $^{12}C^{6+}$, and $^{20}Ne^{9+}$ ions up to ~900 keV/μm, at 25 °C, is shown in parts (a) and (b) of Figure 7, respectively. As one can see from Figure 7a, our calculated primary $H^{\bullet}$ atom yield values present a slight maximum near 6.5 keV/μm before decreasing steeply at higher LET. The origin of this maximum was discussed in detail previously.[99] Below ~10 keV/μm, the behavior of $G_{H^{\bullet}}$ is essentially independent of radiation quality. This is to be expected since in this low-LET region (that is, at high radiation particle energies), the tracks of heavy ions can be viewed, as seen above, as a random succession of (on average) isolated, nearly spherical spurs, and the observed chemistry of such particles should therefore be much like that of fast protons.[10,12] Our simulated results also show that, as do the yields of e^-_{aq} and $^{\bullet}OH$ (see Figure 6), for incident ions of a given LET > 10 keV/μm, $G_{H^{\bullet}}$ increases with ion velocity, from protons to neon ions.[85] In the LET range studied, our calculated $G_{H^{\bullet}}$ values are in good agreement with the experimental data of Appleby and Schwarz[15] and of Bisby et al.,[95] but are slightly higher than the $G_{H^{\bullet}}$ value determined by Elliot et al.[83] at room temperature for irradiations with a 23-MeV $^2H^+$ beam. It should be noted, however, that the $H^{\bullet}$ atom yield reported by these latter authors is estimated from the difference between the measured values of (G_{H_2} + $G_{H^{\bullet}}$) and G_{H_2}, and therefore has a

rather large experimental uncertainty. As for our calculated primary H_2 yields, Figure 7b shows that they increase monotonically with increasing LET for the four impacting ions studied. For instance, in the case of deaerated liquid water irradiated by $^{12}C^{6+}$ ions, our computed G_{H_2} values are found to increase continuously from ~0.64 to 1.15 molec./100 eV on going from ~12 to 600 keV/μm. As can be seen, the available experimental data[15,18,96] are generally well reproduced by our calculated H_2 escape yields over the whole LET range covered here. However, extrapolation of our values to higher LET seems to be somewhat lower than the yield of ~2 molec./100 eV estimated for the decomposition of water by fission recoil fragments with an LET close to ~5000 keV/μm.[16,97,98] In view of the fact that the fission fragment data may have large uncertainties because of dosimetry,[11] further measurements of the H_2 yield using various ion types and ion energies over a wide range of LET values above ~100-200 keV/μm would be needed to clarify the results observed. Figure 7 also shows that, in the case of protons, the incorporation of the double, triple, and quadruple ionizations of water molecules in the simulations has no effect on the variations of $G_{H^\bullet}$ and G_{H_2} with LET. However, in the case of $^4He^{2+}$, $^{12}C^{6+}$, and $^{20}Ne^{9+}$ ions, we observe at high LET a slight gradual decrease of our $G_{H^\bullet}$ and G_{H_2} values calculated with multiple ionization of water in comparison with those obtained without including the multiple-ionization mechanism. This decrease of $G_{H^\bullet}$ and G_{H_2} at low ion energies is more pronounced for heavier ions in the order $^4He^{2+} < {}^{12}C^{6+} < {}^{20}Ne^{9+}$ and mainly results from the increase in the yields of $HO_2^\bullet/O_2^{\bullet-}$ and O_2 (see below) that occurs at high LET in the presence of the multiple ionization of water. In the case of H_2, for example, the main reactions that account for its formation in pure, deaerated liquid water irradiated with ~500-keV/μm $^{12}C^{6+}$ ions are, in order of decreasing importance (data not shown):

$$H^\bullet + e^-_{aq} \rightarrow H_2 + OH^- \qquad \text{(R20)}$$

$$e^-_{aq} + e^-_{aq} \rightarrow H_2 + 2\,OH^- \qquad \text{(R21)}$$

and

$$H^{\bullet} + H^{\bullet} \rightarrow H_2 . \qquad \text{(R22)}$$

As $H^{\bullet}$ reacts with O_2 and $HO_2^{\bullet}/O_2^{\bullet-}$ in the dense $^{12}C^{6+}$ ion tracks by reactions (R11)-(R13) (see Table 3 and Figures 4 and 5), these reactions normally compete with reactions (R20) and (R22) at early time and during track expansion thereby causing a decrease in the observed H_2 yield at high LET. For the example under consideration, the overall variation of G_{H_2} with and without incorporation of multiple ionization of water is $\Delta G(H_2) \approx -0.07$ molec./100 eV at 10^{-6} s (data not shown).

Oxygen is a powerful radiation sensitizer.[100] The biological response to irradiation is greater under oxygenated conditions than under hypoxic conditions. The ratio of hypoxic to aerated doses needed to achieve the *same* biological effect is known as the "oxygen enhancement ratio" (OER). The OER is generally recognized as a dose-modifying factor of fundamental importance in radiobiology as well as of practical importance in radiotherapy. For most cellular organisms, it is well established that the value of OER decreases progressively with increasing LET of the radiation.[101,102] The "oxygen-in-the-track" hypothesis, proposed many years ago to account for this effect,[103] presupposes that molecular oxygen is a product of the radiolysis of water at high LET. In fact, the radiolytic formation of O_2 in the tracks of highly charged particles is presumed to convert an initially "hypoxic" solution to a partially "oxygenated" microenvironment around the relevant cellular target molecules, which justifies the low OER values observed in the experiments.[17,102,104] This hypothesis of the generation of molecular oxygen in heavy-ion tracks has often been invoked for a variety of biological materials, but the conclusion is not clear yet.[105] On the viewpoint of pure radiation chemistry, the creation of O_2 along the tracks of highly charged particles has been proposed by several studies.[16,17,20,106-109] Those measurements all support the proposal that track oxygen is a product of the radiolysis of water at high LET. Most remarkably, Bibler[16] estimated from his studies of the radiolysis of 0.4 *M* H_2SO_4 solutions with ^{252}Cf fission fragments that G_{O_2} could be as

large as ~0.8 molec./100 eV at an LET of ~4000 keV/μm (to make up the material balance).

In the present work, upon incorporation of the double, triple, and quadruple ionizations of water molecules in our simulations of the radiolysis of pure, deaerated liquid water, we find, for the four irradiating ions used ($^{1}H^{+}$, $^{4}He^{2+}$, $^{12}C^{6+}$, and $^{20}Ne^{9+}$), a steep increase in both the initial (at 10^{-13} s) (Figure 8a) and the primary (at 10^{-6} s) (Figure 8b) yields of O_2 as a function of LET. In contrast, in the absence of the multiple ionization of water, these yields remain very small throughout the range of LET studied and show only a slight gradual increase with increasing LET. It is difficult, unfortunately, to offer a quantitative comparison between our calculated initial *G*-values for molecular oxygen and the corresponding experimental data of Baverstock and Burns.[17] In fact, the latter authors obtained, for several different impacting ions, the initial yields of O_2 as the lowest limiting yields when the concentration of Fe^{2+} ions was increased (usually to 10^{-2}-10^{-1} *M*) in deaerated Fricke dosimeter solutions (10^{-3} *M* ferrous ammonium sulfate in aqueous 0.4 *M* H_2SO_4) (Table 1 of ref 17). However, they subsequently showed in more detailed experiments using higher ferrous ion concentrations,[108] that with increasing concentration of Fe^{2+} ions the observed yield of oxygen passes through a minimum, which is dependent upon LET, and rises thereafter. It is clear, under such circumstances, that the initial yields of track oxygen reported by Baverstock and Burns[17] are certainly subject to large uncertainty on an absolute basis. We note, nevertheless, that the initial $G(O_2)$ value (~0.005 molec./100 eV) that these authors estimated for 5-MeV $^{4}He^{2+}$ ions (LET ~ 90 keV/μm)[17] agrees very well with our calculated value of 0.0064 molec./100 eV (Figure 8a). However, for 30-MeV $^{20}Ne^{9+}$ ions (LET ~ 1570 keV/μm),[17,108] their observed initial O_2 yield (0.031 molec./100 eV) is about a factor of 10 smaller than our calculated value (~0.3 molec./100 eV, obtained by extrapolation of the data of Figure 8a). As opposed to the difficulties encountered with the initial O_2 yields, a reliable quantitative comparison of our simulated results for ($G_{HO_2^{\bullet}/O_2^{\bullet-}} + G_{O_2}$) as a function of

LET (Figures 2 and 8b) can be made with experiment,[17-20,108] *bearing in mind that the yields generally quoted for* $HO_2^{\bullet}$ *in the literature also include* O_2 *as a direct radiolysis product.*[11,17] For instance, for ~140-keV/μm $^4He^{2+}$ ions, Figures 2 and 8b (when the mechanism of multiple ionization of water is included in the calculations) give $G_{HO_2^{\bullet}/O_2^{\bullet-}} = 0.046$ molec./100 eV and $G_{O_2} = 0.034$ molec./100 eV, respectively, so that $(G_{HO_2^{\bullet}/O_2^{\bullet-}} + G_{O_2}) = 0.08$ molec./100 eV. This value reproduces very well the corresponding experimental values of 0.08 (Table 1 of ref 17), 0.085,[18] 0.099,[19-20] and ~0.093[108] molec./100 eV. It is also consistent with other experimental data at similar or slightly lower LET, including those of Lefort and Tarrago[14] (0.11 molec./100 eV) and Senvar and Hart[110] (0.10 molec./100 eV) for 5.3- and 3.4-MeV ^{210}Po α particles, respectively, and of Appleby and Schwarz[15] (0.07 molec./100 eV) for 12-MeV $^4He^{2+}$ ions. The same kind of comparison can be done at higher LET, for example for $^{20}Ne^{9+}$ ions at ~1570 keV/μm. By extrapolation of our results of Figures 2 and 8b, we obtain for this case $G_{HO_2^{\bullet}/O_2^{\bullet-}} \approx 0.11$ molec./100 eV and $G_{O_2} \approx 0.17$ molec./100 eV, so that $(G_{HO_2^{\bullet}/O_2^{\bullet-}} + G_{O_2}) \approx 0.28$ molec./100 eV. This value is in quite good agreement with the corresponding measured yields of 0.25,[17,108] 0.27,[18] and 0.24[19-20] molec./100 eV reported in the literature for $^{20}Ne^{9+}$ ions at this particular LET. This good agreement between calculated and experimental yield values gives strong support to the validity and consistency of the model,[111] and in turn to the importance of the role of multiple ionization in the radiolysis of water under high-LET irradiation conditions. A final remark that is worthwhile to mention here concerns the relative yields of $HO_2^{\bullet}/O_2^{\bullet-}$ and O_2 in the tracks of highly charged particles. As can be seen from Figures 2 and 8b, not only does the sum $(G_{HO_2^{\bullet}/O_2^{\bullet-}} + G_{O_2})$ increase with increasing LET, but also the amount of O_2 produced, which is low at low LET, becomes greater than that of $HO_2^{\bullet}/O_2^{\bullet-}$ for very high-LET ions. In fact, using the same examples as those cited just above, the ratio $G_{O_2}:G_{HO_2^{\bullet}/O_2^{\bullet-}}$ is calculated to increase from about 0.73 to 1.55 as the LET is raised from ~140 to 1570 keV/μm. These results clearly demonstrate the usefulness of the present computer simulation studies to elucidate the problem of the sepa-

ration of the combined yields of $HO_2^{\bullet}$ and O_2 in high-LET heavy-ion radiolysis experiments using deaerated Fe^{2+}/Cu^{2+} aqueous solutions under acidic conditions.[109]

Further insights into the effects of multiple ionization of water on G_{O_2} in the heavy-ion water radiolysis can be gained by examining the unfolding of the various reactions that contribute to the formation or decay of O_2 in the ion tracks as they expand by diffusion. The main reactions that are involved in the primary yield of O_2 in the case of deaerated liquid water irradiated by 24-MeV $^{12}C^{6+}$ ions (~500 keV/μm) at neutral pH and 25 °C are listed in Table 5. As noted above, the importance of these reactions can be quantified by the yield variations $\Delta G(O_2)$ that they cause over the time interval of nonhomogeneous track chemistry (~10^{-12}-10^{-6} s). In Figure 9, we compare, with and without including the mechanism of multiple ionization of water, our calculated time profiles of $\Delta G(O_2)$ for each of these reactions. Figure 9a shows that, in the absence of multiple ionization, the production and disappearance of molecular oxygen are predominantly due to intratrack reactions (R6) and (R7), and (R10) and (R11), respectively. Overall, the amount of O_2 produced is slightly larger than that removed, so that our calculated G_{O_2} value at the microsecond time scale is low (~0.013 molec./100 eV; see Figures 8b and 10a). When the double, triple, and quadruple ionizations of water molecules are incorporated in the simulations (Figure 9b), O_2 is formed within the tracks mainly by reaction (R6) and to a much lower extent by reaction (R7), whereas there is a chemical production of O_2 at early times originating from the reactions (R14) and (R21) of the $O(^3P)$ atom[112] with $HO_2^{\bullet}$ and with itself, respectively. As for the O_2 decay, it largely occurs through the two track reactions (R10) and especially (R11). Compared to the results obtained in the absence of multiple ionization, there is overall a marked (about five times) increase in the production of O_2 over its disappearance, our calculated value of G_{O_2} being equal, in this case, to ~0.062 molec./100 eV (see Figures 8b and 10b). A detailed inspection of Figure 9 also reveals the presence of a maximum in the time dependence of the O_2 yield (Figure 10), which is mainly accounted for by the different formation and decay kinetics of molecular oxygen. In

fact, reaction (R6), which is the dominant chemical route for formation of O_2, takes place at very short times and its importance in producing O_2 increases rapidly around $\sim 10^{-11}$ s. By contrast, the reactions (R10) and (R11), which are the principal causes of the decay of O_2, show a comparatively slower initial increase in importance but this trend is reversed on the time scale from $\sim 10^{-10}$ to 10^{-9} s with an increasingly faster decay of O_2. This leads, in turn, to the appearance of a maximum in the O_2 yield at around 10^{-9} s. As it is clearly seen in Figure 10, for 24-MeV $^{12}C^{6+}$ ions (~500 keV/μm), this maximum is very shallow in the absence of the multiple-ionization mechanism, but becomes quite pronounced (~0.13 molec./100 eV at $\sim 4 \times 10^{-10}$ s) when the double, triple, and quadruple ionizations of water molecules are incorporated in the simulations.

Parts (a) and (b) of Figure 10 show the effect of LET on the temporal variation of the yield of O_2 at 25 °C, over the range 10^{-12}-10^{-6} s, obtained from our simulations of the radiolysis of pure, deaerated liquid water by $^{12}C^{6+}$ ions of various initial energies in the range ~18-2 MeV/nucleon (~100-500 keV/μm). As can be seen from Figures 9a and 10a, in the absence of multiple ionization of water, the initial yield of molecular oxygen is almost non-existent for all LET values considered, while at longer times there is a small amount of O_2 produced via intratrack reactions occurring during the nonhomogeneous chemical stage. In contrast, upon incorporation of multiple ionization of water molecules in our simulations, the production of O_2 increases considerably with increasing LET.[113] Figures 9b and 10b demonstrate that, in this case, the amount of O_2 produced by the very short-time track reactions (R6), (R14), and (R21) is the primary cause of the overall increase in the yield of O_2. The results in Figure 10b also show that, as the LET is increased, the maximum of the O_2 yield becomes more and more pronounced as a function of time, while its position continuously shifts toward shorter times. Unfortunately, there are at present no experimental or theoretical information available in the literature with which to

compare our results on the time variations of the yield of molecular oxygen at high LET.

A few final words should be added here regarding the oxygen production in high-LET ion tracks. Using our calculated *G*-values for O_2 reported above for 24-MeV $^{12}C^{6+}$ ions (~500 keV/μm) (see Figures 8a and 10b), we can estimate the track concentration of O_2 as a function of time. In fact, assuming that the oxygen molecules are produced *evenly* in a cylinder whose initial radius r_0 is equal to the radius of the physicochemical core of the impacting ion track (at 10^{-13} s),[8,9] this concentration can simply be derived from[2,17,56]

$$[O_2] \approx G(O_2) \times \left(\frac{\text{LET}}{\pi \, r(t)^2} \right),$$

where

$$r(t)^2 \approx r_0^2 + 6\,D\,t$$

represents the change with time of r_0 due to the diffusive expansion of the track. Here, t is the time and D is the diffusion coefficient of O_2 ($D = 2.42 \times 10^{-9}$ m^2 s^{-1} at 25 °C).[50] For the case of 24-MeV $^{12}C^{6+}$ ions, the LET is ~500 keV/μm, $G(O_2)$ at 10^{-13} s is ~0.1 molec./100 eV (Figure 8a), and r_0 obtained from our simulations is ~2.0 nm. Under these conditions, the initial track concentration of oxygen $[O_2]_0$ is ~63.5 m*M*, a value that is about three orders of magnitude higher than the concentration of O_2 found in typical human cells (~30 μ*M*).[114] At ~4×10^{-10} s (that is, at the O_2 yield maximum; see Figure 10b), we have r ~ 3.1 nm, $G(O_2)$ ~ 0.13 molec./100 eV, and thus $[O_2]$ ~ 32.8 m*M*. Finally, at the microsecond time scale, r ~ 121 nm, G_{O_2} ~ 0.063 molec./100 eV, and the oxygen concentration in the irradiated track volume is ~11 μ*M*. All of these values clearly indicate that there is an excess production *in situ* of molecular oxygen in high-LET, heavy-ion tracks at early time that is not observed with lower LET radiations. One must nevertheless be cautious in relating these substantial O_2 yields and concentrations, which are for water, to the situation where energy is deposited in or

near a cell.[105] However, it seems certain that this O_2 formation can be an important factor in the increased biological efficiency of radiations of high LET with, in turn, profound consequences in radiobiology, oxidative processes, and other applications. In view of the above results, the present work largely pleads in favor of the "oxygen in the heavy-ion track" hypothesis.

4. Conclusion

In this study, we have used Monte Carlo track structure simulations to investigate the effects of multiple ionization of water on the *G*-values of the radiolytic free radical and molecular species, including O_2, produced in the radiolysis of pure, air-free liquid water by several different types of radiation, including $^{1}H^{+}$, $^{4}He^{2+}$, $^{12}C^{6+}$, and $^{20}Ne^{9+}$ ions, at high LET up to ~900 keV/μm, at neutral pH and 25 °C. Taking into account the double, triple, and quadruple ionizations of water molecules, the primary (or "escape") yields $G_{HO_2^{\bullet}/O_2^{\bullet-}}$, $G_{H_2O_2}$, $G_{e_{aq}^-}$, $G_{^{\bullet}OH}$, $G_{H^{\bullet}}$, G_{H_2}, and G_{O_2}, have been calculated as a function of LET. A good agreement has been obtained between the calculated yields and the available experimental data. In particular, our results quantitatively reproduce the large increase observed in the $HO_2^{\bullet}/O_2^{\bullet-}$ yield with increasing LET. With the exception of protons, they also simultaneously predict a maximum in the yield of H_2O_2 around 100-200 keV/μm in remarkable accord with experiment. In addition, for each ion investigated, this maximum of $G_{H_2O_2}$ occurs precisely at the point where $G_{HO_2^{\bullet}/O_2^{\bullet-}}$ begins to rise sharply, showing, in agreement with previous experimental data, that the yields of $HO_2^{\bullet}/O_2^{\bullet-}$ and H_2O_2 are closely linked. However, we find that, over the whole LET range considered, the incorporation of multiple ionization of water in the simulations has almost no effect on the variation of our computed $G_{e_{aq}^-}$ and $G_{^{\bullet}OH}$ values. It is also found that $G_{e_{aq}^-}$ and $G_{^{\bullet}OH}$ diminish steeply as the LET is increased; for the highest LET studied, there is almost no escape of e_{aq}^- and $^{\bullet}OH$ from the ion track at the microsecond time scale. In contrast, we observe for $^{4}He^{2+}$, $^{12}C^{6+}$, and $^{20}Ne^{9+}$ ions at high LET a slight gradual decrease of our $G_{H^{\bullet}}$ and G_{H_2}

values calculated with multiple ionization of water in comparison with those obtained without including the multiple-ionization mechanism. This decrease of $G_{H^\bullet}$ and G_{H_2} at low ion energies is found to be more pronounced for heavier ions in the order $^{4}He^{2+}$ < $^{12}C^{6+}$ < $^{20}Ne^{9+}$ and mainly results from the increase in $HO_2^\bullet/O_2^{\bullet-}$ and O_2 yields that occurs at high LET in the presence of the multiple ionization of water. As expected, $G_{H^\bullet}$ at first increases and then decreases at high LET, whereas G_{H_2} monotonically rises with increasing LET. For the four irradiating ions used, our results also show, upon incorporation of multiple ionization of water molecules in the simulations, a steep increase in both the initial (at 10^{-13} s) and the primary (at 10^{-6} s) yields of O_2 as a function of LET. Moreover, detailed examination of the temporal variation of the yield of O_2 reveals the presence of a maximum at around 10^{-9} s. For 24-MeV $^{12}C^{6+}$ ions (~500 keV/μm), this maximum is very shallow in the absence of the multiple-ionization mechanism, but reaches a value of ~0.13 molec./100 eV when the double, triple, and quadruple ionizations of water molecules are incorporated in the simulations. Such an excess production *in situ* of molecular oxygen in high-LET, heavy-ion tracks, that is not observed with lower LET radiations, can be a key factor in the increased biological efficiency of radiations of high LET with, in turn, important consequences in radiobiology, oxidative processes, and other applications. Based on these results, the present work clearly pleads in favor of the "oxygen in the heavy-ion track" hypothesis. Finally, it is worthwhile noting that, under the conditions of this study, the mechanisms of triple and quadruple ionizations contribute only weakly to the production of $HO_2^\bullet/O_2^{\bullet-}$ and O_2, respectively. In other words, the mechanism of double ionization of water is found to largely predominate at high LET whereas it is insignificant at low LET.

The good overall agreement found between calculated and experimental yield values gives strong support to the validity and consistency of the model used in this study, and in turn to the importance of the role of multiple ionization in the radiolysis of water under high-LET irradiation conditions.

Acknowledgment

We are grateful to Professor Hans Bichsel, Dr. Christophe Champion, Professor Yosuke Katsumura, Professor Jay A. LaVerne, Dr. John H. Miller, Professor Dr. Clemens von Sonntag, and Professor David E. Watt for valuable discussions and useful correspondence, and to Mr. Carol Gauthier for his skillful assistance with the computer programs. We would also like to thank the "Réseau québécois de calcul de haute performance" (RQCHP) for providing generous computing facilities. Financial support from the Canadian Institutes of Health Research (Grant No. MT-14617) and the Natural Sciences and Engineering Research Council of Canada (Grant No. 9020-04) is gratefully acknowledged.

TABLE 1: Revised branching ratios used in our simulations for the different competing mechanisms in the fate of (A) Vibrationally excited water molecules ($H_2O^*_{vib}$) formed by recombination of a subexcitation electron (e^-_{sub}) with its water parent cation ($H_2O^{\bullet+}$)[a] and (B) Directly excited electronic states ($\tilde{A}^1B_1$ and $\tilde{B}^1A_1$) of water molecules[b]

(A)

$H_2O^{\bullet+} + e^- \rightarrow H_2O^*_{vib}$

$H_2O^*_{vib}$	→	Nondissociative deexcitation	45% (35%)	→	H_2O + release of thermal energy
	→	Dissociative deexcitation	55% (65%)	→	$H^\bullet + {}^\bullet OH$ 79% (79.8%) $2H^\bullet + O(^3P)$ 8% (5.5%) $H_2 + O(^1D)$ 13% (14.7%)

[a] Previously employed values from ref 32 are given in parentheses.

(B)

$H_2O^*(\tilde{A}^1B_1)$	→	Nondissociative deexcitation	45% (35%)	→	H_2O
	→	Dissociative deexcitation	55% (65%)	→	$H^\bullet + {}^\bullet OH$
$H_2O^*(\tilde{B}^1A_1)$	→	Autoionization	50% (50%)	→	$H_2O^{\bullet+} + e^-$
	→	Nondissociative deexcitation	22.5% (17.5%)	→	H_2O
	→	Dissociative deexcitation	27.5% (32.5%)	→	$H^\bullet + {}^\bullet OH$ 79% (78%) $2H^\bullet + O(^3P)$ 8% (12%) $H_2 + O(^1D)$ 13% (10%)

[b] Previously employed values from ref 28 are given in parentheses.

TABLE 2: Reaction scheme considered in our simulations to model the radiolysis of deaerated 0.005 *M* H_2SO_4 solutions of $FeSO_4$-$CuSO_4$ (pH ~ 2.1) at 25 °C

Reaction	k (M^{-1} s^{-1})
$H^{\bullet} + Fe^{2+} \rightarrow Fe^{3+} + H^-$	1.3×10^7 (*a*, *b*)
$H^{\bullet} + Cu^{2+} \rightarrow Cu^{+} + H^+$	9.1×10^7 (*c*)
$H^{\bullet} + Fe^{3+} \rightarrow Fe^{2+} + H^+$	1.0×10^8 (*a*, *b*)
$H^{\bullet} + Cu^{+} \rightarrow CuH^+$	5.0×10^9 (*c*)
$H^{\bullet} + SO_4^{\bullet -} \rightarrow HSO_4^-$	1.0×10^{10} (*d*)
$H^{\bullet} + S_2O_8^{2-} \rightarrow SO_4^{\bullet -} + HSO_4^-$	2.5×10^7 (*c*)
$^{\bullet}OH + Fe^{2+} \rightarrow Fe^{3+} + OH^-$	3.4×10^8 (*a*, *b*)
$^{\bullet}OH + Cu^{2+} \rightarrow Cu^{3+} + OH^-$	3.5×10^8 (*c*)
$^{\bullet}OH + Cu^{+} \rightarrow Cu^{2+} + OH^-$	2.0×10^{10} (*e*)
$^{\bullet}OH + HSO_4^- \rightarrow H_2O + SO_4^{\bullet -}$	1.5×10^5 (*f*, *g*)
$e_{aq}^- + Fe^{2+} \rightarrow Fe^{+}$ (*o*)	1.2×10^8 (*b*)
$e_{aq}^- + Cu^{2+} \rightarrow Cu^{+}$ (*o*)	3.8×10^{10} (*h*)
$e_{aq}^- + Fe^{3+} \rightarrow Fe^{2+}$ (*o*)	2.0×10^{10} (*a*, *b*)
$e_{aq}^- + Cu^{+} \rightarrow Cu$ (*o*)	2.7×10^{10} (c)
$e_{aq}^- + S_2O_8^{2-} \rightarrow SO_4^{\bullet -} + SO_4^{2-}$ (*o*)	1.2×10^{10} (*c*)
$H_2O_2 + SO_4^{\bullet -} \rightarrow HO_2^{\bullet} + HSO_4^-$	1.2×10^7 (i)
$HO_2^{\bullet} + Fe^{2+} \rightarrow Fe^{3+} + HO_2^-$	7.9×10^5 (*a*)
$HO_2^{\bullet} + Cu^{2+} \rightarrow Cu^{+} + O_2 + H^+$	1.2×10^8 (*a*, *j*, *k*)
$HO_2^{\bullet} + Fe^{3+} \rightarrow Fe^{2+} + O_2 + H^+$	2.0×10^4 (*k*)
$HO_2^{\bullet} + Cu^{+} \rightarrow Cu^{2+} + HO_2^-$	2.3×10^9 (*k*)
$O_2^{\bullet -} + Cu^{2+} \rightarrow Cu^{+} + O_2$	1.1×10^{10} (*j*, *k*)
$O^{\bullet -} + Fe^{2+} \rightarrow Fe^{3+} + OH^-$	3.8×10^9 (*c*)

TABLE 2 (Continued)

Reaction	k (M^{-1} s^{-1})
$O_2 + Cu^+ \rightarrow Cu^{2+} + O_2^{\bullet-}$	4.6×10^5 [l]
$CuH^+ + H^+ \rightarrow Cu^{2+} + H_2$	1.0×10^6 [m]
$OH^- + SO_4^{\bullet-} \rightarrow {}^{\bullet}OH + SO_4^{2-}$	8.3×10^7 [i]
$Fe^{2+} + SO_4^{\bullet-} \rightarrow Fe^{3+} + SO_4^{2-}$	9.9×10^8 [i]
$Cu^+ + SO_4^{\bullet-} \rightarrow Cu^{2+} + SO_4^{2-}$	1.8×10^{10} [n]
$Cu^+ + Fe^{3+} \rightarrow Cu^{2+} + Fe^{2+}$	5.5×10^6 [l]
$Cu^{3+} + Fe^{2+} \rightarrow Cu^{2+} + Fe^{3+}$	3.3×10^8 [l]
$CuH^+ + Cu^{2+} \rightarrow 2\,Cu^+ + H^+$	7.0×10^6 [m]
$SO_4^{\bullet-} + SO_4^{\bullet-} \rightarrow S_2O_8^{2-}$	4.4×10^8 [i]

[a] ref 65 [e] ref 69 [i] ref 72 [m] ref 76
[b] ref 66 [f] ref 31 [j] ref 73 [n] ref 77
[c] ref 67 [g] ref 70 [k] ref 74
[d] ref 68 [h] ref 71 [l] ref 75

[o] Since under the considered acidic conditions (0.005 *M* H_2SO_4, pH ~ 2.1) the H^+ ions capture most of the e_{aq}^- radicals in the expanding spurs/tracks to form H• atoms, the reactions of e_{aq}^- with the various solutes Fe^{2+}, Cu^{2+}, Fe^{3+}, Cu^+, and $S_2O_8^{2-}$ present in the solutions in low concentrations play practically no role in the radiolytic process.

TABLE 3: Main track reactions that contribute to the formation and decay of $HO_2^{\bullet}/O_2^{\bullet-}$ in our Monte Carlo simulations of the radiolysis of pure, deaerated liquid lwater by 24-MeV $^{12}C^{6+}$ ions (~500 keV/μm) at 25 °C and in the time interval ~10^{-12}–10^{-6} s.

Reaction[a]	Symbol[b]
$^{\bullet}OH + O(^3P) \rightarrow HO_2^{\bullet}$	(R2)
$^{\bullet}OH + HO_2^{\bullet} \rightarrow O_2 + H_2O$	(R6)
$^{\bullet}OH + O_2^{\bullet-} \rightarrow O_2 + OH^-$	(R7)
$e_{aq}^- + HO_2^{\bullet} \rightarrow HO_2^-$	(R8)
$e_{aq}^- + O_2^{\bullet-} \rightarrow H_2O_2 + 2\,OH^-$	(R9)
$e_{aq}^- + O_2 \rightarrow O_2^{\bullet-}$	(R10)
$H^{\bullet} + O_2 \rightarrow HO_2^{\bullet}$	(R11)
$H^{\bullet} + HO_2^{\bullet} \rightarrow H_2O_2$	(R12)
$H^{\bullet} + O_2^{\bullet-} \rightarrow HO_2^-$	(R13)
$HO_2^{\bullet} + O(^3P) \rightarrow O_2 + {}^{\bullet}OH$	(R14)
$H^+ + O_2^{\bullet-} \rightarrow HO_2^{\bullet}$	(R15)
$HO_2^{\bullet} \rightarrow H^+ + O_2^{\bullet-}$	
$O_2^{\bullet-} + H_2O \rightarrow HO_2^{\bullet} + OH^-$	(R16)
$HO_2^{\bullet} + OH^- \rightarrow O_2^{\bullet-} + H_2O$	

[a] $O(^3P)$ denotes the oxygen atom in its ^3P ground state.

[b] Reaction symbols used in the text.

TABLE 4: Main track reactions that contribute to the formation and decay of H_2O_2 in our Monte Carlo simulations of the radiolysis of pure, deaerated liquid water by 24-MeV $^{12}C^{6+}$ ions (~500 keV/μm) at 25 °C and in the time interval ~10^{-12}–10^{-6} s.

Reaction	Symbol[a]
$^{\bullet}OH + {}^{\bullet}OH \rightarrow H_2O_2$	(R5)
$H^{\bullet} + HO_2^{\bullet} \rightarrow H_2O_2$	(R12)
$H_2O_2 + e_{aq}^- \rightarrow {}^{\bullet}OH + OH^-$	(R17)
$H^+ + HO_2^- \rightarrow H_2O_2$	(R18)
$H_2O_2 + OH^- \rightarrow HO_2^- + H_2O$	(R19)
$HO_2^- + H_2O \rightarrow H_2O_2 + OH^-$	

[a] Reaction symbols used in the text.

TABLE 5: Main track reactions that contribute to the formation and decay of O_2 in our Monte Carlo simulations of the radiolysis of pure, deaerated liquid water by 24-MeV $^{12}C^{6+}$ ions (~500 keV/μm) at 25 °C and in the time interval ~10^{-12}–10^{-6} s.

Reaction	Symbol[a]
$^{\bullet}OH + HO_2^{\bullet} \rightarrow O_2 + H_2O$	(R6)
$^{\bullet}OH + O_2^{\bullet -} \rightarrow O_2 + OH^-$	(R7)
$e_{aq}^- + O_2 \rightarrow O_2^{\bullet -}$	(R10)
$H^{\bullet} + O_2 \rightarrow HO_2^{\bullet}$	(R11)
$HO_2^{\bullet} + O(^3P) \rightarrow O_2 + {}^{\bullet}OH$	(R14)
$O(^3P) + O(^3P) \rightarrow O_2$	(R21)

[a] Reaction symbols used in the text.

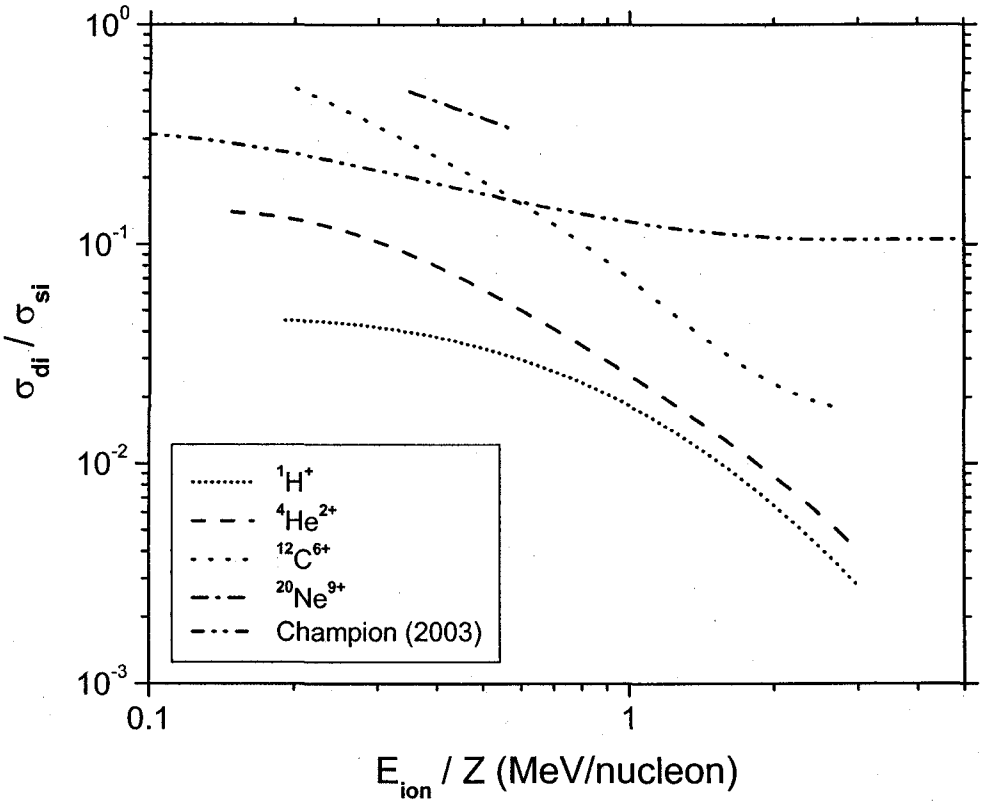

Figure 1: Ratio of the double-to-single ionization cross-sections ($\alpha = \sigma_{di}/\sigma_{si}$) as a function of E_{ion}/Z, where E_{ion} is the ion energy per nucleon and Z is the projectile charge state. The short-dot, dash, dot, and dash-dot lines represent the values of α obtained from our Monte Carlo simulations of the radiolysis of air-free aqueous $FeSO_4$ (1 m*M*)–$CuSO_4$ (10 m*M*) solutions under acidic (0.005 *M* H_2SO_4) conditions for $^1H^+$, $^4He^{2+}$, $^{12}C^{6+}$, and $^{20}Ne^{9+}$ ions, respectively. In those simulations, performed at 25 °C, α is treated as an adjustable parameter chosen to get the best fit of the experimental data of LaVerne and Schuler (ref 20) of ($G_{HO_2\cdot} + G_{O_2}$) as a function of LET (see text). The values of α reported by Champion for a variety of ions at intermediate velocities and gaseous water (solid line in Fig. 1 of ref 27) are also shown for the sake of comparison (dash-dot-dot line).

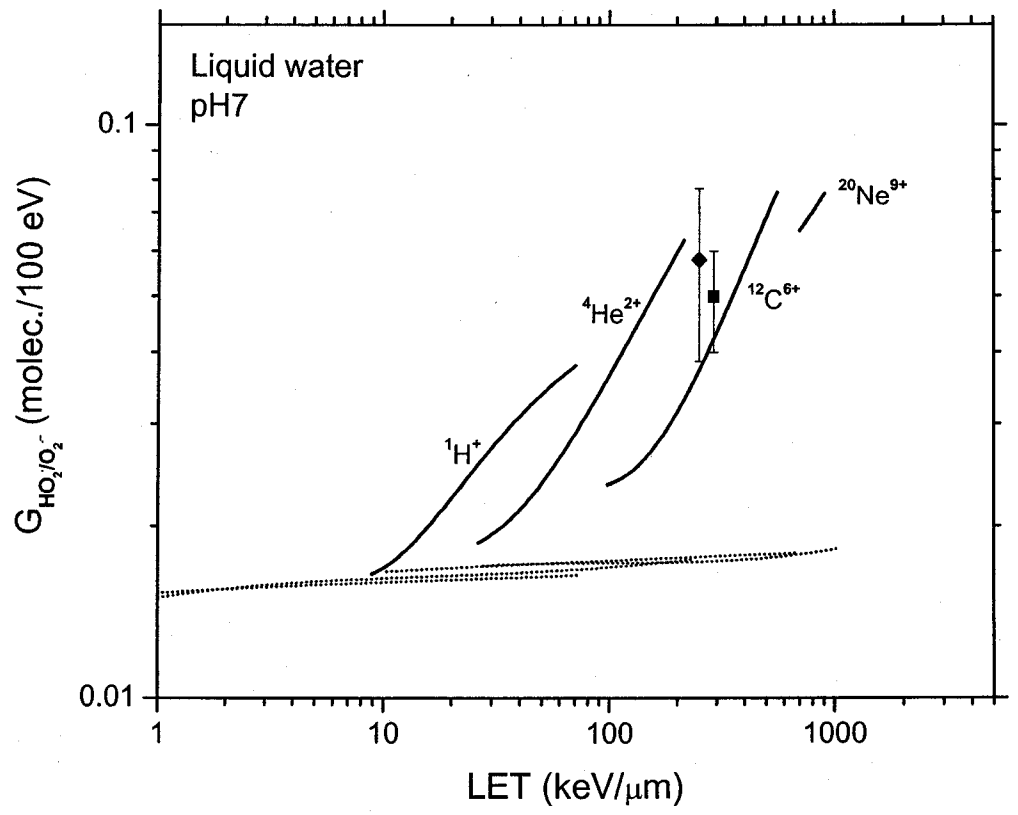

Figure 2: Variation of the primary $HO_2^{\bullet}/O_2^{\bullet-}$ yield ($G_{HO_2^{\bullet}/O_2^{\bullet-}}$) (in molec./100 eV) of the radiolysis of deaerated liquid water by $^{1}H^{+}$, $^{4}He^{2+}$, $^{12}C^{6+}$, and $^{20}Ne^{9+}$ ions as a function of LET up to ~900 keV/μm, at neutral pH and 25 °C. The solid lines represent the results of our Monte Carlo simulations incorporating the double, triple, and quadruple ionizations of water molecules, obtained at 10^{-6} s (see text). The short-dot lines correspond to our $G_{HO_2^{\bullet}/O_2^{\bullet-}}$ values calculated as a function of LET without including the mechanism of multiple ionization of water. Experimental yields (pH ≈ 7): (◆) $^{36}S^{16+}$ ions (77 MeV/nucleon, LET ~ 250 keV/μm) (ref 21), and (■) $^{40}Ar^{18+}$ ions (70 MeV/nucleon, LET ~ 290 keV/μm) (ref 81).

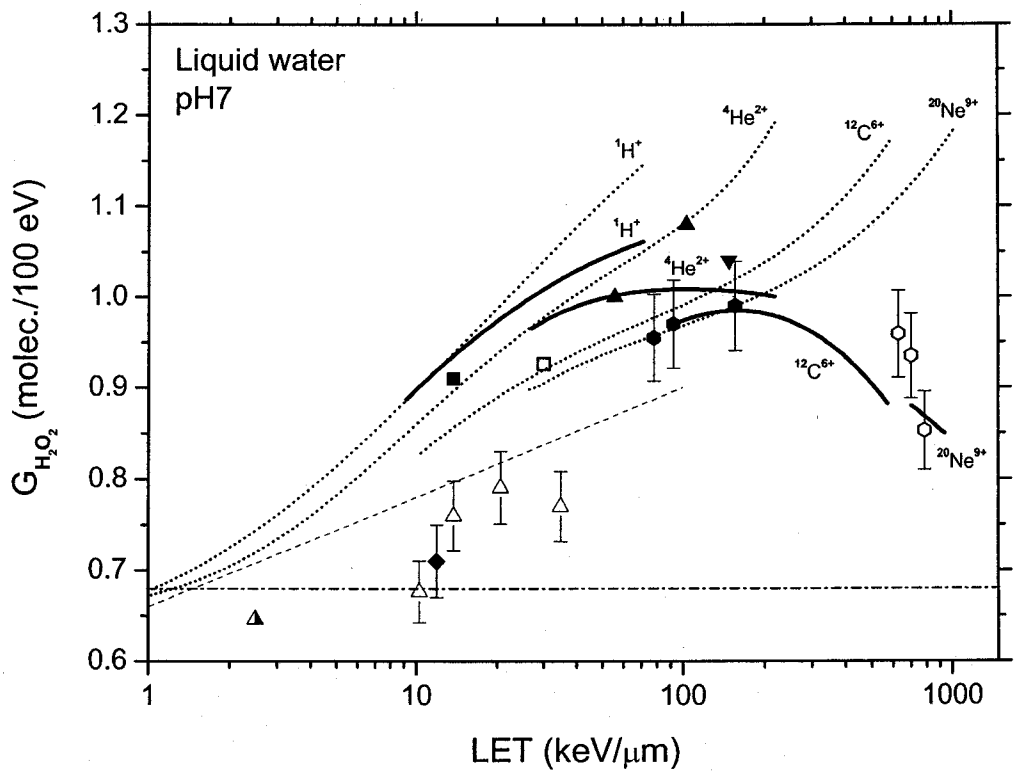

Figure 3: Variation of the primary H_2O_2 yield ($G_{H_2O_2}$) (in molec./100 eV) of the radiolysis of deaerated liquid water by $^1H^+$, $^4He^{2+}$, $^{12}C^{6+}$, and $^{20}Ne^{9+}$ ions as a function of LET up to ~900 keV/μm, at neutral pH and 25 °C. The solid lines represent the results of our Monte Carlo simulations incorporating the double, triple, and quadruple ionizations of water molecules, obtained at 10^{-6} s (see text). The short-dot lines correspond to our $G_{H_2O_2}$ values calculated as a function of LET without including the mechanism of multiple ionization of water. Experimental yields (pH ≈ 7): $^1H^+$ [(△), ref 23; (◭), ref 82], $^2H^+$, at one-half energy [(■), ref 15; (◆), ref 83], $^4He^{2+}$ [(▲), ref 15; (●), ref 23; (▼), ref 84], and $^{12}C^{6+}$ [(○), ref 23; (□), ref 82]. It is worth noting that the simulations of the $^{12}C^{6+}$ radiolysis are not extended above ~600 keV/μm (which corresponds to an incident ion energy of ~1.25 MeV/nucleon) to meet the experimental results of ref 23 because the Z^2 scaling law used in this work to obtain the interaction cross sections is no longer a good approximation below ~1 MeV/nucleon (see text). The dash-dot line represents the limiting primary H_2O_2 yield obtained with ^{60}Co γ-rays or fast electrons (~0.68 molec./100 eV) (ref. 2).

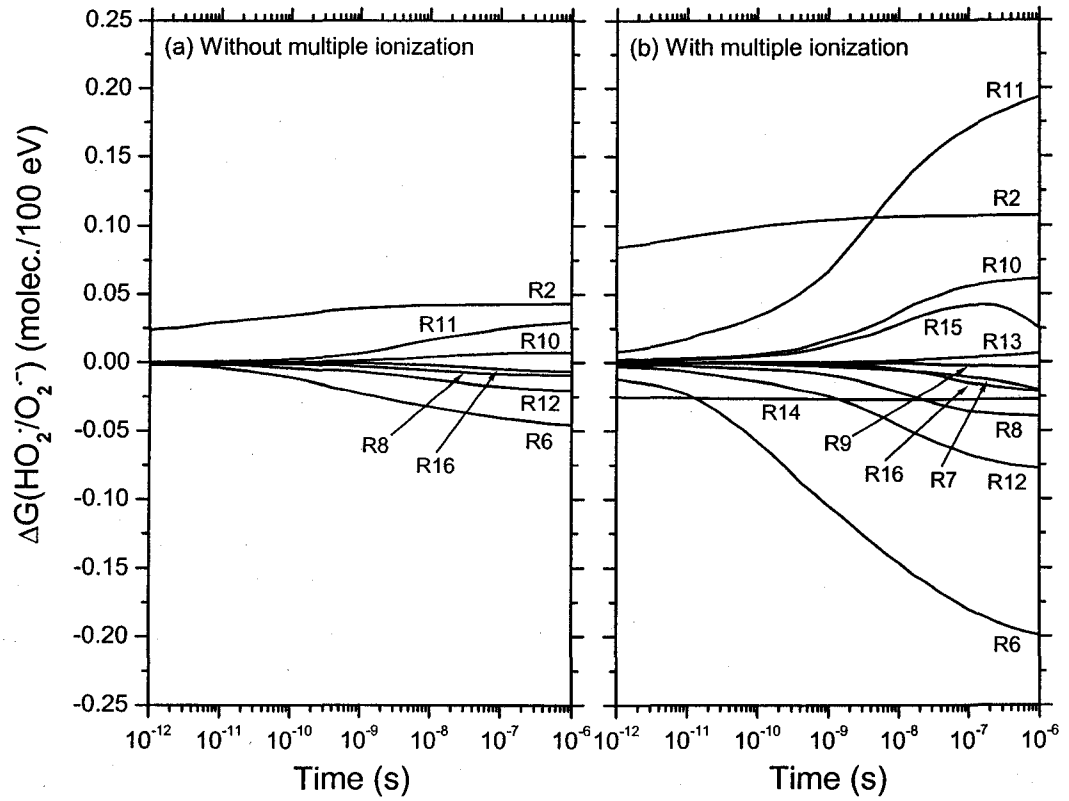

Figure 4: Time dependence of the extents $\Delta G(HO_2^{\bullet}/O_2^{\bullet-})$ (in molec./100 eV) of the main intratrack reactions (R2) and (R6)–(R16) that contribute to the formation and decay of $HO_2^{\bullet}/O_2^{\bullet-}$ (see text and Table 3), calculated from our Monte Carlo simulations of the radiolysis of deaerated liquid water by 24-MeV $^{12}C^{6+}$ ions (~500 keV/μm) at neutral pH, 25 °C, and in the time interval 10^{-12}–10^{-6} s: (a) without including the mechanism of multiple ionization of water, and (b) with incorporating the double, triple, and quadruple ionizations of water molecules. Note that, in the absence of multiple ionization of water, the contributions of reactions (R7), (R9), and (R13)–(R15) are very small and have been omitted from the figure for the sake of clarity.

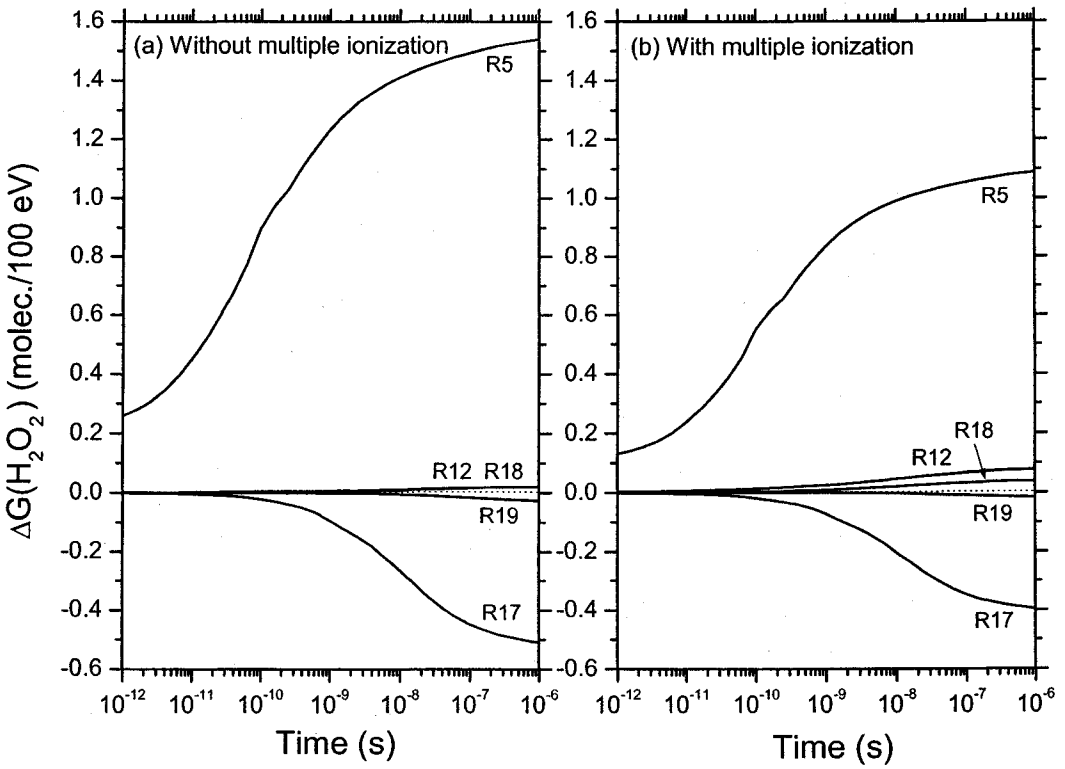

Figure 5: Time dependence of the extents $\Delta G(H_2O_2)$ (in molec./100 eV) of the main intratrack reactions (R5), (R12), and (R17)–(R19) that are involved in the formation and decay of H_2O_2 (see text and Table 4) calculated from our Monte Carlo simulations of the radiolysis of deaerated liquid water by 24-MeV $^{12}C^{6+}$ ions (~500 keV/μm) at neutral pH, 25 °C, and in the time interval 10^{-12}–10^{-6} s: (a) without including the mechanism of multiple ionization of water, and (b) with incorporating the double, triple, and quadruple ionizations of water molecules.

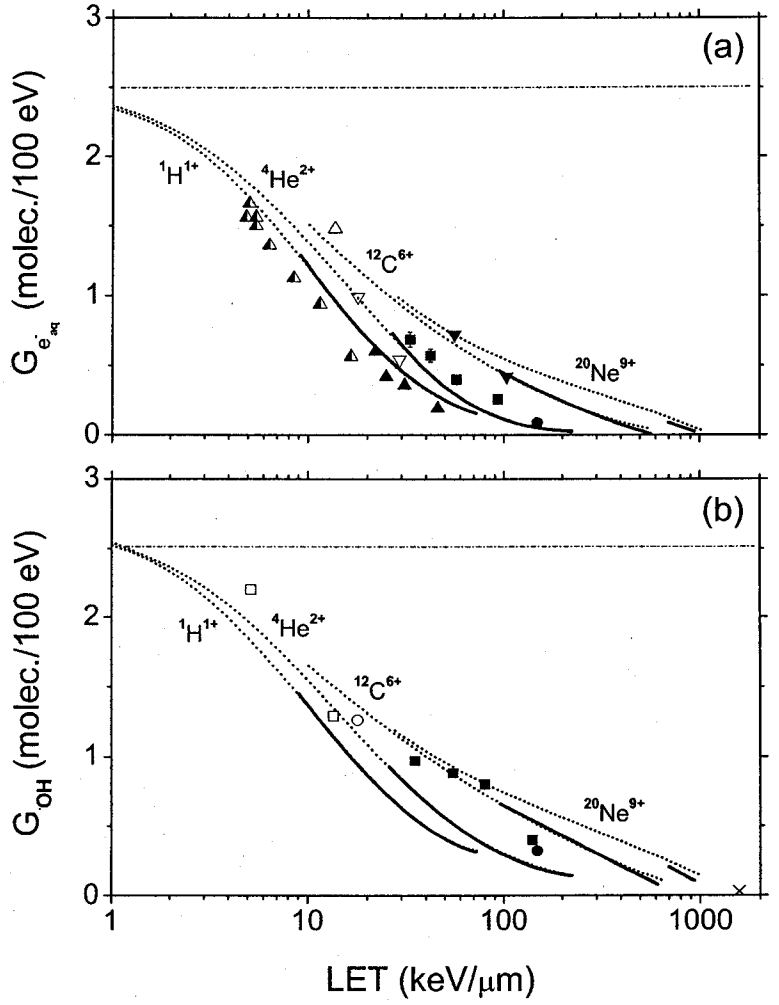

Figure 6: Variation of the primary yields of (a) hydrated electrons ($G_{e^-_{aq}}$) and (b) hydroxyl radicals ($G_{\cdot OH}$) (in molec./100 eV) of the radiolysis of air-free liquid water by $^1H^+$, $^4He^{2+}$, $^{12}C^{6+}$, and $^{20}Ne^{9+}$ ions as a function of LET up to ~900 keV/μm, at neutral pH and 25 °C. The solid lines represent the results of our Monte Carlo simulations incorporating the double, triple, and quadruple ionizations of water molecules, obtained at 10^{-6} s. The short-dot lines correspond to our results calculated without including the mechanism of multiple ionization of water. Experimental yields: (a) $^1H^+$ [(▽), ref 93], $^2H^+$, at one-half energy [(△), ref 15; (▲), ref 88], and $^4He^{2+}$ [(▼), ref 15; (●), ref 84; (▲), ref 88; (■), ref 94]; (b) $^1H^+$ [(□), ref 18; (○), ref 93], $^4He^{2+}$ [(■), ref 18; (●), ref 84], and $^{20}Ne^{9+}$ [(×), ref 18]. The dash-dot lines represent the limiting primary e^-_{aq} and $^{\cdot}OH$ yields obtained with ^{60}Co γ-rays or fast electrons (~2.5 molec./100 eV) (ref 11).

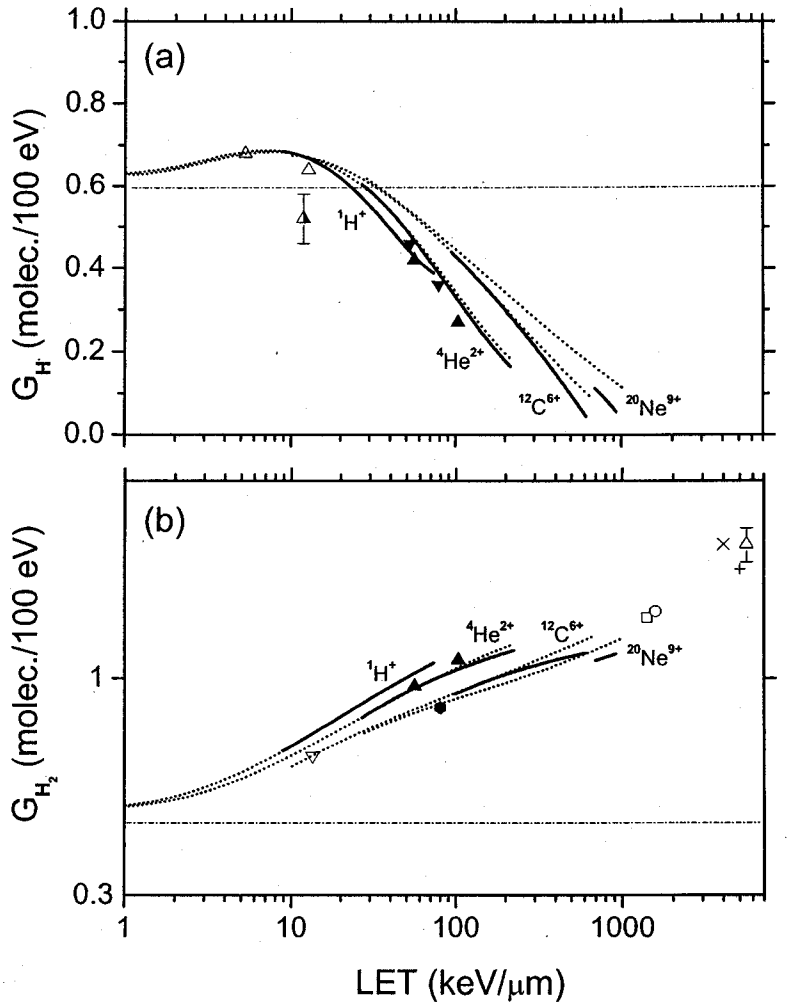

Figure 7: Variation of the primary yields of (a) hydrogen atoms ($G_{H^\bullet}$) and (b) molecular hydrogen (G_{H_2}) (in molec./100 eV) of the radiolysis of air-free liquid water by $^1H^+$, $^4He^{2+}$, $^{12}C^{6+}$, and $^{20}Ne^{9+}$ ions as a function of LET up to ~900 keV/μm, at neutral pH and 25 °C. The solid lines represent the results of our Monte Carlo simulations incorporating the double, triple, and quadruple ionizations of water molecules, obtained at 10^{-6} s. The short-dot lines correspond to our results calculated without including the mechanism of multiple ionization of water. Experimental yields: (a) $^1H^+$ [(△), ref 95], $^2H^+$, at one-half energy [(◭), ref 83], and $^4He^{2+}$ [(▲), ref 15; (▼), ref 95]; (b) $^1H^+$ [(▽), ref 18], $^4He^{2+}$ [(▲), ref 15; (⬢), ref 18], $^{20}Ne^{5+}$ [(□), ref 96], $^{20}Ne^{9+}$ [(○), ref 18], and fission fragments [(×), ref 16; (+), ref 97; (△), ref 98]. The dash-dot lines represent the limiting primary H• and H_2 yields obtained with ^{60}Co γ-rays or fast electrons (~0.60 and 0.45 molec./100 eV, respectively) (ref 2).

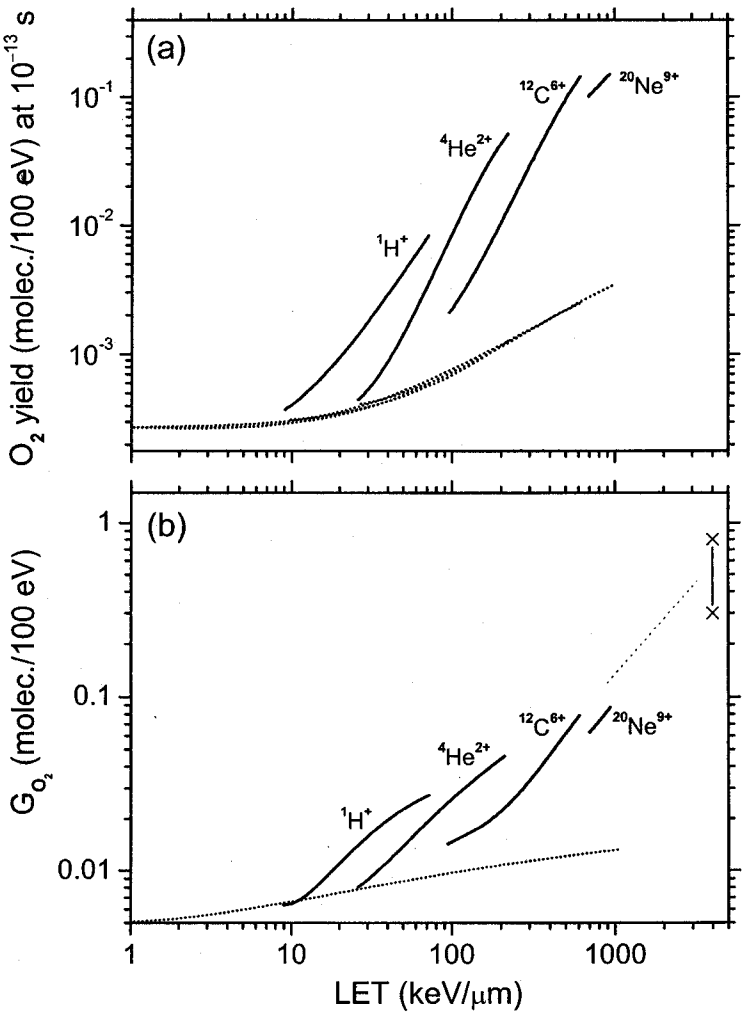

Figure 8: Variation of the initial (a) and primary (b) yields of molecular oxygen (obtained at 10^{-13} and 10^{-6} s, respectively) (in molec./100 eV) of the radiolysis of liquid water by $^{1}H^{+}$, $^{4}He^{2+}$, $^{12}C^{6+}$, and $^{20}Ne^{9+}$ ions as a function of LET, at neutral pH and 25 °C. The solid lines represent the results of our Monte Carlo simulations incorporating the double, triple, and quadruple ionizations of water molecules. The short-dot lines correspond to our calculated values without including the mechanism of multiple ionization of water. The yields $G_{O_2} \sim 0.3$ and 0.8 molec./100 eV estimated by Bibler (ref 16) (×) in the ^{252}Cf fission fragment radiolysis of 0.4 *M* H_2SO_4 solutions at very high LET (~4000 keV/μm) are also shown in part (b) of the figure for the sake of comparison. The dot line is drawn here as a guide for the eye to show that extrapolation to higher LET of our calculated O_2 escape yields for the four ions studied reproduces well Bibler's estimates.

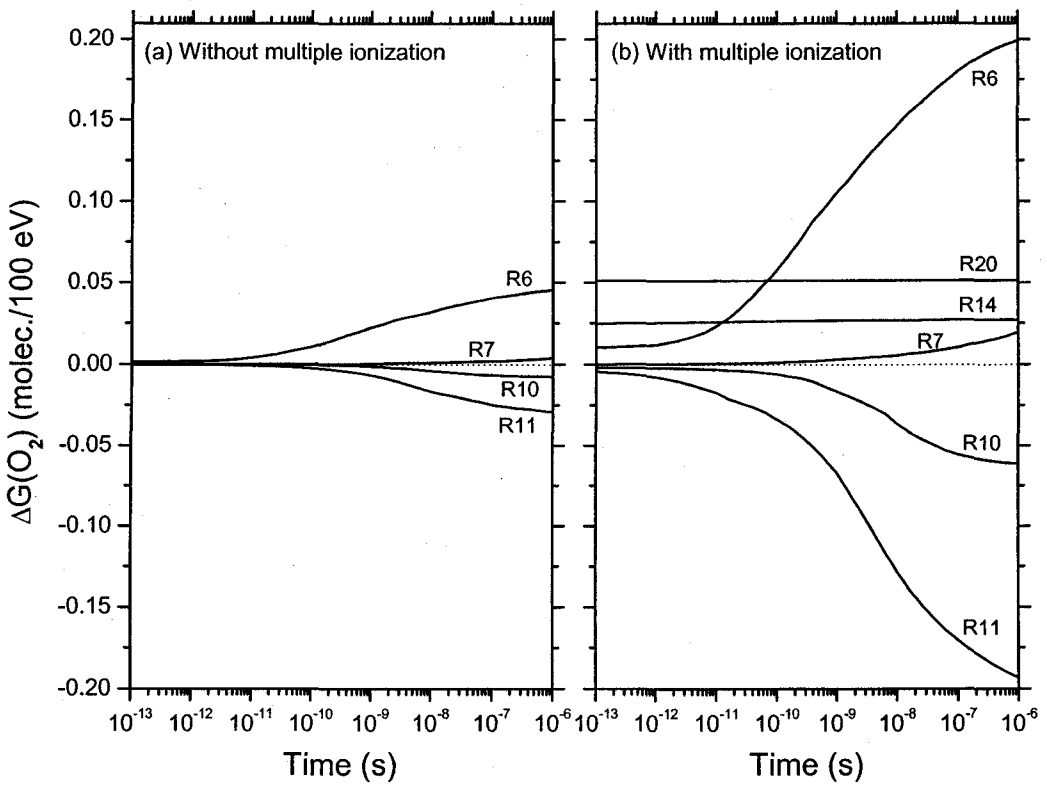

Figure 9: Time dependence of the extents $\Delta G(O_2)$ (in molec./100 eV) of the main intratrack reactions (R6), (R7), (R10), R(11), (R14), and (R21) that contribute to the formation and decay of molecular oxygen (see text and Table 5), calculated from our Monte Carlo simulations of the radiolysis of deaerated liquid water by 24-MeV $^{12}C^{6+}$ ions (~500 keV/μm) at neutral pH, 25 °C, and in the time interval 10^{-12}–10^{-6} s: (a) without including the mechanism of multiple ionization of water, and (b) with incorporating the double, triple, and quadruple ionizations of water molecules. Note that, in the absence of multiple ionization of water, the contributions of reactions (R14) and (R21) are very small and have been omitted from the figure for the sake of clarity.

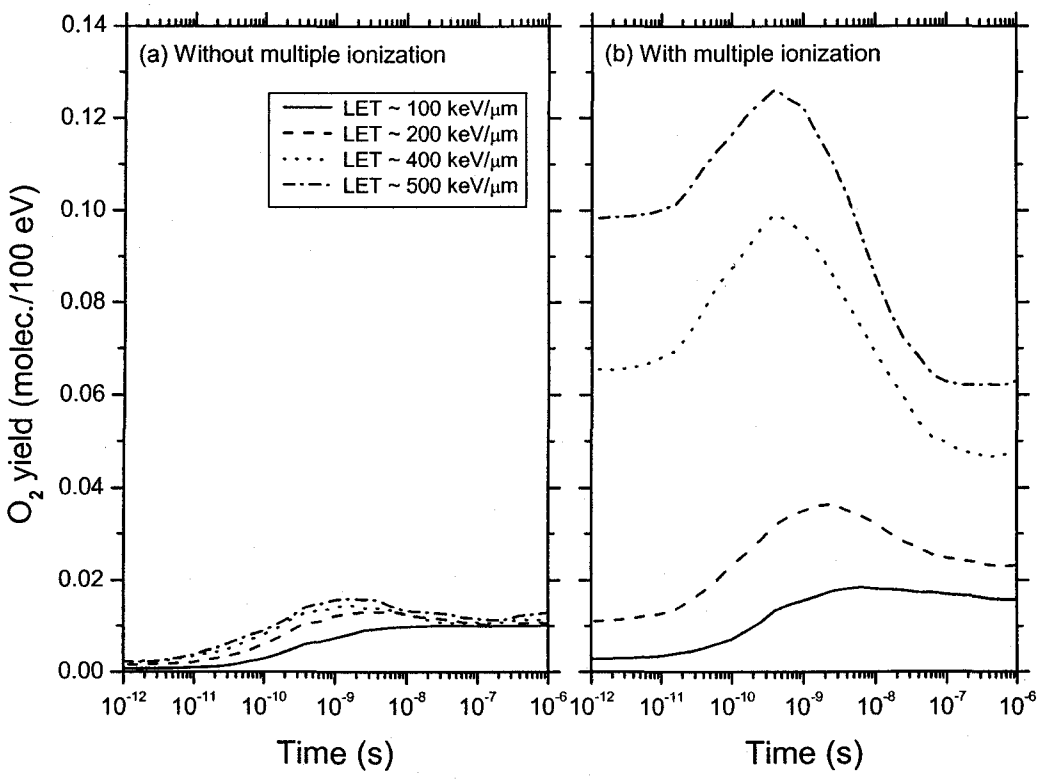

Figure 10: Time dependences of the O_2 yields (in molec./100 eV) calculated from our Monte Carlo simulations of the radiolysis of pure, deaerated liquid water at neutral pH, 25 °C, and in the time scale of 10^{-12}–10^{-6} s, for impacting $^{12}C^{6+}$ ions of various initial energies: 18 (~100 keV/µm), 8 (~200 keV/µm), 3 (~400 keV/µm), and 2 (~500 keV/µm) MeV/nucleon (see text), without mutiple ionization of water (a), and with including the double, triple, and quadruple ionizations of water molecules (b).

References and notes

(1) Spinks, J. W. T.; Woods, R. J. *An Introduction to Radiation Chemistry*, 3rd ed.; Wiley: New York, 1990; p 243.

(2) Ferradini, C.; Jay-Gerin, J.-P. *Can. J. Chem.* **1999**, *77*, 1542.

(3) Buxton, G. V. In *Charged Particle and Photon Interactions with Matter. Chemical, Physicochemical, and Biological Consequences with Applications*; Mozumder, A., Hatano, Y., Eds.; Marcel Dekker: New York, 2004; p 331.

(4) Magee, J. L. *Annu. Rev. Nucl. Sci.* **1953**, *3*, 171.

(5) See, for example: Plante, I. L.; Filali-Mouhim, A.; Jay-Gerin, J.-P. *Radiat. Phys. Chem.* **2005**, *72*, 173.

(6) Throughout this paper, radiation chemical yields (*G*-values) are given in the units of molecules per 100 eV (molec./100 eV). For conversion into SI units (mol/J): 1 molec./100 eV ≈ 0.10364 μmol/J.

(7) Ferradini, C. *J. Chim. Phys.* **1979**, *76*, 636.

(8) Magee, J. L.; Chatterjee, A. In *Kinetics of Nonhomogeneous Processes*; Freeman, G. R., Ed.; Wiley: New York, 1987; p 171.

(9) Mozumder, A. *Fundamentals of Radiation Chemistry*; Academic Press: San Diego, CA, 1999.

(10) LaVerne, J. A. *Radiat. Res.* **2000**, *153*, 487.

(11) LaVerne, J. A. In *Charged Particle and Photon Interactions with Matter. Chemical, Physicochemical, and Biological Consequences with Applications*; Mozumder, A., Hatano, Y., Eds.; Marcel Dekker: New York, 2004; p 403.

(12) Appleby, A. *Radiat. Phys. Chem.* **1989**, *34*, 121.

(13) Note that, for low-LET radiolysis, the production of $HO_2^{\bullet}/O_2^{\bullet-}$ is usually neglected because its very small yield of ~0.02 molec./100 eV (see: Bjergbakke, E.; Hart, E. J. *Radiat. Res.* **1971**, *45*, 261) accounts for less than 1% of the other primary radiolytic species.

(14) Lefort, M.; Tarrago, X. *J. Phys. Chem.* **1959**, *63*, 833.

(15) Appleby, A.; Schwarz, H. A. *J. Phys. Chem.* **1969**, *73*, 1937. Schwarz, H. A.; Caffrey, J. M., Jr.; Scholes, G. *J. Am. Chem. Soc.* **1959**, *81*, 1801.

(16) Bibler, N. E. *J. Phys. Chem.* **1975**, *79*, 1991.

(17) Baverstock, K. F.; Burns, W. G. *Nature* **1976**, *260*, 316.

(18) Burns, W. G.; Sims, H. E. *J. Chem. Soc., Faraday Trans. 1* **1981**, *77*, 2803. See also: Sims, H. E. Ph.D. Thesis, University of Salford, Salford, U.K., 1978.

(19) LaVerne, J. A.; Schuler, R. H.; Burns, W. G. *J. Phys. Chem.* **1986**, *90*, 3238.

(20) LaVerne, J. A.; Schuler, R. H. *J. Phys. Chem.* **1987**, *91*, 6560.

(21) Baldacchino, G.; Le Parc, D.; Hickel, B.; Gardès-Albert, M.; Abedinzadeh, Z.; Jore, D.; Deycard, S.; Bouffard, S.; Mouton, V.; Balanzat, E. *Radiat. Res.* **1998**, *149*, 128.

(22) McCracken, D. R.; Tsang, K. T.; Laughton, P. J. *Aspects of the Physics and Chemistry of Water Radiolysis by Fast Neutrons and Fast Electrons in Nuclear Reactors*, Report AECL-11895; Atomic Energy of Canada Limited: Chalk River, Ontario, 1998.

(23) Pastina, B.; LaVerne, J. A. *J. Phys. Chem. A* **1999**, *103*, 1592.

(24) Meesungnoen, J.; Filali-Mouhim, A.; Snitwongse Na Ayudhya, N.; Mankhetkorn, S.; Jay-Gerin, J.-P. *Chem. Phys. Lett.* **2003**, *377*, 419.

(25) Ferradini, C.; Jay-Gerin, J.-P. *Radiat. Phys. Chem.* **1998**, *51*, 263.

(26) It is worth noting here that a similar conclusion was pointed out more than fifty years ago by Platzman (Platzman, R. L. In *Symposium on Radiobiology. The Basic Aspects of Radiation Effects on Living Systems*; Nickson, J. J., Ed. Wiley: New York, 1952; p 97) in a discussion of the possible role of multiple ionization in radiation action.

(27) Champion, C. *Nucl. Instrum. Methods Phys. Res. B* **2003**, *205*, 671.

(28) Cobut, V.; Frongillo, Y.; Patau, J. P.; Goulet, T.; Fraser, M.-J.; Jay-Gerin, J.-P. *Radiat. Phys. Chem.* **1998**, *51*, 229.

(29) Frongillo, Y.; Goulet, T.; Fraser, M.-J.; Cobut, V.; Patau, J. P.; Jay-Gerin, J.-P. *Radiat. Phys. Chem.* **1998**, *51*, 245.

(30) Hervé du Penhoat, M.-A.; Goulet, T.; Frongillo, Y.; Fraser, M.-J.; Bernat, Ph.; Jay-Gerin, J.-P. *J. Phys. Chem. A* **2000**, *104*, 11757. See also: Hervé du Penhoat, M.-A.; Meesungnoen, J.; Goulet, T.; Filali-Mouhim, A.; Mankhetkorn, S.; Jay-Gerin, J.-P. *Chem. Phys. Lett.* **2001**, *341*, 135.

(31) Meesungnoen, J.; Benrahmoune, M.; Filali-Mouhim, A.; Mankhetkorn, S.; Jay-Gerin, J.-P. *Radiat. Res.* **2001**, *155*, 269.

(32) Muroya, Y.; Meesungnoen, J.; Jay-Gerin, J.-P.; Filali-Mouhim, A.; Goulet, T.; Katsumura, Y.; Mankhetkorn, S. *Can. J. Chem.* **2002**, *80*, 1367.

(33) Michaud, M.; Wen, A.; Sanche, L. *Radiat. Res.* **2003**, *159*, 3.

(34) Goulet, T.; Jay-Gerin, J.-P.; Frongillo, Y.; Cobut, V.; Fraser, M.-J. *J. Chim. Phys.* **1996**, *93*, 111.

(35) Bartels, D. M.; Cook, A. R.; Mudaliar, M.; Jonah, C. D. *J. Phys. Chem. A* **2000**, *104*, 1686.

(36) Muroya, Y.; Lin, M.; Wu, G.; Iijima, H.; Yoshii, K.; Ueda, T.; Kudo, H.; Katsumura, Y. *Radiat. Phys. Chem.* **2005**, *72*, 169.

(37) Pimblott, S. M.; LaVerne, J. A.; Bartels, D. M.; Jonah, C. D. *J. Phys. Chem.* **1996**, *100*, 9412.

(38) Pastina, B.; LaVerne, J. A.; Pimblott, S. M. *J. Phys. Chem. A* **1999**, *103*, 5841.

(39) Schwarz, H. A. *J. Phys. Chem.* **1969**, *73*, 1928.

(40) LaVerne, J. A.; Pimblott, S. M. *J. Phys. Chem.* **1991**, *95*, 3196.

(41) Subexcitation electrons are those that have kinetic energies lower than the first electronic excitation threshold of the medium (~7.3 eV in liquid water, see: Michaud, M.; Cloutier, P.; Sanche, L. *Phys. Rev. A* **1991**, *44*, 5624). They lose energy relatively slowly, the dominant mode of energy loss being the excitation of molecular vibrations. See, for example, ref 9.

(42) Goulet, T.; Patau, J. P.; Jay-Gerin, J.-P. *J. Phys. Chem.* **1990**, *94*, 7312; *Radiat. Prot. Dosim.* **1990**, *31*, 33.

(43) Pimblott, S. M.; LaVerne, J. A. *J. Phys. Chem. A* **1997**, *101*, 5828.

(44) Pimblott, S. M.; Mozumder, A. In *Charged Particle and Photon Interactions with Matter. Chemical, Physicochemical, and Biological Consequences with Applications*; Mozumder, A., Hatano, Y., Eds.; Marcel Dekker: New York, 2004; p 75.

(45) Our average electron thermalization distance of ~11.7 nm should be compared with $\langle r \rangle = 2\sqrt{2}\,\sigma/\sqrt{\pi}$, where σ is the width of the three-dimensional Gaussian distribution that describes the local spatial distribution of e^-_{aq} in deterministic "average" spur models of liquid water radiolysis by low-LET radiation (see: Goulet, T.; Jay-Gerin, J.-P. *Radiat. Res.* **1989**, *118*, 46). Most recent estimations of σ are 4–5 nm (refs 10 and 43) and 5.2 nm (ref 44). This relatively large average electron thermalization distance value comes from the presence of a long tail in our simulated distribution of thermalization distances, which indicates that a number of electrons travel large distances (up to ~40 nm) from subexcitation to thermal energies (refs 28 and 34).

(46) Bartels, D. M.; Gosztola, D.; Jonah, C. D. *J. Phys. Chem. A* **2001**, *105*, 8069.

(47) Cobut, V.; Jay-Gerin, J.-P.; Frongillo, Y.; Patau, J. P. *Radiat. Phys. Chem.* **1996**, *47*, 247.

(48) Melton, C. E. *J. Chem. Phys.* **1972**, *57*, 4218.

(49) Severs, J. C.; Harris, F. M.; Andrews, S. R.; Parry, D. E. *Chem. Phys.* **1993**, *175*, 467.

(50) *CRC Handbook of Chemistry and Physics*, 84th ed.; Lide, D. R., Ed.; CRC Press: Boca Raton, FL, 2003.

(51) Rudd, M. E. *Radiat. Prot. Dosim.* **1990**, *31*, 17. See also: Rudd, M. E.; Kim, Y.-K.; Madison, D. H.; Gay, T. J. *Rev. Mod. Phys.* **1992**, *64*, 441.

(52) See, for example: ICRU Report 55. *Secondary Electron Spectra from Charged Particle Interactions*; International Commission of Radiation Units and Measurements: Bethesda, MD, 1996. Inokuti, M. *Rev. Mod. Phys.* **1971**, *43*, 297.

(53) LaVerne, J. A. *Radiat. Phys. Chem.* **1989**, *34*, 135.

(54) The principle of this method to measure $HO_2^{\bullet}$ is to generate molecular oxygen by the reaction of $HO_2^{\bullet}$ with cupric ion (see: Hart, E. J. *Radiat. Res.* **1955**, *2*, 33. Donaldson, D. M.; Miller, N. *Trans. Faraday Soc.* **1956**, *52*, 652). It should be noted here that any primary molecular oxygen, produced directly or by track reactions, will also be measured using this method. Hence, the yields generally quoted for $HO_2^{\bullet}$ in the literature also include O_2. See refs 11 and 17.

(55) Watt, D. E. *Quantities for Dosimetry of Ionizing Radiations in Liquid Water*; Taylor and Francis: London, 1996. Note that, for $^{20}Ne^{9+}$ ions, we have used the stopping-power compilations of Northcliffe and Schilling (Northcliffe, L. C.; Schilling, R. F. *Nucl. Data Tables A* **1970**, *7*, 233), as suggested by LaVerne et al. (ref 19).

(56) Pimblott, S. M.; LaVerne, J. A. *J. Phys. Chem. A* **2002**, *106*, 9420.

(57) Kuppermann, A. In *Radiation Research: Proceedings of the Third International Congress of Radiation Research, Cortina d'Ampezzo, Italy, June 26-July 2, 1966*; Silini, G., Ed.; North-Holland Publishing Co.: Amsterdam, 1967; p 212.

(58) Gardès-Albert, M.; Jore, D.; Abedinzadeh, Z.; Rouscilles, A.; Deycard, S.; Bouffard, S. *J. Chim. Phys.* **1996**, *93*, 103.

(59) Olivera, G. H.; Caraby, C.; Jardin, P.; Cassimi, A.; Adoui, L.; Gervais, B. *Phys. Med. Biol.* **1998**, *43*, 2347.

(60) Taube, H. *Trans. Faraday Soc.* **1957**, *53*, 656.

(61) Biedenkapp, D.; Hartshorn, L. G.; Bair, E. J. *Chem. Phys. Lett.* **1970**, *5*, 379.

(62) Amichai, O.; Treinin, A. *Chem. Phys. Lett.* **1969**, *3*, 611.

(63) Clifford, P.; Green, N. J. B.; Oldfield, M. J.; Pilling, M. J.; Pimblott, S. M. *J. Chem. Soc., Faraday Trans. 1* **1986**, *82*, 2673. Pimblott, S. M.; Pilling, M. J.; Green,

N. J. B. *Radiat. Phys. Chem.* **1991**, *37*, 377. Pimblott, S. M.; Green, N. J. B. *Res. Chem. Kinet.* **1995**, *3*, 117.

(64) Goulet, T.; Fraser, M.-J.; Frongillo, Y.; Jay-Gerin, J.-P. *Radiat. Phys. Chem.* **1998**, *51*, 85.

(65) Lundström, T.; Christensen, H.; Sehested, K. *Radiat. Phys. Chem.* **2004**, *69*, 211.

(66) Bjergbakke, E.; Draganić, Z. D.; Sehested, K.; Draganić, I. G. *Radiochim. Acta* **1989**, *48*, 65.

(67) Buxton, G. V.; Greenstock, C. L.; Helman, W. P.; Ross, A. B. *J. Phys. Chem. Ref. Data* **1988**, *17*, 513.

(68) Jiang, P.-Y.; Katsumura, Y.; Nagaishi, R.; Domae, M.; Ishikawa, K.; Ishigure, K.; Yoshida, Y. *J. Chem. Soc. Faraday Trans.* **1992**, *88*, 1653.

(69) Goldstein, S.; Czapski, G.; Cohen, H.; Meyerstein, D. *Inorg. Chim. Acta* **1992**, *192*, 87.

(70) Tang, Y.; Thorn, R. P.; Mauldin III, R. L.; Wine, P. H. *J. Photochem. Photobiol. A* **1988**, *44*, 243.

(71) Chen, R.; Avotinsh, Y.; Freeman, G. R. *Can. J. Chem.* **1994**, *72*, 1083.

(72) Neta, P.; Huie, R. E.; Ross, A. B. *J. Phys. Chem. Ref. Data* **1988**, *17*, 1027.

(73) Cabelli, D. E.; Bielski, B. H. J.; Holcman, J. *J. Am. Chem. Soc.* **1987**, *109*, 3665.

(74) Bielski, B. H. J.; Cabelli, D. E.; Arudi, R. L.; Ross, A. B. *J. Phys. Chem. Ref. Data* **1985**, *14*, 1041.

(75) Bjergbakke, E.; Sehested, K.; Rasmussen, O. L. *Radiat. Res.* **1976**, *66*, 433.

(76) Johnson, G. R. A.; Nazhat, N. B. *J. Chem. Soc., Faraday Trans. 1* **1984**, *80*, 3455.

(77) Gogolev, A. V.; Shilov, V. P.; Fedoseev, A. M.; Pikaev, A. K. *Mendeleev Commun.* **1993**, 155.

(78) See, for example: Robinson, R. A.; Stokes, R. H. *Electrolyte Solutions. The Measurement and Interpretation of Conductance, Chemical Potential and Diffusion in Solutions of Simple Electrolytes*, 2nd ed. (revised); Butterworths Publications Ltd.: London, 1959; p 229.

(79) A detailed description of our simulations of the radiolysis of aqueous solutions under acidic conditions will be given elsewhere.

(80) See, for example: Latimer, C. J. *Adv. At. Mol. Opt. Phys.* **1993**, *30*, 105.

(81) Baldacchino, G.; Bouffard, S.; Balanzat, E.; Gardès-Albert, M.; Abedinzadeh, Z.; Jore, D.; Deycard, S.; Hickel, B. *Nucl. Instrum. Methods Phys. Res. B* **1998**, *146*, 528.

(82) Wasselin-Trupin, V.; Baldacchino, G.; Bouffard, S.; Hickel, B. *Radiat. Phys. Chem.* **2002**, *65*, 53.

(83) Elliot, A. J.; Chenier, M. P.; Ouellette, D. C.; Koslowsky, V. T. *J. Phys. Chem.* **1996**, *100*, 9014.

(84) LaVerne, J. A. In *Radiation Research: Proceedings of the 11th International Congress of Radiation Research, Dublin, Ireland, July 18-23, 1999*, Vol. 2; Moriarty, M., Mothersill, C., Seymour, C., Edington, M., Ward, J. F., Fry, R. J. M., Eds.; Allen Press: Lawrence, KS, 2000; p 46.

(85) For kinetic energies of ions small compared to their rest-mass energy, the nonrelativistic Bethe stopping power equation (see: Bethe, H. A.; Ashkin, J. In *Experimental Nuclear Physics*, Vol. 1; Segrè, E., Ed.; Wiley: New York, 1953; p 166) is well approximated by (in SI units):

$$-\frac{dE}{dx} = \left(\frac{1}{4\pi\varepsilon_0}\right)^2 \frac{4\pi Z^2 e^4}{m_0 V^2} N \ln\left(\frac{2m_0 V^2}{I}\right),$$

where Ze is the charge on the incident ion, V is the ion velocity, m_0 is the rest mass of an electron, N is the number of electrons per m^3 of the absorbing medium, and I is the mean excitation and ionization potential of the bound electrons in the absorber (for liquid water, $I = 79.7 \pm 0.5$ eV, see: Bichsel, H.; Hiraoka, T. *Nucl. Instrum. Methods*

Phys. Res. B **1992**, *66*, 345). It follows from this equation that for two different ions of equal LET, the one with the higher charge will have the higher velocity.

(86) Schuler, R. H.; Allen, A. O. *J. Am. Chem. Soc.* **1957**, *79*, 1565.

(87) Sauer, M. C., Jr.; Schmidt, K. H.; Hart, E. J.; Naleway, C. A.; Jonah, C. D. *Radiat. Res.* **1977**, *70*, 91.

(88) Naleway, C. A.; Sauer, M. C., Jr.; Jonah, C. D.; Schmidt, K. H. *Radiat. Res.* **1979**, *77*, 47.

(89) Kaplan, I. G.; Miterev, A. M. In *Advances in Chemical Physics*, Vol. 68; Prigogine, I., Rice, S. A., Eds.; Wiley: New York, 1987; p 255.

(90) Ferradini, C. In *Actions Biologique et Chimique des Radiations Ionisantes*, Vol. 1; Tilquin, B., Ed.; Éditions Ciaco: Bruxelles, 1990; p 52.

(91) Mozumder, A.; Magee, J. L. *Radiat. Res.* **1966**, *28*, 203; *J. Chem. Phys.* **1966**, *45*, 3332.

(92) We recall here that, like molecular oxygen, the free oxygen atom is a biradical and has two unpaired electrons.

(93) Sims, H. E.; Ashmore, C. B.; Tait, P. K.; Walters, W. S. In *Proceedings of JAIF (Japan Atomic Industrial Forum, Inc.) International Conference on Water Chemistry in Nuclear Power Plants, Kashiwazaki, Japan, October 13-16, 1998*; p 894.

(94) LaVerne, J. A.; Yoshida, H. *J. Phys. Chem.* **1993**, *97*, 10720.

(95) Bisby, R. H.; Cundall, R. B.; Sims, H. E.; Burns, W. G. *Faraday Discuss. Chem. Soc.* **1977**, *63*, 237.

(96) Baverstock, K. F.; Cundall, R. B.; Burns, W. G. In *Proceedings of the Third Tihany Symposium on Radiation Chemistry, Balatonfüred-Tihany, Hungary, May 10-15, 1971*, Vol. 2; Dobó, J., Hedvig, P., Eds.; Akadémiai Kiadó: Budapest, 1972; p 1133.

(97) Boyle, J. W.; Hochanadel, C. J.; Sworski, T. J.; Ghormley, J. A.; Kieffer, W. F. In *Proceedings of the International Conference on the Peaceful Uses of Atomic*

Energy, Geneva, Switzerland, August 1955, Vol. 7, P/741; United Nations: New York, 1956; p 576.

(98) Steele, L. R.; Gordon, S.; Dryden, C. K. *Nucl. Sci. Eng.* **1963**, *15*, 458.

(99) Meesungnoen, J.; Jay-Gerin, J.-P.; Filali-Mouhim, A.; Mankhetkorn, S. *Chem. Phys. Lett.* **2001**, *335*, 458.

(100) See, for example: Hall, E. J. *Radiobiology for the Radiologist*, 5th ed.; Lippincott Williams & Wilkins: Philadelphia, 2000; p 91.

(101) We can cite here the elegant work of Barendsen et al. (Barendsen, G. W.; Koot, C. J.; van Kersen, G. R.; Bewley, D. K.; Field, S. B.; Parnell, C. J. *Int. J. Radiat. Biol.* **1966**, *10*, 317), who used cultured cells of human origin to investigate the OER for a wide range of radiation types. These authors showed that as the LET increases, the OER falls slowly at first, from ~2.6 to 2.05 between ~5.6 and 61 keV/μm, after which the OER decreases more rapidly and approaches unity at an LET value of ~165 keV/μm.

(102) Alper, T.; Bryant, P. E. *Int. J. Radiat. Biol.* **1974**, *26*, 203. Bryant, P.E.; Alper, T. In *Proceedings of the 5th Symposium on Microdosimetry, Verbania Pallanza, Italy, September 22-26, 1975*, Report EUR 5452 d-e-f; Booz, J., Ebert, H. G., Smith, B. G. R., Eds.; Commission of the European Communities: Luxembourg, 1976; p 871.

(103) Neary, G. J. *Int. J. Radiat. Biol.* **1965**, *9*, 477. See also: Swallow, A. J.; Velandia, J. A. *Nature* **1962**, *195*, 798.

(104) Baverstock, K. F.; Burns, W. G. *Radiat. Res.* **1981**, *86*, 20.

(105) Stuglik, Z. *Radiat. Res.* **1995**, *143*, 1995. See also, for example: Michael, B. D.; Prise, K. M. *Int. J. Radiat. Biol.* **1996**, *69*, 351. Frankenberg-Schwager, M.; Frankenberg, D.; Harbich, R.; Beckonert, S. *Radiat. Environ. Biophys.* **1994**, *33*, 1. Kiefer, J. *Biological Radiation Effects*; Springer-Verlag: Berlin, 1990; p 157. Jonah, C. D. *Radiat. Res.* **1985**, *104*, S-47. Sauer, M. C., Jr.; Schmidt, K. H.; Jonah, C. D.; Naleway, C. A.; Hart, E. J. *Radiat. Res.* **1978**, *75*, 519.

(106) Lefort, M. In *Actions Chimiques et Biologiques des Radiations*, Vol. 1; Haïssinsky, M., Ed.; Masson: Paris, 1955; p 93, and references cited therein.

(107) Allen, A. O. *Radiat. Res. Suppl.* **1964**, *4*, 54.

(108) Burns, W. G.; May, R.; Baverstock, K. F. *Radiat. Res.* **1981**, *86*, 1.

(109) LaVerne, J. A.; Schuler, R. H. *J. Phys. Chem.* **1996**, *100*, 16034.

(110) Senvar, C. B.; Hart, E. J. In *Proceedings of the Second United Nations International Conference on the Peaceful Uses of Atomic Energy, Geneva, Switzerland, September 1-13, 1958*, Vol. 29, P/1128; United Nations: Geneva, 1958; p 19.

(111) Examination of the material balance equation between the "reducing" (e^-_{aq}, $H^\bullet$, and H_2) and "oxidizing" ($^\bullet OH$, H_2O_2, $HO_2^\bullet/O_2^{\bullet-}$, O_2, etc.) species formed in the decomposition of pure, deaerated liquid water can also serve as a criterion for a consistent set of *G*-values. Under high-LET, heavy-ion irradiation conditions, this equation (refs 11 and 30):

$$G_{e^-_{aq}} + G_{H^\bullet} + 2\,G_{H_2} = G_{^\bullet OH} + 2\,G_{H_2O_2} + 3\,G_{HO_2^\bullet/O_2^{\bullet-}} + 4\,G_{O_2} + \ldots$$

is found to be well satisfied by the results of our simulations throughout the range of LET values studied here.

(112) Interestingly, Brown et al. (Brown, W. G.; Hart, E. J.; Sauer, M. C., Jr. *Radiat. Res.* **1978**, *76*, 533) measured the production of the $O(^3P)$ atom in the radiolysis of water by 20-MeV $^2H^+$ (LET ~ 10 keV/μm) and 40-MeV $^4He^{2+}$ (LET ~ 37 keV/μm) ions, using the reaction of $O(^3P)$ with cyclopentene. The values that these authors obtained for $G[O(^3P)]$ are ~0.0047 and 0.0045 molec./100 eV for deuterons and helium ions, respectively. They also estimated the characteristic time of their measurements (inverse of the cyclopentene scavenging power) to be ~5×10^{-8} s. These experimental data can directly be compared with the results of our simulations. In fact, when the multiple ionization of water is included in the calculations, we find that, at 5×10^{-8} s, $G[O(^3P)] \approx 0.0094$ and 0.0048 molec./100 eV for ~10-keV/μm $^2H^+$ and ~37-keV/μm

$^4He^{2+}$ ions, respectively. Judging from the reported experimental errors (measured yields may be on the order of 15% too low), these results are in remarkable agreement with Brown et al.'s experiments.

(113) We have found by independent simulations incorporating the sole mechanism of double ionization of water molecules that triply and quadruply charged water ions make in fact a negligible contribution to G_{O_2} under the conditions $\sigma_{ti} = \alpha^2 \sigma_{si}$ and $\sigma_{qi} = \alpha^3 \sigma_{si}$ (where $\sigma_{di}/\sigma_{si} = \alpha < 0.5$) adopted in this study (data not shown).

(114) See, for example: Zander, R. In *Proceedings of the Second International Symposium on Oxygen Transport to Tissue, Mainz, Germany, March 12-14, 1975*; Grote, J., Reneau, D. D., Thews, G., Eds.; Plenum Press: New York, 1976; p 463. Halliwell, B.; Gutteridge, J. M. C. *Free Radicals in Biology and Medicine*, 3rd ed.; Oxford University Press: Oxford, 1999; p 1. von Sonntag, C. *Free-Radical-Induced DNA Damage and its Repair – A Chemical Perspective*; Springer-Verlag: Berlin, 2006.

IV. Article No. 3

In this chapter, we investigate the effects of multiple ionization of water on the primary yield of H_2O_2 in the radiolysis of deaerated 0.4 *M* sulfuric acid aqueous solutions by $^{12}C^{6+}$ and $^{20}Ne^{9+}$ ions as a function of LET up to ~900 keV/μm at 25 °C. Our calculated values of $G_{H_2O_2}$ are compared with available experimental data for various radiation types and energies at pH 0.46 and with the corresponding H_2O_2 escape yields obtained at high LET in air-free, neutral liquid water.

This work is presented in the following article, entitled: "**Effect of multiple ionization on the yield of H_2O_2 produced in the radiolysis of aqueous 0.4 *M* H_2SO_4 solutions by high-LET $^{12}C^{6+}$ and $^{20}Ne^{9+}$ ions**", by J. Meesungnoen and J.-P. Jay-Gerin.

This article is published in *Radiation Research*, Vol. **164**, Issue 5, Pages 688-694 (November 2005).

Effect of multiple ionization on the yield of H_2O_2 produced in the radiolysis of aqueous 0.4 *M* H_2SO_4 solutions by high-LET $^{12}C^{6+}$ and $^{20}Ne^{9+}$ ions

by

Jintana Meesungnoen and Jean-Paul Jay-Gerin[1]

Département de Médecine Nucléaire et de Radiobiologie, Faculté de Médecine et des Sciences de la Santé, Université de Sherbrooke, 3001, 12ème Avenue Nord, Sherbrooke (Québec) J1H 5N4, Canada

Manuscript category: **"Regular paper"**

Number of figures: **2**

Number of footnotes: **11**

Running head: **H_2O_2 yield from ion radiolysis of acidic solutions**

[1] *Address for correspondence*:

Prof. Jean-Paul Jay-Gerin
Département de Médecine Nucléaire et de Radiobiologie
Faculté de Médecine et des Sciences de la Santé
Université de Sherbrooke
3001, 12ème Avenue Nord,
Sherbrooke (Québec) J1H 5N4
Canada

Tel. (1) (819) 346-1110, ext.
Fax: (1) (819) 564-5442
E-mail address:

Radiation Research **164**, 688-694 (2005)

Meesungnoen, J. and Jay-Gerin, J.-P. Effect of Multiple Ionization on the Yield of H_2O_2 Produced in the Radiolysis of Aqueous 0.4 *M* H_2SO_4 Solutions by High-LET $^{12}C^{6+}$ and $^{20}Ne^{9+}$ Ions. *Radiat. Res.*

ABSTRACT

Monte Carlo track structure simulations were performed to investigate the effect of multiple ionization of water on the primary (or "escape") (at ~10^{-6} s) yield of hydrogen peroxide ($G_{H_2O_2}$) produced in the radiolysis of deaerated 0.4 *M* H_2SO_4 solutions by $^{12}C^{6+}$ and $^{20}Ne^{9+}$ ions at high linear energy transfer (LET) up to ~900 keV/μm. It was found that, upon incorporating the mechanisms of double, triple, and quadruple ionizations of water in the calculations, a quantitative agreement between theory and experiment can be obtained. The curve for $G_{H_2O_2}$ as a function of LET reaches a well-defined maximum of ~1.4 molecules/100 eV at ~180-200 keV/μm, in very good accord with the available experimental data. Our results also show that, for the highest LET values considered in this study, the H_2O_2 escape yields obtained in 0.4 *M* sulfuric acid solutions are about 45% higher in magnitude than those found in neutral water. Contrary to a recent assumption suggesting that the limiting value of $G_{H_2O_2}$ at infinite LET should be ~1 molecule/100 eV, somewhat similar for neutral and acidic water, our simulations show a clear decrease of the primary H_2O_2 yields with increasing LET at high LET, indicating that the question of the limiting value of $G_{H_2O_2}$ at very high LET for both neutral and acidic liquid water is still open.

Keywords: Liquid water, aqueous 0.4 *M* H_2SO_4 solutions, radiolysis, accelerated heavy ions, linear energy transfer, multiple ionization of water, Monte Carlo track structure simulations, hydrogen peroxide, radiolytic yields.

INTRODUCTION

The radiolysis of pure deaerated liquid water by low- or high-linear energy transfer (LET) radiation can be adequately described, under normal irradiation conditions, by the following *global* equation, written for an absorbed energy of 100 eV (*1-4*):

$$G_{-H_2O}\,H_2O \rightsquigarrow G_{e^-_{aq}}\,e^-_{aq} + G_{OH^-}\,OH^- + G_{H^+}\,H^+ + G_{H^\cdot}\,H^\cdot + G_{H_2}\,H_2 + G_{^\cdot OH}\,{}^\cdot OH + G_{H_2O_2}\,H_2O_2 + G_{HO_2^\cdot/O_2^{\cdot-}}\,HO_2^\cdot/O_2^{\cdot-} + G_{O_2}\,O_2 + \ldots, \quad (1)$$

where the coefficients G_X are the so-called primary free-radical and molecular yields ("long time" or "escape" yields), representing the numbers of the various radiolytic species X (e^-_{aq}, OH^-, H^+, $H^\cdot$, H_2, $^\cdot OH$, H_2O_2, $HO_2^\cdot/O_2^{\cdot-}$, O_2,...) that remain throughout the bulk of the solution at the end of the nonhomogeneous chemical stage,[2] that is, when the spur or track processes are complete (at ~10^{-6} s) after the initial energy deposition.[3,4] G_{-H_2O} denotes, at this stage, the corresponding yield of decomposition of water. From considerations of charge conservation and material balance between the "reducing" and "oxidizing" species, these primary yield values are connected by the equations (*3, 4, 7*):

$$G_{e^-_{aq}} = G_{H^+} - G_{OH^-}$$

$$G_{e^-_{aq}} + G_{H^\cdot} + 2\,G_{H_2} = G_{^\cdot OH} + 2\,G_{H_2O_2} + 3\,G_{HO_2^\cdot/O_2^{\cdot-}} + 4\,G_{O_2} + \ldots . \quad (2)$$

For low-LET, sparsely ionizing radiation such as ^{60}Co γ-rays, fast electrons and high-energy protons, molecular oxygen (O_2) formation is expected to be negligible, and the production of hydroperoxyl/superoxide anion ($HO_2^\cdot/O_2^{\cdot-}$, pK_a = 4.8) radicals can usually be ignored because its small yield of ~0.02 molec./100 eV (*8*) accounts for less than 1% of the other primary radiolytic species.

Under heavy-ion irradiation conditions, the general trends on increasing LET of the radiation are for free-radical yields to decrease and molecular yields to increase (*3, 6, 9, 10*). This is explained by the increased intervention of radical-radical reactions as the local concentration of radicals along the path of the impacting ion increases. In fact,

high-LET charged particles form an essentially continuous track of intense ionization and electronic excitation referred to as the track "core" surrounded by a region of radiation effects due to knocked-out secondary electrons (δ-rays) called the "penumbra" (*11, 12*). This should allow, as the LET increases, fewer radicals to escape combination and recombination reactions during the expansion of the tracks, and in turn the higher yields of molecular products. However, there are two important exceptions to this rule: (1) Unlike the behavior of other radicals, the primary yield of $HO_2^{\cdot}/O_2^{\cdot-}$ increases with increasing LET (*3, 6, 9, 13, 14*), and (2) the primary yield of H_2O_2 rises with increasing LET to a maximum, after which it falls (*9, 15*). These two peculiar behaviors of $G_{HO_2^{\cdot}/O_2^{\cdot-}}$ and $G_{H_2O_2}$ observed in the heavy-ion radiolysis of *neutral* water at high LET have been well reproduced recently by using Monte Carlo simulations that incorporate the mechanism of multiple ionization of water molecules (*4, 16, 17*). It was shown, in particular, that the maximum of $G_{H_2O_2}$ occurs precisely at the point where $G_{HO_2^{\cdot}/O_2^{\cdot-}}$ begins to rise sharply, suggesting, in agreement with experiments (*9*), that the yields of $HO_2^{\cdot}/O_2^{\cdot-}$ and H_2O_2 are closely linked (*4, 16*).

The purpose of this study was to examine further the dependence of $G_{H_2O_2}$ on LET. In fact, there is a large experimental scatter in hydrogen peroxide yields with increasing LET (*3, 6*). This uncertainty in H_2O_2 yields after exposure to high-LET radiation becomes even greater when pH effects are considered. However, a wide variety of studies indicate that, at a given LET, the production of H_2O_2 is *higher* in acidic solutions than in neutral solutions (*18*). For example, the values of $G_{H_2O_2}$ found for 5.3-MeV polonium α-particles in aqueous 0.4 *M* H_2SO_4 solutions (LET ~ 145 keV/μm) (*19-21*) are ~45-50% higher than the H_2O_2 escape yield value measured for 5-MeV $^4He^{2+}$ ions in a near neutral (pH 6.5) solution (*15*). For 10-MeV $^{12}C^{6+}$ ions (LET ~ 725 keV/μm), the data of LaVerne (*22*) in acidic solutions (0.4 *M* sulfuric acid) are also about 50% higher than those reported by Pastina and LaVerne (*15*) in neutral solutions. Even for ^{60}Co γ-rays (~0.3 keV/μm), the primary yield of H_2O_2 obtained in 0.4 *M* H_2SO_4 solutions is about 15% higher than that obtained in neutral liquid water (*18*). In contrast

with these results, LaVerne (*3*) recently suggested in a review article on the chemical effects of heavy-ion radiolysis of water that $G_{H_2O_2}$ should have a limiting value at infinite LET of ~1 molec./100 eV that is somewhat similar for neutral and acidic solutions. This conclusion was obtained, however, on the basis of a fit of different sets of measurements of $G_{H_2O_2}$ at high LET in *both* neutral and acidic (pH 0.46, 2, and 3) liquid water.

In the past four years, we have studied the influence of LET on $G_{H_2O_2}$ in irradiated liquid water at neutral pH and 25 and 300 °C in our laboratory by Monte Carlo track structure simulations using several different types of radiation, including $^{1}H^{+}$, $^{4}He^{2+}$, $^{12}C^{6+}$, and $^{20}Ne^{9+}$ ions, over a wide range of LET (*4, 16, 23, 24*). The primary yields of H_2O_2 produced in the radiolysis of deaerated 0.4 *M* H_2SO_4 aqueous solutions have also been calculated by Monte Carlo simulations as a function of LET, but only for the range ~0.3 to 6.5 keV/μm (*23*). In the present work, we extend this latter study to a wider range of LET up to ~900 keV/μm, using $^{12}C^{6+}$ and $^{20}Ne^{9+}$ ions of various incident energies as irradiating particles, with the aim of investigating the effect of multiple ionization of water molecules on $G_{H_2O_2}$ in the radiolysis of *acidic* (0.4 *M* H_2SO_4) solutions at high LET.

This paper deals only with results at 25 °C. A brief presentation of our simulation approach is given in the next section, followed by the results and their discussion. Conclusions are drawn in the final section.

MONTE CARLO SIMULATIONS

The radiolysis of liquid water has been modeled by using our Monte Carlo simulation code IONLYS-IRT (*4*). In brief, during the physical stage (< 10^{-15} s),[2] the energy deposition by the incident radiation and by all the secondary electrons that it has generated occurs through the slowing down of those particles through a variety of elastic and inelastic scattering processes, including ionization, electronic and vibrational excitation of single water molecules, and excitation of plasmon-type collective modes. The details

of our track structure simulation modeling and the scattering cross sections used have been given previously (see ref. *4* and references therein). To take into account the effects of multiple ionizations under high-LET heavy-ion impact, the model has been extended to incorporate double, triple, and quadruple ionization processes in single ion-water collisions (*4, 16, 17*). Ionizations of higher multiplicity are neglected since their occurrence is much less probable in the range of LET considered here. In this study, the values of the cross sections for the double ionization of water (σ_{di}) are deduced from the knowledge of the ratio $\alpha = \sigma_{di}/\sigma_{si}$ and Rudd's semi-empirical single ionization cross sections (σ_{si}) for proton impact on water vapor (*25*) adapted here to the liquid phase as described previously (*26*) and extended to collisions by any other ion projectile of the same velocity according to a Z^2 scaling law, where Z is the charge state of the ion [see, for example, ref. (*27*)]. Following the approach used in refs. (*4*) and (*16*), we have treated α in our simulations as an adjustable parameter chosen to get the best fit of the experimental values of ($G_{HO_2\cdot} + G_{O_2}$) as a function of LET in the radiolysis of air-free aqueous $FeSO_4$ (1 n*M*)–$CuSO_4$ (10 n*M*) solutions with $^{12}C^{6+}$ and $^{20}Ne^{9+}$ ions under acidic (0.005 *M* H_2SO_4) conditions (*13, 22, 28*).[5] As shown in our previous papers (*4, 16*), this approach offers an original tool to estimate the ratio σ_{di}/σ_{si} for heavy ion–water collisions in the *liquid* phase.[6] The values of α so obtained are shown in Fig. 1 of ref. (*4*) as a function of the ion energy per nucleon divided by the projectile charge state (E_{ion}/Z). As for the triple (σ_{ti}) and quadruple (σ_{qi}) ionizations, we assume that, for the range of impacting ion energies considered in this work, $\sigma_{ti} = \alpha^2\ \sigma_{si}$ and $\sigma_{qi} = \alpha^3\ \sigma_{si}$, where $\alpha < 0.5$ (*30*). We have also multiplied the total cross sections for all ion-induced interaction processes by an energy-dependent factor that constrains the LET of the irradiating ions to conform to the standard LET compilations (*31, 32*). Finally, at the incident ion energies of interest here, interactions involving electron capture and loss by the moving ion (charge-changing collisions) have been neglected (*33*).

The energy that has been so deposited in the medium is then used to produce the "initial" radical and molecular species of the radiolysis, distributed in a specific, highly

nonhomogeneous track structure that depends on the primary ion type and energy. The physicochemical stage ($\sim 10^{-15}$–10^{-12} s)[2] consists of the processes that lead to the establishment of thermal equilibrium in the bulk medium. Among those processes, the production of $HO_2^{\cdot}/O_2^{\cdot-}$ through the double ionization of water is assumed to involve oxygen atoms (*28, 34-36*) formed in their ^3P ground state (*17*), according to

$$H_2O^{2+} + 2\,H_2O \rightarrow 2\,H_3O^+ + O(^3P) \qquad \text{(R1)}$$

at very short times, followed by[7]

$$^{\cdot}OH + O(^3P) \rightarrow HO_2^{\cdot}. \qquad \text{(R2)}$$

For the triple and quadruple ionizations of water molecules, we assume that they lead directly to the formation of $HO_2^{\cdot}/O_2^{\cdot-}$ and molecular oxygen by acid-base re-equilibrations, respectively, according to the following overall reactions (*17*):

$$H_2O^{\cdot 3+} + 4\,H_2O \rightarrow 3\,H_3O^+ + HO_2^{\cdot} \qquad \text{(R3)}$$

and

$$H_2O^{4+} + 5\,H_2O \rightarrow 4\,H_3O^+ + O_2\,. \qquad \text{(R4)}$$

All of the events of the physical and physicochemical stages are handled by our IONLYS step-by-step simulation program that incorporates multiple ionization of water molecules as described above. The complex spatial distribution of reactants at the end of the physicochemical stage, which is provided as an output of this program, is then used directly as the starting point for the nonhomogeneous chemical stage.[2] This third and final stage, during which the various radiolytic species diffuse and react with one another (or with the environment) until all spur/track reactions are complete ($\sim 10^{-6}$ s),[3] is covered by our IRT program. This program employs the independent reaction times (IRT) method (*40, 41*) to model the chemical development that occurs during this stage and to simulate the formation of measurable product yields. Its detailed implementation has been given previously (*42*). Only slight adjustments have been made in some reaction rate constants and diffusion coefficients to take account of the latest data available

from the literature. The simulations of the radiolysis of the Fe^{2+}/Cu^{2+} system in deaerated 0.005 *M* H_2SO_4 aqueous solutions (pH 2.1) and of 0.4 *M* H_2SO_4 aqueous solutions (pH 0.46) are described elsewhere (*4, 23*).[8]

Finally, the influence of the LET on the yields of H_2O_2 produced in neutral water and in 0.4 *M* H_2SO_4 solutions at 25 °C has been investigated by varying the incident ion energy from ~300 to 1.25 MeV/nucleon (~12-604 keV/μm) for $^{12}C^{6+}$ and from ~300 to 3.2 MeV/nucleon (~25-938 keV/μm) for $^{20}Ne^{9+}$. The calculations are performed by simulating short (~1.5-50 μm) ion track segments, over which the energy and LET of the ion are well defined and remain nearly constant. Typically, ~10^4 to 4 × 10^5 reactive chemical species are generated in those simulated track segments (depending on ion type and energy), thus ensuring only small statistical fluctuations in the determination of average yields.

RESULTS AND DISCUSSION

Figure 1 displays our calculated values of $G_{H_2O_2}$ (at 10^{-6} s) as a function of LET for deaerated 0.4 *M* H_2SO_4 aqueous solutions irradiated by $^{12}C^{6+}$ and $^{20}Ne^{9+}$ ions up to ~900 keV/μm at 25 °C. Available experimental data for various radiation types and energies at pH 0.46 (*19-22, 43-57*) are also included in the figure. As can be seen, our curve for $G_{H_2O_2}$ as a function of LET for $^{12}C^{6+}$ ions[9] calculated without including the mechanism of multiple ionization of water increases continuously with increasing LET, in disagreement with experimental data, which indicate a decrease in $G_{H_2O_2}$ at high LET. However, when the double, triple, and quadruple ionizations of water molecules are incorporated in the simulations,[10] we find that the curve of $G_{H_2O_2}$ as a function of LET reaches a maximum around 180-200 keV/μm, after which it falls. This decrease of $G_{H_2O_2}$ observed for $^{12}C^{6+}$ ions at high LET is well confirmed by our curve for $G_{H_2O_2}$ as a function of LET for $^{20}Ne^{9+}$ ions calculated in the presence of the multiple ionization of water between ~700 and 938 keV/μm.[11] Furthermore, extrapolation of our H_2O_2 escape yield values to higher LET is seen to reproduce very well the yield of 0.96

molec./100 eV estimated for the radiolysis of 0.4 *M* H_2SO_4 solutions by dissolved ^{252}Cf fission recoil fragments with an LET close to ~4000 keV/μm (*43*). Overall, our $G_{H_2O_2}$ values so obtained are in good agreement with experiment.

For the sake of comparison, our corresponding calculated values of $G_{H_2O_2}$ as a function of LET for air-free, *neutral* liquid water (*4*) are also shown in Fig. 1, along with experimentally determined yields from the literature at pH 7 (*15, 58-62*). As can be seen, the well-defined maximum of ~1.4 molec./100 eV observed in $G_{H_2O_2}$ in the case of the radiolysis of 0.4 *M* sulfuric acid solutions is ~45% greater in magnitude than that found in neutral solutions. About the same difference also exists in our $G_{H_2O_2}$ values between acidic and neutral liquid water at the highest LET values considered. Such results differ from a recent assumption by LaVerne (*3*) suggesting that the limiting value of $G_{H_2O_2}$ at infinite LET should be ~1 molec./100 eV, somewhat similar for neutral and acidic water. In fact, since our simulations show a clear decrease of $G_{H_2O_2}$ with increasing LET at high LET, one could wonder whether the limit of H_2O_2 yields would not be zero for infinite LET. On the basis of the results presented in Fig. 1, however, predicting trends is difficult. In the absence of more experimental work or model studies for LET above 1000 keV/μm, we are led to conclude that the question of the limiting value of $G_{H_2O_2}$ at very high LET for both neutral and acidic liquid water is still open.

The variations of $G_{H_2O_2}$ with LET in the high-LET heavy-ion radiolysis of neutral liquid water and acidic solutions arise from the main reactions that account for the formation and decay of H_2O_2 in the nonhomogeneous chemical stage, namely:

$$^{\cdot}OH + {}^{\cdot}OH \rightarrow H_2O_2 \qquad \text{(R5)}$$

$$H^{\cdot} + HO_2^{\cdot} \rightarrow H_2O_2 \qquad \text{(R6)}$$

$$H_2O_2 + e_{aq}^{-} \rightarrow {}^{\cdot}OH + OH^{-} \qquad \text{(R7)}$$

$$H^{+} + HO_2^{-} \rightarrow H_2O_2 \qquad \text{(R8)}$$

$$H_2O_2 + OH^{-} \rightarrow HO_2^{-} + H_2O \qquad \text{(R9)}$$

$$HO_2^{-} + H_2O \rightarrow H_2O_2 + OH^{-}$$

The importance of these reactions can be quantified by the yield variations $\Delta G(H_2O_2)$ that they cause over the time interval ~10^{-12}–10^{-6} s. Figure 2 compares, for pure, deaerated liquid water and 0.4 *M* H_2SO_4 aqueous solutions irradiated by 24-MeV $^{12}C^{6+}$ ions (~500 keV/μm) at 25 °C, the time profiles of $\Delta G(H_2O_2)$ of each of these reactions when the double, triple, and quadruple ionizations of water molecules are included in the simulations. As can be seen in Fig. 2a, in neutral water, H_2O_2 is formed within the tracks almost entirely by the reaction (R5) of the 'OH with itself, whereas its decay is dominated by reaction (R7). However, in 0.4 *M* H_2SO_4 solutions, the removal of H_2O_2 due to the occurrence of reaction (R7) is decreased by almost 100% (Fig. 2b). Such a decrease can readily be explained by the fact that, at such a high acid concentration, the H^+ ions capture most, if not all, of the e^-_{aq} radicals in the spurs/tracks to form H' atoms (*18*):

$$e^-_{aq} + H^+ \rightarrow H^{\cdot} \qquad \text{(R10)}$$

Since e^-_{aq} reacts with H^+ in acidic solutions, this reaction competes with reaction (R7), leading to the survival of more H_2O_2 in the expanding spurs/tracks and therefore to an increase of $G_{H_2O_2}$ as compared with the primary H_2O_2 yield observed in neutral water (see Fig. 1).

CONCLUSIONS

In this study, we used Monte Carlo track structure simulations to investigate the effect of multiple ionization of water on the primary yield of H_2O_2 produced in the radiolysis of deaerated 0.4 *M* H_2SO_4 solutions by $^{12}C^{6+}$ and $^{20}Ne^{9+}$ ions at high LET up to ~900 keV/μm at 25 °C. Taking into account the double, triple, and quadruple ionizations of water molecules, a quantitative agreement was obtained between our calculated yields and the available experimental data. In particular, our results predict a maximum in the curve for $G_{H_2O_2}$ versus LET of ~1.4 molec./100 eV around 180-200 keV/μm, in remarkable accord with experiment. They also show that, for the highest LET values

considered in this study, the H_2O_2 escape yields obtained in 0.4 *M* H_2SO_4 solutions are about 45% greater in magnitude than those found in neutral water. In contrast to a recent assumption suggesting that the limiting value of $G_{H_2O_2}$ at infinite LET should be ~1 molec./100 eV, somewhat similar for neutral and acidic water, our simulations show a clear decrease of $G_{H_2O_2}$ with increasing LET at high LET, indicating that the question of the limiting value of $G_{H_2O_2}$ at infinite LET for both neutral and acidic liquid water is still open. Further experiments on the H_2O_2 yields at very high LET are needed to help clarify this question. Finally, it is worthwhile noting that, under the conditions of this study, triply and quadruply charged water ions make only a minor contribution to $G_{H_2O_2}$. In other words, the mechanism of double ionization of water is found to largely predominate at high LET, whereas it is insignificant at low LET.

The good overall agreement found between calculated and experimental H_2O_2 yields largely corroborates our previous results in refs. *4* and *16*, giving strong support to the validity and consistency of the model used in this study and in turn to the importance of the role of multiple ionization in the radiolysis of water under high-LET irradiation conditions.

ACKNOWLEDGMENTS

We thank Dr. Norman V. Klassen (National Research Council of Canada, Ottawa) for helpful suggestions on the manuscript. We would also like to thank the "Réseau québécois de calcul de haute performance" (RQCHP) for providing generous computing facilities. The financial assistance of the Natural Sciences and Engineering Research Council of Canada (Grant No. 9020-04) is gratefully acknowledged.

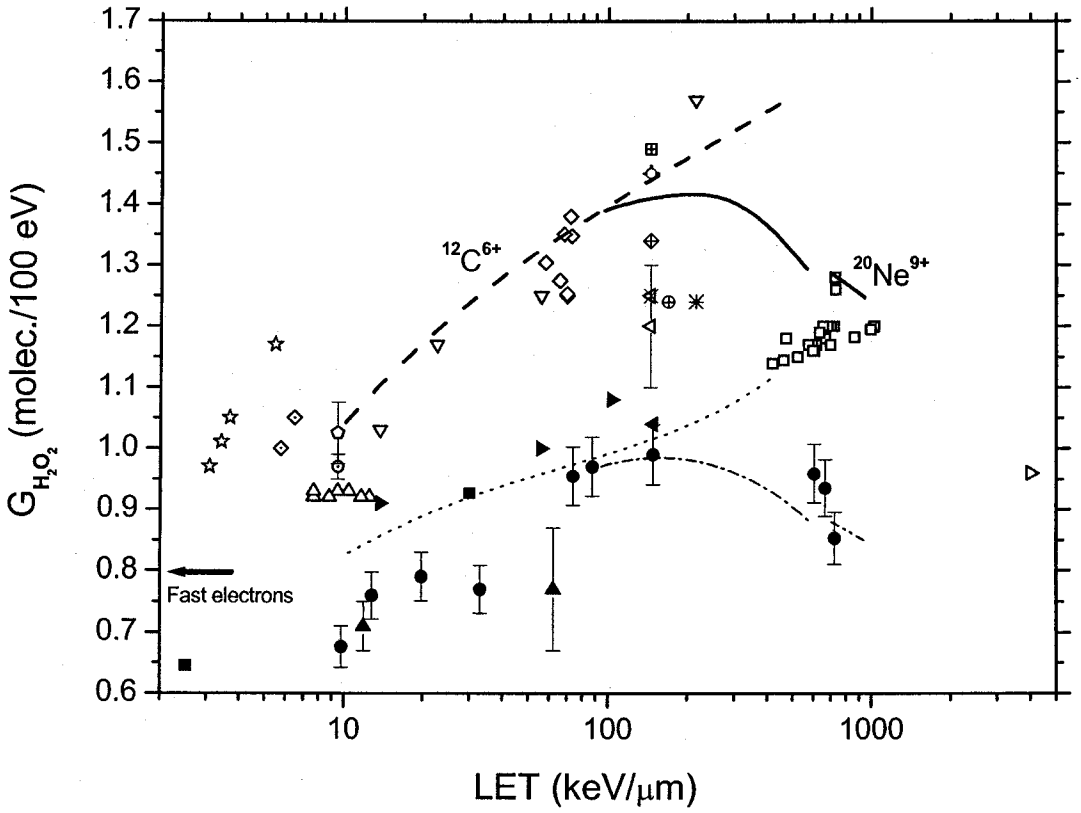

Figure 1: Variation of the primary H_2O_2 yield ($G_{H_2O_2}$) (in molec./100 eV) of the radiolysis of deaerated 0.4 *M* H_2SO_4 aqueous solutions (pH 0.46) by $^{12}C^{6+}$ and $^{20}Ne^{9+}$ ions as a function of LET up to ~900 keV/μm at 25 °C. The solid lines represent the results of our Monte Carlo simulations incorporating the double, triple, and quadruple ionizations of water molecules, obtained at 10^{-6} s (see text). The dashed line corresponds to our $G_{H_2O_2}$ values for impacting $^{12}C^{6+}$ ions calculated as a function of LET without including the mechanism of multiple ionization of water (corresponding results for $^{20}Ne^{9+}$ are not shown in the figure for clarity; see footnote 9). For the sake of comparison, our primary H_2O_2 yields of the radiolysis of deaerated neutral liquid water by $^{12}C^{6+}$ (dash-dot line) and $^{20}Ne^{9+}$ (dash-dot-dot line) ions, calculated when multiple ionization of water is incorporated in the simulations (see ref. *4*), are also included in the figure. The dotted line corresponds to our results for $^{12}C^{6+}$ ions obtained in the absence of multiple ionization of water (see ref. *4*). Experimental yields in 0.4 *M* H_2SO_4 solutions: X-rays [(⟐), ref. *53*; (☆), refs. *55* and *56*], $^1H^+$ [(◇), ref. *47*; (△), ref. *51*], $^2H^+$ [(▽), ref. *46*], $^3H^+$ β-particles [(⊙), ref. *52*; (⬠), ref. *57*], $^4He^{2+}$ [(+), ref. *19*; (⊞), ref. *20*; (○), ref. *21*; (▽), ref. *46*; (⊕), ref. *48*; (⟐), ref. *49*; (×), ref. *50*; (◁), ref. *54*], $^{12}C^{6+}$

[(□), ref. *22*], ^{252}Cf fission fragments [(▷), ref. *43*], and $^{10}B(n, \alpha)^{7}Li$ recoils [(∗), refs. *44* and *45*; (▽), ref. *46*]. Experimental yields in neutral liquid water (closed symbols): $^{1}H^{+}$ [(●), ref. *15*; (■), ref. *58*], $^{2}H^{+}$ [(▲), ref. *59*; (▶), refs. *60* and *61*], $^{4}He^{2+}$ [(●), ref. *15*; (▶), refs. *60* and *61*; (◀), ref. *62*], $^{7}Li^{3+}$ [(▲), ref. *59*], and $^{12}C^{6+}$ [(●), ref. *15*; (■), ref. *58*]. The arrow represents the limiting primary H_2O_2 yield obtained with ^{60}Co γ-rays or fast electrons (~0.80 molec./100 eV) (*1, 2, 18*).

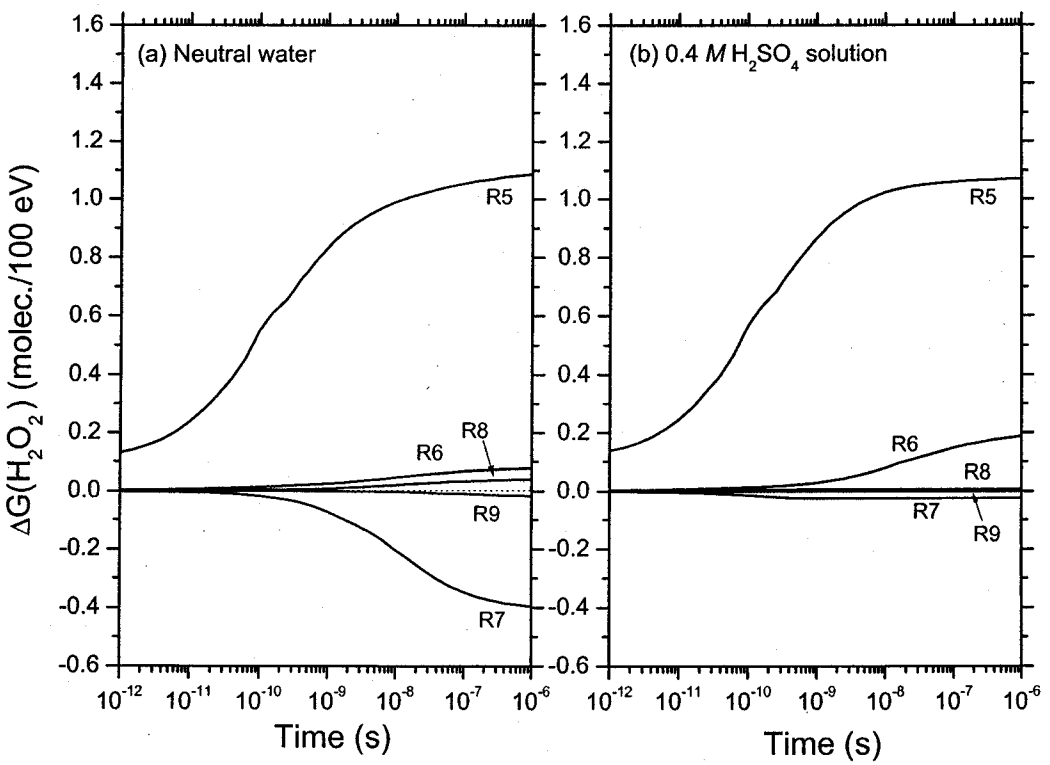

Figure 2: Time dependence of the extents $\Delta G(H_2O_2)$ (in molec./100 eV) of the main intratrack reactions (R5)-(R9) that are involved in the formation and decay of H_2O_2, calculated from our Monte Carlo simulations of the radiolysis of (a) neutral liquid water (see ref. *4*) and (b) 0.4 *M* H_2SO_4 aqueous solutions by 24-MeV $^{12}C^{6+}$ ions (~500 keV/μm) at 25 °C and in the time interval 10^{-12}–10^{-6} s, incorporating the mechanism of multiple ionization of water (see text).

REFERENCES

1. C. Ferradini and J.-P. Jay-Gerin, La radiolyse de l'eau et des solutions aqueuses: historique et actualité. *Can. J. Chem.* **77**, 1542-1575 (1999).

2. J. W. T. Spinks and R. J. Woods, *An Introduction to Radiation Chemistry*, 3rd ed. Wiley, New York, 1990.

3. J. A. LaVerne, Radiation chemical effects of heavy ions. In *Charged Particle and Photon Interactions with Matter. Chemical, Physicochemical, and Biological Consequences with Applications* (A. Mozumder and Y. Hatano, Eds.), pp. 403-429. Marcel Dekker, New York, 2004.

4. J. Meesungnoen and J.-P. Jay-Gerin, High-LET radiolysis of liquid water with $^{1}H^{+}$, $^{4}He^{2+}$, $^{12}C^{6+}$, and $^{20}Ne^{9+}$ ions: Effects of multiple ionization. *J. Phys. Chem. A* **109**, 6406-6419 (2005).

5. R. L. Platzman, The physical and chemical basis of mechanisms in radiation biology. In *Radiation Biology and Medicine. Selected Reviews in the Life Sciences* (W. D. Claus, Ed.), pp. 15-72. Addison-Wesley, Reading, MA, 1958.

6. D. R. McCracken, K. T. Tsang and P. J. Laughton, *Aspects of the Physics and Chemistry of Water Radiolysis by Fast Neutrons and Fast Electrons in Nuclear Reactors*. Report AECL-11895, Atomic Energy of Canada Ltd., Chalk River, Ontario, 1998.

7. M.-A. Hervé du Penhoat, T. Goulet, Y. Frongillo, M.-J. Fraser, P. Bernat and J.-P. Jay-Gerin, Radiolysis of liquid water at temperatures up to 300 °C: A Monte Carlo simulation study. *J. Phys. Chem. A* **104**, 11757-11770 (2000).

8. E. Bjergbakke and E. J. Hart, Oxygen formation in the γ-ray irradiation of Fe^{2+}-Cu^{2+} solutions. *Radiat. Res.* **45**, 261-273 (1971).

9. W. G. Burns and H. E. Sims, Effect of radiation type in water radiolysis. *J. Chem. Soc., Faraday Trans. 1* **77**, 2803-2813 (1981).

10. A. Appleby, Effect of early track structure on the radiation chemistry of water irradiated with heavy ions. *Radiat. Phys. Chem.* **34**, 121-127 (1989).

11. J. L. Magee and A. Chatterjee, Track reactions of radiation chemistry. In *Kinetics of Nonhomogeneous Processes. A Practical Introduction for Chemists, Biologists, Physicists, and Materials Scientists* (G. R. Freeman, Ed.), pp. 171-214. Wiley-Interscience, New York, 1987.

12. A. Mozumder, *Fundamentals of Radiation Chemistry*, pp. 41-69. Academic Press, San Diego, 1999.

13. J. A. LaVerne and R. H. Schuler, Track effects in radiation chemistry: Production of $HO_2^{\cdot}$ in the radiolysis of water by high-LET ^{58}Ni ions. *J. Phys. Chem.* **91**, 6560-6563 (1987).

14. G. Baldacchino, D. Le Parc, B. Hickel, M. Gardès-Albert, Z. Abedinzadeh, D. Jore, S. Deycard, S. Bouffard, V. Mouton and E. Balanzat, Direct observation of HO_2/O_2^- free radicals generated in water by a high-linear energy transfer pulsed heavy-ion beam. *Radiat. Res.* **149**, 128-133 (1998).

15. B. Pastina and J. A. LaVerne, Hydrogen peroxide production in the radiolysis of water with heavy ions. *J. Phys. Chem. A* **103**, 1592-1597 (1999).

16. J. Meesungnoen, A. Filali-Mouhim, N. Snitwongse Na Ayudhya, S. Mankhetkorn and J.-P. Jay-Gerin, Multiple ionization effects on the yields of $HO_2^{\cdot}/O_2^{\cdot-}$ and H_2O_2 produced in the radiolysis of liquid water with high-LET $^{12}C^{6+}$ ions: A Monte Carlo simulation study. *Chem. Phys. Lett.* **377**, 419-425 (2003).

17. C. Ferradini and J.-P. Jay-Gerin, Does multiple ionization intervene for the production of $HO_2^{\cdot}$ radicals in high-LET liquid water radiolysis? *Radiat. Phys. Chem.* **51**, 263-267 (1998).

18. C. Ferradini and J.-P. Jay-Gerin, The effect of pH on water radiolysis: A still open question. A minireview. *Res. Chem. Intermed.* **26**, 549-565 (2000).

19. M. Lefort and X. Tarrago, Radiolysis of water by particles of high linear energy transfer. The primary chemical yields in aqueous acid solutions of ferrous sulfate, and in mixtures of thallous and ceric ions. *J. Phys. Chem.* **63**, 833-836 (1959).

20. M. C. Anta and M. H. Mariano, Réduction des ions cériques sous rayonnement α. Influence de l'acide formique. *J. Chim. Phys.* **57**, 59-62 (1960).

21. J. Pucheault, Action des rayons alpha sur les solutions aqueuses. In *Actions Chimiques et Biologiques des Radiations* (M. Haïssinsky, Ed.), 5ème Série, pp. 31-84. Masson, Paris, 1961.

22. J. A. LaVerne, Radical and molecular yields in the radiolysis of water with carbon ions. *Radiat. Phys. Chem.* **34**, 135-143 (1989).

23. J. Meesungnoen, M. Benrahmoune, A. Filali-Mouhim, S. Mankhetkorn and J.-P. Jay-Gerin, Monte Carlo calculation of the primary radical and molecular yields of liquid water radiolysis in the linear energy transfer range 0.3-6.5 keV/μm: Application to ^{137}Cs gamma rays. *Radiat. Res.* **155**, 269-278 (2001).

24. J. Meesungnoen, J.-P. Jay-Gerin, A. Filali-Mouhim and S. Mankhetkorn, Monte Carlo calculation of the primary yields of H_2O_2 in the $^{1}H^{+}$, $^{2}H^{+}$, $^{4}He^{2+}$, $^{7}Li^{3+}$, and $^{12}C^{6+}$ radiolysis of liquid water at 25 and 300 °C. *Can. J. Chem.* **80**, 68-75 (2002).

25. M. E. Rudd, Cross sections for production of secondary electrons by charged particles. *Radiat. Prot. Dosim.* **31**, 17-22 (1990).

26. V. Cobut, Y. Frongillo, J. P. Patau, T. Goulet, M.-J. Fraser and J.-P. Jay-Gerin, Monte Carlo simulation of fast electron and proton tracks in liquid water. I. Physical and physicochemical aspects. *Radiat. Phys. Chem.* **51**, 229-243 (1998).

27. ICRU, *Secondary Electron Spectra from Charged Particle Interactions*. Report 55, International Commission on Radiation Units and Measurements, Bethesda, MD, 1996.

28. J. A. LaVerne, R. H. Schuler and W. G. Burns, Track effects in radiation chemistry: Production of $HO_2^{\cdot}$ within the track core in the heavy-particle radiolysis of water. *J. Phys. Chem.* **90**, 3238-3242 (1986).

29. E. J. Hart, Radiation chemistry of aqueous ferrous sulfate-cupric sulfate solutions. Effect of γ-rays. *Radiat. Res.* **2**, 33-46 (1955).

30. C. Champion, Multiple ionization of water by heavy ions: a Monte Carlo approach. *Nucl. Instrum. Methods Phys. Res. B* **205**, 671-676 (2003).

31. D. E. Watt, *Quantities for Dosimetry of Ionizing Radiations in Liquid Water.* Taylor and Francis, London, 1996.

32. L. C. Northcliffe and R. F. Schilling, Range and stopping-power tables for heavy ions. *Nucl. Data Tables* **A7**, 233-463 (1970).

33. S. M. Pimblott and J. A. LaVerne, Effects of track structure on the ion radiolysis of the Fricke dosimeter. *J. Phys. Chem. A* **106**, 9420-9427 (2002).

34. A. Kuppermann, Diffusion model of the radiation chemistry of aqueous solutions. In *Radiation Research: Proceedings of the Third International Congress of Radiation Research, Cortina d'Ampezzo, Italy, June 26-July 2, 1966* (G. Silini, Ed.), pp. 212-234. North-Holland Publishing Co., Amsterdam, 1967.

35. M. Gardès-Albert, D. Jore, Z. Abedinzadeh, A. Rouscilles, S. Deycard and S. Bouffard, Réduction du tétranitrométhane par les espèces primaires formées lors de la radiolyse de l'eau par des ions lourds Ar^{18+}. *J. Chim. Phys.* **93**, 103-110 (1996).

36. G. H. Olivera, C. Caraby, P. Jardin, A. Cassimi, L. Adoui and B. Gervais, Multiple ionization in the earlier stages of water radiolysis. *Phys. Med. Biol.* **43**, 2347-2360 (1998).

37. H. Taube, Photochemical reactions of ozone in solution. *Trans. Faraday Soc.* **53**, 656-665 (1957).

38. D. Biedenkapp, L. G. Hartshorn and E. J. Bair, The $O(^1D) + H_2O$ reaction. *Chem. Phys. Lett.* **5**, 379-380 (1970).

39. O. Amichai and A. Treinin, Chemical reactivity of $O(^3P)$ atoms in aqueous solution. *Chem. Phys. Lett.* **3**, 611-613 (1969).

40. P. Clifford, N. J. B. Green, M. J. Oldfield, M. J. Pilling and S. M. Pimblott, Stochastic models of multi-species kinetics in radiation-induced spurs. *J. Chem. Soc., Faraday Trans. 1*, **82**, 2673-2689 (1986).

41. S. M. Pimblott, M. J. Pilling and N. J. B. Green, Stochastic models of spur kinetics in water. *Radiat. Phys. Chem.* **37**, 377-388 (1991).

42. Y. Frongillo, T. Goulet, M.-J. Fraser, V. Cobut, J. P. Patau and J.-P. Jay-Gerin, Monte Carlo simulation of fast electron and proton tracks in liquid water. II. Nonhomogeneous chemistry. *Radiat. Phys. Chem.* **51**, 245-254 (1998).

43. N. E. Bibler, Radiolysis of 0.4 *M* sulfuric acid solutions with fission fragments from dissolved californium-252. Estimated yields of radical and molecular products that escape reactions in fission fragment tracks. *J. Phys. Chem.* **79**, 1991-1995 (1975).

44. J. Pucheault and P. Sigli, Réactions intratrajectoires dans la radiolyse de solutions aqueuses par les particules de recul de $^{10}B(n, \alpha)^7Li$. *Int. J. Radiat. Phys. Chem.* **8**, 613-619 (1976).

45. P. Sigli, C. Ferradini and J. Pucheault, Radiolyses de solutions aqueuses par des rayonnements à ionisations denses. II. Radioréductions de O_2 et de V^V induites par la réaction nucléaire $^{10}B(n, \alpha)^7Li$. *J. Chim. Phys.* **67**, 412-417 (1970).

46. N. F. Barr and R. H. Schuler, Dependence of radiation chemical yields on rate of energy loss: The yields of molecular and radical products from 0.8 *N* sulfuric acid solutions. *Radiat. Res.* **7**, 302-303 (1957).

47. R. Julien and J. Pucheault, Radiolyses de solutions aqueuses par des rayonnements à ionisations denses. III. Oxydation de Fe^{II} et réduction de Ce^{IV} dans les solutions

sulfuriques irradiées par des protons de faible énergie. *J. Chim. Phys.* **69**, 1561-1568 (1972).

48. A. R. Anderson and E. J. Hart, Molecular product and free radical yields in the decomposition of water by protons, deuterons, and helium ions. *Radiat. Res.* **14**, 689-704 (1961).

49. M. C. Anta, M. H. Mariano and M. L. Santos, Rendements de H_2O_2 lors de la radiolyse de solutions aqueuses par les rayons α de 5,3 MeV. *J. Chim. Phys.* **61**, 577-583 (1964).

50. M. H. Mariano and M. L. Santos, Radiolysis of dilute aerated sulfuric acid solutions with 5.3-MeV alpha particles. *Radiat. Res.* **32**, 905-914 (1967).

51. G. L. Kochanny, Jr., A. Timnick, C. J. Hochanadel and C. D. Goodman, Radiation chemistry studies of water as related to the initial linear energy transfer of 11-Mev to 23-Mev protons. *Radiat. Res.* **19**, 462-473 (1963).

52. E. Collinson, F. S. Dainton and J. Kroh, The radiation chemistry of aqueous solutions. II. Radical and molecular yields for tritium β-particles. *Proc. Roy. Soc. A* **265**, 422-429 (1962).

53. M. Lefort, Radiation chemistry. *Annu. Rev. Phys. Chem.* **9**, 123-156 (1958).

54. M. V. Vladimirova, Effect of α-radiation of Po on aqueous solutions (history of French and Russian research). *Czechoslovak J. Phys.* **49**, 493-497 (1999), Suppl. S1.

55. T. J. Hardwick, The effect of the energy of the ionizing electron on the yield in irradiated aqueous systems. *Discuss. Faraday Soc.* **12**, 203-211 (1952).

56. A. O. Allen, The yields of free H and OH in the irradiation of water. *Radiat. Res.* **1**, 85-96 (1954).

57. G. Lemaire, C. Ferradini and J. Pucheault, Radiolysis of water by tritium β rays: Scavenging of hydrogen peroxide precursors. *J. Phys. Chem.* **76**, 1542-1546 (1972).

58. V. Wasselin-Trupin, G. Baldacchino, S. Bouffard and B. Hickel, Hydrogen peroxide yields in water radiolysis by high-energy ion beams at constant LET. *Radiat. Phys. Chem.* **65**, 53-61 (2002).

59. A. J. Elliot, M. P. Chenier, D. C. Ouellette and V. T. Koslowsky, Temperature dependence of *g* values for aqueous solutions irradiated with 23 MeV $^{2}H^{+}$ and 157 MeV $^{7}Li^{3+}$ ion beams. *J. Phys. Chem.* **100**, 9014-9020 (1996).

60. A. Appleby and H. A. Schwarz, Radical and molecular yields in water irradiated by γ rays and heavy ions. *J. Phys. Chem.* **73**, 1937-1941 (1969).

61. H. A. Schwarz, J. M. Caffrey, Jr. and G. Scholes, Radiolysis of neutral water by cyclotron produced deuterons and helium ions. *J. Am. Chem. Soc.* **81**, 1801-1809 (1959).

62. J. A. LaVerne, Fundamental aspects of heavy-ion radiolysis. In *Radiation Research: Proceedings of the 11th International Congress of Radiation Research, Dublin, Ireland, July 18-23, 1999* (M. Moriarty, C. Mothersill, C. Seymour, M. Edington, J. F. Ward and R. J. M. Fry, Eds.), Vol. 2, pp. 46-48. Allen Press, Lawrence, KS, 2000.

FOOTNOTES

1. Address for correspondence: Département de médecine nucléaire et de radiobiologie, Faculté de médecine et des sciences de la santé, Université de Sherbrooke, Sherbrooke (Québec) J1H 5N4, Canada; e-mail: jean-paul.jay-gerin@USherbrooke.ca.

2. The division of the complex succession of events that follow absorption in matter of ionizing radiation into three, more or less distinct, consecutive, temporal stages (physical, physicochemical, and chemical) was first given by Platzman (*5*).

3. Strictly speaking, in nearly all high-LET, heavy-ion radiolysis studies, the yields are measured by reactions with solutes at a particular time or for a specific "scavenging capacity" (product of a solute's concentration and its rate constant for reaction with one species, in s^{-1}; the reciprocal of the scavenging power gives a measure of the time scale over which the scavenging is occurring). Up to now, modelers have tended to use values for yields that correspond to solute concentrations that scavenge primary species on a time scale of $\sim 10^{-6}$ s (concentrations that are involved in many experimental conditions) (*3, 6*).

4. Throughout this paper, radiation chemical yields (*G*-values) are expressed in the units of molecules per 100 eV (molec./100 eV). For conversion into SI units (mol/J): 1 molec./100 eV $\approx$ 0.10364 μmol/J (*1*).

5. The principle of this method to measure $HO_2^{\cdot}$ is to generate molecular oxygen by the reaction of $HO_2^{\cdot}$ with cupric ion (*29*). It should be noted here that any primary molecular oxygen, produced directly or by track reactions, will also be measured using this method. Hence the yields generally quoted for $HO_2^{\cdot}$ in the literature also include O_2. See ref. (*3*).

6. Very little is known yet about the values of the cross-sections for the multiple ionization of water molecules by high-LET heavy ions. To our knowledge, the only relevant work is that of Champion (*30*), who recently reported *n*-fold ioniza-

tion cross-section values for various heavy ions and gaseous targets, including water. No information is available for the liquid phase.

7. It should be recalled here that the O atoms produced in their singlet ^1D state react rapidly with water (*37*, *38*). In contrast, the ground-state O(^3P) atoms are rather inert to water (*37*, *39*) and will then react efficiently with $^{\bullet}OH$ radicals in the heavy particle track core because of the very high local concentration of radicals (*17*).

8. Note that, in our simulations, the *direct* action of ionizing radiation on HSO_4^- anions is neglected, which is a good approximation for 0.4 *M* sulfuric acid solutions. In fact, at this concentration of H_2SO_4, about 4% of the total energy expended in the solution is initially absorbed by direct action of the radiation on HSO_4^- rather than on H_2O.

9. Quite similarly to what we found previously for neutral liquid water (*4*), the curve for $G_{H_2O_2}$ as a function of LET for $^{20}Ne^{9+}$ ions calculated without including the mechanism of multiple ionization of water is very close (slightly lower) to that for $^{12}C^{6+}$ ions, especially below ~100-200 keV/μm, and has not been shown in Fig. 1 for the sake of clarity.

10. It is worth noting that independent simulations incorporating the sole mechanism of double ionization of water molecules have shown that triply and quadruply charged water ions in fact make only a minor contribution to $G_{H_2O_2}$ under the conditions adopted in this study (data not shown).

11. As explained in our previous study (*4*), our curve for $G_{H_2O_2}$ as a function of LET curve for $^{20}Ne^{9+}$ ions could not be extended below ~700 keV/μm due to a lack of experimental data of ($G_{HO_2^{\bullet}} + G_{O_2}$) in the radiolysis of the Fe^{2+}/Cu^{2+} aqueous system with high-energy $^{20}Ne^{9+}$ ions under acidic conditions (*13*, *28*).

V. Discussion

V.1. The radiolysis of liquid water at high LET

The results of our studies presented in Chapters II–IV clearly show that two radiolytic species play a major role in the high-LET, heavy-ion radiolysis of pure, deaerated liquid water, namely, $HO_2^{\bullet}$ and/or its conjugate base $O_2^{\bullet-}$ (bearing in mind that these radicals are produced in only very small yield from low-LET radiolysis), and O_2 (molecular oxygen formation is not observed at low LET). In particular, our calculations support the proposal of a substantial production of O_2 in the track of a heavy ion. Accordingly, under high-LET irradiation conditions, Eq. (7) of Chapter I (traditionally given for low-LET radiolysis of water) should be rewritten as follows:

$$G_{-H_2O}\ H_2O \rightsquigarrow G_{e^-_{aq}}\ e^-_{aq} + G_{H\cdot}\ H^{\bullet} + G_{\cdot OH}\ {}^{\bullet}OH + G_{H^+}\ H^+ + G_{OH^-}\ OH^-$$
$$+ G_{H_2}\ H_2 + G_{H_2O_2}\ H_2O_2 + G_{HO_2\cdot/O_2\cdot^-}\ HO_2^{\bullet}/O_2^{\bullet-} + G_{O_2}\ O_2 + \ldots \quad (1)$$

(with the same conventions as before). The overall electroneutrality and stoichiometry equations connecting these product yields then become

$$G_{e^-_{aq}} + G_{OH^-} = G_{H^+} \quad (2)$$

$$G_{e^-_{aq}} + G_{H\cdot} + 2G_{H_2} = G_{\cdot OH} + 2G_{H_2O_2} + 3G_{HO_2\cdot/O_2\cdot^-} + 4G_{O_2} + \ldots, \quad (3)$$

while the net yield of water decomposition is given by

$$G_{-H_2O} = G_{e^-_{aq}} + G_{H\cdot} + 2G_{H_2} - G_{HO_2\cdot/O_2\cdot^-} - 2G_{O_2} \quad (4)$$
$$= G_{\cdot OH} + 2G_{H_2O_2} + 2G_{HO_2\cdot/O_2\cdot^-} + 2G_{O_2}\,.$$

Of course, the material balance does not specify the source of hydroperoxyl/superoxide anion radicals and molecular oxygen. Our present Monte Carlo track structure simulations show that multiple ionization of water can successfully explain

both the large yields of $HO_2^{\bullet}/O_2^{\bullet-}$ and the excess O_2 produced in the heavy-ion radiolysis of water at high LET.

V.2. Multiple ionization cross sections and fate of multiply ionized water molecules

V.2.1. Cross sections for multiple ionization of water molecules

The successful Monte Carlo modeling of heavy-ion radiation effects in water relies on knowledge of the cross sections of all interaction processes. Multiple ionization (MI) of a single water molecule induced by swift heavy-ion impact has been observed in many circumstances (see Chapter I). However, a survey of the literature shows that most of experiments have been performed with ions in water vapor but not in *liquid* water, as measurements with liquid are either impractical or very difficult. As well, all existing heavy-ion cross-section calculations have been performed for water vapor. Due to this scarcity of reliable "condensed-phase" cross-section data, a quantitative description of multiple ionization effects in liquid water represents a challenging problem. In this work, however, in an effort to overcome these difficulties, we infer MI cross sections *indirectly* from measurements made in the liquid phase. As described in Chapters II and III, our strategy mainly consists in treating the ratio of the double-to-single ionization cross sections ($\alpha = \sigma_{di}/\sigma_{si}$, where σ_{si} is known) in our track simulations as an adjustable parameter chosen to best fit the available experimental data of ($G_{HO_2^{\bullet}} + G_{O_2}$) as a function of LET in the heavy-ion radiolysis of air-free aqueous $FeSO_4$–$CuSO_4$ solutions under acidic conditions (pH ~ 2.1) (LAVERNE et al., 1986; LAVERNE and SCHULER, 1987*b*). As for the triple and quadruple ionizations of water (which are shown, under the conditions of this study, to contribute only weakly to the production of $HO_2^{\bullet}/O_2^{\bullet-}$ and O_2), σ_{ti} and σ_{qi} are assumed to be equal to $\alpha^2\ \sigma_{si}$ and $\alpha^3\ \sigma_{si}$ ($\alpha < 0.5$), respectively, in accordance with the calculated ratios of

σ_j/σ_1 (where σ_j is the cross section for the ejection of j electrons) for collisions of various heavy ions on gas-phase H_2O molecules (CHAMPION, 2003; CHAMPION et al., 2005; GERVAIS et al., 2005, 2006). The values of α so obtained are shown in Fig. 1 for the four impacting ions used in this work (namely, $^{1}H^{+}$, $^{4}He^{2+}$, $^{12}C^{6+}$, and $^{20}Ne^{9+}$) as a function of the ion energy per nucleon divided by the projectile charge number (E_{ion}/Z). The corresponding σ_{di}/σ_{si} values reported by CHAMPION (2003) and GERVAIS et al. (2006) for various ions and gaseous water are also included in the figure for the sake of comparison (see also Fig. 1 of Chapter III). It is seen that our values of α depend on the type of the projectile ion (in contrast to CHAMPION's values, which follow a unique law, independent of the impacting ion) and, for a given value of E_{ion}/Z, increase from protons to neon ions ($Z = 9$). As can also be seen from the figure, our ratios of σ_{di}/σ_{si} compare reasonably well with those obtained from the MI cross-section calculations of GERVAIS et al. (2006) for protons and carbon ions ($Z = 6$).[1] Although such an accord is here satisfactory, it should be emphasized that the process of multiple ionization of polyatomic molecules (including H_2O) in heavy-ion collisions and in particular the effects due to the phase, are an area where very little is known and where more experimental and theoretical work is clearly needed.

[1] Note that these latter authors also showed that, under high-LET, heavy-ion impact, the multiple ionization of water is indeed not negligible with respect to single ionization. For example, for 1-MeV/nucleon $^{12}C^{5+}$ ions (LET ~ 665 keV/μm), they found that the fraction of MI amounts to 28%, while for LET above 10^3 keV/μm it becomes as high as 35% (GERVAIS et al., 2005, 2006).

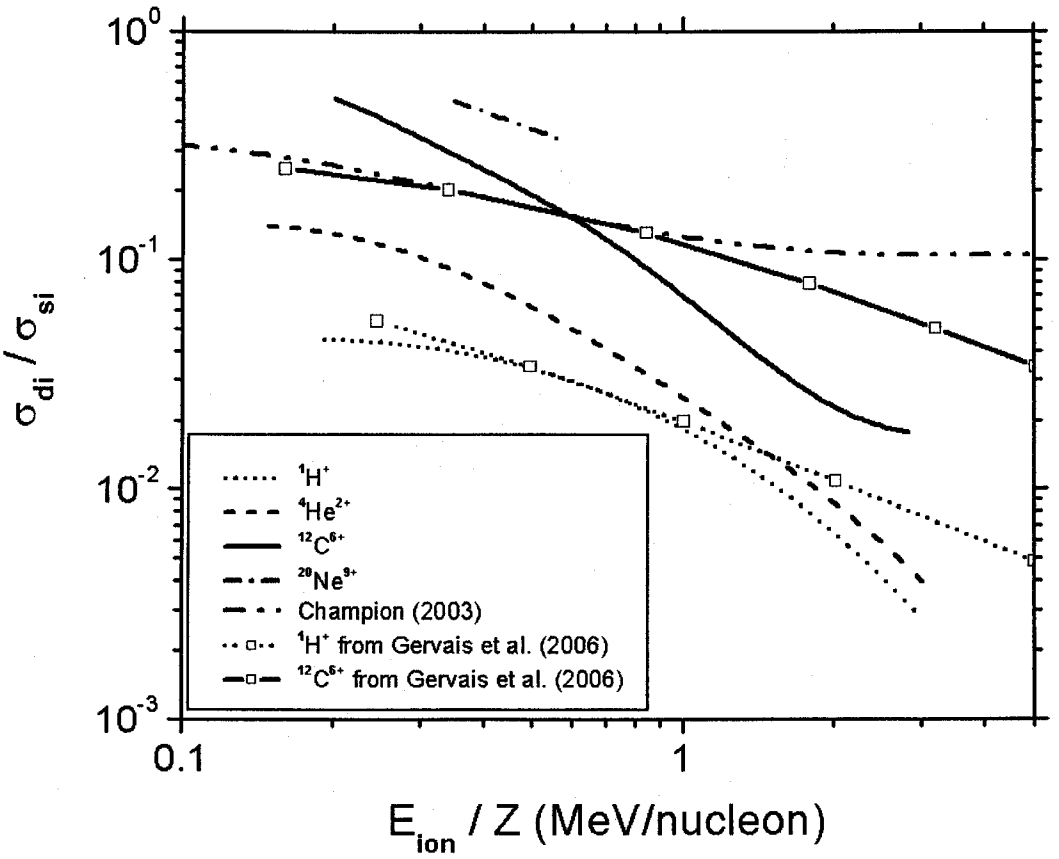

Figure 1. Plot of the ratio of double-to-single ionization cross sections ($\alpha = \sigma_{di}/\sigma_{si}$) against E_{ion}/Z, where E_{ion} is the ion energy per nucleon and Z is the projectile charge number. The short-dot, dash, solid, and dash-dot lines represent, respectively, the α values for $^1H^+$, $^4He^{2+}$, $^{12}C^{6+}$, and $^{20}Ne^{9+}$ impacting ions, obtained from our Monte Carlo simulations (see text and Chapters II and III). The dash-dot-dot line shows the α values reported by CHAMPION (2003) and the symbols (□) with dot and solid lines represent the α values calculated by GERVAIS et al. (2006) for protons and carbon ions, respectively.

V.2.2. Fate of multicharged water cations

V.2.2.1. Acid-base re-equilibration reactions

Very little is known about the fate of multiply ionized water molecules *in solution*. In this work, the rearrangement of these thermodynamically unstable multiply

charged water cations is treated following the general mechanism proposed by FERRADINI and JAY-GERIN (1998), which assumes that, in *liquid* water, H_2O^{n+} dissociates through acid-base re-equilibration processes. For example, for the predominantly formed doubly ionized water molecules, the overall dissociation reaction is [see Eq. (23) of Chapter I]:[2]

$$H_2O^{2+} + 2\,H_2O \rightarrow 2\,H_3O^+ + O\,, \qquad (5)$$

which can be regarded as resulting from a two-step process involving two deprotonation reactions (the two protons being taken away by water molecules), namely,

$$H_2O^{2+} + H_2O \rightarrow H_3O^+ + OH^+\,,$$

followed by

$$OH^+ + H_2O \rightarrow H_3O^+ + O\,.$$

As for the triply and quadruply charged water cations, we have [see Eqs. (25) and (26) of Chapter I]

$$H_2O^{\bullet 3+} + 4\,H_2O \rightarrow 3\,H_3O^+ + HO_2^{\bullet} \qquad (6)$$

$$H_2O^{4+} + 5\,H_2O \rightarrow 4\,H_3O^+ + O_2\,. \qquad (7)$$

Similar reactions can be written for higher degree of ionization ($n > 4$) (see Table 1).

---

[2] As mentioned earlier (see Chapter I), the oxygen atoms formed in their ^3P ground state through reaction (5) are rather inert to water; they subsequently produce, among other things, $HO_2^{\bullet}/O_2^{\bullet -}$ and O_2 by reactions with $^{\bullet}OH$ radicals and with themselves in the track core of the impacting ion, respectively. In contrast, the excited $O(^1D)$ atoms produced in reaction (5) are known to react rapidly with water (to form H_2O_2 or possibly also $2\,^{\bullet}OH$).

Table 1. Radiolytic products inferred from the dissociation of multiply charged water cations (H_2O^{n+}, n = 1–10) (the molecule of water has 10 bound electrons), as obtained by acid-base re-equilibration, in the heavy-ion radiolysis of pure liquid water at high LET.

n	Products
1	$H_3O^+ + {}^{\bullet}OH$
2	$2\,H_3O^+ + O$
3	$3\,H_3O^+ + HO_2^{\bullet}$
4	$4\,H_3O^+ + O_2$
5	$5\,H_3O^+ + {}^{\bullet}OH + O_2$
6	$6\,H_3O^+ + O + O_2$
7	$7\,H_3O^+ + HO_2^{\bullet} + O_2$
8	$8\,H_3O^+ + 2\,O_2$
9	$9\,H_3O^+ + {}^{\bullet}OH + 2\,O_2$
10	$10\,H_3O^+ + O + 2\,O_2$

V.2.2.2. Fragmentation caused by "Coulomb explosions"

In *gaseous* water, MI is followed by fragmentation of the ionized target as a result of the so-called "Coulomb explosion".[3] The mechanism of Coulomb explosion (for example, see: CARLSON and WHITE, 1963, 1966; GEMMELL, 1980; LATIMER, 1993) is based on the simplified scenario where two or more electrons from a molecule are suddenly removed by the incident projectile, so that the transiently formed highly ionized parent ion becomes unstable [due to the Coulomb repulsion between the positive atomic fragment ions (holes) that can repel one another apart] and rapidly dissociates into both charged and neutral fragments.

[3] Fragmentation originating from violent binary collisions (involving small impact parameters) has also been observed (see STOLTERFOHT et al., 2007).

According to experimental results in the gas phase (WERNER et al., 1995*a*, *b*; OLIVERA et al., 1998; GOBET et al., 2001; SIEGMANN et al., 2001; PEŠIĆ et al., 2004; LEGENDRE et al., 2005; ALVARADO et al., 2005; LUNA and MONTENEGRO, 2005; SOBOCINSKI et al., 2005; STOLTERFOHT et al., 2007, and references therein), three main, competing water dication fragmentation channels have been identified (by the coincident detection of correlated fragments from a particular molecular breakup), namely,

$$H_2O^{2+} \rightarrow H^+ + H^+ + O \tag{8}$$

$$H_2O^{2+} \rightarrow H^+ + OH^+ \tag{9}$$

$$H_2O^{2+} \rightarrow H^+ + O^+ + H^\bullet , \tag{10}$$

while for ionization of higher multiplicity ($q \geq 3$) the dominating fragmentation pathway involves a three-body breakup of the multi-ionized water molecule as follows:

$$H_2O^{q+} \rightarrow H^+ + H^+ + O^{(q-2)+} . \tag{11}$$

Only very few data exist on the cross sections (or probabilities) for these various possible water polycation dissociation channels. For instance, OLIVERA et al. (1998) reported the values ~6.3×10^{-15}, 1.3×10^{-15}, and 1.5×10^{-15} cm^2 (with an estimated uncertainty of ~30%) for the fragment production channels (8)–(10) coming from the double ionization of water under 6.7-MeV/nucleon Xe^{44+} ion impact, respectively. These values are found to be ~4–18 times less than the corresponding single-ionization cross section measured by these authors (~2.4×10^{-14} cm^2). As for the triple ionization, the cross section for the $H^+ + H^+ + O^+$ fragmentation channel (11) obtained by OLIVERA et al. (1998) amounts to 2.5×10^{-15} cm^2, an order of magnitude smaller than the cross section for single-ionization fragment production. WERNER et al. (1995*b*) also reported that, for 100–350-keV proton-H_2O collisions, the fragmentation

channel (8) $H_2O^{2+} \rightarrow H^+ + H^+ + O$ has a cross section about twice higher than the $H^+ + H^+ + O^+$ fragmentation (11), a result that is consistent with OLIVERA et al. (1998)'s data. In another, more recent study, PEŠIĆ et al. (2004) investigated the fragmentation of water molecules following interaction with 2–90-keV Ne^{p+} ions (p = 1, 3, 5, 7, and 9). These authors observed a strong dependence of the fragment ion production cross sections on the projectile charge state. They also found that their cross sections are almost two orders of magnitude larger than those reported by WERNER et al. (1995*b*) for fragmentation of H_2O following proton impact. Although a great deal of attention is being devoted currently by different laboratories to studies of the influence of the type, energy, and charge state of the impinging ion on the ion impact-induced fragmentation of water vapor, a detailed knowledge of the basic features of the explosive fragmentation pattern of multiply charged water cations remains, at present, fragmentary. Clearly, there is a need to explore these phenomena further.

In the *liquid* phase, it has been suggested (see Chapter I) that, following (single) ionization (from the uncertainty principle, $\Delta t\ \Delta E \sim \hbar$, the collision time required to know that an energy loss has taken place in ionization is, typically, $\sim 10^{-16}$ s), the $H_2O^{\bullet+}$ hole can migrate rapidly by resonance electron transfer with neighboring water molecules until the ion-molecule reaction

$$H_2O^{\bullet+} + H_2O \rightarrow H_3O^+ + {}^{\bullet}OH \qquad (12)$$

localizes the hole (MOZUMDER, 1999).[4] This proton transfer reaction (12) occurs on the time scale of $\sim 10^{-14}$ s (i.e., ~10 fs), consistent with the characteristic time of a vibrational period of a water molecule (recall here that the O–H stretching frequency of H_2O in the liquid phase is ~3400 cm^{-1}). Unfortunately, very little is known about the

[4] By itself $H_2O^{\bullet+}$ is stable, but in the presence of water it dissociates, giving H_3O^+ and an $^{\bullet}OH$ radical.

different dissociation pathways of H_2O^{n+} ($n \geq 2$) in liquid water. To the best of our knowledge, the only previous studies devoted to this question are those of OLIVERA et al. (1998) and GAIGEOT et al. (2007). Using qualitative arguments based on the ability of the medium to neutralize a charged species, OLIVERA et al. (1998) tentatively extrapolated their water-vapor multi-ionization results to the case of liquid water. Among other things, they concluded that, at least for the process of double ionization, the result of the multi-ionization in liquid water may not be a direct Coulomb explosion of the molecule, but rather a quick neutralization of the water polycation by the surrounding medium. In essence, this conclusion was based on a comparison of the time involved in a dissociative Coulomb explosion process [>1–15 fs, estimated from molecular dynamics calculations; see: GAIGEOT et al. (2007)] and some estimates of characteristic time scales of the competitive neutralization processes, such as hole migration, geminate electron-cation recombination [before thermalization of secondary electrons is complete (<10 fs); see, for example: MEESUNGNOEN et al. (2002*b*)], and proton transfer reactions, in combination with energy transfer to various modes of excitation of the surrounding medium. One further argument against Coulomb explosion-induced fragmentation of the molecule (at least for the lowest degree of ionization) is the "cage effect" observed for molecules in the condensed phase (FRANCK and RABINOWITSCH, 1934), which forces the ejected fragments to stay together (OLIVERA et al., 1998). This cage recombination effect may significantly alter product yields between the two phases (gas phase versus liquid).

In their recent multi-scale *ab initio* theoretical study employing density functional theory-based Car-Parrinello molecular dynamics simulations of a doubly ionized water molecule in the condensed phase, GAIGEOT et al. (2007) were able to confirm the formation of two H_3O^+ ions and an atomic oxygen atom. However, these authors could not completely clarify the early stage of the dissociation of H_2O^{2+} in solution as

they modeled the initial dynamics of the water dication in the absence of the surrounding water molecules assuming a Coulomb explosion mechanism of fragmentation. Based on their molecular dynamics calculations, GAIGEOT et al. (2007) showed that double ionization leads to two main dissociation pathways (in proportion to 84% of all H_2O^{2+} fragmentations) for the production of oxygen atoms in liquid water, namely,

$$H_2O^{2+} \rightarrow H^+ + H^+ + O \xrightarrow{2\,H_2O} 2\,H_3O^+ + O \quad (55\%) \qquad (13)$$

$$H_2O^{2+} \rightarrow H^+ + OH^+ \xrightarrow{2\,H_2O} 2\,H_3O^+ + O \quad (29\%)\,. \qquad (14)$$

These authors also considered the three-body breakup of the doubly ionized water molecule (a minor process, contributing only 16% to the total fragmentation):

$$H_2O^{2+} \rightarrow H^+ + O^+ + H^\bullet \xrightarrow{3\,H_2O} 2\,H_3O^+ + H^\bullet + {}^\bullet OH + O\,, \qquad (15)$$

which, in addition to O atoms, leads to the formation of $H^\bullet$ and $^\bullet OH$ radicals. Finally, for a higher degree of ionization ($q \geq 3$), they proposed the following fragmentation channel:

$$H_2O^{q+} \rightarrow H^+ + H^+ + O^{(q-2)+} \xrightarrow{2(q-1)\,H_2O} q\,H_3O^+ + (q-2)\,{}^\bullet OH + O\,. \qquad (16)$$

GERVAIS et al. (2005, 2006) used this dissociation scheme (13)–(16) to simulate the formation of $HO_2^\bullet/O_2^{\bullet-}$ and O_2 in the heavy-ion radiolysis of liquid water at high LET.

Whatever the mechanism that actually controls the dissociation of the multicharged water cations *in solution* (either Coulomb explosion or acid-base re-equilibration), it is worth noting that the fragments $2\,H_3O^+ + O$ originating from the two most dominant Coulomb-induced reaction channels (13) and (14) are identical to those formed via the corresponding dissociation pathway (5) based on acid-base re-equili-

bration reactions. These fragmentation mechanisms, however, differ at the end in the spatial distribution of the H_3O^+ and atomic oxygen species taking account of the energy distributions that are involved in the Coulomb explosion processes. In fact, the Coulomb breakup of H_2O^{2+} leads to target fragments that should have some kinetic energy[5] and therefore move farther away from the interaction point than they would do in the case of acid-base re-equilibration (or proton transfer) processes. In the case of the two-body H^+–OH^+ dissociation channel (14), the total kinetic energy of the H^+ and OH^+ fragments ejected from collisions of H_2O with 5.9 MeV/nucleon Xe^{18+} and Xe^{43+} ions was measured to be about 6.5 eV (SIEGMANN et al., 2001). Similar results were obtained by SOBOCINSKI et al. (2006) in He^{2+}–H_2O collisions at impact energies of 1 and 5 keV. The three-body dissociation channel $H^+ + H^+ + O$ (13) was also observed by these latter authors, who showed that it gives rise to H^+ fragments with kinetic energies also near 5 eV. For 4–23-keV H^+ and He^+ projectiles, more energetic fragment protons (14.5 eV) were identified by ALVARADO et al. (2005) in the (minor) three-body H_2O^{2+} asymmetric breakup channel (15). These results tend to indicate that fragment ions emitted in the Coulomb explosion of doubly ionized water molecules will most probably have energy lower than the lowest ionization and electronic excitation theshold of (condensed) water, which are ~9 and 7.3 eV (MICHAUD et al., 1991; BERNAS et al., 1997; COBUT et al., 1998), respectively.

[5] The mutual Coulomb energy can be estimated from the simple model of a point-charge interaction between charges [i.e., $V = q_1 q_2/(4\pi\varepsilon_0)\ \varepsilon_s r$, where ε_0 is the vacuum permittivity, ε_s is the dielectric constant of the medium, and r is the separation distance between the charges q_1 and q_2. Note that charges do not interact as strongly in a solvent of high dielectric constant (such as liquid water, with $\varepsilon_s \approx 79$ at room temperature)] under the assumption that charges are localized and can be treated as point charges. This potential energy is converted into kinetic energy of the separating fragments as the Coulomb explosion develops.

This in turn implies that these fragments should not be energetic enough to generate their own physical tracks in the radiolysis of water and, as a consequence, only their subsequent chemistry should be taken into account in the radiolytic processes. Although recent studies have provided valuable new insights, more work is expected and clearly desirable in this area.

V.3. Yields of $HO_2^{\bullet}/O_2^{\bullet-}$ radicals

When compared with such highly reactive species as $^{\bullet}OH$, $O_2^{\bullet-}$ (superoxide anion radical) and its conjugate acid $HO_2^{\bullet}$ (hydroperoxyl radical) ($O_2^{\bullet-}$ is always in a pH-dependent equilibrium with $HO_2^{\bullet}$, $pK_a = 4.8$) (BIELSKI et al., 1985) are far less reactive with DNA in aqueous solution. However, the radiobiological consequences of the production of $HO_2^{\bullet}/O_2^{\bullet-}$ could be important since both species can generate more reactive species. For example, the dismutation of $HO_2^{\bullet}/O_2^{\bullet-}$ generates H_2O_2 and O_2 (in a pH-dependent fashion), according to the following (second-order) reactions:

$$HO_2^{\bullet} + HO_2^{\bullet} \rightarrow H_2O_2 + O_2 \qquad k_{17} = 8.3 \times 10^5\ M^{-1}\ s^{-1} \qquad (17)$$

$$HO_2^{\bullet} + O_2^{\bullet-} \xrightarrow{H^+} H_2O_2 + O_2 \qquad k_{18} = 9.7 \times 10^7\ M^{-1}\ s^{-1} \qquad (18)$$

$$O_2^{\bullet-} + O_2^{\bullet-} \xrightarrow{2\,H^+} H_2O_2 + O_2 \qquad k_{19} < 0.3\ M^{-1}\ s^{-1}\ . \qquad (19)$$

In living cells, the presence of copper/zinc-superoxide dismutase (SOD) greatly accelerates this $HO_2^{\bullet}/O_2^{\bullet-}$ dismutation and then facilitates the cytotoxicity of H_2O_2 via the generation of $^{\bullet}OH$ radicals ($^{\bullet}OH$ is the most reactive oxygen radical known; as soon as it is formed, it reacts very quickly with almost every type of molecule found in its immediate vicinity) by the superoxide-assisted Fenton reaction:

$$Fe^{2+} + H_2O_2 \rightarrow Fe^{3+} + {}^{\bullet}OH + OH^-\ . \qquad (20)$$

or, equivalently, the so-called transition metal (iron/copper)-catalyzed Haber-Weiss reaction:

$$H_2O_2 + O_2^{\bullet-} \rightarrow O_2 + {}^{\bullet}OH + OH^- \qquad (21)$$

(see, for example: HALLIWELL and GUTTERIDGE, 1999; VON SONNTAG, 2006). Another cytotoxic species is *peroxynitrite* ($ONOOH/ONOO^-$; $pK_a = 6.8$ at 37 °C), produced *in vivo* by the fast reaction of $HO_2^{\bullet}/O_2^{\bullet-}$ with nitric oxide ($^{\bullet}NO$) that is released in $^{\bullet}NO$-generating cells in response to oxidative stress:

$$HO_2^{\bullet}/O_2^{\bullet-} + {}^{\bullet}NO \rightarrow ONOOH/ONOO^- . \qquad (22)$$

The rate constant of this reaction (~1.9×10^9–1.9×10^{10} M^{-1} s^{-1}) (HUIE and PADMAJA, 1993; GOLDSTEIN and CZAPSKI, 1995; KISSNER et al., 1997) is comparable to that for the enzymatic dismutation (in the presence of catalysis by SOD) of $O_2^{\bullet-}$ at physiological pH (~4×10^9 M^{-1} s^{-1}). $ONOO^-$ and its protonated form (peroxinitrous acid) are powerful oxidants, capable of attacking a wide range of biological targets (BECKMAN and KOPPENOL, 1996; HALLIWELL and GUTTERIDGE, 1999; FARAGGI and HOUÉE-LEVIN, 1999; RADI et al., 2000; JAY-GERIN and FERRADINI, 2000). Irrespective of its low chemical reactivity, $HO_2^{\bullet}/O_2^{\bullet-}$ itself can also react with and damage specific intracellular constituents directly. For example, superoxide radicals are able of inactivate certain enzymes such as catalase and glutathione peroxidase (GSHPx) and oxidize epinephrine, glutathione, 6-hydroxydopamine, α-tocopherol, etc. (for example, see: BENOV, 2001). The toxicology of $O_2^{\bullet-}$ for biologically relevant targets has been reviewed by FRIDOVICH (1986, 1997).

Increase of the radiation LET increases the molecular yields of H_2 and H_2O_2, at the expense of the radical yields e_{aq}^-, $^{\bullet}OH$, and $H^{\bullet}$ (see Chapter I). However,

$HO_2^{\bullet}/O_2^{\bullet-}$ is an exception to this general observation. $HO_2^{\bullet}/O_2^{\bullet-}$ is a radical, but it behaves like a molecular product, increasing in yield with increasing LET. Recent experiments performed in deaerated neutral water with $^{36}S^{16+}$ (77 MeV/nucleon, LET ~ 250 keV/μm) and $^{40}Ar^{18+}$ (70 MeV/nucleon, LET ~ 290 keV/μm) ions have shown that the yields of $O_2^{\bullet-}$ (0.06 ± 0.02 and 0.05 ± 0.01 molec./100 eV, respectively) are about a factor of 3 greater than that found in fast-electron or ^{60}Co γ-ray radiolysis (~0.02 molec./100 eV, LET ~ 0.3 keV/μm) (BALDACCHINO et al., 1998*a*, *b*). This observed increase in $G_{HO_2^{\bullet}/O_2^{\bullet-}}$ with increased LET is even more pronounced for 70.4-MeV/nucleon $^{78}Kr^{33+}$ ions, where the LET in water is in the range ~1500–2000 keV/μm (TAGUCHI et al., 2005). In fact, preliminary results reported by the latter authors indicate that this yield could be as high as ~0.53 molec./100 eV under those irradiation conditions, that is, more than 25 times the yield found for fast electrons.

Although the $HO_2^{\bullet}/O_2^{\bullet-}$ radical is especially interesting in the context of high-LET, heavy-ion tracks (it is the major radical product, since the other primary-radical *G*-values, i.e., those of $^{\bullet}OH$, $H^{\bullet}$, and e_{aq}^{-}, are virtually zero), the reaction mechanism for its production at high LET is probably the most uncertain in water radiolysis. Several hypotheses have been proposed and discussed previously (see, for example: SIMS, 1978; BURNS and SIMS, 1981; BURNS et al., 1981; LAVERNE et al., 1986; LAVERNE, 1989; FERRADINI and JAY-GERIN, 1998; BALDACCHINO et al., 1998*a*; OLIVERA et al., 1998). Early studies assumed $HO_2^{\bullet}$ to be produced in the reaction:

$$^{\bullet}OH + H_2O_2 \rightarrow HO_2^{\bullet} + H_2O\,, \qquad k_{23} = 2.87 \times 10^7\, M^{-1}\,s^{-1} \qquad (23)$$

but diffusion-kinetic models of track theory (APPLEBY and SCHWARZ, 1969) and Monte Carlo simulations (FRONGILLO et al., 1996) have shown that this reaction is not fast enough to account quantitatively for the totality of the observed yields at high

LET. Without excluding definitely other possible mechanisms, the alternative model of FERRADINI and JAY-GERIN (1998) suggesting that the production of $HO_2^{\bullet}/O_2^{\bullet-}$ by a multicharged heavy ion involves the multiple ionization of water is strongly supported by our present Monte Carlo track structure calculations (MEESUNGNOEN et al., 2003; MEESUNGNOEN and JAY-GERIN, 2005*a*, *b*). This same conclusion is corroborated by the recent simulation studies of GERVAIS et al. (2005, 2006) who also confirmed the hypothesis that MI is responsible for an increasing production of $HO_2^{\bullet}/O_2^{\bullet-}$ at high LET. In essence, $HO_2^{\bullet}/O_2^{\bullet-}$ is found to be produced mainly at an early stage of radiolysis by O atoms, formed predominantly from the double ionization of water [see reaction (5)], reacting with $^{\bullet}OH$ in the track of heavy ions. We should note that such a mechanism involving, at high LET, the production of oxygen atoms followed by their intratrack reaction with $^{\bullet}OH$ was originally proposed by KUPPERMANN as early as 1967, and later by LAVERNE et al. (1985).

As clearly shown in Fig. 2 of Chapter III, our curves of $G_{HO_2^{\bullet}/O_2^{\bullet-}}$ versus LET calculated by ignoring the mechanism of multiple ionization of water cannot account for more than a small fraction of the measured $HO_2^{\bullet}/O_2^{\bullet-}$ escape yields at high LET, even if reaction (23) and all other possible reactions that can produce $HO_2^{\bullet}/O_2^{\bullet-}$ (such as, for example:

$$e_{aq}^{-} + O_2 \rightarrow O_2^{\bullet-} \qquad k_{24} = 1.74 \times 10^{10}\, M^{-1}\, s^{-1} \qquad (24)$$

$$H^{\bullet} + O_2 \rightarrow HO_2^{\bullet} \qquad k_{25} = 2.1 \times 10^{10}\, M^{-1}\, s^{-1} \qquad (25)$$

$$^{\bullet}OH + O(^3P) \rightarrow HO_2^{\bullet} \qquad k_{26} = 2.02 \times 10^{10}\, M^{-1}\, s^{-1}) \qquad (26)$$

(see Table 1 of Chapter I) are included in the simulations. However, when the mechanism of MI is accounted for, we observe a marked increase of $G_{HO_2^{\bullet}/O_2^{\bullet-}}$ with increasing LET, which is in very good agreement with the experimental data of

BALDACCHINO et al. (1998*a*, *b*). Moreover, extrapolation of our calculated $HO_2^{\bullet}/O_2^{\bullet-}$ yields to higher LET comes close to TAGUCHI et al. (2005)'s estimates around ~1500–2000 keV/μm. In their recent Monte Carlo studies, GERVAIS et al. (2005, 2006) also found a very smooth increase in the primary yields of $HO_2^{\bullet}/O_2^{\bullet-}$ with increasing LET in the absence of multiple ionization of water. However, upon incorporation of the MI mechanism, their calculations show, in close similarity with our results, a sharp increase in $G_{HO_2^{\bullet}/O_2^{\bullet-}}$ above ~100–200 keV/μm (depending on the impinging ion studied), in good agreement with experiment.

V.4. Yields of H_2O_2

Hydrogen peroxide is the main oxidizing molecular product formed during the radiolysis of water. It is formed primarily by combination reactions of two $^{\bullet}OH$ radicals produced in the radiolytic decomposition of water:

$$^{\bullet}OH + {}^{\bullet}OH \rightarrow H_2O_2 . \qquad (27)$$

From our Monte Carlo track structure simulations, performed at neutral pH (Chapters II and III) and also in aqueous 0.4 *M* H_2SO_4 solutions (pH ~ 0.46) (Chapter IV), it is shown that the yields of H_2O_2 are sensitive to multiple ionization for irradiating high-LET heavy ions. As can be seen in Fig. 3 of Chapter III and Fig. 1 of Chapter IV, significant differences exist between calculations including MI and those restricted to single ionizations. In the absence of MI, our calculated values of $G_{H_2O_2}$ continuously increase with increasing LET. However, when the mechanism of MI of water is incorporated in the simulations, the curves for $G_{H_2O_2}$ as a function of LET first rise, then bend downward (in the case of incident protons) and, at higher LET, reach a maximum (in the case of impacting $^4He^{2+}$ and $^{12}C^{6+}$ ions), after which they fall (see Fig. 3 of Chapter III). While this maximum is relatively narrow for $^4He^{2+}$ ions, it is more pro-

nounced for $^{12}C^{6+}$ ions. Its position also slightly shifts to higher LET as the ion charge increases. In fact, if we consider the curve of $G_{H_2O_2}$ versus LET that includes the ensemble of our four calculated $G_{H_2O_2}$(LET) curves for the different ions studied ($^{1}H^{+}$, $^{4}He^{2+}$, $^{12}C^{6+}$, and $^{20}Ne^{9+}$), the overall maximum can be estimated around 100–200 keV/μm, which is in good accord with experiment (BIBLER, 1975; SIMS, 1978; BURNS and SIMS, 1981; PASTINA and LAVERNE, 1999; WASSELIN-TRUPIN et al., 2002). Moreover, for each ion investigated, this maximum of $G_{H_2O_2}$ occurs precisely at the point where $G_{HO_2^{\bullet}/O_2^{\bullet-}}$ begins to rise sharply, showing, in agreement with previous experimental data (SIMS, 1978; BURNS and SIMS, 1981), that the yields of $HO_2^{\bullet}/O_2^{\bullet-}$ and H_2O_2 are closely linked. This is readily explained by the fact that H_2O_2 is formed within the tracks mainly by the combination reaction (27). As $^{\bullet}OH$ reacts with $O(^3P)$ by reaction (26), this latter reaction competes with reaction (27), thereby causing a drop in the observed hydrogen peroxide yields at high LET.

As is seen in Fig. 3 of Chapter III (see also Fig. 1 of Chapter IV), there is a significant amount of scatter in the yields of H_2O_2 measured by different investigators as a function of LET (see, for reviews: McCRACKEN et al., 1998; LAVERNE, 2004). This uncertainty in H_2O_2 yields after exposure to high-LET radiation becomes even greater when pH effects are considered (Fig. 1 of Chapter IV). However, a wide variety of studies indicate that, at a given LET, the production of H_2O_2 is higher in acidic solutions than in neutral water (FERRADINI and JAY-GERIN, 2000). Unfortunately, some confusion in predicting trends exists in the literature as some authors have inferred their conclusion by comparing different sets of measurements of $G_{H_2O_2}$ at high LET in *both* neutral and acidic liquid water. For example, LAVERNE (2004) recently suggested in a review article on the radiation chemical effects of heavy ions in water that $G_{H_2O_2}$ should have a "limiting" value at infinite LET of ~1 molec./100 eV, somewhat similar for neutral and acidic solutions. This conclusion, however, is un-

certain as it is based on a fit of different $G_{H_2O_2}$ data measured at various pH (namely, 0.46, 2, 3, and 7). In fact, measurements of the H_2O_2 yield as a function of LET by a number of workers in deaerated 0.4 *M* H_2SO_4 aqueous solutions (pH 0.46) clearly show a well-defined maximum of ~1.4 molec./100 eV (i.e., ~45% greater in magnitude than that found in neutral solutions) around ~180–200 keV/μm, with the yield decreasing thereafter to the value of 0.96 molec./100 eV (BIBLER, 1975) at an LET close to ~4000 keV/μm. As can be seen in Fig. 1 of Chapter IV, this dependence of $G_{H_2O_2}$ on LET is *quantitatively* reproduced by our Monte Carlo simulations using irradiating $^{12}C^{6+}$ and $^{20}Ne^{9+}$ ions and incorporating the mechanism of multiple ionization of water. Furthermore, extrapolation of our H_2O_2 escape yield values to higher LET reproduces very well BIBLER (1975)'s value of $G_{H_2O_2}$ for dissolved ^{252}Cf fission recoil fragments (LET ~ 4000 keV/μm). As can also be seen in the figure, our curve for $G_{H_2O_2}$ as a function of LET for $^{12}C^{6+}$ ions calculated without including MI increases continuously with increasing LET, in disagreement with experiment.

Similar findings have been obtained by GERVAIS et al. (2006) from their simulations of the radiolysis of neutral liquid water with carbon and argon ions. These authors found that, above ~100 keV/μm, $G_{H_2O_2}$ is sensitive to multiple ionization. In fact, they observed a marked decrease in the values of $G_{H_2O_2}$ (up to 30% for their largest LET investigated) upon incorporating MI in the calculations. However, in contrast to our results (and also to experiment), they did not find any maximum in their $G_{H_2O_2}$ curves versus LET calculated in the presence of the MI mechanism. The source of such a difference in the dependence of $G_{H_2O_2}$ on LET between our work and that of GERVAIS et al. (2006) is examined below.

As seen above, the three (Coulomb-induced) fragmentation channels (13)–(15) that GERVAIS et al. (2006) considered for the (predominantly formed) doubly ionized water molecules lead all to the production of atomic oxygen, either directly or after

neutralization of O^+ with water. This is essentially equivalent to the acid-base re-equilibration reaction (5) used in our study and which also produces O atoms. In other words, the difference in the formation mechanism of O atoms should not be the reason of the observed difference in $G_{H_2O_2}$ between our work and that of GERVAIS et al. (2006). We have confirmed this point by incorporating in our simulation program the three dissociation channels of H_2O^{2+} used by GERVAIS et al. (2006) [in place of reaction (5)]; indeed, no significant change in our $G_{H_2O_2}$ values was observed [it is important to note that the respective proportions (or branching ratios) of the various fragmentation pathways are not critical for the simulations, mainly because they all generate atomic oxygen].

In another facet of our work, we have assumed that all O atoms produced in reaction (5) are in their ^3P ground state. By contrast, GERVAIS et al. (2006) tentatively considered in their simulations that 85% of O atoms are generated in an excited state, while 15% are left in the ^3P state. These latter authors also showed that changing the proportion of excited states from 80% to 20% does not change the variation of the $HO_2^{\bullet}/O_2^{\bullet-}$ and O_2 yields with the LET, but only changes their absolute value by a small constant factor (GERVAIS et al., 2005, 2006). This is readily explained by the fact that when the concentration of radicals becomes larger and larger, the reaction of an oxygen atom, either in an excited state or in its ground state, with another radical becomes more and more likely. Also, at high LET, the relative number of available water molecules should decrease because of the high density of interactions of water molecules with impacting ions along their paths.

Actually, the difference between our Monte Carlo simulations and those of GERVAIS et al. (2006) regarding the LET dependence of $G_{H_2O_2}$ can be shown to originate mainly from the different ratios for the double-to-single ionization cross sections ($\alpha = \sigma_{di}/\sigma_{si}$) used by the two groups (see Fig. 1). As can be seen from this

figure for the case of $^{12}C^{6+}$ ions (shown for the sake of comparison), at low impacting ion energies (i.e., at high LET), our σ_{di}/σ_{si} values are higher than those used by GERVAIS et al. (2006). As a result, our simulations produce more doubly ionized water molecules and therefore more O atoms. This increased formation of oxygen atoms [as compared to GERVAIS et al. (2006)'s simulations] leads to an increased intervention of reaction (26) with an exacerbated competition with reaction (27), thereby causing the drop in the hydrogen peroxide yields that is seen at high LET (Fig. 3 of Chapter III and Fig. 1 of Chapter IV).

V.5. Production of O_2 and the "oxygen-in-the-track" hypothesis

A specially important aspect of the action of radiations on living systems – in relation to the radiotherapy of tumors – is that cells which are hypoxic at the time of irradiation are generally much less damaged by a given dose of X- or γ-radiation than those which are well oxygenated (see Chapter I). In other words, the absence of oxygen enhances the resistance of cells to low-LET ionizing radiations. By contrast, for high-LET radiation, the survival of tumor cells is practically the same in the presence or in the absence of O_2 (CURTIS et al., 1982). As mentioned in Chapter I, there are several different hypotheses (not all mutually exclusive) that have been invoked in the literature to account for this experimental finding. At present, however, the mechanism of radiobiological action underlying the reduction of the "oxygen enhancement ratio" (OER) with increasing LET is not yet completely clear. Among the hypotheses advanced to explain the LET dependence of the OER either independently, or as parts of a single mechanism, the "oxygen-in-the-track" hypothesis (SCHOLES and WEISS, 1959; SWALLOW and VELANDIA, 1962; NEARY, 1965; ALPER and BRYANT, 1974) proposes that molecular oxygen is generated *in situ* by heavy-ion

tracks passing through water, in quantities which depend on the radiation quality: the denser the track, the greater the effective concentration of oxygen. This hypothesis has often been invoked for a variety of biological systems. Other possible explanations have also been considered, including the "interacting-radicals" hypothesis (ALPER, 1956; ALPER and HOWARD-FLANDERS, 1956; HOWARD-FLANDERS, 1958), the "oxygen depletion in the vicinity of heavy-ion tracks" hypothesis (KIEFER, 1975, 1990; STUGLIK, 1995), and more recently the "radical multiplicity" hypothesis (FRANKENBERG-SCHWAGER et al., 1994; MICHAEL and PRISE, 1996). In addition to these proposed (radiation-chemical) mechanisms and irrespective of whichever of them is true, there is available evidence pointing to the involvement of biological factors, such as repair processes, to explain (at least in part) why OER goes down as LET rises (for example, see: KIEFER, 1975, 1990). In fact, reduced repair capabilities of cells after high-LET irradiation have been observed consistent with an increase in the complexity (severity) of DNA lesions (HENDRY, 1999; VON SONNTAG, 2006). Even though a definite conclusion has not yet been forthcoming, it may be stated that there is probably more than one mechanism responsible for the lower OER found at high LET.

On the viewpoint of pure radiation chemistry, the "oxygen-in-the-track" hypothesis presupposes that O_2 is a product of the radiolysis of water at high LET (we recall that, for radiation of low LET, oxygen is *not* a radiolytic product). Oxygen generated in this way has been identified in several previous experiments (LEFORT, 1955; ALLEN, 1961; BIBLER, 1975; BAVERSTOCK and BURNS, 1976; LAVERNE and SCHULER, 1987*b*, 1996; BURNS et al., 1981). Most remarkably, BIBLER (1975) estimated from his studies of the radiolysis of 0.4 *M* H_2SO_4 solutions with ^{252}Cf fission fragments that G_{O_2} could be as high as ~0.3–0.8 molec./100 eV at an LET of ~4000 keV/μm (to make up the material balance) (see Fig. 8*b* of Chapter I). For the

biological point of view, such "track" oxygen would then be available immediately after the passage of the incident ion to react with adjacent potential cellular lesions (mainly measured as alterations in DNA) formed by the same ionizing particle (BAVERSTOCK and BURNS, 1981). These combination events of oxygen with DNA radicals (converting them into the corresponding peroxyl radicals):

$$DNA^{\bullet} + O_2 \rightarrow DNA\text{-}O_2^{\bullet} \qquad (28)$$

are said to result in nonrepairable damage (oxygen is also said to "fix" or make permanent the radiation lesion).[6] These "nonrestorable" lesions ultimately increase the amount of stable DNA damage – and thus the extent of cellular lethality – from a given radiation dose. Hence, the radiolytic formation of O_2 in the tracks of heavy ions would likely be a determinant of increased radiation sensitivity.

In support to the "oxygen-in-the-track" hypothesis, our Monte Carlo simulations clearly suggest that there is, indeed, an excess production *in situ* of molecular oxygen in high-LET, heavy-ion tracks at early time that is not observed with lower LET radiations (see Chapter III). They show, in particular, that the mechanism of multiple (mainly double) ionization of water, even though infrequent relative to single-ionization events, is responsible for such an O_2 production (through the formation of

[6] The "oxygen fixation" hypothesis is widely regarded as the most satisfactory explanation of why O_2 is a radiation sensitizer. According to this hypothesis, oxygen sensitizes cells because DNA lesions that are produced by ionizing radiation with the chemical participation of oxygen are difficult or impossible to restore chemically back to an original, undamaged state (repair enzymes cannot adequately work on such sites) (for recent discussions on the subject, see, for example: EWING, 1998; VON SONNTAG, 2006).

oxygen atoms).[7] In fact, as can be seen from Fig. 9*b* of Chapter III, there is a chemical production of O_2 at early times originating from the reactions:

$$O(^3P) + O(^3P) \rightarrow O_2 \qquad (29)$$

and

$$^{\bullet}OH + O(^3P) \rightarrow HO_2^{\bullet} \qquad (26)$$

followed by

$$HO_2^{\bullet} + O(^3P) \rightarrow O_2 + {}^{\bullet}OH\,, \qquad (30)$$

whereas in the time interval ~10^{-12}–10^{-6} s (i.e., during spur/track expansion), O_2 is formed mainly by

$$^{\bullet}OH + HO_2^{\bullet} \rightarrow O_2 + H_2O \qquad (31)$$

and, but to a much lower extent, by

$$^{\bullet}OH + O_2^{\bullet-} \rightarrow O_2 + OH^-\,. \qquad (32)$$

In addition, as observed with $HO_2^{\bullet}/O_2^{\bullet-}$ and H_2O_2, the O_2 yields at early times as well as at the microsecond time scale are both LET and irradiating-ion dependent. As is clearly seen in Fig. 8 of Chapter III, upon incorporating the MI mechanism, our calculations indicate that:

(i) the initial and primary yields of O_2 increase steeply with increasing LET (in contrast, in the absence of MI of water, these yields remain very small throughout the range of LET studied and show only a slight gradual increase with increasing LET);

(ii) for different incident ions (including $^1H^+$, $^4He^{2+}$, $^{12}C^{6+}$, and $^{20}Ne^{9+}$ ions) of equal LET but different velocities, G_{O_2} decreases as the ion velocity increases, a

[7] Similar findings have also been obtained by GERVAIS et al. (2005, 2006) in their recent Monte Carlo simulations of water radiolysis by swift ions.

behavior that is akin to the other molecular yields (note that, according to the Bethe stopping power equation [see Eq. (6) of Chapter I; see also Chapter III], for two different ions of equal LET, the one with the higher charge will have the higher velocity).

To further test the veracity of the "oxygen-in-the-track" hypothesis, we need to know the extent to which O_2 is formed in heavy-ion tracks. This information is obviously of considerable importance for biologically based treatment planning in radiation oncology because high levels of tumor hypoxia have a positive correlation with treatment failure for many human cancers (for example, see: CARLSON et al., 2006). If it is correct to invoke that the greater efficiency of high-LET radiation for the inactivation of tumor hypoxic cells can be attributable to the formation of oxygen in tracks, then estimates of the track concentration of O_2 as a function of time could significantly help quantify and predict changes in the observed differences in radiosensitivity for hypoxic and aerobic tumor cells, and therefore achieve a better level of cell killing in hypoxic regions of a tumor in clinical applications. Using the *G*-values for O_2 obtained from our Monte Carlo simulations of the radiolysis of pure, deaerated water in the time scale of ~10^{-12}–10^{-6} s, for impacting 24-MeV $^{12}C^{6+}$ (LET ~ 500 keV/μm) and 4-MeV $^{4}He^{2+}$ (LET ~ 120 keV/μm) ions, with including the mechanism of MI of water,[8] we have calculated the concentrations of O_2 generated in the tracks of those ions as a function of time (see Chapter III). Our calculation relies on the assumption that the O_2 molecules are produced *evenly* in a cylinder whose initial radius r_0 is equal to the radius of the physical track "core", which corresponds to the tiny radial region within

[8] As seen in Fig. 10*a* of Chapter III, in the absence of MI of water in the simulations, the yields of O_2 at early times are almost nonexistent for all LET values investigated, while at longer times there is a small amount of O_2 produced via intratrack reactions occurring during the nonhomogeneous chemical stage with corresponding yields rising only very slightly and gradually with increasing LET.

the first few nanometers around the impacting ion path (at ~10^{-13} s) (MAGEE and CHATTERJEE, 1987; MOZUMDER, 1999). Under these conditions, the oxygen concentration can simply be derived from (BAVERSTOCK and BURNS, 1976; PIMBLOTT and LAVERNE, 2002):

$$[O_2] \approx G(O_2) \times \left(\frac{\text{LET}}{\pi r^2} \right) \tag{33}$$

where

$$r^2 \approx r_0^2 + 4Dt \tag{34}$$

represents the change with time of r_0 due to the diffusive expansion of the track. Here, r_0 obtained from our simulations is ~2.0 nm for the irradiating ions considered, t is the time, and D is the diffusion coefficient of O_2 [$D = 2.42 \times 10^{-9}$ m^2 s^{-1} at 25 °C (LIDE, 2003)]. The values of $[O_2]$ so obtained are shown in Fig. 2 along with the corresponding values of $G(O_2)$ for the two different types of heavy ions used (namely, 24-MeV $^{12}C^{6+}$ and 4-MeV $^{4}He^{2+}$ ions), as well as for 300-MeV protons (corresponding to the low-LET limiting case of fast electrons or ^{60}Co γ-radiolysis), as a function of time (see also Fig. 10*b* of Chapter III). As can be seen from Figs. 2*a* and 2*b*, $G(O_2)$ and $[O_2]$ at early times are, respectively, ~0.1 molec./100 eV and 63 m*M* for 24-MeV $^{12}C^{6+}$ ions (LET ~ 500 keV/μm), and ~0.015 molec./100 eV and 2.2 m*M* for 4-MeV $^{4}He^{2+}$ (LET ~ 120 keV/μm). These initial track concentrations of O_2 are much higher (in fact, more than 3 orders of magnitude) than the oxygen levels present in normally oxygenated tumor regions (which are found to vary widely, almost homogeneously from zero to above 20 μ*M*) and in hypoxic tumor regions (where a large proportion of the vessels appear to have near zero oxygenation) (POGUE et al., 2001), as well as in normal human cells (typical values are around 30 μ*M*) (HALLIWELL and GUTTERIDGE, 1999; VON SONNTAG, 2006). The results in Fig. 2*b* also show that, for the two $^{12}C^{6+}$

and $^4He^{2+}$ ions investigated, $[O_2]$ remains almost constant as a function of time between ~10^{-12} and 1–3 × 10^{-10} s, and then decreases steeply to ~2.2 m*M* and 260 μ*M* at ~10^{-8} s, ~165 and 21 μ*M* at ~10^{-7} s, and ~17 and 2 μ*M* at the microsecond time scale, respectively. It is remarkable to note that these track oxygen concentrations compare very well with the experimental estimates of BAVERSTOCK and BURNS (1976) who found that, for typical α-particles with LET ~ 100 keV/μm, $[O_2]$ would be 4.2 m*M* at

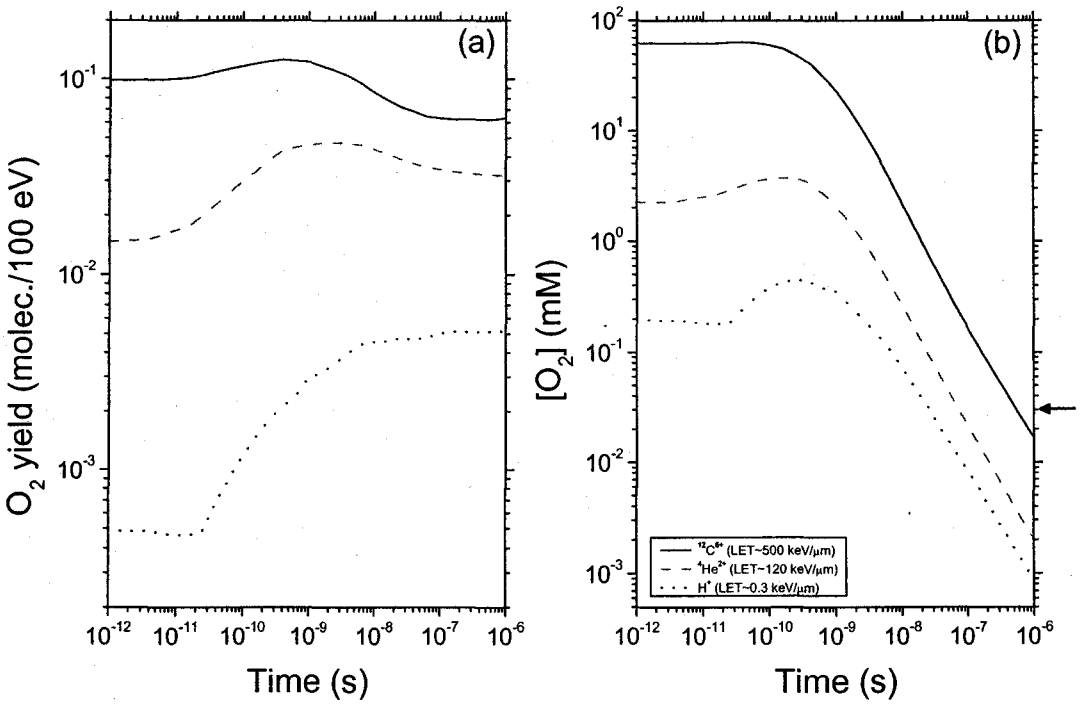

Figure 2. (*a*) Time dependences of the O_2 yields (in molec./100 eV) calculated from our Monte Carlo simulations of the radiolysis of pure, air-free liquid water at pH 7, 25 °C, for impacting 24-MeV $^{12}C^{6+}$ (LET ~ 500 keV/μm, solid line) and 4-MeV $^4He^{2+}$ (LET ~ 120 keV/μm, dash line) ions, with including multiple ionizations of water molecules. The dot line corresponds to our calculated $G(O_2)$ values for the low-LET limiting case of 300-MeV protons (LET ~ 0.3 keV/μm) and is shown in the figure for the sake of comparison. (*b*) Time dependence of the corresponding track concentrations of O_2 (in m*M*) calculated from Eqs. (33) and (34) for the different irradiating ions considered, using the $G(O_2)$ values shown in (*a*). Typical O_2 concentrations in normal human cells (~30 μM) are shown by the arrow on the right of the figure.

early time and 51 μ*M after* 10^{-8} s. These O_2 concentrations provide clear evidence which supports the hypothesis that O_2 is engendered in substantial yields in the tracks of densely ionizing radiation.

The effect of LET on the concentration of oxygen formed at the end of spur/ track expansion (i.e., ~10^{-6} s) in deaerated liquid water irradiated by $^4He^{2+}$ and $^{12}C^{6+}$ ions of varying incident energies, at neutral pH and for two different temperatures, namely, 25 and 37 °C, is shown in Fig. 3. As described above, the values of $[O_2]$ are directly obtained from Eqs. (33) and (34) using the O_2 escape yields computed from our Monte Carlo simulations with incorporating the multiple ionizations of water, over the whole LET ranges covered for the two impacting ions studied [namely, ~28–215 keV/μm (~6–0.3 MeV/nucleon) for $^4He^{2+}$ and ~97–605 keV/μm (~20–1.25 MeV/ nucleon) for $^{12}C^{6+}$]. As can be seen from the figure, our calculated $[O_2]$ values steeply increase monotonically with increasing LET for both impacting ions, showing an approximate (the lines of Fig. 3 being not precisely straight) proportionality given by $[O_2] \propto (LET)^n$, with $n \approx 1.8–2$. It is also seen from Fig. 3 that, for both $^4He^{2+}$ and $^{12}C^{6+}$ ions, the O_2 concentrations at a given LET are slightly lower at 37 °C than at 25 °C, which is readily explicable by the fact that the diffusion coefficient of oxygen [which intervenes in Eq. (34)] increases with temperature ($D = 3.13 \times 10^{-9}$ m^2 s^{-1} at 37 °C) (HERVÉ DU PENHOAT et al., 2000). For the case of $^4He^{2+}$ ions in the range of LET studied, it is instructive to compare our calculated values of $[O_2]$ for water at 37 °C to the so-called "effective concentrations" of oxygen in the tracks [defined as that amount of O_2 which, if present under "anoxic" conditions, would produce the observed reduction in OER with increasing LET (see Fig. 7 of Chapter I)] estimated by ALPER and BRYANT (1974) (see also: BRYANT and ALPER, 1976; BAVERSTOCK and BURNS, 1976, 1981; BAVERSTOCK et al., 1978; SAUER et al., 1978) from their results on two different cellular systems: the bacterium *S. flexneri* and the alga *C.*

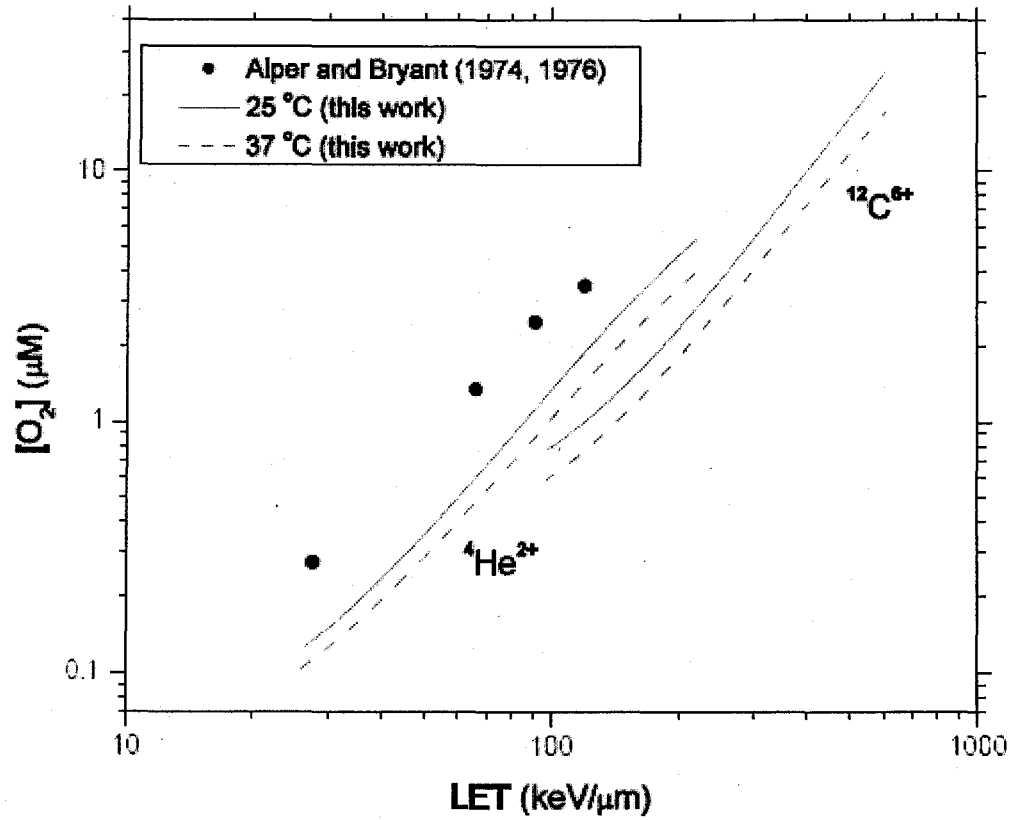

Figure 3. Variation of the concentration of O_2 (in μM) formed in the radiolysis of pure, deaerated liquid water by $^{12}C^{6+}$ and $^{4}He^{2+}$ ions as a function of LET (see text). The solid and dot lines represent our $[O_2]$ values calculated at 25 and 37 °C, respectively, using Eqs. (33) and (34) with the O_2 escape yields (at ~10^{-6} s) obtained from our Monte Carlo simulations incorporating MI of water. In the calculations, the radius of the physical track "core" (r_0) is taken to be ~2.0 nm for the two irradiating ions considered (whatever their energies), and the diffusion coefficient of O_2 (D) is 2.42 × 10^{-9} and 3.13 × 10^{-9} m^2 s^{-1} at 25 and 37 °C, respectively. The closed circles correspond to the "effective concentrations" of track-generated O_2 estimated by ALPER and BRYANT (1974) (see also BRYANT and ALPER, 1976) from the observed reduction in OER with LET (assuming this decrease is attributable to the formation of O_2 in the tracks) for two different organisms, *S. flexneri* and *C. reinhardii*, irradiated with several energies of helium ions. These effective oxygen concentrations were found to be independent of the type of cells being irradiated within experimental error [they were found also to account satisfactorily for the changes in OER with LET for human T_1 kidney cells (BARENDSEN et al., 1966)], a result that was taken as corroboration of the "oxygen-in-the-track" hypothesis.

reinhardii. This comparison is shown in Fig. 3, assuming that O_2 acts at homogeneity (i.e., at the end of spur/track expansion at ~10^{-6} s). As can be seen from this figure, our values reproduce very well the trend of the observed variation of ALPER and BRYANT (1974)'s [O_2] estimates with LET, but, as Fig. 4 illustrates, their magnitude strongly depends on the time scale assumed for the radiobiological action of O_2 in the cellular environment. In fact, these authors did not specify the time scale of events occurring between the oxygen engendered by the helium ions and the O_2-susceptible lesions formed (either directly or indirectly) by the same ionizing particles or by ejected secondary electrons [for example, see reaction (28)]. However, according to HALL and GIACCIA (2006), for the oxygen effect to be observed, oxygen must be present during the irradiation or, to be precise, *during or within microseconds after* the radiation exposure. Support for this view comes from the fact that at high LET the high concentrations of track oxygen and potentially lethal radiation-induced lesions, formed in close proximity to one another, cause their reaction together to be important at an early stage of radiation chemical action (in the time scale below ~10^{-6} s), before the other reactions of self-repair (e.g., fast "chemical repair" of DNA radicals by glutathione and thiols or "biological repair" by cellular repair processes) and self-fixation of lesions (half-lives in the range of ~10^{-5} to 10^{-3} s) can become competitive (SAUER et al., 1978; BAVERSTOCK et al., 1978; BAVERSTOCK and BURNS, 1981; KIEFER, 1975, 1990; VON SONNTAG, 2006). On the basis of the results presented in Fig. 4, our curves of [O_2] versus LET, calculated for *water* irradiated by $^4He^{2+}$ ions of varying energies assuming different values of the oxygen-effect time scale between 10^{-12} and 10^{-6} s, unambiguously indicate that there is a substantial production *in situ* of molecular oxygen that is available immediately after the passage of the ions to produce, *in cells*, the observed drop in OER with increasing LET. However, as we can see from the figure, this production of "radiolytic" track oxygen largely exceeds (by up to

about two orders of magnitude if the oxygen effect is assumed to be determined in a time scale in the range ~10^{-12}–10^{-9} s) the "effective" amounts of O_2 that are actually needed to account for ALPER and BRYANT (1974)'s data. Although one should be

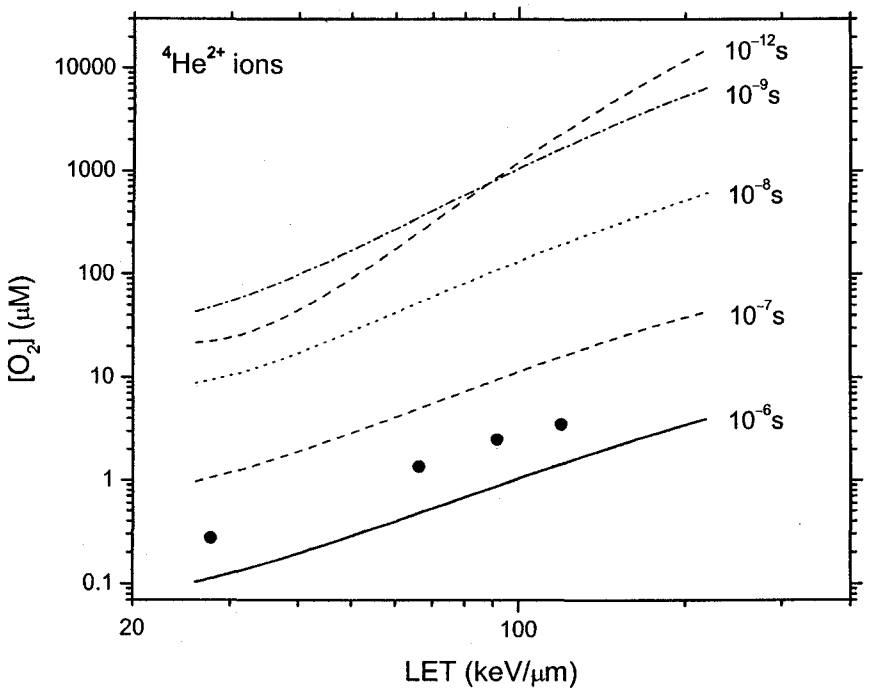

Figure 4. Plot of the curves of the concentration of O_2 (in μM) formed in pure, deaerated liquid water at 37 °C irradiated by $^4He^{2+}$ ions of varying energies in the range ~6–0.3 MeV/nucleon (~28–215 keV/μm) as a function of LET, assuming different values of the oxygen-effect time scale between 10^{-12} and 10^{-6} s. The $[O_2]$ values are calculated using Eqs. (33) and (34) with $r_0 \sim 2.0$ nm, $D(O_2) = 3.13 \times 10^{-9}$ m^2 s^{-1}, and the O_2 yields obtained from our Monte Carlo simulations of the radiolysis of water including the mechanism of MI of water. The closed circles correspond to the "effective concentrations" of track-generated O_2 estimated by ALPER and BRYANT (1974) (see also BRYANT and ALPER, 1976) from the observed reduction in OER with LET (assuming this decrease is attributable to the formation of O_2 in the tracks) for *S. flexneri* and *C. reinhardii*, irradiated with several energies of helium ions (see caption of Fig. 3).

cautious in relating these calculated O_2 yields and concentrations, which are for water, to the situation where energy is deposited in or near a cell (SAUER et al., 1978), the present results strongly suggest that a large proportion of the oxygen generated in the tracks of the ions is consumed in track reactions with free-radical lesions on cellular components that are, in fact, *not* critical for the cells. This can easily be understood in view of the heterogeneity of the target material. In essence, if the critical target in cells is DNA in chromatin, the potentially lethal damage is likely to be at sites where there is also a high protein concentration and where, therefore, the competition for radicals between cellular components and track oxygen is greatly enhanced. Even if the present calculations cannot exclude the possibility of other mechanisms that may also be involved to fully account for the decrease of OER with LET, or equivalently for the increased efficiency of high-LET radiations for the inactivation of tumor hypoxic cells, they appear to indicate that the excess production *in situ* of O_2 in the high-LET tracks is a key intervening factor. In view of these results, the present work largely pleads in favor of the "oxygen-in-the-track" hypothesis.

V.6. Yields of e^-_{aq}, $^{\bullet}OH$, $H^{\bullet}$, and H_2

The nonhomogeneous distribution of reactive species initially produced by the energy deposition relaxes in time toward a homogeneous distribution. This spur/track expansion is essentially complete on the microsecond time scale. As is well known, a key phenomenon in the radiolysis of water and aqueous solutions is the variation of yields with the type and quality of radiation (see Chapter I). The most evident effect of increasing the LET of the radiation is to give lower free-radical and higher molecular primary yields. As mentioned in Chapter I, this behavior reflects the increased intervention of radical-radical combination reactions as the local concentration of radicals

within spurs/tracks increases. In other words, high LET favors high reaction rates for radicals within the dense columnar regions of tracks.

Figures 6 and 7 of Chapter III show that the incorporation of multiple ionizations of water molecules in our simulations of the high-LET, heavy-ion radiolysis of pure, deaerated water has only little effect on the primary yields of e^-_{aq}, $^{\bullet}OH$, $H^{\bullet}$, and H_2 (obtained at 10^{-6} s) for irradiating $^1H^+$, $^4He^{2+}$, $^{12}C^{6+}$, and $^{20}Ne^{9+}$ ions up to ~900 keV/μm, at 25 °C. However, among these radiolytic species, the hydroxyl radicals are certainly the most sensitive, at least at early times, to MI. In fact, as shown in Table 1, most of the $^{\bullet}OH$ radicals arise from single-ionization events [see reactions (12) and (18) of Chapter I], but upon incorporation of MI, double, triple, and quadruple ionizations of water take the place of approximately 2, 3, and 4 single ionizations (to produce O atoms, $HO_2^{\bullet}/O_2^{\bullet-}$, and O_2), respectively. For instance, for the case of double ionizations, 1 O atom takes the place of two $^{\bullet}OH$ radicals. This decrease in single ionizations at high LET readily explains the observed *reduction* (about 15% for ~500 keV/μm $^{12}C^{6+}$ impacting ions; see Fig. 5) in the initial $^{\bullet}OH$ yield (obtained at ~10^{-12} s) when MI is incorporated in our simulations (see also GERVAIS et al., 2006). Since $G(^{\bullet}OH)$ at early times is particularly sensitive to MI, the initial yield of H_2O_2 [which arises mainly from reaction (27)] is itself sensitive, as it can be seen in Fig. 5. In contrast to $^{\bullet}OH$ and H_2O_2, our calculated initial yields of e^-_{aq}, $H^{\bullet}$, and H_2 are essentially identical to those obtained without MI of water. This is easily seen, for example, in the case of e^-_{aq}, since a multiple ionization of degree q is equivalent to q single ionizations with respect to electron emission. Hence, the number of ejected electrons is nearly the same in both kinds of simulations (with and without including MI), so that the physicochemical e^-_{aq} yields are more or less the same. It is worth noting, however, that the reduction in the initial $^{\bullet}OH$ and H_2O_2 yields does not affect in general the corresponding primary radical and molecular yields at the microsecond time scale, except in the case of hydrogen

peroxide for which $G_{H_2O_2}$ remains significantly lower when the multiple ionization of water is included in the simulations (see Chapters III and IV). Unfortunately, there is at present no experimental data available in the literature with which to compare our calculated *G*-values at early times, as well as a function of time in the interval ~10^{-12}–10^{-6} s, at high LET.

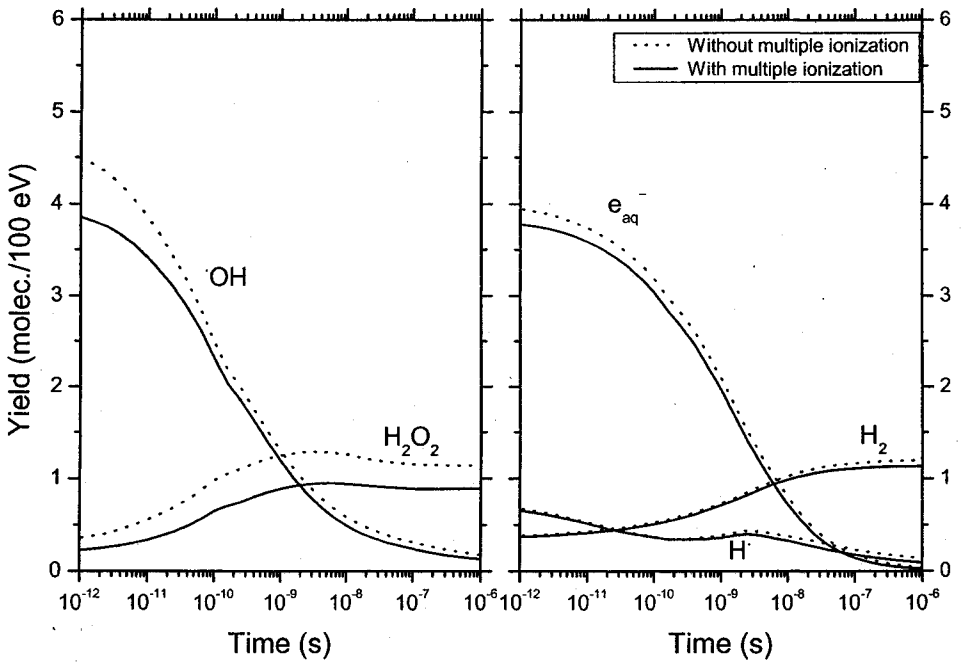

Figure 5. Time dependences of the yields of •OH, H_2O_2, e^-_{aq}, H_2, and H• (in molec./100 eV) calculated from our Monte Carlo simulations of the radiolysis of pure, deaerated liquid water at neutral pH, 25 °C, and in the time scale of 10^{-12}–10^{-6} s, for impacting 2-MeV/nucleon $^{12}C^{6+}$ ions (LET ~ 500 keV/μm). The solid and dot lines represent the results of our simulations with and without including the multiple ionization of water, respectively.

VI. Conclusion

In this work, we have used Monte Carlo track structure simulations to investigate the effect of multiple ionization (MI) of water on the yields of the radiolytic free radical and molecular species, including molecular oxygen, produced in the radiolysis of pure, deaerated liquid water and 0.4 *M* H_2SO_4 aqueous solutions by using several different types of radiation, including $^{1}H^{+}$, $^{4}He^{2+}$, $^{12}C^{6+}$, and $^{20}Ne^{9+}$ ions, at high LET up to ~900 keV/μm, at room temperature. Taking into account the double, triple, and quadruple ionizations of water molecules, the primary (or "escape") yields $G_{HO_2^{\cdot}/O_2^{\cdot-}}$, $G_{H_2O_2}$, $G_{e^-_{aq}}$, $G_{^{\cdot}OH}$, $G_{H^{\cdot}}$, G_{H_2}, and G_{O_2}, have been calculated as a function of LET. A good overall agreement has been obtained between the calculated yields and the available experimental data.

Most remarkably, our results quantitatively reproduce the large increase observed in the $HO_2^{\bullet}/O_2^{\bullet-}$ yield with increasing LET, confirming, for the first time, a hypothesis put forward several years ago by FERRADINI and JAY-GERIN (1998) that multiple ionization of water should intervene in the high-LET, heavy-ion radiolysis of water in the form of the production of $HO_2^{\bullet}/O_2^{\bullet-}$ radicals. This result is all the more important since, under high-LET irradiation conditions, $HO_2^{\bullet}/O_2^{\bullet-}$ is the major radical product that survives spur/track expansion.

With the exception of protons, our results also simultaneously predict a maximum in the curve for $G_{H_2O_2}$ as a function of LET around 180-200 keV/μm, in accord with experiment (although there are large uncertainties in measured hydrogen peroxide yields for different kinds of radiation). In addition, for each ion investigated, this maximum of $G_{H_2O_2}$ occurs precisely at the point where $G_{HO_2^{\cdot}/O_2^{\cdot-}}$ begins to rise sharply, suggesting, in agreement with previous experimental data, that the yields of $HO_2^{\bullet}/O_2^{\bullet-}$ and H_2O_2 are closely linked. In accordance with experiment, we find that

the maximum observed in $G_{H_2O_2}$ in the case of the radiolysis of 0.4 *M* sulphuric acid solutions is more pronounced than that found in neutral solutions and about 45% greater in magnitude. This same difference also exists between our calculated $G_{H_2O_2}$ values for acidic and neutral water at the highest LET values considered in this study. Such results are apparently at variance with a recent assumption by LAVERNE (2004) suggesting that the limiting value of $G_{H_2O_2}$ at infinite LET should be around ~1 molec./100 eV, somewhat similar for both neutral and acidic water. In fact, since our simulations show a marked decrease of $G_{H_2O_2}$ above ~200 keV/μm (this is especially true for acidic solutions), one could be tempted to speculate that the H_2O_2 yields would, instead, tend to zero (or to a value close to it) at very high LET. In the absence of more experimental work, we are led to the conclusion that the question of the limiting value of $G_{H_2O_2}$ at very high LET for both neutral and acidic liquid water is still open. Further experiments on the H_2O_2 yields above 1000 keV/μm would be highly desirable to help clarify this question.

Another point that would need special attention in the problem at hand is the determination of reliable "condensed-phase" multiple-ionization cross-section data. All existing heavy-ion cross sections have been obtained in water vapor but not in liquid water. To overcome these difficulties, we have adopted in this study a strategy consisting in inferring MI cross sections *indirectly* from measurements ($G_{HO_2^\cdot} + G_{O_2}$ in the heavy-ion radiolysis of air-free aqueous $FeSO_4$-$CuSO_4$ solutions at pH ≈ 2.1) made in the *liquid* phase. Using these cross sections in our Monte Carlo simulations allowed us to reproduce, among other things, the maximum in $G_{H_2O_2}$ vs. LET that is observed experimentally. Other published reports have used cross-section data derived directly from gas-phase measurements or from gas-phase-based calculations with various theoretical adjustments to take into account the effects due to the phase, but

they could not reproduce any maximum in the variation of $G_{H_2O_2}$ with LET. More experimental and theoretical work is clearly needed in this area.

For the four irradiating ions used, our results show, upon incorporation of MI of water in the simulations, a steep increase in both the initial (at ~10^{-13} s) and the primary (at ~10^{-6} s) yields of O_2 as a function of LET, giving support to the radiobiological "oxygen in the heavy-ion track" hypothesis. Such an excess production of molecular oxygen in high-LET, heavy-ion tracks is not observed with lower LET radiations. We have shown, in particular, that the dissociation of doubly ionized water molecules is responsible, to a large extent, for this O_2 production *via* the formation of oxygen atoms. The radiolytic formation, at high LET, of substantial amounts of O_2 in heavy-ion tracks can have profound consequences in radiobiology and, in turn, be of great practical relevance in radiotherapy. In fact, being immediately available after the passage of the incident ion, this track oxygen can readily react, in *cells*, with adjacent potentially lethal lesions formed by the same ionizing particle (e.g., the so-called "O_2 fixation" of DNA damage) to produce the observed reduction in the "oxygen enhancement ratio" (OER) with increasing LET. Even if the present calculations cannot exclude the possibility of other mechanisms that may also be involved to fully account for the decrease of OER with LET, or equivalently for the increased efficiency of high-LET radiations for the inactivation of tumor hypoxic cells, they appear to clearly indicate that the excess production *in situ* of O_2 in the high-LET tracks is a key intervening factor.

In contrast to $G_{HO_2^{\cdot}/O_2^{\cdot-}}$, $G_{H_2O_2}$, and G_{O_2}, the incorporation of the mechanism of MI in our simulations has almost no effect on the primary yields of e_{aq}^-, $^{\bullet}OH$, $H^{\bullet}$, and H_2. As expected, $G_{e_{aq}^-}$ and $G_{^{\bullet}OH}$ diminish steeply as the LET is increased, and for the highest LET studied, there is almost no e_{aq}^- and $^{\bullet}OH$ surviving at the microsecond time scale. Our calculated primary $H^{\bullet}$ atom yield values present a slight maximum near 6.5 keV/μm before decreasing steeply at higher LET (similarly to the

behavior of other radicals). As for molecular hydrogen, we find that G_{H_2} monotonically rises with increasing LET for the four impacting ions studied. The available experimental data are generally well reproduced by our calculated escape yields over the whole LET range covered here.

As a consequence of the fact that the LET does not exactly or uniquely define the densities of species in heavy-ion tracks, and therefore the subsequent radiation chemical effects, we observe, for all the species formed during the radiolysis, an irradiating-ion dependence of the yields at a given LET. In other words, two different incident ions of equal LET but different velocities produce different yields due to differences in the effects of track structure on the radiation chemistry.

Finally, it is worthwhile noting that, under the conditions of this study, the mechanisms of triple and quadruple ionizations contribute only weakly to the production of $HO_2^{\bullet}/O_2^{\bullet-}$ and H_2O_2. In other words, the mechanism of double ionization of water is found to largely predominate at high LET, whereas it is insignificant at low LET.

In closing, this study strongly supports the importance of the role of MI in the radiolysis of water under high-LET irradiation conditions. As suggested by PLATZMAN (1952) more than fifty years ago, direct multiple (mainly double) ionization processes, although infrequent relative to single-ionization events, are, indeed, "extremely efficient chemically".

Acknowledgements

I would like to express my sincere gratitude to Prof. Jean-Paul Jay-Gerin for his constant guidance, inspiration, and support, both academic and financial, throughout the course of this study. He is the ideal mentor and this dissertation would not have been possible without him.

I am grateful to Dr. Abdelali Filali-Mouhim for his guidance, encouragement, and helpful discussions in the early stages of this work.

I also wish to thank my colleague, Ianik Plante, for his assistance and many interesting discussions. His help has been very much appreciated.

I thank Prof. M'hamed Bentourkia, Prof. Michael Huels, Prof. Michel Barrette, Prof. Abdelouahed Khalil, and Dr. Craig R. Stuart for having accepted to be on my dissertation Committee and for their helpful critical reviews of this thesis.

Appreciation is also extended to Dr. Samlee Mankhetkorn for his support during my M.Sc. studies in Burapha University (Thailand) and for the encouragement he gave me to come to Sherbrooke to continue for a Ph.D.

I am grateful to Mr. Daniel Robillard and Mr. Carol Gauthier for their most efficient computer technical assistance. I would also like to thank the "Réseau québécois de calcul de haute performance" (RQCHP) for providing generous computing facilities.

It is a pleasure to thank the professors of the Department of Nuclear Medicine and Radiobiology for their excellent courses and constructive suggestions, and all the students and members, past and present, of the Department, for their kind cooperation and friendship.

My deepest thanks and love go to my family who have always supported my education and all of my endeavors.

Bibliography

ALLEN, A.O., 1948. Radiation chemistry of aqueous solutions. *J. Phys. Colloid Chem.* **52**, 479-490.

ALLEN, A.O., 1961. *The Radiation Chemistry of Water and Aqueous Solutions*. D. Van Nostrand Co., Princeton, New Jersey.

ALPER, T., 1956. The modification of damage caused by primary ionization of biological targets. *Radiat. Res.* **5**, 573-586.

ALPER, T. and HOWARD-FLANDERS, P., 1956. Role of oxygen in modifying the radiosensitivity of *E. Coli* B. *Nature (London)* **178**, 978-979.

ALPER, T. and BRYANT, P.E., 1974. Reduction in oxygen enhancement ratio with increase in LET: Tests of two hypotheses. *Int. J. Radiat. Biol.* **26**, 203-218.

ALVARADO, F., HOEKSTRA, R., and SCHLATHÖLTER, T., 2005. Dissociation of water molecules upon keV H^+- and He^{q+}-induced ionization. *J. Phys. B: At. Mol. Opt. Phys.* **38**, 4085-4094.

AMICHAI, O. and TREININ, A., 1969. Chemical reactivity of $O(^3P)$ atoms in aqueous solution. *Chem. Phys. Lett.* **3**, 611-613.

ANDERSON, D.W., 1984. *Absorption of Ionizing Radiation*. University Park Press, Baltimore, MD.

ANDERSON, A.R. and HART, E.J., 1961. Molecular product and free radical yields in the decomposition of water by protons, deuterons, and helium ions. *Radiat. Res.* **14**, 689-704.

APPLEBY, A., 1989. Effects of early track structure on the radiation chemistry of water irradiated with heavy ions. *Radiat. Phys. Chem.* **34**, 121-127.

APPLEBY, A. and SCHWARZ, H.A., 1969. Radical and molecular yields in water irradiated by γ rays and heavy ions. *J. Phys. Chem.* **73**, 1937-1941.

AUTSAVAPROMPORN, N., 2006. The effects of pH and radiation quality (LET) on the radiolysis of liquid water and aqueous solutions: A study by using Monte-Carlo simulations. M.Sc. Thesis, Burapha University, Bangsaen (Thailand).

AUTSAVAPROMPORN, N., MEESUNGNOEN, J., PLANTE, I., and JAY-GERIN, J.-P., 2007. Monte Carlo simulation study of the effects of acidity and LET on the

primary free-radical and molecular yields of water radiolysis. Application to the Fricke dosimeter. *Can. J. Chem.* **85**, 214-229.

AZZAM, E.I., DE TOLEDO, S., and LITTLE, J.B., 2003. Oxidative metabolism, gap junctions and the ionizing radiation-induced bystander effect. *Oncogene* **22**, 7050-7057.

BALDACCHINO, G., LE PARC, D., HICKEL, B., GARDÈS-ALBERT, M., ABEDINZADEH, Z., JORE, D., DEYCARD, S., BOUFFARD, S., MOUTON, V., and BALANZAT, E., 1998*a*. Direct observation of HO_2/O_2^- free radicals generated in water by a high-linear energy transfer pulsed heavy-ion beam. *Radiat. Res.* **149**, 128-133.

BALDACCHINO, G., BOUFFARD, S., BALANZAT, E., GARDÈS-ALBERT, M., ABEDINZADEH, Z., JORE, D., DEYCARD, S., and HICKEL, B., 1998*b*. Direct time-resolved measurement of radical species formed in water by heavy ions irradiation. *Nucl. Instrum. Methods Phys. Res. B* **146**, 528-532.

BALLARINI, F., BIAGGI, M., MERZAGORA, M., OTTOLENGHI, A., DINGFELDER, M., FRIEDLAND, W., JACOB, P., and PARETZKE, 2000. Stochastic aspects and uncertainties in the prechemical and chemical stages of electron tracks in liquid water: A quantitative analysis based on Monte Carlo simulations. *Radiat. Environ. Biophys.* **39**, 179-188.

BARENDSEN, G.W., 1968. Responses of cultured cells, tumours and normal tissues to radiations of different linear energy transfer. *Curr. Top. Radiat. Res. Quarterly* **4**, 293-356.

BARENDSEN, G.W., KOOT, C.J., VAN KERSEN, G.R., BEWLEY, D.K., FIELD, S.B., and PARNELL, C.J., 1966. The effect of oxygen on impairment of the proliferative capacity of human cells in culture by ionizing radiations of different LET. *Int. J. Radiat. Biol.* **10**, 317-327.

BARILLA, J. and LOKAJÍČEK, M., 2000. The role of oxygen in DNA damage by ionizing particles. *J. Theor. Biol.* **207**, 405-414.

BASS, A.D. and SANCHE, L., 2003. Dissociative electron attachment and charge transfer in condensed matter. *Radiat. Phys. Chem.* **68**, 3-13.

BAVERSTOCK, K.F. and BURNS, W.G., 1976. Primary production of oxygen from irradiated water as an explanation for decreased radiobiological oxygen enhancement at high LET. *Nature (London)* **260**, 316-318.

BAVERSTOCK, K.F., BURNS, W.G., and MAY, R., 1978. The oxygen in the track hypothesis: Microdosimetric implications. In: Booz, J. and Ebert, H.G. (Eds.), *Sixth Symposium on Microdosimetry, Brussels, Belgium, May 22-26, 1978*, vol. 2. Harwood Academic Publ., London, pp. 1151-1158.

BAVERSTOCK, K.F. and BURNS, W.G., 1981. Oxygen as a product of water radiolysis in high-LET tracks. II. Radiobiological implications. *Radiat. Res.* **86**, 20-33.

BAVERSTOCK, K.F. and CHARLTON, D.E. (Eds.), 1988. *DNA Damage by Auger Emitters*. Taylor & Francis, London.

BECKER, D. and SEVILLA, M.D., 1993. The chemical consequences of radiation damage to DNA. *Adv. Radiat. Biol.* **17**, 121-180.

BECKMAN, J.S. and KOPPENOL, W.H., 1996. Nitric oxide, superoxide, and peroxynitrite: The good, the bad, and the ugly. *Am. J. Physiol.: Cell Physiol.* **271**, C1424-C1437.

BEDNÁŘ, J., 1985. Electronic excitations in condensed biological matter. *Int. J. Radiat. Biol.* **48**, 147-166.

BENOV, L., 2001. How superoxide radical damages the cell. *Protoplasma* **217**, 33-36.

BERNAS, A., FERRADINI, C., and JAY-GERIN, J.-P., 1996. Électrons en excès dans les milieux polaires homogènes et hétérogènes. *Can. J. Chem.* **74**, 1-23.

BERNAS, A., FERRADINI, C., and JAY-GERIN, J.-P., 1997. On the electronic structure of liquid water: Facts and reflections. *Chem. Phys.* **222**, 151-160.

BERNHARD, W.A. and CLOSE, D.M., 2004. DNA damage dictates the biological consequences of ionizing irradiation: The chemical pathways. In: Mozumder, A. and Hatano, Y. (Eds.), *Charged Particle and Photon Interactions with Matter: Chemical, Physicochemical, and Biological Consequences with Applications*. Marcel Dekker, New York, pp. 431-470.

BETHE, H., 1930. Zur Theorie des Durchgangs schneller Korpuskularstrahlen durch Materie. *Ann. Physik (Leipzig)* **5**, 325-400.

BETHE, H.A. and ASHKIN, J., 1953. Passage of radiations through matter. In: Segrè, E. (Ed.), *Experimental Nuclear Physics*, vol. 1. Wiley, New York, pp. 166-357.

BIBLER, N.E., 1975. Radiolysis of 0.4 M sulfuric acid solutions with fission fragments from dissolved californium-252. Estimated yields of radical and

molecular products that escape reactions in fission fragment tracks. *J. Phys. Chem.* **79**, 1991-1995.

BICHSEL, H., 2006. A method to improve tracking and particle identification in TPCs and silicon detectors. *Nucl. Instrum. Methods Phys. Res. A* **562**, 154-197.

BICHSEL, H. and HIRAOKA, T., 1992. Energy loss of 70 MeV protons in elements. *Nucl. Instrum. Methods Phys. Res. B* **66**, 345-351.

BIEDENKAPP, D., HARTSHORN, L.G., and BAIR, E.J., 1970. The $O(^1D)$ + H_2O reaction. *Chem. Phys. Lett.* **5**, 379-380.

BIELSKI, B.H., CABELLI, D.E., ARUDI, R.L., and ROSS, A.B., 1985. Reactivity of HO_2/O_2^- radicals in aqueous solution. *J. Phys. Chem. Ref. Data* **14**, 1041-1100.

BJERGBAKKE, E. and HART, E.J., 1971. Oxygen formation in the γ-ray irradiation of Fe^{2+}-Cu^{2+} solutions. *Radiat. Res.* **45**, 261-273.

BOUDAÏFFA, B., CLOUTIER, P., HUNTING, D., HUELS, M.A., and SANCHE, L., 2000*a*. Les électrons de très faible énergie produisent des lésions de l'ADN. *Med. Sci.* **16**, 1281-1283.

BOUDAÏFFA, B., CLOUTIER, P., HUNTING, D., HUELS, M.A., and SANCHE, L., 2000*b*. Resonant formation of DNA strand breaks by low-energy (3 to 20 eV) electrons. *Science* **287**, 1658-1660.

BREEN, A.P. and MURPHY, J.A., 1995. Reactions of oxyl radicals with DNA. *Free Radic. Biol. Med.* **18**, 1033-1077.

BRYANT, P.E. and ALPER, T., 1976. Reduction in OER with LET: Evidence supporting the "oxygen-in-the-track" hypothesis. In: Booz, J., Ebert, H.G., and Smith, B.G.R. (Eds.), *Proceedings of the 5th Symposium on Microdosimetry, Verbania Pallanza, Italy, Sept. 22-26, 1975*. Report EUR-5452 d-e-f. Commission of the European Communities, Luxembourg, pp. 871-884.

BURNS, W.G. and SIMS, H.E., 1981. Effect of radiation type in water radiolysis. *J. Chem. Soc., Faraday Trans. 1*, **77**, 2803-2813.

BURNS, W.G., MAY, R., and BAVERSTOCK, K.F., 1981. Oxygen as a product of water radiolysis in high-LET tracks. I. The origin of the hydroperoxyl radical in water radiolysis. *Radiat. Res.* **86**, 1-19.

BURTON, M., 1969. Radiation chemistry: A godfatherly look at its history and its relation to liquids. *Chem. Eng. News* **47**, 86-96 (Feb. 10, 1969).

BUXTON, G.V., 2004. The radiation chemistry of liquid water: Principles and applications. In: Mozumder, A. and Hatano, Y. (Eds.), *Charged Particle and Photon Interactions with Matter: Chemical, Physicochemical, and Biological Consequences with Applications*. Marcel Dekker, New York, pp. 331-363.

BUXTON, G.V., GREENSTOCK, C.L., HELMAN, W.P., and ROSS, A.B., 1988. Critical review of rate constants for reactions of hydrated electrons, hydrogen atoms and hydroxyl radicals ($^{\bullet}OH/^{\bullet}O^{-}$) in aqueous solution. *J. Phys. Chem. Ref. Data* **17**, 513-886.

CADET, J., BERGER, M., DOUKI, T., and RAVANAT, J.-L., 1997. Oxidative damage to DNA: Formation, measurement, and biological significance. *Rev. Physiol. Biochem. Pharmacol.* **131**, 1-87.

CADET, J., DOUKI, T., GASPARUTTO, D., and RAVANAT, J.-L., 2005. Radiation-induced damage to cellular DNA: Measurement and biological role. *Radiat. Phys. Chem.* **72**, 293-299.

CARLSON, T.A. and WHITE, R.M., 1963. Formation of fragment ions from CH_3Te^{125} and $C_2H_5Te^{125}$ following the nuclear decays of CH_3I^{125} and $C_2H_5I^{125}$. *J. Chem. Phys.* **38**, 2930-2934.

CARLSON, T.A. and WHITE, R.M., 1966. Measurement of the relative abundances and recoil-energy spectra of fragment ions produced as the initial consequences of X-ray interaction with CH_3I, HI, and DI. *J. Chem. Phys.* **44**, 4510-4520.

CARLSON, D.J., STEWART, R.D., and SEMENENKO, V.A., 2006. Effects of oxygen on intrinsic radiation sensitivity: A test of the relationship between aerobic and hypoxic linear-quadratic (LQ) model parameters. *Med. Phys.* **33**, 3105-3115.

CHAMPION, C., 2003. Multiple ionization of water by heavy ions: A Monte Carlo approach. *Nucl. Instrum. Methods Phys. Res. B* **205**, 671-676.

CHAMPION, C., L'HOIR, A., POLITIS, M.F., FAINSTEIN, P.D., RIVAROLA, R.D., and CHETIOUI, A., 2005. A Monte Carlo code for the simulation of heavy-ion tracks in water. *Radiat. Res.* **163**, 222-231.

CHATTERJEE, A. and SCHAEFER, H.J., 1976. Microdosimetric structure of heavy ion tracks in tissue. *Radiat. Environ. Biophys.* **13**, 215-227.

CHATTERJEE, A. and HOLLEY, W.R., 1993. Computer simulation of initial events in the biochemical mechanisms of DNA damage. *Adv. Radiat. Biol.* **17**, 181-226.

CHATTORJI, D., 1976. *The Theory of Auger Transitions.* Academic Press, New York.

CHRISTOPHOROU, L.G., McCORKLE, D.L., and CHRISTODOULIDES, A.A., 1984. Electron attachment processes. In: Christophorou, L.G. (Ed.), *Electron-Molecule Interactions and their Applications*, vol. 1. Academic Press, Orlando, FL, pp. 477-617.

CLIFFORD, P., GREEN, N.J.B., OLDFIELD, M.J., PILLING, M.J., and PIMBLOTT, S.M., 1986. Stochastic models of multi-species kinetics in radiation-induced spurs. *J. Chem. Soc., Faraday Trans. 1* **82**, 2673-2689.

COBUT, V., FRONGILLO, Y., JAY-GERIN, J.-P., and PATAU, J.P., 1994. Calculs des rendements des produits de la radiolyse de l'eau en fonction du temps par une méthode Monte Carlo. *J. Chim. Phys.* **91**, 1018-1024.

COBUT, V., JAY-GERIN, J.-P., FRONGILLO, Y., and PATAU, J.P., 1996. On the dissociative electron attachment as a potential source of molecular hydrogen in irradiated liquid water. *Radiat. Phys. Chem.* **47**, 247-250.

COBUT, V., FRONGILLO, Y., PATAU, J.P., GOULET, T., FRASER, M.-J., and JAY-GERIN, J.-P., 1998. Monte Carlo simulation of fast electron and proton tracks in liquid water. I. Physical and physicochemical aspects. *Radiat. Phys. Chem.* **51**, 229-243.

COCKE, C.L. and OLSON, R.E., 1991. Recoil ions. *Phys. Rep.* **205**, 153-219.

CURIE, P. and DEBIERNE, A., 1901. Sur la radio-activité induite et les gaz activés par la radium. *Comptes Rendus Acad. Sci. Paris* **132**, 768-770.

CURTIS, S.B., SCHILLING, W.A., TENFORDE, T.S., CRABTREE, K.E., TENFORDE, S.D., HOWARD, J., and LYMAN, J.T., 1982. Survival of oxygenated and hypoxic tumor cells in the extended-peak regions of heavy charged-particle beams. *Radiat. Res.* **90**, 292-309.

DEBIERNE, A., 1914. Recherches sur les gaz produits par les substances radioactives. Décomposition de l'eau. *Ann. Phys. (Paris)* **2**, 97-127.

DINGFELDER, M., INOKUTI, M., and PARETZKE, H.G., 2000. Inelastic-collision cross sections of liquid water for interactions of energetic protons. *Radiat. Phys. Chem.* **59**, 255-275.

DRAGANIĆ, I.G. and DRAGANIĆ, Z.D., 1971. *The Radiation Chemistry of Water.* Academic Press, New York.

DUANE, W. and SCHEUER, O., 1913. Recherches sur la decomposition de l'eau par les rayons α. *Radium (Paris)* **10**, 33-46.

DUBOIS, R.D. and MANSON, S.T., 1987. Multiple-ionization channels in proton-atom collisions. *Phys. Rev. A* **35**, 2007-2025.

DURUP, J. and PLATZMAN, R.L., 1975. Rendements absolus de l'ionisation en couche profonde sous l'action des rayonnements ionisants. II. Hydrocarbures et quelques substances d'intérêt biologique. *Int. J. Radiat. Phys. Chem.* **7**, 121-136.

ELLIOT, A.J., CHENIER, M.P., OUELLETTE, D.C., and KOSLOWSKY, V.T., 1996. Temperature dependence of g values for aqueous solutions irradiated with 23 MeV $^{2}H^{+}$ and 157 MeV $^{7}Li^{3+}$ ion beams. *J. Phys. Chem.* **100**, 9014-9020.

EVANS, R.D., 1955. *The Atomic Nucleus*. Krieger Publ. Co., Malabar, FL.

EWING, D., 1998. The oxygen fixation hypothesis: A reevaluation. *Am. J. Clin. Oncol.* **21**, 355-361.

FALCONE, J.M., BECKER, D., SEVILLA, M.D., and SWARTS, S.G., 2005. Products of the reactions of the dry and aqueous electron with hydrated DNA: hydrogen and 5,6-dihydropyrimidines. *Radiat. Phys. Chem.* **72**, 257-264.

FANO, U., 1963. Penetration of protons, alpha particles, and mesons. *Annu. Rev. Nucl. Sci.* **13**, 1-66.

FARAGGI, M. and DÉSALOS, J., 1969. Effect of positively charged ions on the "molecular" hydrogen yield in the radiolysis of aqueous solutions. *Int. J. Radiat. Phys. Chem.* **1**, 335-344.

FARAGGI, M., FERRADINI, C., and JAY-GERIN, J.-P., 1995. Migration et devenir des charges formées initialement dans l'ADN irradié: une synthèse. *New J. Chem.* **19**, 1203-1215.

FARAGGI, M. and HOUÉE-LEVIN, C., 1999. Some aspects of the chemistry and biology of the superoxide radical anion. *J. Chim. Phys.* **96**, 71-84.

FERRADINI, C., 1979. Actions chimiques des radiations ionisantes. *J. Phys. Chim.* **76**, 636-644.

FERRADINI, C., 1990. Aspect hétérogène des phénomènes radiolytiques. In: Tilquin, B. (Ed.), *Actions Biologique et Chimique des Radiations*, vol. 1. Éditions Ciaco, Bruxelles, pp. 52-63.

FERRADINI, C. and JAY-GERIN, J.-P., 1998. Does multiple ionization intervene for the production of $HO_2^{\bullet}$ radicals in high-LET liquid water radiolysis. *Radiat. Phys. Chem.* **51**, 263-267.

FERRADINI, C. and JAY-GERIN, J.-P., 1999. La radiolyse de l'eau et des solutions aqueuses : historique et actualité. *Can. J. Chem.* **77**, 1542-1575.

FERRADINI, C. and JAY-GERIN, J.-P., 2000. The effect of pH on water radiolysis: A still open question. A minireview. *Res. Chem. Intermed.* **26**, 549-565.

FRANCK, J. and RABINOWITSCH, E., 1934. Some remarks about free radicals and the photochemistry of solutions. *Trans. Faraday Soc.* **30**, 120-131.

FRANKENBERG-SCHWAGER, M., FRANKENBERG, D., HARBICH, R., and BECKONERT, S., 1994. Evidence against the "oxygen-in-the-track" hypothesis as an explanation for the radiobiological low oxygen enhancement ratio at high linear energy transfer radiation. Radiat. Environ. Biophys. **33**, 1-8.

FREEMAN, G.R., 1987. Ionization and charge separation in irradiated materials. In: Freeman, G.R. (Ed.), *Kinetics of Nonhomogeneous Processes*. Wiley, New York, pp. 19-87.

FRIDOVICH, I., 1986. Biological effects of the superoxide radical. *Arch. Biochem. Biophys.* **247**, 1-11.

FRIDOVICH, I., 1997. Superoxide anion radical ($O_2^{\bullet -}$), superoxide dismutases, and related matters. *J. Biol. Chem.* **272**, 18515-18517.

FRONGILLO, Y., FRASER, M.-J., COBUT, V., GOULET, T., JAY-GERIN, J.-P., and PATAU, J.P., 1996. Évolution des espèces produites par le ralentissement de protons rapides dans l'eau liquide : simulation fondée sur l'approximation des temps de réaction independents. *J. Chim. Phys.* **93**, 93-102.

FRONGILLO, Y., GOULET, T., FRASER, M.-J., COBUT, V., PATAU, J.P., and JAY-GERIN, J.-P., 1998. Monte Carlo simulation of fast electron and proton tracks in liquid water. II. Nonhomogeneous chemistry. *Radiat. Phys. Chem.* **51**, 245-254.

FUCIARELLI, A.F. and ZIMBRICK, J.D. (Eds.), 1995. *Radiation Damage in DNA: Structure/Function Relationships at Early Times*. Battelle Press, Columbus.

GAIGEOT, M.P., VUILLEUMIER, R., STIA, C., GALASSI, M.E., RIVAROLA, R., GERVAIS, B., and POLITIS, M.F., 2007. A multi-scale ab initio theoretical study of the production of free radicals in swift ion tracks in liquid water. *J. Phys. B: At. Mol. Opt. Phys.* **40**, 1-12.

GANGULY, A.K. and MAGEE, J.L., 1956. Theory of radiation chemistry. III. Radical reaction mechanism in the tracks of ionizing radiations. *J. Chem. Phys.* **25**, 129-134.

GARDÈS-ALBERT, M., JORE, D., ABEDINZADEH, Z., ROUSCILLES, A., DEYCARD, S., and BOUFFARD, S., 1996. Réduction du tétranitrométhane par les espèces primaires formées lors de la radiolyse de l'eau par des ions lourds Ar^{18+}. *J. Chim. Phys.* **93**, 103-110.

GÄUMANN, T. and SCHULER, R.H., 1961. The radiolysis of benzene by densely ionizing radiations. *J. Phys. Chem.* **65**, 703-704.

GEMMELL, D.S., 1980. Determining the stereochemical structures of molecular ions by "Coulomb-explosion" techniques with fast (MeV) molecular ion beams. *Chem. Rev.* **80**, 301-311.

GERVAIS, B., BEUVE, M., OLIVERA, G.H., GALASSI, M.E., and RIVAROLA, R.D., 2005. Production of HO_2 and O_2 by multiple ionization in water radiolysis by swift carbon ions. *Chem. Phys. Lett.* **410**, 330-334.

GERVAIS, B., BEUVE, M., OLIVERA, G.H., and GALASSI, M.E., 2006. Numerical simulation of multiple ionization and high LET effects in liquid water radiolysis. *Radiat. Phys. Chem.* **75**, 493-513.

GIESEL, F., 1902. Ueber Radium und radioactive Stoffe. *Ber. Dtsch. Chem. Ges. (Berlin)* **35**, 3608-3611.

GIESEL, F., 1903. Ueber den Emanationskörper aus Pechblende und über Radium. *Ber. Dtsch. Chem. Ges. (Berlin)* **36**, 342-347.

GOBET, F., FARIZON, B., FARIZON, M., GAILLARD, M.J., CARRÉ, M., LEZIUS, M., SCHEIER, P., and MÄRK, 2001. Total, partial, and electron-capture cross sections for ionization of water vapor by 20–150 keV protons. *Phys. Rev. Lett.* **86**, 3751-3754.

GOLDSTEIN, S. and CZAPSKI, G., 1995. The reaction of $^{\bullet}NO$ with $O_2^{\bullet-}$ and $HO_2^{\bullet}$: A pulse radiolysis study. *Free Radical Biol. Med.* **19**, 505-510.

GOODHEAD, D.T., 1994. Initial events in the cellular effects of ionizing radiations: Clustered damage in DNA. *Int. J. Radiat. Biol.* **65**, 7-17.

GOULET, T. and JAY-GERIN, J.-P., 1988. Thermalization distances and times for subexcitation electrons in solid water. *J. Phys. Chem.* **92**, 6871-6874.

GOULET, T. and JAY-GERIN, J.-P., 1989. Thermalization of subexcitation electrons in solid water. *Radiat. Res.* **118**, 46-62.

GOULET, T. and JAY-GERIN, J.-P., 1992. On the reactions of hydrated electrons with $^{\bullet}OH$ and H_3O^+. Analysis of photoionization experiments. *J. Chem. Phys.* **96**, 5076-5087.

GOULET, T., FRASER, M.-J., FRONGILLO, Y., and JAY-GERIN, J.-P., 1998. On the validity of the independent reaction times approximation for the description of the nonhomogeneous kinetics of liquid water radiolysis. *Radiat. Phys. Chem.* **51**, 85-91.

GRAY, L.H., CONGER, A.D., EBERT, M., HORNSEY, S., and SCOTT, O.C.A., 1953. The concentration of oxygen dissolved in tissues at the time of irradiation as a factor in radiotherapy. *Brit. J. Radiol.* **26**, 638-648.

GREEN, N.J.B., PILLING, M.J., PIMBLOTT, S.M., and CLIFFORD, P., 1990. Stochastic modeling of fast kinetics in a radiation track. *J. Phys. Chem.* **94**, 251-258.

HALL, E.J. and GIACCIA, A.J., 2006. *Radiobiology for the Radiologist*, 6th ed. Lippincott, Williams & Wilkins, Philadelphia, PA.

HALLIWELL, B. and GUTTERIDGE, J.M.C., 1999. *Free Radicals in Biology and Medicine*, 3rd ed. Oxford University Press, Oxford.

HAMM, R.N., TURNER, J.E., RITCHIE, R.H., and WRIGHT, H.A., 1985. Calculation of heavy-ion tracks in liquid water. *Radiat. Res.* **104**, S-20–S-26.

HELLER, J.M., Jr., HAMM, R.N., BIRKHOFF, R.D., and PAINTER, L.R., 1974. Collective oscillation in liquid water. *J. Chem. Phys.* **60**, 3483-3486.

HENDRY, J.H., 1999. Repair of cellular damage after high LET irradiation. *J. Radiat. Res.* **40** (Suppl.), 60-65.

HERVÉ DU PENHOAT, M.-A., GOULET, T., FRONGILLO, Y., FRASER, M.-J., BERNAT, Ph., and JAY-GERIN, J.-P., 2000. Radiolysis of liquid water at temperatures up to 300 °C: A Monte Carlo simulation study. *J. Phys. Chem. A* **104**, 11757-11770.

HOWARD-FLANDERS, P., 1958. Physical and chemical mechanisms in the injury of cells by ionizing radiations. *Adv. Biol. Med. Phys.* **6**, 553-603.

HUELS, M.A., BOUDAÏFFA, B., CLOUTIER, P., HUNTING, D., and SANCHE, L., 2003. Single, double, and multiple double strand breaks induced in DNA by 3-100 eV electrons. *J. Am. Chem. Soc.* **125**, 4467-4477.

HUIE, R.E. and PADMAJA, S., 1993. The reaction of NO with superoxide. *Free Radical Res. Commun.* **18**, 195-199.

IAEA-TECDOC-799, 1995. *Atomic and Molecular Data for Radiotherapy and Radiation Research.* International Atomic Energy Agency, Vienna.

ICRU REPORT 16, 1970. *Linear Energy Transfer.* International Commission on Radiation Units and Measurements, Washington, DC.

ICRU REPORT 31, 1979. *Average Energy Required to Produce an Ion Pair.* International Commission on Radiation Units and Measurements, Washington, DC.

ICRU REPORT 55, 1996. *Secondary Electron Spectra from Charged Particle Interactions.* International Commission on Radiation Units and Measurements, Bethesda, MD.

ICRU REPORT 60, 1998. *Fundamental Quantities and Units for Ionizing Radiation.* International Commission on Radiation Units and Measurements, Bethesda, MD.

INOKUTI, M., 1971. Inelastic collisions of fast charged particles with atoms and molecules – The Bethe theory revisited. *Rev. Mod. Phys.* **43**, 297-347.

JARDIN, P., CASSIMI, A., GRANDIN, J.-P., and UNVERZAGT, M., 1994. Multi-ionisation de la molécule d'eau en phase gazeuse par les ions lourds. Book of Abstracts, "7$^{\text{ièmes}}$ Journées d'Études sur la Chimie sous Rayonnement, Caen, France, 5-9 September 1994", p. C45.

JAY-GERIN, J.-P. and FERRADINI, C., 2000. Are there protective enzymatic pathways to regulate high local nitric oxide ($^{\bullet}$NO) concentrations in cells under stress conditions? *Biochimie* **82**, 161-166.

JOACHAIN, C.J., 1983. *Quantum Collision Theory*, 3rd ed. North-Holland, Amsterdam.

JONAH, C.D., 1985. Discussion. *Radiat. Res.* **104**, S-47–S-51.

JONAH, C.D., 1995. A short history of the radiation chemistry of water. *Radiat. Res.* **144**, 141-147.

KAPLAN, I.G. and MITEREV, A.M., 1987. Interaction of charged particles with molecular medium and track effects in radiation chemistry. *Adv. Chem. Phys.* **68**, 255-386.

KARA-MICHAILOVA, E. and LEA, D.E., 1940. The interpretation of ionization measurements in gases at high pressures. *Proc. Cambridge Phil. Soc.* **36**, 101-126.

KATZ, R., 1970. RBE, LET and z/β^{α}. *Health Phys.* **18**, 175.

KATZ, R., 1978. Track structure theory in radiobiology and in radiation detection. *Nucl. Track Detect.* **2**, 1-28.

KERNBAUM, M., 1910. Sur la décomposition de l'eau par divers rayonnements. *Radium (Paris)* **7**, 242.

KIEFER, J., 1975. Theoretical aspects and implications of the oxygen effect. In: Nygaard, O.F., Adler, H.I., and Sinclair, W.K. (Eds.), *Radiation Research: Biomedical, Chemical, and Physical Perspectives – Proceedings of the Fifth International Congress of Radiation Research, Seattle, WA, U.S.A., July 14-20, 1974.* Academic Press, New York, pp. 1025-1037.

KIEFER, J., 1990. *Biological Radiation Effects*. Springer-Verlag, Berlin.

KIMMEL, G.A., ORLANDO, T.M., VÉZINA, C., and SANCHE, L., 1994. Low-energy electron-stimulated production of molecular hydrogen from amorphous water ice. *J. Chem. Phys.* **101**, 3282-3286.

KISSNER, R., NAUSER, T., BUGNON, P., LYE, P.G., and KOPPENOL, W.H., 1997. Formation and properties of peroxynitrite as studied by laser flash photolysis, high-pressure stopped-flow technique, and pulse radiolysis. *Chem. Res. Toxicol.* **10**, 1285-1292.

KRAFT, G. and KRÄMER, M., 1993. Linear energy transfer and track structure. *Adv. Radiat. Biol.* **17**, 1-52.

KROH, J. (Ed.), 1989. *Early Developments in Radiation Chemistry*. The Royal Society of Chemistry, Thomas Graham House, Cambridge.

KUPPERMANN, A., 1967. Diffusion model of the radiation chemistry of aqueous solutions. In: Silini, G. (Ed.), *Radiation Research: Proceedings of the Third International Congress of Radiation Research, Cortina d'Ampezzo, Italy, June 26-July 2, 1966*. North-Holland, Amsterdam, pp. 212-234.

LATIMER, C.J., 1993. The dissociative ionization of simple molecules by fast ions. *Adv. At. Molec. Opt. Phys.* **30**, 105-138.

LAVERNE, J.A., 1989. Radical and molecular yields in the radiolysis of water with carbon ions. *Radiat. Phys. Chem.* **34**, 135-143.

LAVERNE, J.A., 2000. Track effects of heavy ions in liquid water. *Radiat. Res.* **153**, 487-496.

LAVERNE, J.A., 2004. Radiation chemical effects of heavy ions. In: Mozumder, A. and Hatano, Y. (Eds.), *Charged Particle and Photon Interactions with Matter: Chemical, Physicochemical, and Biological Consequences with Applications*. Marcel Dekker, New York, pp. 403-429.

LAVERNE, J.A., BURNS, W.G., and SCHULER, R.H., 1985. Production of HO_2 within the track core in the heavy particle radiolysis of water. *J. Phys. Chem.* **89**, 242-243.

LAVERNE, J.A., SCHULER, R.H., and BURNS, W.G., 1986. Track effects in radiation chemistry: Production of $HO_2^{\bullet}$ within the track core in the heavy-particle radiolysis of water. *J. Phys. Chem.* **90**, 3238-3242.

LAVERNE, J.A. and SCHULER, R.H., 1987*a*. Radiation chemical studies with heavy ions: Oxidation of ferrous ion in the Fricke dosimeter. *J. Phys. Chem.* **91**, 5770-5776.

LAVERNE, J.A. and SCHULER, R.H., 1987*b*. Track effects in radiation chemistry: Production of $HO_2^{\bullet}$ in the radiolysis of water by high-LET ^{58}Ni ions. *J. Phys. Chem.* **91**, 6560-6563.

LAVERNE, J.A. and MOZUMDER, A., 1993. Concerning plasmon excitation in liquid water. *Radiat. Res.* **133**, 282-288.

LAVERNE, J.A. and PIMBLOTT, S.M., 1995. Electron energy-loss distributions in solid, dry DNA. *Radiat. Res.* **141**, 208-215.

LAVERNE, J.A. and SCHULER, R.H., 1996. Radiolysis of the Fricke dosimeter with ^{58}Ni and ^{238}U ions: Response for particles of high linear energy transfer. *J. Phys. Chem.* **100**, 16034-16040.

LEFORT, M., 1955. Chimie des radiations des solutions aqueuses. Aspect actuel des résultats expérimentaux. In: Haïssinsky, M. (Ed.), *Actions Chimiques et Biologiques des Radiations*, vol. 1. Masson, Paris, pp. 93-204.

LEFORT, M. and TARRAGO, X., 1959. Radiolysis of water by particles of high linear energy transfer. The primary chemical yields in aqueous acid solutions of ferrous sulfate, and in mixtures of thallous and ceric ions. *J. Phys. Chem.* **63**, 833-836.

LEGENDRE, S., GIGLIO, E., TARISIEN, M., CASSIMI, A., GERVAIS, B., and ADOUI, L., 2005. Isotopic effects in water dication fragmentation. *J. Phys. B.: At. Mol. Opt. Phys.* **38**, L233-L241.

LE SECH, C., FROHLICH, H., SAINT-MARC, C., and CHARLIER, M., 1996. DNA breakage upon K-shell excitation of phosphorus as a model for direct effects in radiation biology. *Radiat. Res.* **145**, 632-635.

LIDE, D.R. (Ed.), 2003. *CRC Handbook of Chemistry and Physics*, 84th ed. CRC Press, Boca Raton, FL.

LUNA, H. and MONTENEGRO, E.C., 2005. Fragmentation of water by heavy ions. *Phys. Rev. Lett.* **94**, 043201-1–043201-4.

MAGEE, J.L., 1953. Radiation chemistry. *Annu. Rev. Nucl. Sci.* **3**, 171-192.

MAGEE, J.L. and CHATTERJEE, A., 1980. Radiation chemistry of heavy-particle tracks. 1. General considerations. *J. Phys. Chem.* **84**, 3529-3536.

MAGEE, J.L. and CHATTERJEE, A., 1987. In: Freeman, G.R. (Ed.), *Kinetics of Nonhomogeneous Processes*. Wiley, New York, pp. 171-214.

MANSON, S.T., DUBOIS, R.D., and TOBUREN, L.H., 1983. Multiple-ionization mechanisms in fast proton-neon collisions. *Phys. Rev. Lett.* **51**, 1542-1545.

McCRACKEN, D.R., TSANG, K.T., and LAUGHTON, P.J., 1998. Aspects of the physics and chemistry of water radiolysis by fast neutrons and fast electrons in nuclear reactors. Report AECL-11895. Atomic Energy of Canada Ltd., Chalk River, Ontario.

McDANIEL, E.W., MITCHELL, J.B.A., and RUDD, M.E., 1993. *Atomic Collisions: Heavy Particle Projectiles*. Wiley, New York.

MEDIN, J., ROSS, C.K., KLASSEN, N.V., PALMANS, H., GRUSELL, E., and GRINDBORG, J.-E., 2006. Experimental determination of beam quality factors, k_Q, for two types of Farmer chamber in a 10 MV photon and a 175 MeV proton beam. *Phys. Med. Biol.* **51**, 1503-1521.

MEESUNGNOEN, J., BENRAHMOUNE, M., FILALI-MOUHIM, A., MANKHETKORN, S., and JAY-GERIN, J.-P., 2001. Monte Carlo calculation of the primary radical and molecular yields of liquid water radiolysis in the linear energy transfer range 0.3-6.5 keV/μm: Application to ^{137}Cs gamma rays. *Radiat. Res.* **155**, 269-278.

MEESUNGNOEN, J., JAY-GERIN, J.-P., FILALI-MOUHIM, A., and MANKHETKORN, S., 2002*a*. Low-energy electron penetration range in liquid water. *Radiat. Res.* **158**, 657-660.

MEESUNGNOEN, J., JAY-GERIN, J.-P., FILALI-MOUHIM, A., and MANKHETKORN, S., 2002*b*. On the temperature dependence of the primary yield and the product $G\varepsilon_{max}$ of hydrated electrons in the low-LET radiolysis of liquid water. *Can. J. Chem.* **80**, 767-773.

MEESUNGNOEN, J., FILALI-MOUHIM, A., SNITWONGSE NA AYUDHYA, N., MANKHETKORN, S., and JAY-GERIN, J.-P., 2003. Multiple ionization effects on the yields of $HO_2^{\bullet}/O_2^{\bullet-}$ and H_2O_2 produced in the radiolysis of liquid water with high-LET $^{12}C^{6+}$ ions: A Monte-Carlo simulation study. *Chem. Phys. Lett.* **377**, 419-425.

MEESUNGNOEN, J. and JAY-GERIN, J.-P., 2005*a*. High-LET radiolysis of liquid water with $^{1}H^{+}$, $^{4}He^{2+}$, $^{12}C^{6+}$, and $^{20}Ne^{9+}$ ions: Effects of multiple ionization. *J. Phys. Chem. A* **109**, 6406-6419.

MEESUNGNOEN, J. and JAY-GERIN, J.-P., 2005*b*. Effect of multiple ionization on the yield of H_2O_2 produced in the radiolysis of aqueous 0.4 *M* H_2SO_4 solutions by high-LET $^{12}C^{6+}$ and $^{20}Ne^{9+}$ ions. *Radiat. Res.* **164**, 688-694.

MICHAEL, B.D. and PRISE, K.M., 1996. A multiple-radical model for radiation action on DNA and the dependence of OER on LET. *Int. J. Radiat. Biol.* **69**, 351-358.

MICHAUD, M., CLOUTIER, P., and SANCHE, L., 1991. Low-energy electron-energy-loss spectroscopy of amorphous ice: Electronic excitations. *Phys. Rev. A* **44**, 5624-5627.

MICHAUD, M., WEN, A., and SANCHE, L., 2003. Cross sections for low-energy (1-100 eV) electron elastic and inelastic scattering in amorphous ice. *Radiat. Res.* **159**, 3-22.

MILLER, N., 1958. Radical yield measurements in irradiated aqueous solutions. II. Radical yields with 10.9-MeV deuterons, 21.3- and 3.4-MeV alpha particles, and B(n,α)Li recoil radiations. *Radiat. Res.* **9**, 633-646.

MONTENEGRO, E.C. and LUNA, H., 2005. Primary radicals production from water fragmentation by heavy ions. *Brazilian J. Phys.* **35**, 927-932.

MOTHERSILL, C. and SEYMOUR, C.B., 2004. Radiation-induced bystander effects – Implications for cancer. *Nature (London)* **4**, 158-164.

MOZUMDER, A., 1999. *Fundamentals of Radiation Chemistry*. Academic Press, San Diego, CA.

MOZUMDER, A. and MAGEE, J.L., 1966*a*. Model of tracks of ionizing radiations for radical reaction mechanisms. *Radiat. Res.* **28**, 203-214.

MOZUMDER, A. and MAGEE, J.L., 1966*b*. Theory of radiation chemistry. VII. Structure and reactions in low LET tracks. *J. Chem. Phys.* **45**, 3332-3341.

MOZUMDER, A., CHATTERJEE, A., and MAGEE, J.L., 1968. Theory of radiation chemistry. IX. Model and structure of heavy particle tracks in water. *Adv. Chem. Series* **81**, 27-48.

MOZUMDER, A. and MAGEE, J.L., 1975. The early events of radiation chemistry. *Int. J. Radiat. Phys. Chem.* **7**, 83-93.

MROCZKA, N.E., MERCER, K.R., and BERNHARD, W.A., 1997. The effects of lattice water on free radical yields in X-irradiated crystalline pyrimidines and purines: A low-temperature electron paramagnetic resonance investigation. *Radiat. Res.* **147**, 560-568.

MUROYA, Y., MEESUNGNOEN, J., JAY-GERIN, J.-P., FILALI-MOUHIM, A., GOULET, T., KATSUMURA, Y., and MANKHETKORN, S., 2002. Radiolysis of liquid water: An attempt to reconcile Monte-Carlo calculations with new experimental hydrated electron yield data at early times. *Can. J. Chem.* **80**, 1367-1374.

MUROYA, Y., PLANTE, I., AZZAM, E.I., MEESUNGNOEN, J., KATSUMURA, Y., and JAY-GERIN, J.-P., 2006. High-LET ion radiolysis of water:

Visualization of the formation and evolution of ion tracks and relevance to the radiation-induced bystander effect. *Radiat. Res.* **165**, 485-491.

NAGASAWA, H. and LITTLE, J.B., 1992. Induction of sister chromatid exchanges by extremely low doses of α-particles. *Cancer Res.* **52**, 6394-6396.

NEARY, G.J., 1965. Chromosome aberrations and the theory of RBE. 1. General considerations. *Int. J. Radiat. Biol.* **9**, 477-502.

NIKJOO, H., O'NEILL, P., WILSON, W.E., and GOODHEAD, D.T., 2001. Computational approach for determining the spectrum of DNA damage induced by ionizing radiation. *Radiat. Res.* **156**, 577-583.

OGURA, H. and HAMILL, W.H., 1973. Positive hole migration in pulse-irradiated water and heavy water. *J. Phys. Chem.* **77**, 2952-2954.

OLIVERA, G.H., CARABY, C., JARDIN, P., CASSIMI, A., ADOUI, L., and GERVAIS, B., 1998. Multiple ionization in the earlier stages of water radiolysis. *Phys. Med. Biol.* **43**, 2347-2360.

O'NEILL, P., AL-KAZWINI, A.T., LAND, E.J., and FIELDEN, E.M., 1991. Early chemical events in the development of radiation damage of DNA – Novel approaches. In: Fielden, E.M. and O'Neill, P. (Eds.), *The Early Effects of Radiation on DNA*. Springer-Verlag, Berlin, pp. 125-140.

O'NEILL, P. and FIELDEN, E.M., 1993. *Adv. Radiat. Biol.* **17**, 53-120.

O'NEILL, P., 2001. Radiation-induced damage in DNA. In: Jonah, C.D. and Rao, B.S.M. (Eds.), *Radiation Chemistry: Present Status and Future Trends*. Elsevier, Amsterdam, pp. 585-622.

PARETZKE, H.G., 1987. Radiation track structure theory. In: Freeman, G.R. (Ed.), *Kinetics of Nonhomogeneous Processes*. Wiley, New York, pp. 89-170.

PARETZKE, H.G., GOODHEAD, D.T., KAPLAN, I.G., and TERRISSOL, M., 1995. Track structure quantities. In: *Atomic and Molecular Data for Radiotherapy and Radiation Research*, IAEA-TECDOC-799. International Atomic Energy Agency, Vienna, pp. 633-721.

PASTINA, B. and LAVERNE, J.A., 1999. Hydrogen peroxide production in the radiolysis of water with heavy ions. *J. Phys. Chem. A* **103**, 1592-1597.

PATT, H.M., 1953. Protective mechanisms in ionizing radiation injury. *Physiol. Rev.* **33**, 35-76.

PEŠIĆ, Z.D., CHESNEL, J.-Y., HELLHAMMER, R., SULIK, B., and STOLTERFOHT, N., 2004. Fragmentation of H_2O molecules following the interaction with slow, highly charged Ne ions. *J. Phys. B: At. Mol. Opt. Phys.* **37**, 1405-1417.

PIMBLOTT, S.M., LAVERNE, J.A., MOZUMDER, A., and GREEN, N.J.B., 1990. Structure of electron tracks in water. 1. Distribution of energy deposition events. *J. Phys. Chem.* **94**, 488-495.

PIMBLOTT, S.M. and MOZUMDER, A., 1991. Structure of electron tracks in water. 2. Distribution of primary ionizations and excitations in water radiolysis. *J. Phys. Chem.* **95**, 7291-7300.

PIMBLOTT, S.M., PILLING, M.J., and GREEN, N.J.B., 1991. Stochastic models of spur kinetics in water. *Radiat. Phys. Chem.* **37**, 377-388.

PIMBLOTT, S.M. and GREEN, N.J.B., 1995. Recent advances in the kinetics of radiolytic processes. *Res. Chem. Kinet.* **3**, 117-174.

PIMBLOTT, S.M. and LAVERNE, J.A., 2002. Effects of track structure on the ion radiolysis of the Fricke dosimeter. *J. Phys. Chem. A* **106**, 9420-9427.

PIMBLOTT, S.M. and MOZUMDER, A., 2004. Modeling of physicochemical and chemical processes in the interactions of fast charged particles with matter. In: Mozumder, A. and Hatano, Y. (Eds.), *Charged Particle and Photon Interactions with Matter: Chemical, Physicochemical, and Biological Consequences with Applications*. Marcel Dekker, New York, pp. 75-103.

PLANTE, I., 2005. Conception d'une interface informatique couplée à un code de simulation Monte-Carlo de la radiolyse de l'eau, permettant la visualisation en trois dimensions de la trajectoire d'une particule chargée incidente et de toutes les espèces radiolytiques formées en fonction du temps. M.Sc. Thesis, University of Sherbrooke, Sherbrooke (Quebec), Canada.

PLANTE, I., FILALI-MOUHIM, A., and JAY-GERIN, J.-P., 2005. SimulRad: A Java interface for a Monte-Carlo simulation code to visualize in 3D the early stages of water radiolysis. *Radiat. Phys. Chem.* **72**, 173-180.

PLATZMAN, R.L., 1952. On the primary processes in radiation chemistry and biology. In: Nickson, J.J. (Ed.), *Symposium on Radiobiology. The Basic Aspects of Radiation Effects on Living Systems*. Wiley, New York, pp. 97-116.

PLATZMAN, R.L., 1955. Subexcitation electrons. *Radiat. Res.* **2**, 1-7.

PLATZMAN, R.L., 1958. The physical and chemical basis of mechanisms in radiation biology. In: Claus, W.D. (Ed.), *Radiation Biology and Medicine. Selected Reviews in the Life Sciences*. Addison-Wesley, Reading, MA, pp. 15-72.

PLATZMAN, R.L., 1962*a*. Superexcited states of molecules. *Radiat. Res.* **17**, 419-425.

PLATZMAN, R.L., 1962*b*. Dissociative attachment of subexcitation electrons in liquid water, and the origin of radiolytic "molecular" hydrogen. In: *Abstracts of Papers*, Second International Congress of Radiation Research, Harrogate, England, August 5-11, 1962, p. 128.

POGUE, B.W., O'HARA, J.A., WILMOT, C.M., PAULSEN, K.D., and SWARTZ, H.M., 2001. Estimation of oxygen distribution in RIF-1 tumors by diffusion model-based interpretation of pimonidazole hypoxia and Eppendorf measurements. *Radiat. Res.* **155**, 15-25.

PUCHEAULT, J., 1961. Action des rayons alpha sur les solutions aqueuses. In: Haïssinsky, M. (Ed.), *Actions Chimiques et Biologiques des Radiations*, vol. 5. Masson, Paris, pp. 31-84.

RADI, R., DENICOLA, A., ALVAREZ, B., FERRER-SUETA, G., and RUBBO, H., 2000. The biological chemistry of peroxynitrite. In: Ignarro, L.J. (Ed.), *Nitric Oxide: Biology and Pathobiology*. Academic Press, San Diego, CA, pp. 57-82.

RAMSAY, W. and SODDY, F., 1903. Experiments in radioactivity, and the production of helium from radium. *Proc. R. Soc. London* **72**, 204-207.

ROWNTREE, P., PARENTEAU, L., and SANCHE, L., 1991. Electron stimulated desorption via dissociative attachment in amorphous H_2O. *J. Chem. Phys.* **94**, 8570-8576.

RUDD, M.E., 1990. Cross sections for production of secondary electrons by charged particles. *Radiat. Prot. Dosim.* **31**, 17-22.

RUDD, M.E., KIM, Y.-K., MADISON, D.H., and GAY, T.J., 1992. Electron production in proton collisions with atoms and molecules: energy distributions. *Rev. Mod. Phys.* **64**, 441-490.

SAENGER, W., 1984. *Principles of Nucleic Acid Structure*. Springer-Verlag, New York.

SAMUEL, A.H. and MAGEE, J.L., 1953. Theory of radiation chemistry. II. Track effects in radiolysis of water. *J. Chem. Phys.* **21**, 1080-1087.

SANCHE, L., 2002. Nanoscopic aspects of radiobiological damage: Fragmentation induced by secondary low-energy electrons. *Mass Spectrom. Rev.* **21**, 349-369.

SAUER, M.C., Jr., SCHMIDT, K.H., HART, E.J., NALEWAY, C.A., and JONAH, C.D., 1977. LET dependence of transient yields in the pulse radiolysis of aqueous systems with deuterons and α particles. *Radiat. Res.* **70**, 91-106.

SAUER, M.C., Jr., SCHMIDT, K.H., JONAH, C.D., NALEWAY, C.A., and HART, E.J., 1978. High-LET pulse radiolysis: O_2^- and oxygen production in tracks. *Radiat. Res.* **75**, 519-528.

SELMAN, J., 1983. *Elements of Radiobiology*. Charles C. Thomas, Springfield, IL.

SCHOLES, G. and WEISS, J., 1959. Oxygen effects and formation of peroxides in aqueous solutions. *Radiat. Res. Suppl.* **1**, 177-189.

SCHULER, R.H., 1965. Radiolysis of benzene by heavy ions. *Trans. Faraday Soc.* **61**, 100-109.

SCHULER, R.H. and ALLEN, A.O., 1957. Radiation chemistry studies with cyclotron beams of variable energy: Yields in aerated ferrous sulfate solution. *J. Am. Chem. Soc.* **79**, 1565-1572.

SCHWARZ, H.A., 1969. Applications of the spur diffusion model to the radiation chemistry of aqueous solutions. *J. Phys. Chem.* **73**, 1928-1937.

SIEGMANN, B., WERNER, U., LUTZ, H.O., and MANN, R., 2001. Multiple ionization and fragmentation of H_2O in collisions with fast highly charged Xe ions. *J. Phys. B: At. Mol. Opt. Phys.* **34**, L587-L593.

SIMS, H.E., 1978. Some effects of linear energy transfer on the radiolysis of aqueous solutions. Ph.D. Thesis, University of Salford, Salford, U.K.

SOBOCINSKI, P., PEŠIĆ, Z.D., HELLHAMMER, R., KLEIN, D., SULIK, B., CHESNEL, J.-Y., and STOLTERFOHT, N., 2006. Anisotropic proton emission after fragmentation of H_2O by multiply charged ions. *J. Phys. B: At. Mol. Opt. Phys.* **39**, 927-937.

SPINKS, J.W.T. and WOODS, R.J., 1990. *An Introduction to Radiation Chemistry*, 3rd ed. Wiley, New York.

STOLTERFOHT, N., CABRERA-TRUJILLO, R., HELLHAMMER, R., PEŠIĆ, Z., DEUMENS, E., ÖHRN, Y., and SABIN, J.R., 2007. Charge exchange and fragmentation in slow collisions of He^{2+} with water molecules. *Adv. Quantum Chem.* **52**, 149-170.

STUGLIK, Z., 1995. On the "oxygen in heavy-ion tracks" hypothesis. *Radiat. Res.* **143**, 343-348.

SUTHERLAND, B.M., BENNETT, P.V., SIDORKINA, O., and LAVAL, J., 2000. Clustered DNA damages induced in isolated DNA and human cells by low doses of ionizing radiation. *Proc. Natl. Acad. Sci. USA* **97**, 103-108.

SWALLOW, A.J. and VELANDIA, J.A., 1962. Oxygen effect as an explanation of differences between the action of α-particles and X- or γ-rays on aqueous solutions of amino-acids and proteins. *Nature (London)* **195**, 798-800.

SWIATLA-WOJCIK, D. and BUXTON, G.V., 1995. Modeling of radiation spur processes in water at temperatures up to 300 °C. J. Phys. Chem. **99**, 11464-11471.

TAGUCHI, M., BALDACCHINO, G., PIN, S., VIGNERON, G., HICKEL, B., and KOJIMA, T., 2005. Direct observation of superoxide radicals produced in water by 70 MeV/u Kr ion irradiations. In: Tagawa, S. (Ed.), *Proceedings of the 48th Annual Meeting of the Japanese Society of Radiation Chemistry, Osaka, Japan, October 12-14, 2005*. Osaka University, Osaka, pp. 31-32.

TAUBE, H., 1957. Photochemical reactions of ozone in solution. *Trans. Faraday Soc.* **53**, 656-665.

TOBUREN, L.H., 2004. Ionization and secondary electron production by fast charged particles. In: Mozumder, A. and Hatano, Y. (Eds.), *Charged Particle and Photon Interactions with Matter: Chemical, Physicochemical, and Biological Consequences with Applications*. Marcel Dekker, New York, pp. 31-74.

TSURUOKA, C., SUZUKI, M., KANAI, T., and FUJITAKA, K., 2005. LET and ion species dependence for cell killing in normal human skin fibroblasts. *Radiat. Res.* **163**, 494-500.

TURNER, J.E., MAGEE, J.L., HAMM, R.N., CHATTERJEE, A., WRIGHT, H.A., and RITCHIE, R.H., 1981. Early events in irradiated water. In: Booz, J., Ebert, H.G., and Hartfiel, H.D. (Eds.), *Seventh Symposium on Microdosimetry, Oxford, U.K., Sept. 8-12, 1980*. Harwood Academic Publ., London, pp. 507-520.

TURNER, J.E., MAGEE, J.L., WRIGHT, H.A., CHATTERJEE, A., HAMM, R.N., and RITCHIE, R.H., 1983. Physical and chemical development of electron tracks in liquid water. *Radiat. Res.* **96**, 437-449.

TURNER, J.E., HAMM, R.N., SOULEYRETTE, M.L., MARTZ, D.E., RHEA, T.A., and SCHMIDT, D.W., 1988*a*. Calculations for β dosimetry using Monte Carlo code (OREC) for electron transport in water. *Health Phys.* **55**, 741-750.

TURNER, J.E., HAMM, R.N., WRIGHT, H.A., RITCHIE, R.H., MAGEE, J.L., CHATTERJEE, A., and BOLCH, W.E., 1988*b*. *Radiat. Phys. Chem.* **32**, 503-510.

UEHARA, S. and NIKJOO, H., 2006. Monte Carlo simulation of water radiolysis for low-energy charged particles. *J. Radiat. Res.* **47**, 69-81.

USHER, F.L., 1911. Die chemische Einzelwirkung und die chemische Gesamtwirkung der α- und der β-Strahlen. *Jahrb. Radioakt. Elektron.* **8**, 323-334.

VON SONNTAG, C., 2006. *Free-Radical-Induced DNA Damage and its Repair.* Springer-Verlag, Berlin.

VON SONNTAG, C., 2007. Free-radical-induced DNA damage as approached by quantum-mechanical and Monte Carlo calculations: An overview from the standpoint of an experimentalist. *Adv. Quantum Chem.* **52**, 5-20.

WALLACE, S.S., 1998. Enzymatic processing of radiation-induced free radical damage in DNA. *Radiat. Res.* **150** (Suppl.), S60-S79.

WARD, J.F., 1988. DNA damage produced by ionizing radiation in mammalian cells: Identities, mechanisms of formation, and repairability. *Prog. Nucleic Acid Res. Mol. Biol.* **35**, 95-125.

WASSELIN-TRUPIN, V., BALDACCHINO, G., BOUFFARD, S., BALANZAT, E., GARDÈS-ALBERT, M., ABEDINZADEH, Z., JORE, D., DEYCARD, S., and HICKEL, B., 2000. A new method for the measurement of low concentrations of OH/O_2^- radical species in water by high-LET pulse radiolysis. A time-resolved chemiluminescence study. *J. Phys. Chem.* **104**, 8709-8714.

WASSELIN-TRUPIN, V., BALDACCHINO, G., BOUFFARD, S., and HICKEL, B., 2002. Hydrogen peroxide yields in water radiolysis by high-energy ion beams at constant LET. *Radiat. Phys. Chem.* **65**, 53-61.

WATT, D.E., 1996. *Quantities for dosimetry of ionizing radiations in liquid water.* Taylor & Francis, London.

WERNER, U., BECKORD, K., BECKER, J., FOLKERTS, H.O., and LUTZ, H.O., 1995*a*. Ion-impact-induced fragmentation of water molecules. *Nucl. Instrum. Methods Phys. Res. B* **98**, 385-388.

WERNER, U., BECKORD, K., BECKER, J., and LUTZ, H.O., 1995*b*. 3D imaging of the collision-induced Coulomb fragmentation of water molecules. *Phys. Rev. Lett.* **74**, 1962-1965.

WILSON, C.D., DUKES, C.A., and BARAGIOLA, R.A., 2001. Search for the plasmon in condensed water. *Phys. Rev. B* **63**, 121101.

ZAIDER, M., FRY, J.L., and ORR, D.E., 1990. Towards an *ab initio* evaluation of the wave-vector- and frequency-dependent dielectric response function for crystalline water. *Radiat. Prot. Dosim.* **31**, 23-28.

ZIMBRICK, J.D., 2002. Radiation chemistry and the Radiation Research Society: A history from the beginning. *Radiat. Res.* **158**, 127-140.

ZIRKLE, R.E., MARCHBANK, D.F., and KUCK, K.D., 1952. Exponential and sigmoid survival curves resulting from alpha and X irradiation of aspergillus spores. *J. Cellular Comp. Physiol.* **39**, Suppl. No. 1, 75-85.

Appendix 1 – Article No. 4

In this Appendix, we report Monte Carlo track structure simulations of the heavy-ion radiolysis of liquid water, aimed at (1) providing a realistic representation of the early physical processes that lead to the creation of the radiation track structure and (2) visualizing the temporal, three-dimensional development of the nonhomogeneous spatial distributions of each of the radiolytic species produced (from ~1 ps to 10 μs).

This work was carried out jointly with the groups of Professor Yosuke KATSUMURA (University of Tokyo, Tokyo and Tokai, Japan) and Professor Edouard I. AZZAM (New Jersey Medical School, Newark, N.J., U.S.A.). It is presented in the following article, entitled: "**High-LET ion radiolysis of water: Visualization of the formation and evolution of ion tracks and relevance to the radiation-induced bystander effect**", by Y. Muroya, I. Plante, E.I. Azzam, J. Meesungnoen, Y. Katsumura, and J.-P. Jay-Gerin.

This article is published in *Radiation Research*, Vol. **165**, Issue 4, Pages 485-491 (April 2006).

High-LET ion radiolysis of water: visualization of the formation and evolution of ion tracks and relevance to the radiation-induced bystander effect

by

Yusa Muroya,[a,b] Ianik Plante,[a] Edouard I. Azzam,[c] Jintana Meesungnoen,[a] Yosuke Katsumura[d] and Jean-Paul Jay-Gerin[a,1]

[a]Département de Médecine Nucléaire et de Radiobiologie, Faculté de Médecine et des Sciences de la Santé, Université de Sherbrooke, 3001, 12ème Avenue Nord, Sherbrooke (Québec) J1H 5N4, Canada; [b]Nuclear Professional School, Graduate School of Engineering, University of Tokyo, 2-22 Shirakata-shirane, Tokai, Naka, Ibaraki 319-1188, Japan; [c]Department of Radiology, New Jersey Medical School, 185 South Orange Avenue, Newark, NJ 07103, U.S.A.; and [d]Department of Nuclear Engineering and Management, Graduate School of Engineering, University of Tokyo, 7-3-1 Hongo, Bunkyo, Tokyo 113-8656, Japan

Manuscript category: **"Short communication"**
Number of figures: **3**
Number of footnotes: **9**
Running head: **Structure of ion tracks in liquid water**

[1]Address for correspondence: Département de Médecine Nucléaire et de Radiobiologie, Faculté de Médecine et des Sciences de la Santé, Université de Sherbrooke, 3001, 12ème Avenue Nord, Sherbrooke (Québec) J1H 5N4, Canada; tel. (819) 346-1110, ext.
fax: (819) 564-5442; e-mail:

Radiation Research **165**, 485-491 (2006)

Muroya, Y., Plante, I., Azzam, E.I., Meesungnoen, J., Katsumura, Y. and Jay-Gerin, J.-P. High-LET Ion Radiolysis of Water: Visualization of the Formation and Evolution of Ion Tracks and Relevance to the Radiation-Induced Bystander Effect. *Radiat. Res.*

ABSTRACT

Ionizing radiation-induced bystander effects, commonly observed in cell populations exposed to high-linear energy transfer (LET) radiations, are initiated by damage to a cellular molecule which then gives rise to a toxic signal exported to neighboring cells not directly hit by radiation. A major goal in studies of this phenomenon is the identification of this initial radiation-induced lesion. Liquid water being the main constituent of biological matter, reactive species produced by water radiolysis in the cellular environment are likely to be major contributors to the induction of this lesion. In this context, the radiation track structure is of crucial importance in specifying the precise location and identity of all the radiolytic species and their subsequent signaling or damaging effects. We report here Monte Carlo track structure simulations of the radiolysis of liquid water by four different impacting ions $^{1}H^{+}$, $^{4}He^{2+}$, $^{12}C^{6+}$, and $^{20}Ne^{10+}$, with the same LET (~70 keV/μm). The initial radial distribution profiles of the various water decomposition products (e^{-}_{aq}, $^{\bullet}OH$, $H^{\bullet}$, H_2, and H_2O_2) for the different ions considered are presented and discussed briefly in the context of track structure theory. As an example, the formation and temporal evolution of simulated 24-MeV $^{4}He^{2+}$ ion tracks (LET ~ 26 keV/μm) are reported for each radiolytic species from 1 ps to 10 μs. The calculations reveal that the ion track structure is completely lost by ~1 μs.

Keywords: Liquid water, radiolysis, accelerated heavy ions, linear energy transfer, Monte Carlo track structure simulations, temporal evolution of ion tracks, radiolytic yields, bystander effect.

INTRODUCTION

It has long been considered that the genotoxic effects of ionizing radiation are a consequence of residual DNA damage that arises from the direct interaction of radiation with the nuclei of exposed cells (*1*). However, evidence accumulated over the past two decades indicates that genetic damage in cells need not be the effect of direct nuclear irradiation. Radiation-induced genomic instability experiments show that the progeny of cells that survive a radiation exposure harbor lesions that are different in nature from those that initially occurred in the irradiated parental cells (*2*). Furthermore, gene mutations may also occur when the cytoplasm (not the nucleus) is specifically targeted with charged particles using microbeam irradiation (*3*). More importantly, bystander effect studies mainly with cell populations exposed to very low fluences of α-particles show that biological changes, including genetic alterations, occur in cells that are not directly irradiated (*4*). These studies indicate that molecular signals transmitted from irradiated to neighboring nonirradiated cells lead to biological responses in bystander cells and that the target for genetic damage is much larger than the nucleus of the irradiated cell [reviewed in refs. (*5-7*)].

Radiation-induced bystander effects have been observed in cells of varying genetic background, lineage and organ origin. Their widespread occurrence is likely to have important consequences for radiation risk assessment, radiotherapy, and diagnostic radiology. While adequate evidence for such effects exists, a clear understanding of the basic mechanisms by which they occur is only beginning to emerge. Gap-junction intercellular communication and diffusible factor(s) secreted by irradiated cells have been implicated in expression of bystander responses. Metabolic redox reactions appear to be common to both mechanisms (*8*). Cellular phenotype, radiation quality or linear energy transfer (LET) (i.e., the stopping power, $-dE/dx$), dose, and dose rate (or intensity) are also likely modulators of the molecular and biochemical signaling events involved.

Liquid water being the main constituent of living cells (~85%), knowledge of the yield and precise location, as a function of time, of water radiolytic species is critical to our

understanding of early events involved in signaling the bystander effect. In fact, the water decomposition products e^-_{aq} (hydrated electron), $^{\bullet}OH$, $H^{\bullet}$, H_2, and H_2O_2 (*9*, *10*) generated initially in the cellular environment traversed by ionizing particle tracks can react efficiently with many cellular molecules, causing both covalent modifications and changes in cell signaling that may subsequently act as triggers of bystander effects (*11-14*).[2,3] The induced molecular changes are likely dependent on the biochemical status and physical organization of the cellular organelle(s) traversed by the irradiating particle. In this context, the radiation track structure is of crucial importance in specifying the spatial distribution and identity of all the radiolytic species and free radical intermediates created by the passage of the impacting ion (*17*, *18*) and the subsequent damage or signaling effects. For example, the finding that similar doses of different radiation types like α-particles or γ-rays lead to biological changes with varying effectiveness [see, for example, refs. (*19*, *20*)], where a more nonuniform geometric distribution of absorbed energy is biologically more efficient, emphasizes the importance of the initial local distribution of reactants in the response of irradiated cells. Such knowledge would be significant in the development of predictive computational models that bridge together data characterizing the various steps involved in chemical and biological processes leading to propagation of bystander effects.

Successful prediction of the effects of radiation type and energy in radiolysis requires not only a realistic description of the early physical aspects of the radiation track structure but also an accurate modeling of the temporal dependence of the spatial distributions of the various radiation-induced reactive species in the tracks. Here, as an example, we have studied the initial, nonhomogeneous deposition of radiation energy in water exposed to 24-MeV helium ions (LET ~ 26 keV/μm). The temporal, three-dimensional development of the track, in which the various water decomposition products are specified and allowed to diffuse and react with one another (or with the milieu), is modeled using Monte Carlo ion track structure simulations between 1 ps and 10 μs. The initial radial distribution profiles of the different radiolytic species for four different impacting ions ($^1H^+$, $^4He^{2+}$,

$^{12}C^{6+}$, and $^{20}Ne^{10+}$) with the same LET (~70 keV/μm) are also presented and discussed briefly in the context of the theory of track structure. Knowledge of track development in cells coupled with refinements in identifying the precise path of irradiating particles (e.g., cytoplasmic, nuclear, mitochondrial traverse, etc.) should be informative of mechanisms underlying expression of bystander effects.

MONTE CARLO SIMULATIONS

The complex succession of events that follow the irradiation of a biological system can usually be divided into four more or less distinct consecutive stages: (1) deposition of radiant energy and formation of initial products in a specific, highly nonhomogeneous track structure geometry ("physical" stage), (2) establishment of thermal equilibrium in the bulk medium with reactions and reorganization of initial products to give stable molecules and chemically reactive species such as free atoms and radicals ("physicochemical" stage), (3) thermal chemistry during which the various reactive species diffuse and react with one another (or with the environment) ("chemical" stage), and (4) biological system response to chemical products of irradiation ("biological" stage) (*21*). Since this study deals with the ion radiolysis of pure, deaerated liquid water, only the first three stages need to be considered here.

In the calculations reported, the complete sequence of all individual stochastic events is modeled using our Monte Carlo code IONLYS-SBS for the simulation of ion track segments in water and their subsequent diffusion-kinetic development up to ~10 μs. This code, which follows the reactant trajectories on an event-by-event basis, enables one to keep control of the spatial distribution and identity of all generated radical and molecular species (e^-_{aq}, $^{\bullet}OH$, $H^{\bullet}$, H_2, and H_2O_2) at all times.[4] The detailed implementation of this code has been given elsewhere [(*24*, *25*) and references cited].

Short (1-5 μm) track segments of four different incident ions $^1H^+$, $^4He^{2+}$, $^{12}C^{6+}$, and $^{20}Ne^{10+}$, have been calculated at the same LET. The chosen LET value is ~70 keV/μm, which is less than the maximum LET at the Bragg peak of the stopping-power curve for

each irradiating ion in water. The corresponding ion energies are 0.15 MeV for $^{1}H^{+}$, 1.75 MeV/nucleon for $^{4}He^{2+}$, 25.5 MeV/nucleon for $^{12}C^{6+}$, and 97.5 MeV/nucleon for $^{20}Ne^{10+}$.[5] Finally, at the incident ion energies considered here, interactions involving electron capture and loss by the moving ions (charge-changing collisions) have been neglected (*28*).

RESULTS AND DISCUSSION

Figure 1 shows typical two-dimensional representations of 1–5-μm track segments of $^{1}H^{+}$, $^{4}He^{2+}$, $^{12}C^{6+}$, and $^{20}Ne^{10+}$ ions generated at the origin and along the *Y* axis, calculated (at ~10^{-13} s) under the same LET conditions (~70 keV/μm). As we can see, the tracks consist of a cylindrical "core" produced by the ion track itself and a surrounding "penumbra" of ejected, comparatively low-LET, secondary electrons [the so-called "short" (~500 eV–5 keV) and "branch" (> 5 keV) tracks in the terminology of Mozumder and Magee (*29*), or "δ-rays"] (*9*, *10*, *17*, *18*, *30*). Our simulated results also show that these energetic secondary electrons travel to a greater average distance away from the track core as the velocity of the incident ion increases, from protons to neon ions. This irradiating-ion dependence of the track structure at a given LET is in accord with Bethe's theory of stopping power[6] and explains why LET is not a unique parameter to correctly describe the radiation chemical effects within heavy-ion tracks (*10*, *18*, *25*, *28*).

The initial radial distribution profiles of the various water decomposition products (e^{-}_{aq}, $^{\bullet}OH$, $H^{\bullet}$, H_2, and H_2O_2) around the trajectory of the different ions of the same LET considered in Fig. 1 are presented in Fig. 2. To generate these distribution profiles, the initial locations of a large number (~2×10^{6}) of each radiation-induced species were collected by accumulating the data obtained from 200 simulations of 5-μm ion track segments (1000 simulations of 1-μm tracks in the case of protons) and projecting in a plane perpendicular to the direction of the incident ion. As seen in Fig. 2, the spatial extent of the distributions of all species increases with increasing energy of the irradiating ion. This is readily explained by the greater penetration range (or thermalization length) of the

ejected secondary electrons from the higher velocity ion (see Fig. 1 and Table 1).[7] Figure 2 also reveals the presence of two different regions. The first, central region extends to radial distances up to ~20–50 nm or so from the ion trajectory and contains a high concentration of chemical reactants. This is larger than the physical core radius calculated by Magee and Chatterjee (*30*, *33*) and Mozumder and LaVerne [(*34*); see also ref. (*17*)], which corresponds to the tiny radial region within the first few nanometers around the path of the irradiating ion where the energy is deposited. In fact, it can be seen that this central region is made up of the reactive species that are generated not only by the heavy ion itself but also by the numerous low-energy secondary electrons that are ejected from the ion trajectory, mainly in glancing collisions. The core of tracks is then initially comprised of "spurs" (< 100 eV) and "blobs" (~100–500 eV) (*29*) with sizes reaching a few tens of nanometers (*32*). As we can see from Fig. 1, these secondary electrons are so dense that this central region appears continuous and radially symmetrical. The second, peripheral region extends beyond ~20–50 nm from the incident ion path. It is much larger and less dense in radiolytic species. Figures 1 and 2 clearly show that this region is almost absent for the proton track while its importance increases with the energy of the irradiating ion, from helium to neon ions (see Table 1). It corresponds, obviously, to the region where energetic secondary electrons (δ-rays), ejected from the core in knock-on collisions, can go. As seen in Fig. 1, the production of these δ-rays is sporadic, and their tracks are generally well separated from each other, giving a highly nonuniform geometric distribution of absorbed energy.

Figure 3 displays, as an example, the three-dimensional expansion of a 5-μm track segment (generated at the origin and along the *Y* axis, and viewed end-on over the plane *XZ*) of 24-MeV $^{4}He^{2+}$ ions. More precisely, this figure shows the time-dependent cross sections of the nonhomogeneous spatial distributions of each of the radiolytic species produced, calculated with our Monte Carlo track structure simulation code IONLYS-SBS from 1 ps to 10 μs. As can be seen, these radial distribution profiles of species essentially reflect the trajectories of the ejected energetic δ-rays. At an early stage of track develop-

ment, it is clear from Figs. 2 and 3 that the e^-_{aq} and •OH radial distributions are far denser than those of the other radiation-induced reactants (H•, H_2, and H_2O_2). This observation is consistent with the much greater radiolytic yields found for these two radical species; in fact, for the case of 24-MeV $^4He^{2+}$ ions (LET ~ 26 keV/μm), our calculated values of $G(e^-_{aq})$ and G(•OH) at 1 ps are, respectively, ~4.2 and 5.0 molec./100 eV,[8] while the corresponding yields of H•, H_2, and H_2O_2 are only ~0.69, 0.33, and 0.18 molec./100 eV, respectively.[9] Finally, Fig. 3 also clearly reveals that the ion track structure, which is very well-defined at early times, is gradually lost as time progresses because of the diffusion of the species, and has completely disappeared by about 1 μs.

CONCLUSION

Liquid water radiolysis studies have contributed greatly to our understanding of the cellular responses to ionizing radiation. Expansion of these studies to include determination of yield, lifetime and spatial distribution of radiolytic species generated by energetic ions in the vicinity of specific target molecules within cells is likely to increase our understanding of mechanisms underlying the propagation of radiation-induced effects within and among cells. Knowledge of these parameters as a function of LET, number of traversals of incident particles, whether stressful or protective effects are propagated from irradiated cells to non-targeted neighbors, and the range of propagation of such effects, coupled with information on the nature, amount and lifetime of secondary long-lived species that result from interaction of water decomposition products with other cellular molecules should be informative of the relationship among water radiolysis products and the lesion(s) that trigger the bystander effect. It is attractive to speculate that signaling molecules (e.g., second messengers) are compartmentalized along radiation track structures. Concentration and stoichiometry of these molecules, as well as cross-talk among them, within such defined compartments may be critical in signaling expression of low dose/low fluence ionizing radiation effects. These studies are of particular significance to health protection issues related to evaluating the effects of galactic cosmic rays to which

astronauts are exposed during prolonged space exploration missions.

ACKNOWLEDGMENTS

The financial assistance of the Natural Sciences and Engineering Research Council of Canada (Grant No. 9020-04) is gratefully acknowledged.

TABLE 1

Maximum δ-ray energies (Q_{max}) (*26*) and average penetration ranges (R_{av}) (*32*) corresponding to these energies. R_{av} gives an estimate of the radius of the penumbra. Comparison is made with the penumbra radii (r_p) reported in refs. (*30*) and (*33*).

Ion	Energy (MeV/nucleon)	Q_{max} (keV)	R_{av} (nm)	r_p (nm)
$^{1}H^{+}$	0.15	0.327	15.7	7.65
$^{4}He^{2+}$	1.75	3.81	3.6×10^{2}	2.0×10^{2}
$^{12}C^{6+}$	25.5	56.3	3.7×10^{4}	7.4×10^{3}
$^{20}Ne^{10+}$	97.5	$2.23 \times\times 10^{2}$	2.4×10^{5} [a]	3.8×10^{4}

[a] Extrapolated value from the electron penetration ranges calculated in ref. (*32*).

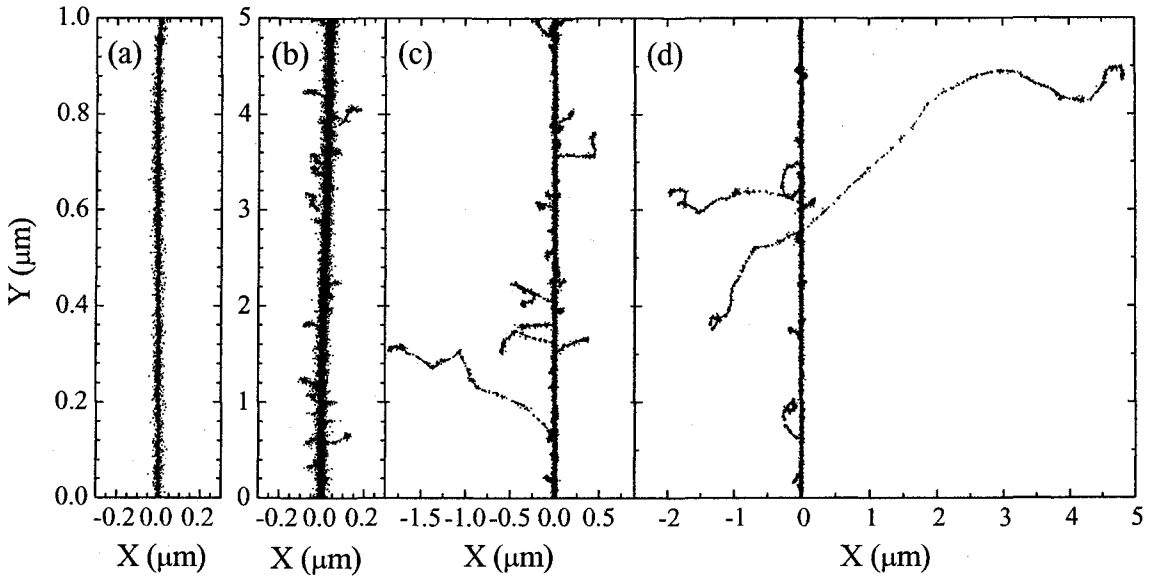

Figure 1: Projections over the *XY* plane of track segments calculated (at ~10^{-13} s) for the following impacting ions: (a) $^{1}H^{+}$ (0.15 MeV), (b) $^{4}He^{2+}$ (1.75 MeV/nucleon), (c) $^{12}C^{6+}$ (25.5 MeV/nucleon), and (d) $^{20}Ne^{10+}$ (97.5 MeV/nucleon). Ions are generated at the origin and along the *Y* axis in liquid water at 25 °C under identical LET conditions (~70 keV/μm) (see text). Dots represent the energy deposited at points where an interaction occurred.

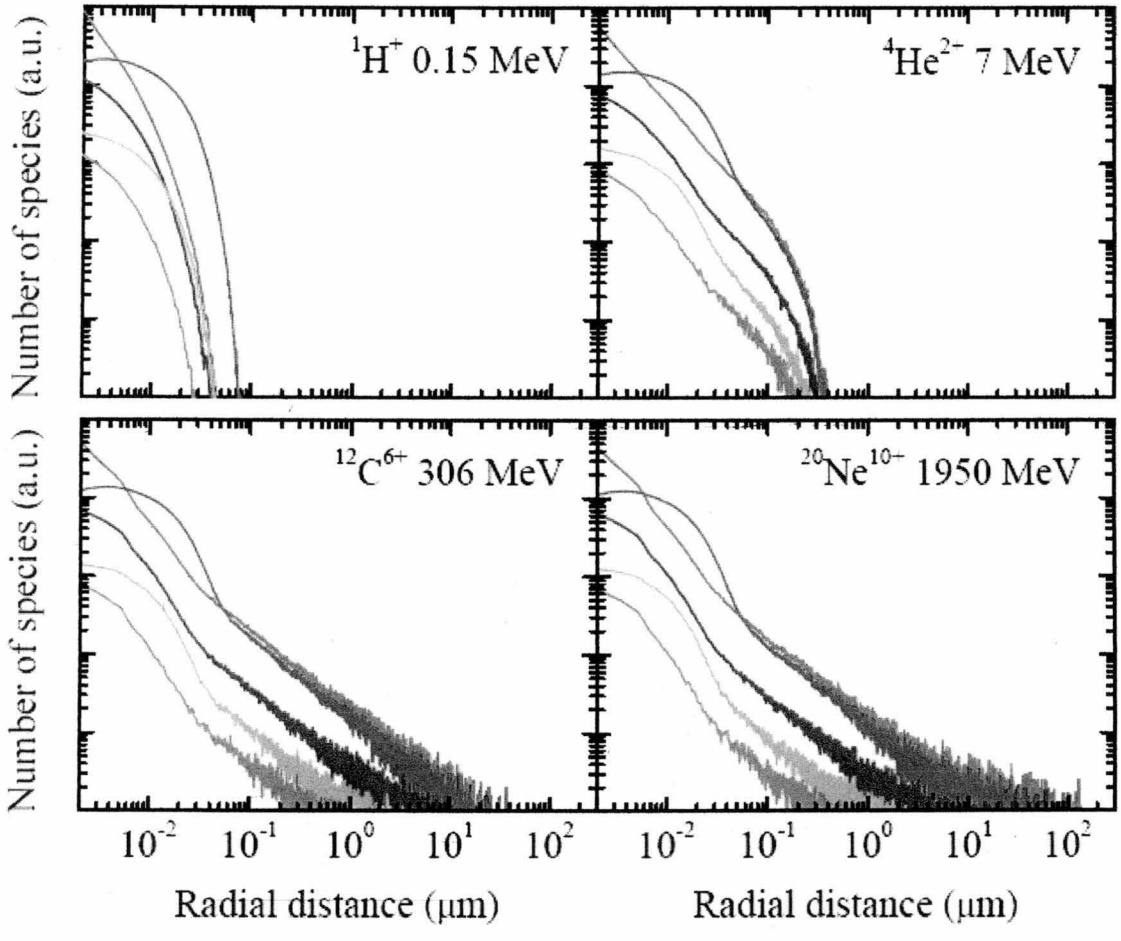

Figure 2: Initial radial distribution profiles of the main water decomposition products perpendicular to the trajectory of the four incident ions from Fig. 1 (see text). The colors green, red, blue, cyan, and magenta are associated with the radiation-induced chemical species e_{aq}^{-}, $^{\bullet}OH$, $H^{\bullet}$, H_2, and H_2O_2, respectively.

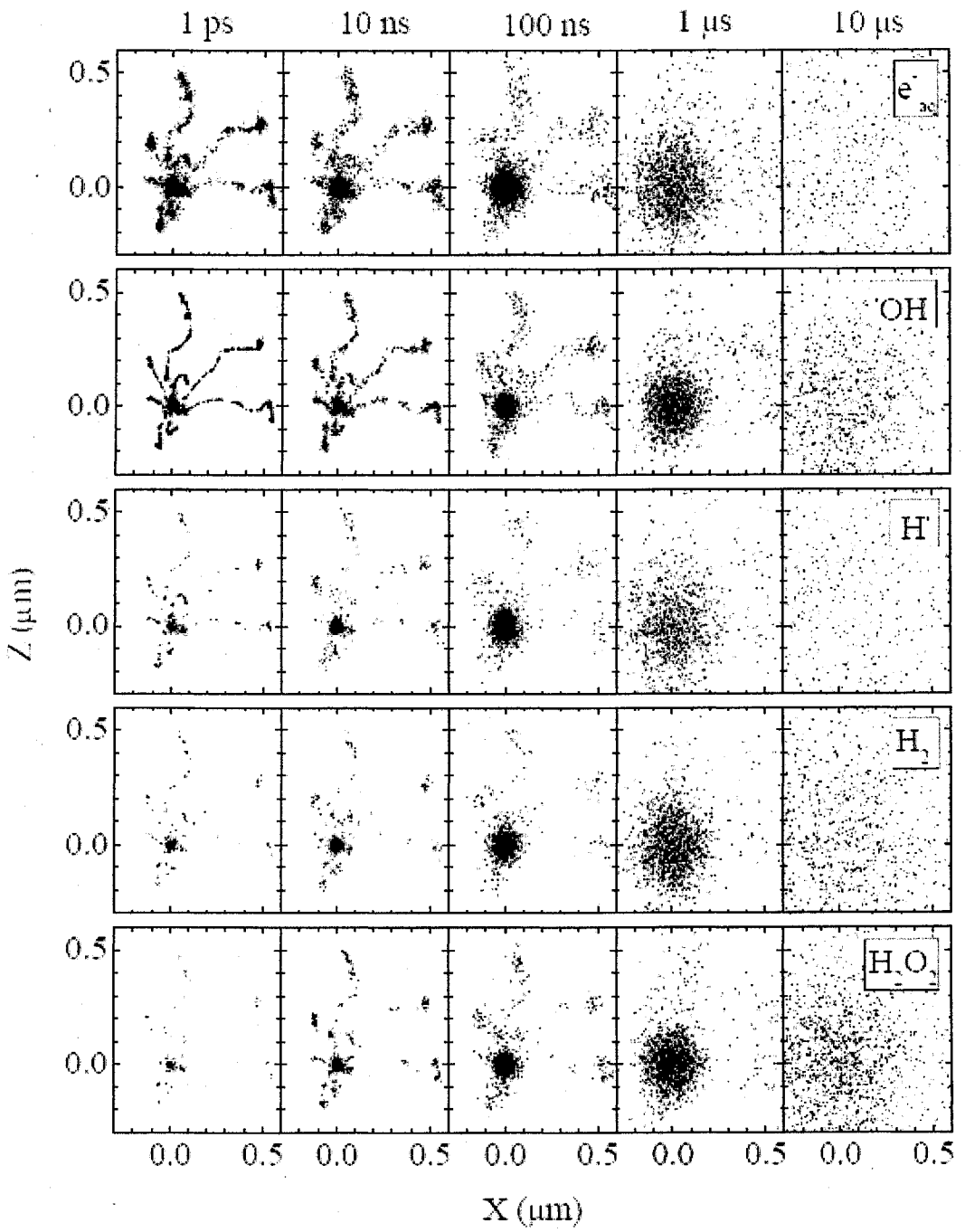

Figure 3: Time-dependent cross sections of the nonhomogeneous spatial distributions of the main radiolytic species (e^-_{aq}, •OH, H•, H_2, and H_2O_2) in liquid water exposed to 24-MeV $^4He^{2+}$ ions (LET ~ 26 keV/μm) from 1 ps to 10 μs (see text). The track geometry is the same as that in Fig. 1, but here the track segment is viewed end-on over the *XZ* plane.

REFERENCES

1. R. E. Zirkle and W. Bloom, Irradiation of parts of individual cells. *Science* **117**, 487-493 (1953).
2. M. A. Kadhim, D. A. Macdonald, D. T. Goodhead, S. A. Lorimore, S. J. Marsden and E. G. Wright, Transmission of chromosomal instability after plutonium α-particle irradiation. *Nature* **355**, 738-740 (1992).
3. L.-J. Wu, G. Randers-Pehrson, A. Xu, C. A. Waldren, C. R. Geard, Z. Yu and T. K. Hei, Targeted cytoplasmic irradiation with alpha particles induces mutations in mammalian cells. *Proc. Natl. Acad. Sci. USA* **96**, 4959-4964 (1999).
4. H. Nagasawa and J. B. Little, Induction of sister chromatid exchanges by extremely low doses of α-particles. *Cancer Res.* **52**, 6394-6396 (1992).
5. J. B. Little, Genomic instability and bystander effects: a historical perspective. *Oncogene* **22**, 6978-6987 (2003).
6. W. F. Morgan, Is there a common mechanism underlying genomic instability, bystander effects and other nontargeted effects of exposure to ionizing radiation? *Oncogene* **22**, 7094-7099 (2003).
7. K. M. Prise, M. Folkard and B. D. Michael, A review of the bystander effect and its implications for low-dose exposure. *Radiat. Prot. Dosim.* **104**, 347-355 (2003).
8. E. I. Azzam, S. M. de Toledo and J. B. Little, Oxidative metabolism, gap junctions and the ionizing radiation-induced bystander effect. *Oncogene* **22**, 7050-7057 (2003).
9. J. W. T. Spinks and R. J. Woods, *An Introduction to Radiation Chemistry*, 3rd ed. Wiley, New York, 1990.
10. C. Ferradini and J.-P. Jay-Gerin, La radiolyse de l'eau et des solutions aqueuses: historique et actualité. *Can. J. Chem.* **77**, 1542-1575 (1999).
11. L. E. Feinendegen, Reactive oxygen species in cell responses to toxic agents. *Hum. Exp. Toxicol.* **21**, 85-90 (2002).
12. J. W. Ward, The radiation-induced lesions which trigger the bystander effect. *Mutat.*

Res. **499**, 151-154 (2002).

13. J.-P. Jay-Gerin, J. Meesungnoen, P. Banville and S. Mankhetkorn, Comment on "The radiation-induced lesions which trigger the bystander effect" by J. F. Ward [Mutat. Res. 499 (2002) 151-154]. *Mutat. Res.* **525**, 125-127 (2003).

14. D. R. Spitz, E. I. Azzam, J. J. Li and D. Gius, Metabolic oxidation/reduction reactions and cellular responses to ionizing radiation: a unifying concept in stress response biology. *Cancer Metastasis Rev.* **23**, 311-322 (2004).

15. B. H. J. Bielski, D. E. Cabelli, R. L. Arudi and A. B. Ross, Reactivity of HO_2/O_2^- radicals in aqueous solution. *J. Phys. Chem. Ref. Data* **14**, 1041-1100 (1985).

16. Z. B. Alfassi (Ed.), *Peroxyl Radicals*. Wiley, Chichester, 1997.

17. A. Mozumder, *Fundamentals of Radiation Chemistry*, pp. 41-69. Academic Press, San Diego, 1999.

18. J. A. LaVerne, Radiation chemical effects of heavy ions. In *Charged Particle and Photon Interactions with Matter. Chemical, Physicochemical, and Biological Consequences with Applications* (A. Mozumder and Y. Hatano, Eds.), pp. 403-429. Marcel Dekker, New York, 2004.

19. G. W. Barendsen, Responses of cultured cells, tumours and normal tissues to radiations of different linear energy transfer. *Curr. Top. Radiat. Res. Quaterly* **4**, 293-356 (1968).

20. C. Tsuruoka, M. Suzuki, T. Kanai and K. Fujitaka, LET and ion species dependence for cell killing in normal human skin fibroblasts. *Radiat. Res.* **163**, 494-500 (2005).

21. R. L. Platzman, The physical and chemical basis of mechanisms in radiation biology. In *Radiation Biology and Medicine. Selected Reviews in the Life Sciences* (W. D. Claus, Ed.), pp. 15-72. Addison-Wesley, Reading, MA, 1958.

22. J. E. Turner, J. L. Magee, R. N. Hamm, A. Chatterjee, H. A. Wright and R. H. Ritchie, Early events in irradiated water. In *Proceedings of the Seventh Symposium on Microdosimetry, Oxford, U.K., September 8-12, 1980*, Report EUR 7147 de-en-fr (J. Booz, H. G. Ebert, and H. D. Hartfiel, Eds.), pp. 507-520. Harwood Academic

Publishers, London, 1981.

23. J. E. Turner, J. L. Magee, H. A. Wright, A. Chatterjee, R. N. Hamm and R. H. Ritchie, Physical and chemical development of electron tracks in liquid water. *Radiat. Res.* **96**, 437-449 (1983).

24. I. L. Plante, A. Filali-Mouhim and J.-P. Jay-Gerin, SimulRad: a Java interface for a Monte Carlo simulation code to visualize in 3D the early stages of water radiolysis. *Radiat. Phys. Chem.* **72**, 173-180 (2005).

25. J. Meesungnoen and J.-P. Jay-Gerin, High-LET radiolysis of liquid water with $^{1}H^{+}$, $^{4}He^{2+}$, $^{12}C^{6+}$, and $^{20}Ne^{9+}$ ions: effects of multiple ionization. *J. Phys. Chem. A* **109**, 6406-6419 (2005).

26. D. E. Watt, *Quantities for Dosimetry of Ionizing Radiations in Liquid Water*. Taylor and Francis, London, 1996.

27. J. Meesungnoen, M. Benrahmoune, A. Filali-Mouhim, S. Mankhetkorn and J.-P. Jay-Gerin, Monte Carlo calculation of the primary radical and molecular yields of liquid water radiolysis in the linear energy transfer range 0.3-6.5 keV/μm: application to ^{137}Cs gamma rays. *Radiat. Res.* **155**, 269-278 (2001).

28. S. M. Pimblott and J. A. LaVerne, Effects of track structure on the ion radiolysis of the Fricke dosimeter. *J. Phys. Chem. A* **106**, 9420-9427 (2002).

29. A. Mozumder and J. L. Magee, Model of tracks of ionizing radiations for radical reaction mechanisms. *Radiat. Res.* **28**, 203-214 (1966).

30. J. L. Magee and A. Chatterjee, Track reactions of radiation chemistry. In *Kinetics of Nonhomogeneous Processes. A Practical Introduction for Chemists, Biologists, Physicists, and Materials Scientists* (G. R. Freeman, Ed.), pp. 171-214. Wiley-Interscience, New York, 1987.

31. H. A. Bethe and J. Ashkin, Passage of radiations through matter. In *Experimental Nuclear Physics* (E. Segrè, Ed.), Vol. 1, pp. 166-357. Wiley, New York, 1953.

32. J. Meesungnoen, J.-P. Jay-Gerin, A. Filali-Mouhim and S. Mankhetkorn, Low-energy electron penetration range in liquid water. *Radiat. Res.* **158**, 657-660

(2002).

33. J. L. Magee and A. Chatterjee, Radiation chemistry of heavy-particle tracks. 1. General considerations. *J. Phys. Chem.* **84**, 3529-3536 (1980).

34. A. Mozumder and J. A. LaVerne, Theoretical aspects of heavy-ion tracks in radiation chemistry. In *Radiation Research: Proceedings of the 8th International Congress of Radiation Research, Edinburgh, July 19-24, 1987* (E. M. Fielden, J. F. Fowler, J. H. Hendry, and D. Scott, Eds.), Vol. 2, pp. 11-16. Taylor & Francis, London, 1987.

FOOTNOTES

1. Address for correspondence: Département de médecine nucléaire et de radiobiologie, Faculté de médecine et des sciences de la santé, Université de Sherbrooke, 3001, 12ème Avenue Nord, Sherbrooke (Québec) J1H 5N4, Canada; e-mail: jean-paul.jay-gerin@USherbrooke.ca.
2. In the presence of oxygen, e_{aq}^- and $H^\bullet$ atoms are rapidly (on the microsecond time scale) converted to the superoxide anion/hydroperoxyl ($O_2^{\bullet-}/HO_2^\bullet$) radicals, where $O_2^{\bullet-}$ is always in a pH-dependent equilibrium with its conjugate acid ($pK_a = 4.8$) (*15*). In an aerobic cellular environment at physiological pH, the major reactive species present at ~1 μs are thus $O_2^{\bullet-}$, $^\bullet OH$, and H_2O_2 (H_2 plays only a limited role in the radiolysis of aqueous solutions, and most of it generally escapes from solution). In biological systems, organic radicals ($R^\bullet$) are also formed, most often by H-abstraction reactions (initiated by $^\bullet OH$ for example). These carbon-centered radicals usually react rapidly with O_2 to give peroxyl radicals ($RO_2^\bullet$), which are better oxidizing agents than their parent radicals (*16*).
3. These reactions are extremely rapid in living cells and are generally difficult to detect directly.
4. It is worth noting here that similar Monte Carlo computer simulations in liquid water were initially conducted by Turner, Hamm, Wright, and Ritchie at Oak Ridge National Laboratory jointly with Magee and Chatterjee at Lawrence Berkeley Laboratory about 25 years ago (*22*, *23*). This earlier work used different particles for its examples and different estimates of cross sections, diffusion coefficients and reaction rate constants, but the results were qualitatively the same.
5. The track segments for the different ions have been chosen equal to 5 μm, except for $^1H^+$, for which we have adopted a track length of 1 μm (see Fig. 1). This reduction in the track length for $^1H^+$ was dictated by the fact that the penetration range of this ion in liquid water, at the considered energy of 0.15 MeV, amounts to only ~2.3 μm (*26*). For the case of a 1-μm segment of 0.15 MeV proton track (LET ~ 70 keV/μm), note

that even if the energy of the ion varies appreciably along its trajectory, the LET remains nearly constant (see ref. *27*).

6. For ions with kinetic energies that are small compared to their rest-mass energy, the nonrelativistic Bethe stopping power equation (*31*) is well approximated by (in SI units):

$$-\frac{dE}{dx} = \left(\frac{1}{4\pi\varepsilon_0}\right)^2 \frac{4\pi Z^2 e^4}{m_0 V^2} N \ln\left(\frac{2m_0 V^2}{I}\right),$$

where Ze is the charge on the incident ion, V is the ion velocity, m_0 is the rest mass of an electron, N is the number of electrons per m^3 of the absorbing medium, and I is the mean excitation and ionization potential of the bound electrons in the absorber. It follows from this equation that for two different ions of equal LET, the one with the higher charge will have the higher velocity.

7. The nature of the initial spatial nonhomogeneity of the chemical species is that their concentrations are high in the vicinity of the sites of energy deposition along the ejected, secondary electron tracks traversing the penumbra.

8. Radiation chemical yields (G-values) are given in the units of molecules per 100 eV (molec./100 eV). For conversion into SI units (mol/J): 1 molec./100 eV ≈ 0.10364 μmol/J.

9. Our calculated primary (or "escape") yield values (at ~1 μs) are: $G_{e^-_{aq}} = 0.81$, $G_{\cdot OH} = 0.92$, $G_{H\cdot} = 0.62$, $G_{H_2} = 0.83$, and $G_{H_2O_2} = 1.03$ molec./100 eV. These values are in good agreement with experimental data (see ref. *25*).

Appendix 2 – Article No. 5

In this Appendix, we use Monte Carlo simulations to investigate the effects of acidity (pH) on the primary yields of the various chemical species produced in the radiolysis of deaerated aqueous sulfuric acid solutions over the range from neutral solution to 0.4 *M* H_2SO_4 and for different values of the LET varying from ~0.3 to 15 keV/μm. As an application, a Monte Carlo study of the radiation-induced oxidation of ferrous sulfate solutions in aerated aqueous 0.4 *M* H_2SO_4 (Fricke dosimeter) is also reported.

This work is presented in the following article, entitled: "**Monte Carlo simulation study of the effects of acidity and LET on the primary free-radical and molecular yields of water radiolysis – Application to the Fricke dosimeter**", by N. Autsavapromporn, J. Meesungnoen, I. Plante, and J.-P. Jay-Gerin.

This article is published in *Canadian Journal of Chemistry*, Vol. **85**, Issue 3, Pages 214-229 (March 2007).

Monte Carlo simulation study of the effects of acidity and LET on the primary free-radical and molecular yields of water radiolysis – Application to the Fricke dosimeter

by

Narongchai Autsavapromporn, Jintana Meesungnoen, Ianik Plante, and Jean-Paul Jay-Gerin[1]

Département de Médecine Nucléaire et de Radiobiologie
Faculté de Médecine et des Sciences de la Santé, Université de Sherbrooke
Sherbrooke (Québec) J1H 5N4, Canada

This work is dedicated to the memory of Professor David A. Armstrong.

---

[1]Address for correspondence: Département de médecine nucléaire et de radiobiologie, Faculté de médecine et des sciences de la santé, Université de Sherbrooke, 3001, 12e Avenue Nord, Sherbrooke (Québec) J1H 5N4, Canada. Tel. (819) 346-1110, ext.
Fax: (819) 564-5442. E-mail:

Canadian Journal of Chemistry **85**, 214-229 (2007)

Abstract

Monte Carlo simulations are used to investigate the effects of acidity (pH) on the primary yields of various chemical species produced in the radiolysis of deaerated aqueous sulfuric acid solutions over the range from neutral solution to 0.4 M H_2SO_4. The effects of the quality of radiation, measured in terms of linear energy transfer (LET), have also been studied for LET varying from ~0.3 to 15 keV/μm at ambient temperature. Our results show that an increase in acidity (1 < pH < 4) leads to an increase in the yield $G_{e^-_{aq}+H^\bullet}$ of the "reducing" free radicals (hydrated electron and H• atom) and a slight increase in $G_{^\bullet OH}$ and $G_{H_2O_2}$, while there is a slight decrease in G_{H_2}. At pH < 1, •OH radicals react with HSO_4^- anions to form $SO_4^{\bullet-}$ radicals, resulting in a steep decrease in $G_{^\bullet OH}$. By contrast, in the range of pH from ~4 to 7, the calculated yield values are independent of sulfuric acid concentration. In both neutral water and 0.4 M H_2SO_4 (pH 0.46) solutions, the primary molecular yields increase upon increasing LET to ~15 keV/μm with a concomitant decrease in those of free radicals. As an exception, $G_{H^\bullet}$ at first increases versus LET, reaching a maximum near 6.5 keV/μm before decreasing steeply at higher LET. The results obtained are generally in good agreement with available experimental data over the whole acidity and LET ranges studied. Finally, as an application, we have simulated the radiation-induced oxidation of ferrous sulfate solutions in aerated aqueous 0.4 M H_2SO_4 (Fricke dosimeter) as a function of time up to ~50 s and addressed the effects of LET on the resulting ferric ion yield at 25 °C. The production of Fe^{3+} ions is highly sensitive to free-radical yields, especially H• atoms (via formation of $HO_2^\bullet$), resulting in a marked decline of $G(Fe^{3+})$ with increasing LET. The general trend of the observed variation of $G(Fe^{3+})$ with radiation quality is well reproduced by our computed Fe^{3+} ion yield values.

Keywords: Liquid water, acidic (H_2SO_4) aqueous solutions, radiolysis, free-radical and molecular yields, linear energy transfer (LET), Fricke dosimeter, Monte Carlo simulations.

Résumé

À l'aide de calculs de simulation Monte Carlo, nous avons étudié l'influence de l'acidité (pH) sur les rendements primaires des diverses espèces chimiques produites lors de la radiolyse de solutions aqueuses désaérées d'acide sulfurique dans la gamme de concentrations ~0–0.4 M en H_2SO_4. L'influence de la qualité du rayonnement, décrite en termes de transfert d'énergie linéique (TEL), a aussi été étudiée pour des valeurs de TEL entre ~0,3 et 15 keV/μm à la température ambiante. Nos résultats montrent que, pour des irradiations avec des rayonnements de faible TEL, une augmentation en acidité ($1 < pH < 4$) conduit à une augmentation du rendement $G_{e^-_{aq}+H^\bullet}$ de l'entité réductrice radicalaire (électron hydraté et atome H•) et à un faible accroissement de $G_{^\bullet OH}$ et $G_{H_2O_2}$, alors que G_{H_2} diminue légèrement. À $pH < 1$, les radicaux •OH réagissent avec les anions HSO_4^- pour former les radicaux $SO_4^{\bullet-}$, entraînant une diminution marquée de $G_{^\bullet OH}$. En revanche, pour des pH entre ~4 et 7, les valeurs des rendements calculées sont indépendantes de la concentration en acide sulfurique. Autant pour l'eau liquide neutre que pour les solutions H_2SO_4 0,4 M (pH 0,46), les rendements primaires moléculaires augmentent avec le TEL alors que ceux des espèces radicalaires diminuent de façon concomitante. Le cas de $G_{H^\bullet}$ est singulier, puisqu'il augmente initialement avec le TEL, atteint un maximum à ~6,5 keV/μm, puis décroît rapidement à TEL plus élevé. Les résultats obtenus s'accordent bien avec les données expérimentales disponibles dans la littérature pour toute la gamme d'acidité et de TEL considérée. À titre d'application, nous avons enfin simulé l'oxydation radio-induite des ions ferreux en milieu H_2SO_4 0,4 M aéré (dosimètre de Fricke) en fonction du temps jusqu'à ~50 s et étudié l'influence du TEL sur le rendement d'apparition des ions ferriques à 25 °C. La production des ions Fe^{3+} est très sensible à la valeur des rendements radicalaires, en particulier les atomes H• (via la formation de $HO_2^\bullet$), résultant en une décroissance marquée de $G(Fe^{3+})$ lorsque le TEL augmente. L'allure générale de la variation expérimentale de $G(Fe^{3+})$ avec la qualité du rayonnement utilisé est bien reproduite par nos valeurs calculées des rendements d'ions Fe^{3+}.

Mots clés : Eau liquide, solutions aqueuses acides (H_2SO_4), radiolyse, rendements radicalaires et moléculaires, transfert d'énergie linéique (TEL), dosimètre de Fricke, simulations Monte Carlo.

Introduction

A large fraction of radiation chemistry has been concerned with studies of water and its solutions[2] mainly because of the unique importance of water, particularly in biological systems (living cells are composed of about 70%-85% water by weight) and also in various domains of nuclear science and technology, such as water-cooled nuclear power reactors (where water is used both as neutron moderator and as the heat-transport medium). A good summary of the present status of aqueous radiation chemistry is given in refs. 1-4.

The radiolysis of pure liquid water (in the absence of oxygen) by low-LET (linear energy transfer or energy loss per unit track length, $-dE/dx$) radiation such as ^{60}Co γ-rays, fast electrons, or high-energy protons, can be described under ordinary irradiation conditions by the following *global* equation, written for an absorbed energy of 100 eV (1):

$$[1]\quad G_{\text{-}H_2O}\ H_2O \rightsquigarrow G_{e^-_{aq}}\ e^-_{aq} + G_{OH^-}\ OH^- + G_{H^+}\ H^+ + G_{H\cdot}\ H^\bullet + G_{H_2}\ H_2 + G_{\cdot OH}\ {}^\bullet OH + G_{H_2O_2}\ H_2O_2 + G_{HO_2\cdot/O_2\cdot-}\ HO_2^\bullet/O_2^{\bullet-} + \ldots,$$

where the coefficients G_X are the so-called "primary" free-radical and molecular yields ("long-time" or "escape" yields) representing the numbers of the various radiolytic species X (e^-_{aq}, OH^-, H^+, $H^\bullet$, H_2, $^\bullet OH$, H_2O_2, $HO_2^\bullet/O_2^{\bullet-}$...) that remain throughout the bulk of the solution after spur expansion owing to diffusion.[3] At ambient temperature, this spur

---

[2] In fact, experiments showing that water is decomposed by the action of dissolved radium salts were carried out shortly after Henri Becquerel's discovery of radioactivity (1896). One reviewer of this paper pointed out that Sir William Ramsay [J. Chem. Soc. Trans. **91**, 931 (1907)] was the first to systematically perform a series of complete experiments relating to the action of radium "emanation" on water. His article, entitled: "The chemical action of the radium emanation. Part I. Action on distilled water", was published in 1907, precisely a century ago. A historical account of the radiation chemistry of water is given in ref. 1 and refs. cited therein.

[3] The symbol G with the formula of the species as subscript is used here to represent the "primary" yield of species X. Note that, following convention, the symbol G(X) with the

expansion is essentially complete on the microsecond time scale after the initial energy deposition. At this time, the species that have diffusively escaped from spur or track reactions become homogeneously distributed in the bulk of the solution and available to react with added solutes (treated as spatially homogeneous) at moderate concentrations. At this stage, G_{-H_2O} denotes the corresponding yield for net water decomposition. For ^{60}Co γ-radiation and neutral water at ambient temperature (LET ~ 0.3 keV/μm, pH 7), the values of the primary yields are (3):

$$G_{e^-_{aq}} = 2.50 \qquad G_{H\cdot} = 0.56 \qquad G_{H_2} = 0.45 \qquad [2]$$

$$G_{\cdot OH} = 2.50 \qquad G_{H_2O_2} = 0.70 \qquad G_{HO_2\cdot/O_2\cdot^-} = 0.02$$

$$G_{-H_2O} = 3.94\,.$$

These values, including the contribution of hydroperoxyl/superoxide anion radicals ($HO_2^\bullet/O_2^{\bullet-}$, $pK_a = 4.8$, is a minor radiolytic product and can be usually omitted in the case of low-LET radiation),[4] are connected by the equations:

[3] $$G_{e^-_{aq}} + G_{OH^-} = G_{H^+}$$

[4] $$G_{e^-_{aq}} + G_{H\cdot} + 2G_{H_2} = G_{\cdot OH} + 2G_{H_2O_2} + 3G_{HO_2\cdot/O_2\cdot^-}$$

$$G_{-H_2O} = G_{e^-_{aq}} + G_{H\cdot} + 2G_{H_2} - G_{HO_2\cdot/O_2\cdot^-} = G_{\cdot OH} + 2G_{H_2O_2} + 2G_{HO_2\cdot/O_2\cdot^-}$$

expressing the charge conservation (electroneutrality) and material balance of eq. [1], respectively.[5] Examination of the material balance eq. [4] normally serves as a stringent

---

formula of the product in parentheses denotes the experimental 100-eV yield of the "final" product X. Throughout this paper, values of G are expressed in units of molecules per 100 eV (abbreviated: molec./100 eV) of absorbed energy; for conversion into SI units: 1 molec./100 eV ≈ 0.10364 μmol/J.

[4] The production of $HO_2^\bullet/O_2^{\bullet-}$ radicals is significant only in high-LET radiation tracks (e.g., see ref. 3).

[5] Equations [3] and [4] can readily be derived by writing that, at any time, the total (algebraic) charge of the transient species and stable products formed in the decomposition of

criterion for a consistent set of *G*-values.

For ^{60}Co γ-irradiated 0.4 M sulfuric acid aqueous solutions at room temperature (pH 0.46), representative values of the primary free-radical and molecular product yields are (e.g., see ref. 5):

[5] $G_{e^-_{aq}+H^\cdot} = 3.66$ $G_{H_2} = 0.40$ $G_{^\cdot OH} = 2.84$ $G_{H_2O_2} = 0.78$

$G_{HO_2^\cdot/O_2^{\cdot-}} = 0.02$ $G_{-H_2O} = 4.44$.

In fact, radiolysis experiments concerning acidic solutions were carried out before those for neutral solutions [the most commonly used acid was H_2SO_4 in 0.4 M aqueous solutions, although a few other acids like HCl, $HClO_4$, and $(COOH)_2$ were also employed in radiation yield determinations at low pH] for historical reasons related to the early development of the standard aerated ferrous sulfate (Fricke) dosimeter (6). One of the reasons that dictated the choice of sulfuric acid came from the fact that the dominant anion HSO_4^- was then considered to not intervene in the course of the radiolysis. The concentration of 0.4 M H_2SO_4 was originally selected to provide the same mass absorption for X-rays in the dosimeter solution as in air (7). At such a high concentration of H_2SO_4, the H^+ ions very rapidly scavenge most, if not all, of the e^-_{aq} radicals in the spurs/tracks to form $H^\bullet$ atoms (5, 8-10):

[6] $e^-_{aq} + H^+ \rightarrow H^\bullet$

with a bimolecular rate constant $k_6 \approx 1.12 \times 10^{10}$ M^{-1} s^{-1} (value corrected to take into account the effects of ionic strength at this acid concentration; see below) (11-15). The total primary yield of the reducing radicals e^-_{aq} and $H^\bullet$ may then be represented by the sum $G_{e^-_{aq}+H^\cdot} = G_{e^-_{aq}} + G_{H^\cdot}$.

A great many experimental and theoretical studies have shown that the yields in the radiolysis of water and aqueous solutions are highly dependent on the distances separating

---

water should be zero and the total number of $H^\bullet$ atoms in the transients and products considered should be equal to twice the number of O atoms.

the primary products from each other along the track of the ionizing radiation. The distribution of separations, commonly referred to as the "track structure" (e.g., see ref. 3), is largely determined by the geometry of the physical energy loss events, or in other words by the quality of the radiation. An often used specifier of beam quality is the LET. The most evident effect of increasing the LET of the radiation is to give lower free-radical and higher molecular primary yields (3, 16-20). This behavior is explained by the increased intervention of radical-radical reactions as the local concentration of radicals within the track increases. In fact, as the LET increases, the initially isolated "spherical" spurs change to a situation in which the spurs overlap to form continuous "cylindrical" tracks consisting of a "core" of intense ionization and electronic excitation surrounded by a region composed of the tracks of knocked-out secondary electrons (δ-rays) called the "penumbra" (21-23). This should permit fewer free radicals to escape combination and recombination reactions during the expansion of the tracks and, in turn, the formation of more molecular products.

One of the best studied systems in radiation chemistry is the aerated dilute solution of ferrous sulfate in aqueous 0.4 M H_2SO_4, which is referred to as the "Fricke dosimeter" after Hugo Fricke who first published accounts of its properties in 1927-1929 (6). The chemistry of this system is based on the oxidation of ferrous ions to ferric ions by the oxidizing species $HO_2^{\bullet}$ (bearing in mind the rapid conversion of e_{aq}^- and $H^{\bullet}$ to $HO_2^{\bullet}$ at low pH and in the presence of oxygen), $^{\bullet}OH$, and H_2O_2 that are produced in the radiolytic decomposition of water (see below) (2, 7, 16, 24). From this mechanism, the yield of Fe^{3+} ions can be expressed in terms of the primary free-radical and molecular yields, given above, by the following stoichiometric equation (2, 24):

$$[7] \quad G(Fe^{3+}) = 3(G_{e_{aq}^- + H^{\bullet}} + G_{HO_2^{\bullet}}) + G_{^{\bullet}OH} + 2G_{H_2O_2}.$$

This relationship, which has been confirmed by experiment, shows that the production of Fe^{3+} ions is highly sensitive to factors that alter the free-radical yields, especially the yield of $H^{\bullet}$ atoms. In particular, $G(Fe^{3+})$ depends on the type of the radiation used. Data by a number of different authors have shown that $G(Fe^{3+})$ steadily decreases with increasing LET, this dependence reflecting the lower yields of radicals that escape the high-LET track

as compared with low-LET radiolysis (e.g., see refs. 7, 11, 16, and 25-33). The Fricke dosimeter is a widely used liquid chemical dosimeter because of the accuracy, reproducibility, and linearity of its response as a function of dose (with care, Fricke dosimetry is capable of 0.1% precision for ^{60}Co γ-rays and high-energy X-rays and electrons) (33). In fact, its well-established characteristics are a standard in radiation-chemical work for comparison of yields under various conditions, both for experimental observations and for theoretical calculations.

For years, it has repeatedly been underlined that the problem of the influence of pH on the primary free-radical and molecular yields of water radiolysis is not yet totally resolved, especially at extreme values of pH where a certain confusion still exists (5, 10, 31). To gain further insights into our understanding of the effects of varying acidity and LET in the radiation chemistry of water, in the present study we have performed Monte Carlo simulations of the radiolysis of aqueous H_2SO_4 solutions (over the range from neutral solution to 0.4 M H_2SO_4) to calculate the variations of $G_{e^-_{aq}+H^\cdot}$, $G_{^\cdot OH}$, G_{H_2}, and $G_{H_2O_2}$ with pH for different values of the LET varying from ~0.3 to 15 keV/μm. This is followed, as an application, by a Monte Carlo study of the radiolytic oxidation of Fe^{2+} to Fe^{3+} ions in the Fricke dosimeter as a function of time (up to ~50 s) to address the influence of the radiation quality on the ferric ion yield. The results in each case are tested against the available experimental data.

This paper deals only with results at 25 °C. The main features of our simulation approach are presented in the next section, followed by the results and their discussion. Conclusions are drawn in the final section.

Monte Carlo simulations

Monte Carlo simulation techniques are used to model the complex succession of events that are generated in liquid water and sulfuric acid aqueous solutions under irradiation. The detailed description and implementation of our Monte Carlo code IONLYS-IRT that simulates the nonhomogeneous distribution of reactive species initially produced by the energy deposition by the incident radiation and by all the secondary

electrons that it has generated (i.e., the radiation track structure) and the subsequent chemical reactions of these species with each other and with available solutes has been given previously (see ref. 34 and the refs. therein). In brief, the IONLYS simulation program models, on an event by event basis, all of the events of the early physical ($<10^{-15}$ s) and physicochemical ($\sim10^{-15}$-10^{-12} s) stages in the track development. The complex spatial distribution of reactants at the end of the physicochemical stage, which is provided as an output of the IONLYS program, is then used directly as the starting point for the subsequent nonhomogeneous chemical stage ($\sim10^{-12}$-10^{-6} s). This third and final stage, during which the individual reactive species diffuse randomly and react with one another (or with the environment) until all spur or track processes are complete, is covered by our IRT program. This program employs the "independent reaction times" (IRT) method (35, 36), a computer efficient stochastic simulation technique that is used to simulate reaction times without following the trajectories of the diffusing species. The IRT method relies on the approximation that the reaction time of each pair of reactants is independent of the presence of other reactants in the system. Within the framework of this approach, the competition between the reactions is simply described via a sorting out of the stochastically sampled reaction times of each potentially reactive pair. The IRT simulation technique also allows one (as is the case in this study) to include in a simple way pseudo first-order reactions of the radiolytic products with various scavengers that are homogeneously distributed in the medium. The ability of our IRT program to give accurate time-dependent chemical yields has been well validated by comparison with a full step-by-step Monte Carlo simulation, which does follow the reactant trajectories in detail (37).

To reproduce the effects of fast electron or ^{60}Co γ-radiolysis, we use short (~100 μm) segments of 300-MeV proton tracks, over which the LET value obtained in the simulations is nearly constant[6] and equal to ~0.3 keV/μm at 25 °C. The number of proton histories

[6] Such an analysis thus gives the track segment yields at a well-defined LET (e.g., see ref. 3).

(~150) is chosen so as to ensure only small statistical fluctuations when calculating average yields, while keeping acceptable computer time limits. We should note that the use of high-energy protons as primary particles was more appropriate here than that of electrons since we wanted to study track segments over which the LET is essentially constant. In fact, a proton that has the same LET as an electron must also have an energy ~2000 times larger, and consequently its LET is much less affected by a given series of energy depositions (11, 36).

The reaction scheme and reaction parameters, as well as the diffusion coefficients of reactive species used in our IRT program for the radiolysis of pure liquid water, are taken from Tables 1 and 2 of ref. 36. Only slight adjustments were made in some reaction rate constants and diffusion coefficients to take account of the latest data available from the literature.

Modeling the effects of acidity

To simulate the radiolysis of water under acidic conditions, we have used aqueous solutions of sulfuric acid of various concentrations in the range ~0-0.4 M (i.e., at different pH values between ~7 to 0.46). As discussed earlier, much experimental and theoretical work has been done over many decades on the radiation chemistry of aqueous H_2SO_4 solutions (especially, in 0.4 M sulfuric acid), at least in part because of the fact that sulfuric acid was widely employed in the early development of the Fricke and other chemical dosimeters (custom then dictated its continued usage) (38). For aqueous H_2SO_4 (a diprotic acid), we have:

$$[8]\quad H_2SO_4 \underset{pK_{a1}}{\overset{H^+}{\rightleftarrows}} HSO_4^- \underset{pK_{a2}}{\overset{H^+}{\rightleftarrows}} SO_4^{2-}$$

with $pK_{a1} \approx -3$ and $pK_{a2} = 1.987$ at 25 °C (39, 40). Hence H_2SO_4 is virtually completely dissociated when dissolved in water above pH ≈ 0, and the solution contains mainly H^+,

HSO_4^-, and a certain amount of SO_4^{2-}.[7] The concentration of each species changes as the total acid concentration changes.

We summarize in the following the model assumptions and procedures we have used to carry out the Monte Carlo simulations of the radiolysis of aqueous H_2SO_4 solutions with IONLYS-IRT (some of the details of our computational modeling have already been given in refs. 11 and 41). As noted before, the effects of the background concentrations of H^+ in solutions were added to the IRT program as pseudo first-order reactions. We also supplemented the pure water reaction scheme to include the reactions listed in Table 1, which account for the species present in irradiated sulfuric acid solutions. At high acidities, a certain proportion of the $^{\bullet}OH$ radicals react with hydrogen sulfate (or bisulfate) ions[8] to form the sulfate radical $SO_4^{\bullet-}$ according to (e.g., see refs. 14, 42, and 44-46):

[9] $^{\bullet}OH + HSO_4^- \rightarrow H_2O + SO_4^{\bullet-}$.

The importance of $SO_4^{\bullet-}$ (or, equivalently, its protonated form $HSO_4^{\bullet}$, although no pK_a value has been determined) as an intermediate in the radiolysis of aqueous H_2SO_4 solutions at low pH has long been recognized. However, the value of the rate constant (k_9) for reaction [9] is not well established, and the data reported thus far in the literature span a range of about an order of magnitude ($1.3\text{-}15 \times 10^5$ M^{-1} s^{-1}) (14, 42, 44, 45). In view of such uncertainty, instead of choosing, somewhat arbitrarily, a particular value of k_9 among

---

[7] In this work, the dissociation of HSO_4^- is simply treated for the entire range of pH studied as a weak-acid problem in dilute aqueous solutions. Under these conditions, the concentrations of H^+ ($F + x$), HSO_4^- ($F - x$), and SO_4^{2-} (x) are readily determined, at equilibrium, by solving the quadratic equation:

$$K_{a2} = [H^+]\,[SO_4^{2-}]/[HSO_4^-] = (F + x)\,(x)/(F - x),$$

where F and K_{a2} are the considered concentration of H_2SO_4 and its second acid dissociation constant ($K_{a2} = 10^{-pK_{a2}} \approx 0.0103$), respectively.

[8] Contrary to the hydrogen sulfate ion HSO_4^-, the sulfate ion, SO_4^{2-}, has been reported to be unreactive toward $^{\bullet}OH$.

those already published, we have selected $k_9 = 1.5 \times 10^5$ M^{-1} s^{-1} in this study by adjusting this parameter so as to match, at low LET, the experimental (47-50) and simulated values of $G_{\cdot OH}$ in the region of pH < 1-2. Concomitantly, the $SO_4^{\bullet-}$ escape yields calculated using this value of k_9 are also found, in this acid range, to be less than the $G_{SO_4^{\bullet-}}$ values measured experimentally (42, 48, 50). This observation is consistent with the fact that there are two distinct formation processes of the $SO_4^{\bullet-}$ radical (for a review, see ref. 51), the indirect process via $^{\bullet}OH$ radical attack on HSO_4^- according to reaction [9] (which we have considered) and the direct action of radiation on the sulfuric acid anions (which we have not considered in our simulations; see below). Unfortunately, a more quantitative comparison between modeling and experiment is difficult to offer at this stage, as the experimental discrimination between the two contributing components of $G_{SO_4^{\bullet-}}$ has not been clearly elucidated yet. The diffusion coefficients of HSO_4^-, $SO_4^{\bullet-}$, SO_4^{2-}, and $S_2O_8^{2-}$, employed in the Monte Carlo simulations are taken to be (in units of 10^{-9} m^2 s^{-1}) 1.385 (for both HSO_4^- and $SO_4^{\bullet-}$), 1.065, and 1.145, respectively (52).

In addition, we have introduced in the IRT program the effects due to the ionic strength of the solutions (e.g., see ref. 53) for reaction [6] and for the recombination of the proton with the hydroxyl ion (11, 34):

[10] $OH^- + H^+ \rightarrow H_2O$,

as well as for all reactions between ions [except for the peculiar bimolecular self-recombination of hydrated electrons for which there is no evidence of any ionic strength effect (54)], including those given in Table 1. To relate rate constant and ionic strength of the solution, we used the following equation, obtained from the Brönsted-Bjerrum model of ionic reactions and the extended Debye-Hückel theory of ionic solutions (55, 56):

$$[11] \quad \log\left(\frac{k}{k_0}\right) = 1.02 Z_a Z_b \left(\frac{I^{1/2}}{1 + I^{1/2}}\right) - 2bI ,$$

where k is the rate constant at ionic strength I, k_0 is the rate constant in the limit of zero

ionic strength (i.e., at infinite dilution), Z_a and Z_b are the algebraic numbers of charges on the reactants (positive for cations and negative for anions), and b is a parameter taken as ($0.15\ Z_a\ Z_b$) in this study. I is defined as (57)

$$[12]\quad I = \frac{1}{2}\sum_i Z_i^2\, C_i\,,$$

where Z_i is the charge number of the ith ion and C_i is its molar concentration. The sum extends over all ionic species present in the solution. According to eq. [11], the rate constant will increase, decrease, or remain the same with increasing ionic strength, depending on whether the reactants have the same sign, opposite signs, or whether one reactant is neutral. For example, in 0.4 M H_2SO_4 solutions, the rate constants for reactions [6] and [10], corrected for these effects, are $k_6 \approx 1.12 \times 10^{10}$ M^{-1} s^{-1} (see above) and $k_{10} \approx 5.97 \times 10^{10}$ M^{-1} s^{-1} (instead of 2.11×10^{10} and 11.3×10^{10} M^{-1} s^{-1} in neutral water at 25 °C, respectively) (11-15, 36).

Finally, in our simulations, the direct action of ionizing radiation on the sulfuric acid anions (mainly HSO_4^-) is neglected, which is a reasonably good approximation over the range of sulfuric acid concentration studied (up to ~0.4 M). In fact, in 0.4 M H_2SO_4 (pH 0.46), only about 3.5% of the total energy expended in the solution is initially absorbed by direct action on HSO_4^- (rather than on H_2O) (assuming that the energy absorbed by each component is proportional to its electron fraction) (58). However, at higher acid concentrations, this effect can no longer be neglected (42, 48, 50, 59).

Modeling the effects of radiation quality (LET)

The influence of the quality of the radiation (or LET) on the yields of the radiolytic species produced in neutral water and in aqueous 0.4 M sulfuric acid solutions at 25 °C has been investigated by performing a series of simulations with protons of various initial energies, and therefore various LET. In this study, we limit ourselves to the incident proton energy range ~300-2.1 MeV, corresponding to LET values between ~0.3 and 15 keV/μm (11, 60, 61).

As mentioned above, the calculations are performed by simulating short (~20-100

μm) proton track segments, over which the energy and LET of the proton are well defined and remain essentially constant. Typically, about 5000 to 35 000 reactive chemical species are generated in the chemical development of such simulated track segments (depending on the LET). Statistically, the kinetics of ~30-150 different proton tracks (depending on the proton energy) are usually simulated to obtain computed averages of chemical yields for comparison with experiment.

Simulations of the Fricke dosimeter

To stochastically model the chemistry of the ferrous-sulfate Fricke dosimeter, we have added in the IRT program the reactions of Fe^{2+} ions with the oxidizing species $HO_2^{\bullet}$, $^{\bullet}OH$, and H_2O_2 that are formed in the water of the irradiated solution under aerated conditions. The mechanism for the radiolytic oxidation of Fe^{2+} ions to Fe^{3+} is well-understood and the rate constants of the individual reactions taking place are known. The reaction scheme is as follows (2, 7, 14-16, 24, 36, 62-64):

[6]	$e_{aq}^- + H^+ \rightarrow H^{\bullet}$	$k_6 \approx 1.12 \times 10^{10}\ M^{-1}\ s^{-1}$ $pK_a\ (H^{\bullet}/e_{aq}^-) = 9.59$
[13]	$H^{\bullet} + O_2 \rightarrow HO_2^{\bullet}$	$k_{13} = 2.1 \times 10^{10}\ M^{-1}\ s^{-1}$
[14]	$Fe^{2+} + {}^{\bullet}OH \rightarrow Fe^{3+} + OH^-$	$k_{14} = 3.4 \times 10^{8}\ M^{-1}\ s^{-1}$
[15]	$Fe^{2+} + HO_2^{\bullet} \rightarrow Fe^{3+} + HO_2^-$	$k_{15} = 7.9 \times 10^{5}\ M^{-1}\ s^{-1}$
[16]	$HO_2^- + H^+ \rightarrow H_2O_2$	$k_{16} \approx 2.66 \times 10^{10}\ M^{-1}\ s^{-1}$ $pK_a\ (H_2O_2/HO_2^-) = 11.62$
[17]	$Fe^{2+} + H_2O_2 \rightarrow Fe^{3+} + {}^{\bullet}OH + OH^-$	$k_{17} = 52\ M^{-1}\ s^{-1}$
[10]	$OH^- + H^+ \rightarrow H_2O$	$k_{10} \approx 5.97 \times 10^{10}\ M^{-1}\ s^{-1}$ $pK_a\ (H_2O/OH^-) = 13.999.$

As we can see, each $H^{\bullet}$ atom forms a hydroperoxyl radical, and each of these radicals oxidizes three Fe^{2+} ions: one by reaction [15] and two by the reaction sequence [16], [17], and [14]. Each $^{\bullet}OH$ radical oxidizes one Fe^{2+} ion, and each molecule of H_2O_2 oxidizes two

Fe^{2+} ions. Summing all sources of Fe^{3+} ions, the yield of ferric ions in aerated solution $G(Fe^{3+})$ is related to the "escape" yields of the free radicals and molecular species of water radiolysis by eq. [7].

Note that the values of k_6, k_{10}, and k_{16} shown above and used in the simulations have been corrected, using eqs. [11] and [12], for the effects due to the ionic strength in the case (under study here) of a solution made of 0.4 M H_2SO_4 and 5 mM $FeSO_4$. Note also that, as we have mentioned above, for solutions 0.4 M in H_2SO_4 there is a small amount of $^{\bullet}OH$ radicals that react with HSO_4^- to form $SO_4^{\bullet-}$ (reaction [9]). However, the overall ferric ion yield remains the same as given by eq. [7] since the sulfate radical reacts with Fe^{2+} in the same way as $^{\bullet}OH$ (24, 43):

[18] $SO_4^{\bullet-} + Fe^{2+} \rightarrow Fe^{3+} + SO_4^{2-}$ $\qquad k_{18} \approx 2.79 \times 10^8\ M^{-1}\ s^{-1}$.

Under normal irradiation conditions, the radical concentrations are low compared with the background concentrations of acid, Fe^{2+} ions, and oxygen (~2.5×10^{-4} M) in solution, and the reactions were treated in the IRT program as pseudo-first order (see above). In modeling the Fricke dosimeter, the slowest component of the kinetics of Fe^{3+} formation is due to the Fenton-type reaction [17] (65). For example, in the case of 5 mM $FeSO_4$ solutions considered here, this reaction takes several seconds to go to completion, which increases the computer time usually chosen for modeling the radiolysis of water (typically ~1 μs). In this work, the time evolution of $G(Fe^{3+})$ has been followed until ~50 s.

Results and discussion

The effects of acidity on the primary free-radical and molecular yields

Figure 1 displays our calculated values of $G_{^{\bullet}OH}$, $G_{e^-_{aq}+H^{\bullet}}$, G_{H_2}, and $G_{H_2O_2}$ for the radiolysis of air-free aqueous sulfuric acid solutions, at 25 °C, as a function of -log $[H^+]$ in the range from neutral solution to 0.4 M H_2SO_4, using 300-MeV incident protons (LET ~ 0.3 keV/μm). Available experimental data (3, 8, 10, 47-50, 66-76) are also included for comparison. Our results show that an increase in acidity ($1 < pH < 4$) leads to an increase in $G_{e^-_{aq}+H^{\bullet}}$ and a slight increase in $G_{^{\bullet}OH}$ and $G_{H_2O_2}$, while there is a slight decrease in

G_{H_2}. At pH < 1, $G_{\cdot OH}$ diminishes steeply. By contrast, in the range of pH from ~4 to 7, the calculated yield values are constant, independent of sulfuric acid concentration. As can be seen from Fig. 1, the computed primary yield values are generally in good agreement with the experimental values over the whole acidity range studied.

As the direct action of radiation on the sulfuric acid anions has been ignored in our simulations, the "initial" yields of the radiolytic species arising from the radiolysis of pure water can be regarded as essentially independent of the H_2SO_4 concentration. Hence, the variation of the yields of those species with acid concentration only results from the various chemical reactions that contribute to their formation or decay while the spurs expand by diffusion. To gain further insight into the effects of acidity on $G_{\cdot OH}$, $G_{e^-_{aq}+H\cdot}$, G_{H_2}, and $G_{H_2O_2}$, it is thus of interest to examine the unfolding of those various reactions that lead to the different primary yields shown in Fig. 1. This can readily be done with our Monte Carlo simulations, which enable us to determine quantitatively the time dependence of each reaction. Table 2 summarizes the major spur/track reactions that are involved in the primary yields of water decomposition products. The importance of these reactions can be quantified by the yield variations ΔG that they cause over the time interval of nonhomogeneous track chemistry (~10^{-12}-10^{-6} s). Figures 2 and 3 compare, for pure neutral water and 0.4 M H_2SO_4 (pH 0.46) aqueous solutions, respectively, the time profiles of the extents ΔG of each of these reactions, calculated from our simulations for low-LET radiolysis.

The hydroxyl radical

The hydroxyl radical is the main oxidizing radical formed when aqueous sulfuric acid solutions are irradiated. As can be seen in Fig. 1*a*, our calculated values of $G_{\cdot OH}$ are independent of pH over the range ~4-7, slightly increase at pH < 4 to reach a weakly pronounced maximum around pH 1, and then fall steeply as the pH is further reduced below 1. From Fig. 2*a*, it is seen that, in neutral water, •OH is produced mainly by reaction [R4], whereas its decay is dominated by reactions [R8], [R5], [R7], and [R6] (in order of decreasing importance). In contrast, in 0.4 M H_2SO_4 solutions (see Fig. 3*a*), the formation of

•OH due to reaction [R4] is decreased by almost 100%, due to the occurrence of the very rapid reaction [6] of the H^+ ions which, at this acid concentration, capture most, if not all, of the e^-_{aq} radicals in the spurs. For the same reason, the removal of •OH due to reaction [R5] is also significantly decreased at low pH in favor of reaction [R7]. Finally, as discussed above, there is a decrease of •OH caused by reaction [9].

The "reducing" free-radical species e^-_{aq} ***and H•***

As shown in Fig. 1*b*, the effect of increasing -log $[H^+]$ from ~0.4 to 7 is to reduce our calculated values of $G_{e^-_{aq}+H\cdot}$ ($= G_{e^-_{aq}} + G_{H\cdot}$) from ~3.7 to 3.1 molec./100 eV (that is by less than 20%), which is in good agreement with experiment. In the pH range ~4-7, $G_{e^-_{aq}+H\cdot}$ is independent of acid concentration. From Figs. 2*b* and 2*c*, it is seen that, in neutral water, the decay of the e^-_{aq} yield up to ~10^{-6} s is mainly due to the reactions [R5] and [R1] (or [6]) of e^-_{aq} with •OH radicals and H^+ ions. In 0.4 M H_2SO_4 solutions, however, it clearly appears from Fig. 3*b* that reaction [R1] largely dominates the decay of e^-_{aq}, which is rapidly converted in the spurs into the hydrogen atom. This reaction occurs mostly at early times (< 10^{-9} s).

As for the H• atom, Figs. 2*c* and 3*c* show that, in both neutral water and 0.4 M sulfuric acid solutions, reaction [R7] is responsible for most of its decay, while its production takes place mainly through the occurrence of reaction [R1].

Molecular hydrogen

As is well established, G_{H_2} slightly decreases with increasing acidity (8, 10, 47, 49, 59, 69, 70, 72-74; see also ref. 5). As one can see from Fig. 1*c*, our calculations reproduce such a decrease in G_{H_2} at pH < 4, in agreement with experiment. In the range of pH ~4-7, G_{H_2} is independent of acidity. The measured microsecond yield value $G_{H_2} \simeq 0.45$ molec./100 eV at pH 7 is also well reproduced by our simulations.

Figure 2*d* shows that, in neutral water, the production of H_2 is predominantly due to reactions [R3] and [R2] (in order of decreasing importance). By contrast, as the acidity increases, reaction [R10] occurs to an increasing extent in the spurs. As it clearly appears from Fig. 3*d*, reactions [R2] and [R3] are only of minor importance in 0.4 M H_2SO_4 solu-

tions, and the production of H_2 under such acidic conditions can be almost entirely attributed to reaction [R10].

Hydrogen peroxide

As is shown in Fig. 1*d*, our calculated values of $G_{H_2O_2}$ remain unaffected by changes of pH in the range ~4-7 and increase as -log [H^+] is decreased from ~4 to 0.4, in good agreement with experiment. It has long been established, from modeling and experimental studies, that the main precursor of the molecular yield of H_2O_2 is •OH through the spur reaction [R8] of •OH with itself. The importance of this reaction is quantified in Figs. 2*e* and 3*e*. As can be seen, there is clear evidence that the combination reaction of •OH radicals is the major source of primary hydrogen peroxide, both in neutral water and 0.4 M H_2SO_4 solutions. Figure 2*e* also shows that, in neutral water, the decay of H_2O_2 is dominated by the back reaction [R4]. In contrast to this situation, in 0.4 M H_2SO_4 solutions, the removal of H_2O_2 due to the occurrence of reaction [R4] is decreased by almost 100%.

Proposed interpretation of the effects of acidity on the primary free-radical and molecular yields

As can be seen in Figs. 1*a-d*, the values of the primary free-radical and molecular product yields do not change in the range ~4 < pH < 7. This can easily be explained if we consider, as mentioned above, that the main effects of acidity on the primary yields of the radiolysis of aqueous solutions at low pH are attributed to the presence of H^+ ions, which can rapidly scavenge hydrated electrons through reaction [6] (or [R1]). At pH 4, for example, one has a H^+ concentration of 10^{-4} M and a scavenging power, defined as the product k_6 [H^+] (for example, see ref. 20), of ~2.05×10^6 s^{-1}. Hence, the time scale over which reaction [6] occurs, measured by the reciprocal of the scavenging power, is ~5×10^{-7} s. Therefore, the addition of 10^{-4} M H^+ ions will contribute only very little to the scavenging of e^-_{aq} in the spurs. Under such conditions, a change of pH from 7 to ~4 has, indeed, no effect on either radical or molecular primary yields.

At pH < 4, the concentration of H^+ ions is high enough to be able to convert the e^-_{aq}

radicals in the spurs or tracks into H• atoms, interfering to some extent with the back reactions forming water (see Figs. 3*b* and 3*c*). According to Hayon (69, 77) and as clearly shown in Fig. 2*b* from our simulations, these electrons, in neutral solution, would have predominantly combined, in the absence of other electron-accepting solutes with which they could react, with •OH to form water:

[R5] $e^-_{aq} + {}^{\bullet}OH \rightarrow OH^-$ $k_{R5} = 2.95 \times 10^{10}\ M^{-1}\ s^{-1}$ (15)

The H• atoms, on the contrary, react less efficiently than e^-_{aq} with •OH in the spurs:

[R7] $H^{\bullet} + {}^{\bullet}OH \rightarrow H_2O$ $k_{R7} = 1.55 \times 10^{10}\ M^{-1}\ s^{-1}$ (15)

This reduction in reactivity is also the result of H• having a larger diffusion coefficient ($7.0 \times 10^{-9}\ m^2\ s^{-1}$) than e^-_{aq} ($4.9 \times 10^{-9}\ m^2\ s^{-1}$) (4, 15, 78). The effect of acid is thus to decrease in the spur time scale the importance of the back reaction [R5]. The conversion of e^-_{aq} to H• in the spurs in acidic solution, and the subsequent "protection" of the •OH radicals against the action of hydrated electrons (69, 77, 79), lead to the following consequences:

(i) The reducing free-radical entities being less reactive while the spurs expand, owing to the intervention of reaction [R7], $G_{e^-_{aq}+H^{\bullet}}$ increases on going from neutral to acidic solutions, as observed experimentally (Fig. 1*b*).

(ii) This mechanism tends, at low pH, to increase $G_{{}^{\bullet}OH}$. This is clearly seen in Fig. 1*a* where $G_{{}^{\bullet}OH}$ slightly increases at pH < 4.

(iii) Due to the dimerization of the •OH radicals, $G_{H_2O_2}$ also increases with increasing acidity up to 0.4 M H_2SO_4, in good agreement with experiment (Fig. 1*d*). At higher sulfuric acid concentrations, however, our simulations predict (data not shown) that $G_{H_2O_2}$ should diminish owing to the removal of •OH radicals due to the increased intervention of reaction [9] (or [R9]) (see Fig. 1*a*). Unfortunately, there is at present no experimental or theoretical data available in the literature with which to compare our results.

(iv) The yield of molecular hydrogen is gradually lowered below pH 4 (Fig. 1*c*). This is explained by the fact that, as the acidity progressively increases, the contribution of the

self reaction of the H• atom:

[R10] $H^{\bullet} + H^{\bullet} \rightarrow H_2$ $k_{R10} = 5.03 \times 10^9\ M^{-1}\ s^{-1}$ (15)

becomes more important. As can be seen in Fig. 3*d*, this reaction is the dominant chemical route for producing H_2 in 0.4 M H_2SO_4 solutions. Under neutral conditions (see Fig. 2*d*), reaction [R10] is only of minor importance, and the production of H_2 can be almost entirely attributed to reaction [R3]:

[R3] $e^-_{aq} + H^{\bullet}\ (+H_2O) \rightarrow H_2 + OH^-$ $k_{R3} = 2.5 \times 10^{10}\ M^{-1}\ s^{-1}$ (80)

and, but to a lesser extent, reaction [R2]. Reaction [R10] being less efficient than reaction [R3], conversion of the e^-_{aq} to H• atom leads to a lowering of G_{H_2} at low pH.

(v) Finally, the yield of decomposition of water, G_{-H_2O} , increases as the pH decreases below ~4 , in order, of course, to maintain the material balance eq. [4].

Overall, our present Monte Carlo calculations generally agree well with experiment (see Fig. 1). Results clearly show that the primary free-radical and molecular yields of the radiolysis of aqueous solutions are influenced by the addition of H^+ ions, especially at high sulfuric acid concentrations. However, in accord with a previous conclusion by Draganić and Draganić (10), there is no strong dependence of those yields on pH.

The effect of LET on the primary free-radical and molecular yields of the radiolysis of neutral liquid water and aqueous 0.4 M H_2SO_4 solutions

Figures 4 and 5 show the variations of our computed primary free-radical and molecular yields as a function of LET over the range ~0.3-15 keV/μm, for deaerated neutral liquid water and aqueous 0.4 M H_2SO_4 solutions, respectively, at 25 °C. For the sake of comparison, available experimental data for various radiation types and different authors (3, 8, 20, 48, 49, 66-76, 81-100) are also included in the figures. Overall, our computed results are in good agreement with the measured yields. In both neutral water and acidic solutions, it is seen that, in general, the primary yields of molecular products increase with increasing LET at the expense of those of free radicals. These variations in radical and

molecular yields reflect the effect of changing conditions on the extent of radical-radical reactions within spurs/tracks; as mentioned above, high LET favors high reaction rates for radicals within the dense columnar regions of tracks. We should notice, however, the peculiar behavior of $G_{H\cdot}$ in neutral water. In fact, unlike the other radical yields, our calculated $G_{H\cdot}$ values exhibit a slight maximum near 6.5 keV/μm before decreasing at higher LET (Fig. 4*a*). The origin of this maximum was discussed in detail previously (101). In essence, this variation of $G_{H\cdot}$ as a function of LET does not arise from a change in the "initial" yield of H• atoms (i.e., at the end of the physicochemical stage), which is nearly constant over the LET range studied, but rather from the various reactions that are involved in their production and decay in the time interval of nonhomogeneous spur/track chemistry (see Table 2). As one can see from Figs. 2*c* and 4*a*, our calculations, which confirm the results previously obtained by Meesungnoen et al. (101), show that the overall effect of LET on $G_{H\cdot}$ is dominated by reaction [R1] (or [6]) up to the maximum of $G_{H\cdot}$ at ~6.5 keV/μm, and by reactions [R7], [R3], and [R10] (by order of decreasing importance) at higher LET.

Together with the yields obtained at 10^{-6} s (solid lines in Figs. 4 and 5), we also show our primary free-radical and molecular yield values calculated at 10^{-7} s after irradiation (dashed lines in Figs. 4 and 5). Such a comparison is given as a means to estimate the sensitivity of our computed "escape" yields as regards the uncertainty in assigning a value for the time (generally quoted ~10^{-6}-10^{-7} s in the literature) marking the end of the nonhomogeneous radiation chemical stage (that is, when the expanding spurs and tracks overlap or, equivalently, when the species are considered to be homogeneously distributed in the solution). As can be seen from Figs. 4 and 5, the differences found between these two sets of yield values at 10^{-6} and 10^{-7} s depend strongly on the particular species and LET. For low-LET radiation, these differences are of the order of a few percent only (but never exceed ~10%), suggesting that, at ~10^{-7} s after the ionizing event, the intratrack reactions in fast electron or γ-radiolysis are already nearly complete. By contrast, there are considerably more reactions of species in high-LET tracks than in the spurs produced by fast electrons. In fact, the differences observed in yield values at 10^{-6} and 10^{-7} s are getting

more important with increasing LET (for example, they amount to ~30-40% at ~15 keV/μm for the particular case of e^-_{aq} and $^{\bullet}OH$, compared to ~3-10% at ~0.3 keV/μm). These differences reflect the changes in the nature of the track structure; at high LET, the species will not escape as they diffuse along the axis of the cylindrical track and will continue to react among themselves to longer times (in the absence of solutes) (for example, see refs. 102 and 103).

The material balance eq. [4] for "reducing" (e^-_{aq}, $H^{\bullet}$, and H_2) and "oxidizing" ($^{\bullet}OH$, H_2O_2, and $HO_2^{\bullet}/O_2^{\bullet-}$) species is found to be satisfied throughout the range of LET studied, for both neutral water and acidic solutions:

(i) For neutral water, we have (at 10^{-6} s), for ^{60}Co γ radiation (LET ~ 0.3 keV/μm): $G_{red} = G_{e^-_{aq}} + G_{H^{\bullet}} + 2G_{H_2} = 4.05 \pm 0.04$ and $G_{ox} = G_{^{\bullet}OH} + 2G_{H_2O_2} + 3G_{HO_2^{\bullet}/O_2^{\bullet-}} = 3.99 \pm 0.05$, in good agreement with the experimental value of ~3.94 molec./100 eV given in eq. [2]; for an LET of ~12.8 keV/μm, our calculated primary yields are: $G_{red} = 3.14 \pm 0.04$ and $G_{ox} = 3.10 \pm 0.03$, which compare well with the values of ~3.09 and 3.05 molec./100 eV deduced for this LET from the room-temperature yield data reported by Elliot et al. (15, 81), respectively.

(ii) For 0.4 M H_2SO_4 solutions, we have similarly (at 10^{-6} s), for ^{60}Co γ radiation: $G_{red} = G_{e^-_{aq}+H^{\bullet}} + 2G_{H_2} = 4.47 \pm 0.04$ and $G_{ox} = 4.26 \pm 0.07$, in good accord with the experimental value of ~4.44 molec./100 eV given in eq. [5]; for an LET of ~13.7 keV/μm, we find $G_{red} = 3.84 \pm 0.03$ and $G_{ox} = 3.73 \pm 0.04$, which compare satisfactorily with the values of ~3.81 and ~3.98 molec./100 eV reported by Barr and Schuler (71) and Schuler and Allen (91) for 18-MeV deuterons, respectively.

The effect of LET on the chemistry and the yield of the Fricke dosimeter

Kinetics of Fe^{3+} formation

As an application and also as a test of the reliability of our primary yields, Monte Carlo simulations have been used to study the LET dependence of the oxidation of ferrous ions in the radiolysis of air-saturated solutions of 5 mM $FeSO_4$ in aqueous 0.4 M H_2SO_4

(the ferrous-sulfate Fricke dosimeter[9]).[10] As described above, the mechanism of this chemical system, well-understood in terms of oxidation of Fe^{2+} ions to Fe^{3+} by H• atoms (via production of HO_2•), •OH radicals, and H_2O_2, includes the sequence of reactions [6] and [13]-[17]. Figure 6 shows the kinetics of Fe^{3+} formation as obtained from our simulations for 300-MeV irradiating protons (LET ~ 0.3 keV/μm) at ambient temperature. As can be seen from this figure, $G(Fe^{3+})$ is time dependent, as a result of the differences in the lifetimes of the reactions making up the radiolysis mechanism (2, 105, 106). The fastest reaction of Fe^{2+} ions is with •OH radicals. It is completed on a microsecond time scale. The oxidation of Fe^{2+} by HO_2• is slower and requires a few milliseconds for completion. The slowest component in the formation of Fe^{3+} is due to Fe^{2+} oxidation by H_2O_2 (both the molecular product yield and that formed by reaction [16]). This latter reaction takes place at times longer than ~0.1 s and is completed by about 30 s.

The accepted value of the ferric ion yield in the Fricke dosimeter, obtained for ^{60}Co γ-rays, high-energy X-rays or fast electrons, is $G(Fe^{3+}) = 15.6 \pm 0.2$ molec./100 eV (for example, see refs. 7, 25, 28, and 107-110) at 25 °C. Under the same low-LET conditions, our computed value of $G(Fe^{3+})$ at ~50 s is found to be equal to ~15.7 molec./100 eV (Fig. 6), in very good agreement with the standard value.

Variation of $G(Fe^{3+})$ with LET

Figure 7 shows the values of $G(Fe^{3+})$ calculated from our Monte Carlo simulations of the radiolysis of aerated solutions of 5 mM $FeSO_4$ in aqueous 0.4 M H_2SO_4 as a function of LET over the range ~0.3-15 keV/μm, at 25 °C. It is seen that, as the LET increases, the yield diminishes. Our computed values are compared with experimental data of ferric ion

---

[9] Note that the commonly used Fricke solution typically contains 1 mM $FeSO_4$ and is saturated with air. The "super-Fricke" dosimeter, saturated with oxygen and containing 10 mM ferrous sulfate, is seldom used. See ref. 30.

[10] A preliminary report of this work has been presented at the "48th Annual Meeting of the Japanese Society of Radiation Chemistry, Osaka, Japan", October 12-14, 2005. See ref. 104.

yields versus LET obtained by a number of different workers (26, 28, 33, 67, 72, 81, 91, 95, 108, 109, 111-123) using a variety of methods for radiations of different energies. Despite the relatively large uncertainties of the reported measurements, there is a good agreement between theory and experiment. Also shown in the figure are the curves of $G(Fe^{3+})$ versus LET calculated at two different times chosen for the completion of spur/track processes (namely, 10^{-7} and 10^{-6} s after the energy deposition event) on the basis of the values of G(primary yields) using eq. [7]. As can be seen, the values of $G(Fe^{3+})$ obtained from our Monte Carlo simulations are found to lie in between the two curves of the yields obtained from eq. [7] at 10^{-7} and 10^{-6} s, over the whole LET range considered.

This dependence of $G(Fe^{3+})$ on LET results from the fact that the production of ferric ions in the Fricke system is most sensitive to radical yields; indeed, according to eq. [7], the lower the yield of radicals which escape the radiation track, the lower the Fricke G-value. Since increasing LET has the effect of reducing the free-radical product yields from water (see Fig. 5), it follows that $G(Fe^{3+})$ also decreases as the LET increases.

Conclusions

In this study, we have used Monte Carlo simulations to investigate the influence of acidity (pH) on the primary yields of the various chemical species produced in the radiolysis of deaerated aqueous sulfuric acid solutions over the range of H_2SO_4 concentrations ~0-0.4 M. The effects of the quality of radiation, a measure of which is its LET, has also been studied for LET varying from ~0.3 to 15 keV/μm at ambient temperature. Our results show that an increase in acidity ($1 < pH < 4$) leads to an increase in the yields of the reducing radicals (e^-_{aq} and H• atom) and the oxidizing products (•OH radical and H_2O_2), while the yield of H_2 decreases. At $pH < 1$, •OH radicals react with HSO_4^- anions to form $SO_4^{\bullet-}$ radicals, resulting in a marked decrease in $G_{\cdot OH}$. By contrast, at $pH > 4$, the yields are essentially independent of sulfuric acid concentration. In both neutral liquid water and 0.4 M H_2SO_4 (pH ~ 0.46) solutions, the most evident effect of increasing LET is an increase in the primary yields of molecular products, accompanied by a corresponding decrease in those of free radicals. As an exception, $G_{H\cdot}$ at first increases

vs. LET, then reaches a maximum near 6.5 keV/μm before decreasing steeply at higher LET. The results obtained are in generally good agreement with available experimental data over the whole acidity and LET ranges studied.

Finally, as an application, we have simulated the chemical development of the Fricke dosimeter (aerated solution of ferrous sulfate in aqueous 0.4 M H_2SO_4) as a function of time up to ~50 s and addressed the effects of LET on the resulting ferric ion yield at 25 °C. The production of Fe^{3+} ions is found to be highly sensitive to free-radical yields, especially $H^{\bullet}$ atoms, and is strongly dependent on the quality of the radiation. Our calculated values of $G(Fe^{3+})$ agree very well with the experimental yields.

The good overall agreement between calculated and experimental yield values obtained for both neutral water and acidic solutions, as well as for the Fricke dosimeter, gives strong support to the validity and consistency of the assumptions employed in this study.

Acknowledgments

One of the authors (N.A.) expresses his appreciation to Dr. Kashane Chalermwat, Dr. Nisa Chawapun, and Dr. Wisatre Kongcharoensuntorn for their support and continuous encouragement during the course of this study. J.-P. J.-G. thanks the Japan Society for the Promotion of Science for a 2005 JSPS Invitation Fellowship for Research in Japan, which allowed him to present preliminary results of this work as part of an invited talk at the 48th Annual Meeting of the Japanese Society of Radiation Chemistry, held in Osaka, Japan, on October 12-14, 2005. The financial assistance of the Natural Sciences and Engineering Research Council of Canada (under Grant No. 9020-04) is gratefully acknowledged.

Table 1. Reactions added to the pure water reaction scheme to simulate the radiolysis of deaerated aqueous H_2SO_4 solutions, at 25 °C. The rate constants given here for the reactions between ions are at ionic strength equal to zero.

Reaction	k (M^{-1} s^{-1})
$H^{\bullet} + SO_4^{\bullet-} \rightarrow HSO_4^-$	1.0×10^{10} [a]
$H^{\bullet} + S_2O_8^{2-} \rightarrow SO_4^{\bullet-} + HSO_4^-$	2.5×10^{7} [b]
$^{\bullet}OH + HSO_4^- \rightarrow H_2O + SO_4^{\bullet-}$	1.5×10^{5} [c]
$e_{aq}^- + S_2O_8^{2-} \rightarrow SO_4^{\bullet-} + SO_4^{2-}$	1.2×10^{10} [b]
$H_2O_2 + SO_4^{\bullet-} \rightarrow HO_2^{\bullet} + HSO_4^-$	1.2×10^{7} [d]
$OH^- + SO_4^{\bullet-} \rightarrow {}^{\bullet}OH + SO_4^{2-}$	8.3×10^{7} [d]
$SO_4^{\bullet-} + SO_4^{\bullet-} \rightarrow S_2O_8^{2-}$	4.4×10^{8} [d]

[a] Reference 42.

[b] Reference 14.

[c] Value used in this work (see text).

[d] Reference 43.

Table 2. Most important spur/track reactions inferred from our Monte Carlo simulations of the nonhomogeneous chemical stage in the low-LET radiolysis of deaerated neutral liquid water and aqueous sulfuric acid solutions at 25 °C and in the time interval ~10^{-12}-10^{-6} s.

Symbol [a]	Reaction
[R1] (or [6])	$e^-_{aq} + H^+ \rightarrow H^\bullet$
[R2]	$e^-_{aq} + e^-_{aq}\ (+2\,H_2O) \rightarrow H_2 + 2\,OH^-$
[R3]	$e^-_{aq} + H^\bullet\ (+H_2O) \rightarrow H_2 + OH^-$
[R4]	$e^-_{aq} + H_2O_2 \rightarrow {}^\bullet OH + OH^-$
[R5]	$e^-_{aq} + {}^\bullet OH \rightarrow OH^-$
[R6]	${}^\bullet OH + OH^- \rightarrow O^{\bullet-} + H_2O$
	$O^{\bullet-} + H_2O \rightarrow {}^\bullet OH + OH^-$
[R7]	${}^\bullet OH + H^\bullet \rightarrow H_2O$
[R8]	${}^\bullet OH + {}^\bullet OH \rightarrow H_2O_2$
[R9] (or [9])	${}^\bullet OH + HSO_4^- \rightarrow H_2O + SO_4^{\bullet-}$
[R10]	$H^\bullet + H^\bullet \rightarrow H_2$

[a] Reaction symbols used in the text.

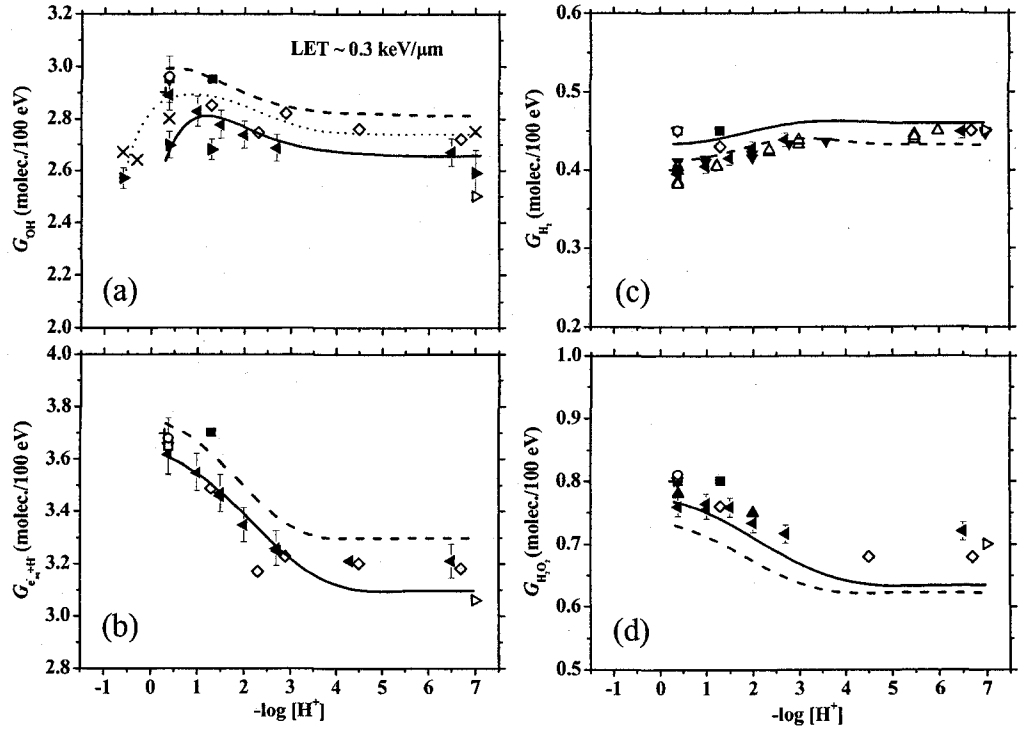

Figure 1: Variations of the primary free-radical and molecular yields (in molec./100 eV) of the radiolysis of deaerated aqueous H_2SO_4 solutions by 300-MeV incident protons (LET ~ 0.3 keV/μm) as a function of -log [H^+] over the sulfuric acid concentration range 0-0.4 M at 25 °C. The solid and broken lines represent the results of our Monte Carlo simulations for (*a*) $G_{\cdot OH}$, (*b*) $G_{e^-_{aq}+H\cdot}$, (*c*) G_{H_2}, and (*d*) $G_{H_2O_2}$, obtained at 10^{-6} and 10^{-7} s after the initial energy deposition, respectively. The calculations were performed with $k_9 = 1.5 \times 10^5$ M^{-1} s^{-1} (see text); this value of k_9 was adjusted to match the experimental and simulated values of $G_{\cdot OH}$ in the region of pH < 1-2. This is shown in (*a*) where the curve of $G_{\cdot OH}$ vs. -log [H^+] calculated at 2.5×10^{-7} s is also presented for H_2SO_4 concentrations up to ~4 M (dotted line), for the sake of comparison. Note that in solutions greater than 0.4 M sulfuric acid, the measured $G_{\cdot OH}$ data were corrected to account for the direct action of radiation on HSO_4^- anions according to a procedure given in ref. 48 based on the formula $(G_{\cdot OH})^0 = G_{\cdot OH}/E_w$, where $(G_{\cdot OH})^0$ is the *G*-value for •OH production that results from energy absorption by water and E_w denotes the electron fraction of water. Experiment: ref. 3 (▷), refs. 8 and 69 (△), refs. 10 and 47 (◇), ref. 48 (▶), ref. 49 (◀), ref. 50 (×), refs. 66 and 67 (□), ref. 68 (○), ref. 70 (▼), ref. 71 (▽), ref. 72 (●), refs. 73 and 74 (+), ref. 75 (■), and ref. 76 (▲). For conversion of yield values into SI units: 1 molec./100 eV ≈ 0.10364 μmol/J.

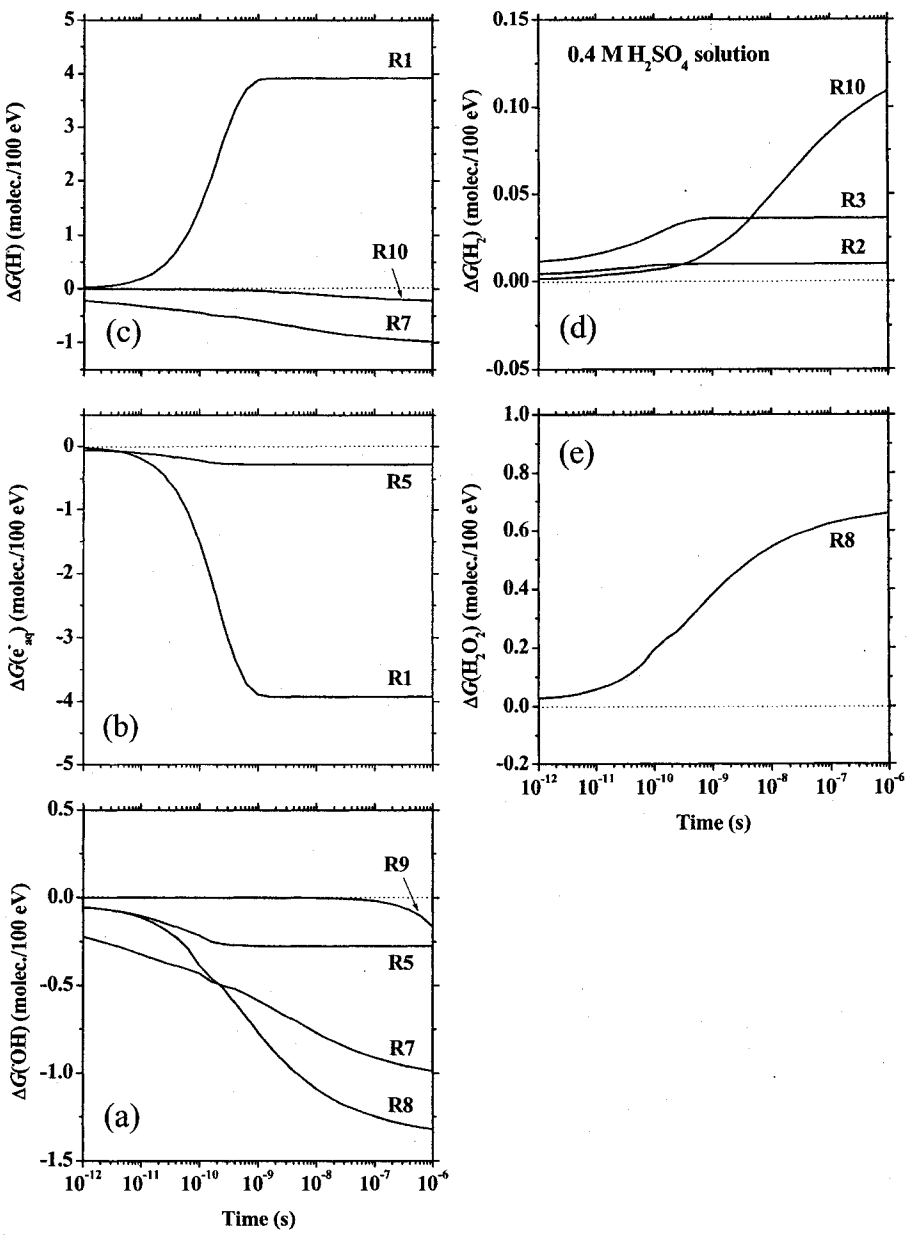

Figure 2: Time dependence of the extents ΔG (in molec./100 eV) of the main spur/ intratrack reactions that are involved in the formation and decay of (*a*) •OH, (*b*) e^-_{aq}, (*c*) H•, (*d*) H_2, and (*e*) H_2O_2 (see text and Table 2), calculated from our Monte Carlo simulations of the radiolysis of deaerated liquid water by ~300-MeV protons (LET ~ 0.3 keV/μm) at neutral pH, 25° C and in the interval 10^{-12}-10^{-6} s. Note that the "initial" yields of •OH, e^-_{aq}, H•, H_2, and H_2O_2, calculated at the end of the physicochemical stage, are ~5.43, 4.26, 0.97, 0.28, and 0.11 molec./100 eV, respectively.

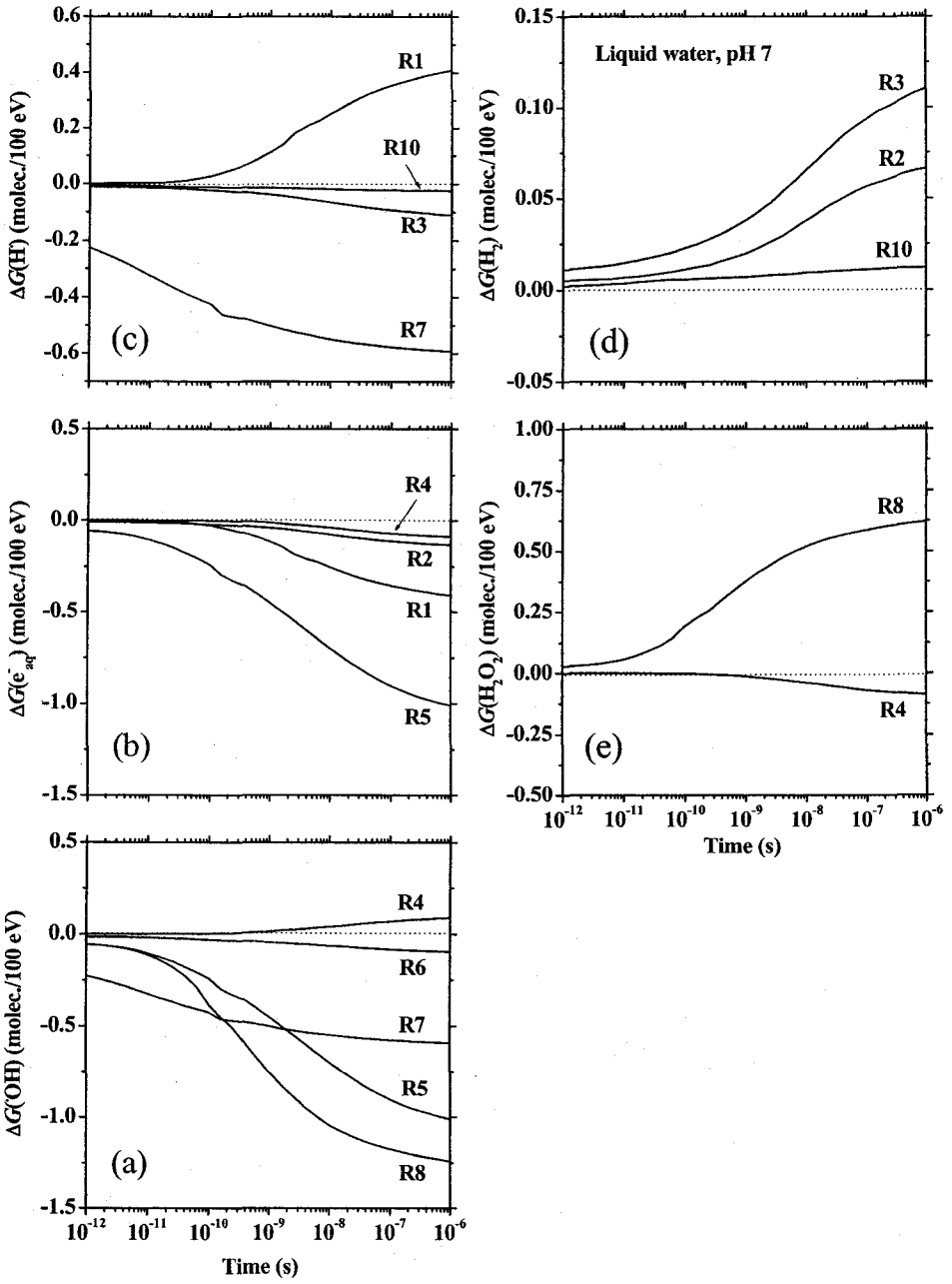

Figure 3: Time dependence of the extents ΔG (in molec./100 eV) of the main spur/ intratrack reactions that contribute to the formation and decay of (*a*) •OH, (*b*) e^-_{aq}, (*c*) H•, (*d*) H_2, and (*e*) H_2O_2 (see text and Table 2), calculated from our Monte Carlo simulations of the radiolysis of deaerated 0.4 M H_2SO_4 aqueous solutions by ~300-MeV protons (LET ~ 0.3 keV/μm) at 25° C and in the interval 10^{-12}-10^{-6} s. The "initial" yields of •OH, e^-_{aq}, H•, H_2, and H_2O_2, calculated at the end of the physicochemical stage, are as in the legend of Fig. 2.

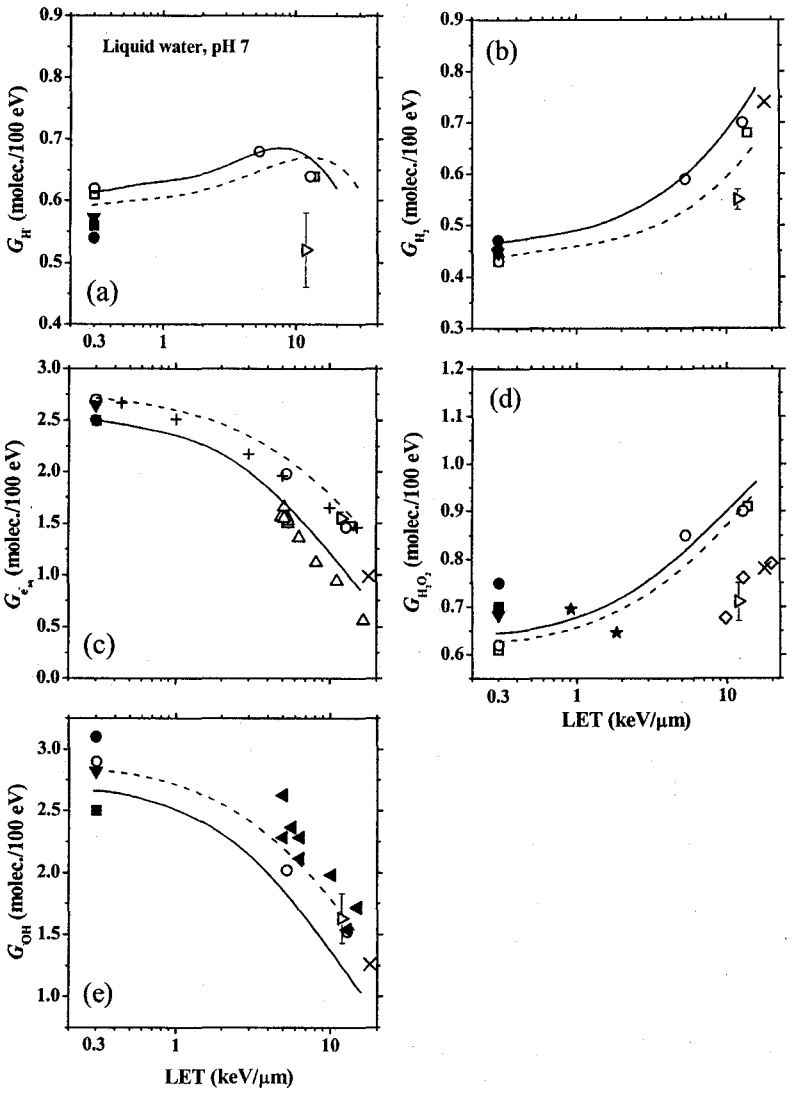

Figure 4: Variations of the primary free-radical and molecular yields (in molec./100 eV) of the radiolysis of deaerated neutral liquid water at 25 °C as a function of LET over the range ~0.3-15 keV/μm (up to ~20 keV/μm for the primary yield of H• atoms). The solid and dashed curves represent the results of our Monte Carlo simulations for (*a*) $G_{H.}$, (*b*) G_{H_2}, (*c*) $G_{e^-_{aq}}$, (*d*) $G_{H_2O_2}$, and (*e*) $G_{.OH}$ at 10^{-6} and 10^{-7} s, respectively. Experiment: ref. 3 (■), ref. 20 (data taken from the line marked "selected" in Fig. 7.7.1, which is a fit of experimental yields from different authors at various LET) (+), ref. 81 (▷), ref. 82 (▼), ref. 83 (□), ref. 84 (○), ref. 85 (△), ref. 86 (◀), ref. 87 (◇), ref. 88 (★), ref. 89 (×), and ref. 90 (●). LET values used here for the various types of radiation considered correspond to dose-average LET values, taken from ref. 60.

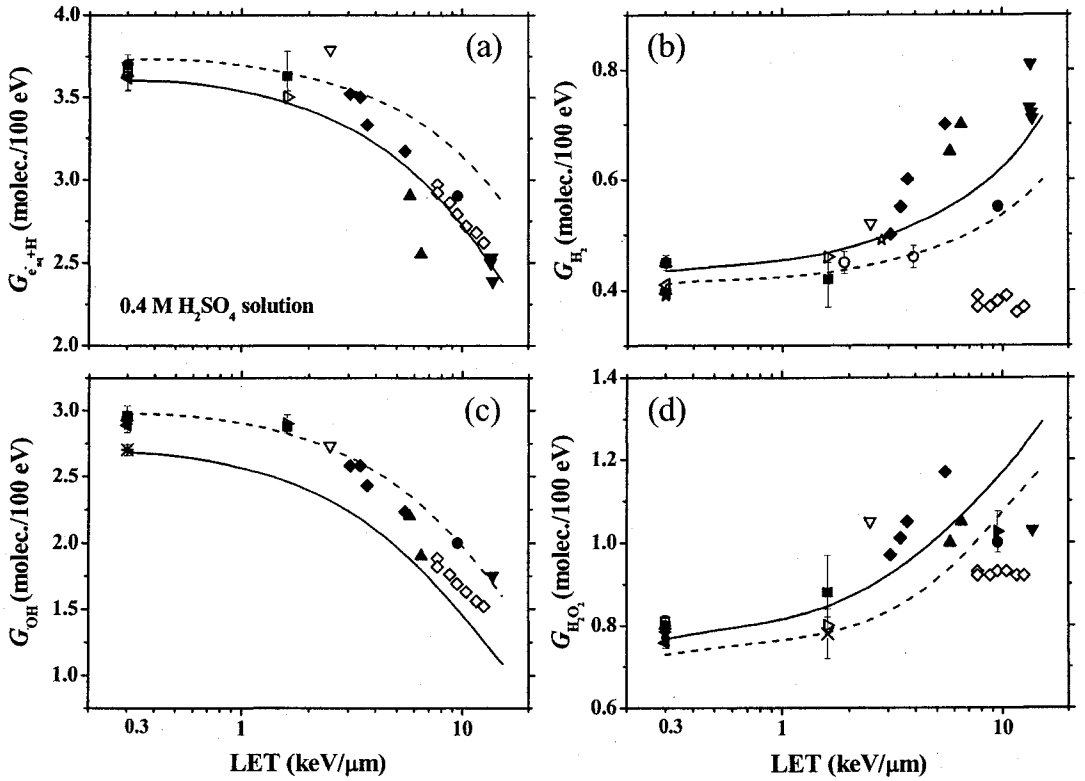

Figure 5: Variations of the primary free-radical and molecular yields (in molec./100 eV) of the radiolysis of deaerated 0.4 M H_2SO_4 aqueous solutions (pH 0.46) at 25 °C as a function of LET over the range ~0.3-15 keV/μm. The solid and dashed curves represent the results of our Monte Carlo simulations for (*a*) $G_{e^-_{aq}+H^\cdot}$, (*b*) G_{H_2}, (*c*) $G_{\cdot OH}$, and (*d*) $G_{H_2O_2}$ at 10^{-6} and 10^{-7} s, respectively. Experiment: refs. 8 and 69 (△), ref. 48 (✳), ref. 49 (◀), refs. 66 and 67 (▲), refs. 66, 68, and 92 (□), ref. 70 (◁), refs. 71 and 91 (▼), ref. 72 (○), refs. 73 and 74 (+), ref. 75 (in 0.05 M H_2SO_4) (●), ref. 76 (★), ref. 93 (◆), ref. 94 (×), ref. 95 (▷), ref. 96 (▽), ref. 97 (◇), ref. 98 (■), ref. 99 (▶), and ref. 100 (☆). Dose-average LET values used here for the various radiations considered are taken from ref. 60.

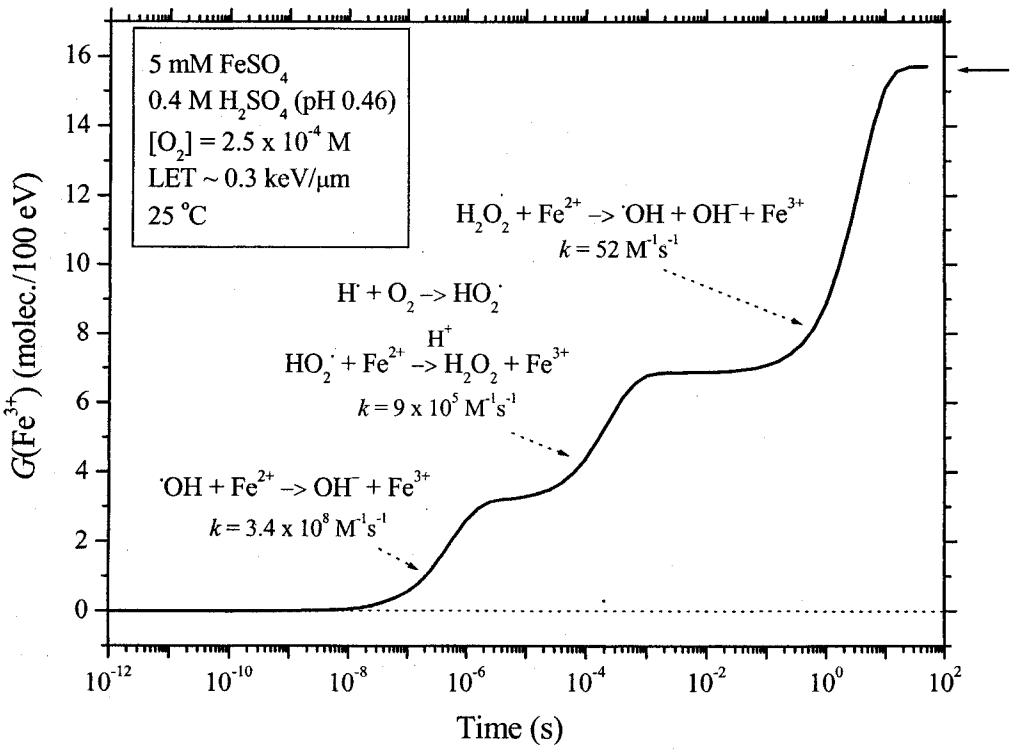

Figure 6: Time evolution of $G(Fe^{3+})$ (in molec./100 eV) in the radiolysis of air-saturated solution of 5 mM $FeSO_4$ in aqueous 0.4 M H_2SO_4 at 25 °C. The concentration of dissolved oxygen used in the calculations is ~2.5 × 10^{-4} M. The solid line shows our simulated kinetics of Fe^{3+} ion formation. The arrow on the right of the figure shows the accepted value (15.6 molec./100 eV) of the yield of the Fricke dosimeter for ^{60}Co γ-rays and fast electrons.

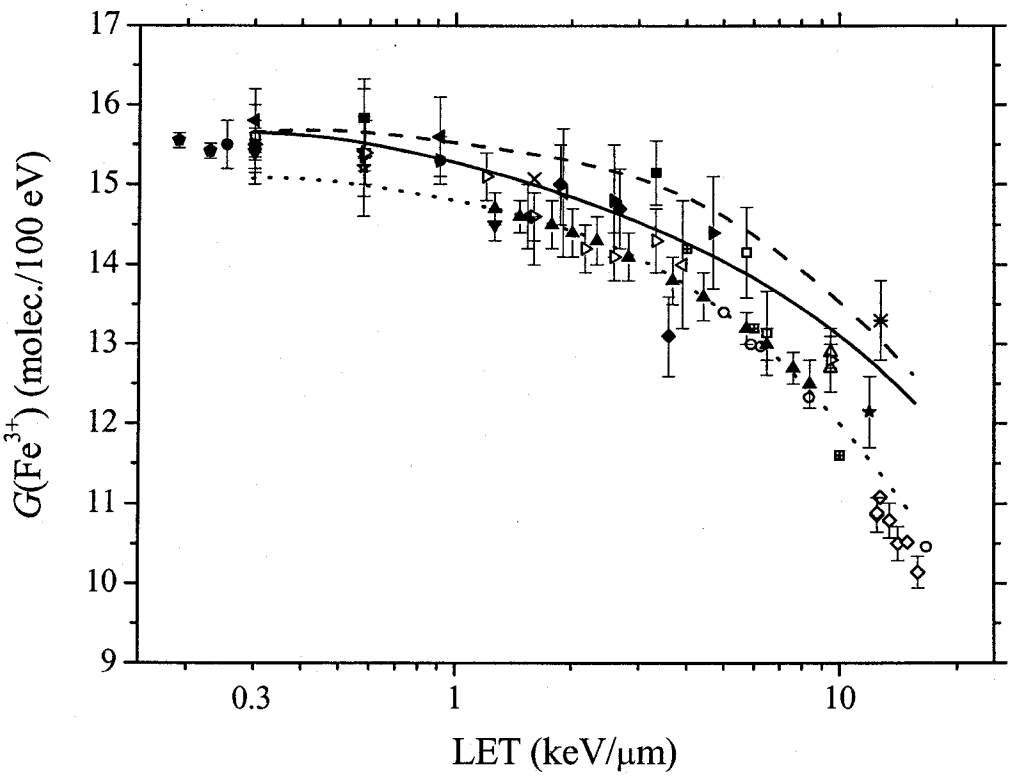

Figure 7: Plot of the ferric ion yield $G(Fe^{3+})$ (in molec./100 eV) for aerated 0.4 M H_2SO_4 aqueous solution (Fricke dosimeter), at 25 °C, against LET in the range ~0.3-15 keV/μm. The solid curve represents the values of $G(Fe^{3+})$ calculated from our Monte Carlo simulations. The dashed and dotted lines correspond to the Fricke *G*-values calculated at 10^{-7} and 10^{-6} s, respectively, from eq. [7] based on *G*(primary products). Experiment: ref. 26 (▲), ref. 28 (●), ref. 33 (⬟), ref. 67 (□), ref. 72 (◁), ref. 81(★), refs. 91, 108, and 121 (○), ref. 95 (×), refs. 109 and 122 (◀), ref. 111 (▼), ref. 112 (▽), ref. 113 (in 0.05 M H_2SO_4) (▷), ref. 114 (in 0.05 M H_2SO_4) (▶), ref. 115 [based on $G(Fe^{3+})$ = 15.6 molec./100 eV for ^{60}Co γ-rays] (■), ref. 116 (△), ref. 117 (◇), ref. 118 (in 0.05 M H_2SO_4) (◆), ref. 119 (☆), ref. 120 (✳), and ref. 123 (⊞). Dose-average LET values used here for the various radiation types considered are taken from ref. 60. Note that, for X-rays, there are, in certain cases, insufficient experimental details for an estimate of the average energy of electrons resulting from photon absorption in the solution to be made. This results in some uncertainty in assigning an average LET value to the corresponding reported $G(Fe^{3+})$ results.

References

1. C. Ferradini and J.-P. Jay-Gerin. Can. J. Chem. **77**, 1542 (1999).
2. J.W.T. Spinks and R.J. Woods. An introduction to radiation chemistry. 3rd ed. Wiley, New York. 1990. p. 243.
3. J.A. LaVerne. Radiat. Res. **153**, 487 (2000); *in* Charged particle and photon interactions with matter: chemical, physicochemical, and biological consequences with applications. *Edited by* A. Mozumder and Y. Hatano. Marcel Dekker, New York. 2004. p. 403.
4. G.V. Buxton. *In* Charged particle and photon interactions with matter: chemical, physicochemical, and biological consequences with applications. *Edited by* A. Mozumder and Y. Hatano. Marcel Dekker, New York. 2004. p. 331.
5. C. Ferradini and J.-P. Jay-Gerin. Res. Chem. Intermed. **26**, 549 (2000).
6. H. Fricke and S. Morse. Am. J. Roentgenol. Radium Ther. **18**, 430 (1927); Phil. Mag., 7th Ser., **7**, 129 (1929).
7. H. Fricke and E.J. Hart. *In* Radiation dosimetry. 2nd ed. Vol. II. *Edited by* F.H. Attix and W.C. Roesch. Academic Press, New York. 1966. p.167.
8. E. Hayon. *In* Radiation chemistry of aqueous systems. *Edited by* G. Stein. The Weizmann Science Press of Israel, Jesuralem. 1968. p. 157.
9. G.V. Buxton. *In* Proceedings of the third international congress of radiation research, Cortina d'Ampezzo, Italy, June 26-July 2, 1966. *Edited by* G. Silini. North-Holland, Amsterdam. 1967. p. 235; Radiat. Res. Rev. **1**, 209 (1968).
10. I.G. Draganić and Z.D. Draganić. The radiation chemistry of water. Academic Press, New York. 1971. p. 123.
11. J. Meesungnoen, M. Benrahmoune, A. Filali-Mouhim, S. Mankhetkorn, and J.-P. Jay-Gerin. Radiat. Res. **155**, 269 (2001).
12. M.J. Bronskill, R.K. Wolff, and J.W. Hunt. J. Chem. Phys. **53**, 4201 (1970).
13. C.D. Jonah, J.R. Miller, and M.S. Matheson. J. Phys. Chem. **81**, 931 (1977).
14. G.V. Buxton, C.L. Greenstock, W.P. Helman, and A.B. Ross. J. Phys. Chem. Ref. Data

17, 513 (1988).

15. A.J. Elliot. Rate constants and *G*-values for the simulation of the radiolysis of light water over the range 0-300 °C. Report AECL-11073. Atomic Energy of Canada Ltd., Chalk River, Ontario. 1994; A.J. Elliot, D.C. Ouellette, and C.R. Stuart. The temperature dependence of the rate constants and yields for the simulation of the radiolysis of heavy water. Report AECL-11658. Atomic Energy of Canada Ltd., Chalk River, Ontario. 1996.
16. A.O. Allen. The radiation chemistry of water and aqueous solutions. D. Van Nostrand Co., Princeton, New Jersey. 1961. p. 49.
17. J. Pucheault. *In* Actions chimiques et biologiques des radiations. 5ème Sér. *Edited by* M. Haïssinsky. Masson, Paris. 1961. p. 31.
18. W.G. Burns and H.E. Sims. J. Chem. Soc., Faraday Trans. 1, **77**, 2803 (1981).
19. A. Appleby. Radiat. Phys. Chem. **34**, 121 (1989).
20. D.R. McCracken, K.T. Tsang, and P.J. Laughton. Aspects of the physics and chemistry of water radiolysis by fast neutrons and fast electrons in nuclear reactors. Report AECL-11895. Atomic Energy of Canada Ltd., Chalk River, Ontario. 1998.
21. J.L. Magee and A. Chatterjee. J. Phys. Chem. **84**, 3529 (1980).
22. C. Ferradini. J. Chim. Phys. **76**, 636 (1979).
23. A. Mozumder. Fundamentals of radiation chemistry. Academic Press, San Diego, California. 1999. p. 41.
24. R.C. Das. Radiat. Res. Rev. **3**, 121 (1971).
25. R. Bensasson, A. Bernas, M. Bodard, L. Bouby, M. Cottin, M. Duflo, F. Kieffer, A. Koulkès, N. Leray, J. Pucheault, and C. Vermeil. *In* Tables of constants and numerical data. Vol. 13. *Edited by* M. Haïssinski and M. Magat. Pergamon, Oxford. 1963.
26. ICRU Report 17. Radiation dosimetry: X rays generated at potentials of 5 to 150 kV. International Commission on Radiation Units and Measurements, Washington, D.C. 1970.
27. A. Chatterjee and J.L. Magee. J. Phys. Chem. **84**, 3537 (1980).
28. ICRU Report 34. The dosimetry of pulsed radiation. International Commission on

Radiation Units and Measurements, Bethesda, Maryland. 1982.

29. J.A. LaVerne and R.H. Schuler. J. Phys. Chem. **91**, 5770 (1987).
30. See ref. 2, p. 71.
31. Y. Tabata, Y. Ito, and S. Tagawa (*Editors*). CRC handbook of radiation chemistry. CRC Press, Boca Raton, Florida. 1991. p. 321 and 571.
32. S.M. Pimblott and J.A. LaVerne. J. Phys. Chem. A **106**, 9420 (2002).
33. N.V. Klassen, K.R. Shortt, J. Seuntjens, and C.K. Ross. Phys. Med. Biol. **44**, 1609 (1999).
34. J. Meesungnoen and J.-P. Jay-Gerin. J. Phys. Chem. A **109**, 6406 (2005).
35. P. Clifford, N.J.B. Green, M.J. Oldfield, M.J. Pilling, and S.M. Pimblott. J. Chem. Soc. Faraday Trans. 1, **82**, 2673 (1986); S.M. Pimblott, M.J. Pilling, and N.J.B. Green. Radiat. Phys. Chem. **37**, 377 (1991); S.M. Pimblott and N.J.B. Green. Res. Chem. Kinet. **3**, 117 (1995).
36. Y. Frongillo, T. Goulet, M.-J. Fraser, V. Cobut, J.P. Patau, and J.-P. Jay-Gerin. Radiat. Phys. Chem. **51**, 245 (1998).
37. T. Goulet, M.-J. Fraser, Y. Frongillo, and J.-P. Jay-Gerin. Radiat. Phys. Chem. **51**, 85 (1998).
38. E.J. Hart. J. Chem. Educ. **34**, 586 (1957).
39. J.A. Dean. Handbook of organic chemistry. McGraw-Hill, New York. 1987. p. 8-56.
40. J.-J. Max, C. Ménichelli, and C. Chapados. J. Phys. Chem. A **104**, 2845 (2000). See also H. Chen and D.E. Irish. J. Phys. Chem. **75**, 2672 (1971).
41. J. Meesungnoen and J.-P. Jay-Gerin. Radiat. Res. **164**, 688 (2005).
42. P.-Y. Jiang, Y. Katsumura, R. Nagaishi, M. Domae, K. Ishikawa, K. Ishigure, and Y. Yoshida. J. Chem. Soc. Faraday Trans. **88**, 1653 (1992).
43. P. Neta, R.E. Huie, and A.B. Ross. J. Phys. Chem. Ref. Data 17, 1027 (1988).
44. C. Ferradini. *In* Actions chimiques et biologiques des radiations. 10ème Sér. *Edited by* M. Haïssinsky. Masson, Paris. 1966. p. 89.
45. Y. Tang, R.P. Thorn, R.L. Mauldin III, and P.H. Wine. J. Photochem. Photobiol. A **44**, 243 (1988).

46. R.E. Huie and L.W. Sieck. *In* S-centered radicals. *Edited by* Z.B. Alfassi. Wiley, Chichester. 1999. p. 63.

47. I.G. Draganić, M.T. Nenadović, and Z.D. Draganić, J. Phys. Chem. **73**, 2564 (1969).

48. R.W. Matthews, H.A. Mahlman, and T.J. Sworski. J. Phys. Chem. **76**, 1265 (1972); Radiat. Res. **39**, 534 (1969).

49. K. Sehested, E. Bjergbakke, and H. Fricke. Radiat. Res. **56**, 385 (1973); K. Sehested, H. Corfitzen, and H. Fricke. J. Phys. Chem. **74**, 211 (1970).

50. B. Lesigne, C. Ferradini, and J. Pucheault. J. Phys. Chem. **77**, 2156 (1973); J. Phys. Chem. **76**, 3676 (1972).

51. Y. Katsumura. *In* Radiation chemistry: present status and future trends. *Edited by* C.D. Jonah and B.S.M. Rao. Elsevier, Amsterdam. 2001. p. 163.

52. D.R. Lide (*Editor*). CRC handbook of chemistry and physics. 84th ed. CRC Press, Boca Raton, Florida. 2003. p. 5-96.

53. D.C. Harris. Exploring chemical analysis. 2nd ed. W.H. Freeman, New York. 2001. p. 233.

54. K.H. Schmidt and D.M. Bartels. Chem. Phys. **190**, 145 (1995).

55. E.A. Guggenheim. Philos. Mag. S. 7. **19**, 588 (1935); C.W. Davies. J. Chem. Soc. 2093 (1938); R.A. Robinson and R.H. Stokes. Electrolyte solutions. The measurement and interpretation of conductance, chemical potential and diffusion in solutions of simple electrolytes. 2nd ed. (revised). Butterworths Publications Ltd., London. 1959. p. 223.

56. G. Czapski and H.A. Schwarz. J. Phys. Chem. **66**, 471 (1962).

57. T. Solomon. J. Chem. Educ. **78**, 1691 (2001).

58. E.R. Johnson and A.O. Allen. J. Am. Chem. Soc. **74**, 4147 (1952).

59. J.W. Boyle. Radiat. Res. **17**, 427 (1962); Radiat. Res. **17**, 450 (1962).

60. D.E. Watt. Quantities for dosimetry of ionizing radiations in liquid water. Taylor & Francis, London. 1996. p. 82.

61. ICRU Report 49. Stopping powers and ranges for protons and alpha particles. International Commission on Radiation Units and Measurements, Bethesda, Maryland.

1993.

62. H. Shiraishi, G.R. Sunaryo, and K. Ishigure. J. Phys. Chem. **98**, 5164 (1994).
63. T. Lundström, H. Christensen, and K. Sehested. Radiat. Phys. Chem. **69**, 211 (2004).
64. See ref. 52, p. 8-46.
65. B. Halliwell and J.M.C. Gutteridge. Free radicals in biology and medicine. 3rd ed. Oxford University Press, Oxford. 1999. p. 36.
66. See ref. 16, p. 32.
67. M. Lefort. J. Chim. Phys. **54**, 782 (1957); Annu. Rev. Phys. Chem. **9**, 123 (1958); M. Cottin and M. Lefort. J. Chim. Phys. **53**, 267 (1956).
68. H.A. Mahlman and J.W. Boyle. J. Am. Chem. Soc. **80**, 773 (1958); H.A. Mahlman. J. Am. Chem. Soc. **81**, 3203 (1959).
69. E. Hayon. J. Phys. Chem. **65**, 1502 (1961); Trans. Faraday Soc. **61**, 734 (1965); J. Phys. Chem. **69**, 2628 (1965).
70. C.H. Cheek, V.J. Linnenbom, and J.W. Swinnerton. Radiat. Res. **19**, 636 (1963); Report of NRL Progress. July 1962. p. 11.
71. N.F. Barr and R.H. Schuler. Radiat. Res. **7**, 302 (1957).
72. M.H. Back and N. Miller. Nature **179**, 321 (1957).
73. C.J. Hochanadel and S.C. Lind. Annu. Rev. Phys. Chem. **7**, 83 (1956).
74. C. Ferradini and J. Pucheault. Biologie de l'action des rayonnements ionisants. Masson, Paris. 1983. p. 25; J. Pucheault and C. Ferradini. J. Chim. Phys. **54**, 659 (1957).
75. E. Collinson, F.S. Dainton, and J. Kroh. Proc. R. Soc. London A, **265**, 422 (1962).
76. T.J. Sworski. J. Am. Chem. Soc. **76**, 4687 (1954).
77. E. Hayon. J. Phys. Chem. **68**, 1242 (1964).
78. K.H. Schmidt, P. Han, and D.M. Bartels. J. Phys. Chem. **96**, 199 (1992).
79. M. Haïssinsky. J. Chim. Phys. **62**, 1141 (1965); *in* Actions chimiques et biologiques des radiations. 11ème Sér. *Edited by* M. Haïssinsky. Masson, Paris. 1967. p. 131.
80. B. Pastina and J.A. LaVerne. J. Phys. Chem. A **105**, 9316 (2001).
81. A.J. Elliot, M.P. Chenier, D.C. Ouellette, and V.T. Koslowsky. J. Phys. Chem. **100**,

9014 (1996); The temperature dependence of *G*-values for aqueous solutions irradiated with a 23 MeV $^{2}H^{+}$ beam. Report AECL-10659. Atomic Energy of Canada Ltd., Chalk River, Ontario. 1992.

82. A.J. Elliot, M.P. Chenier, and D.C. Ouellette. J. Chem. Soc. Faraday Trans. **89**, 1193 (1993).
83. A. Appleby and H.A. Schwarz. J. Phys. Chem. **73**, 1937 (1969); H.A. Schwarz, J.M. Caffrey, Jr., and G. Scholes. J. Am. Chem. Soc. **81**, 1801 (1959).
84. R.H. Bisby, R.B. Cundall, H.E. Sims, and W.G. Burns. Faraday Discuss. Chem. Soc. **63**, 237 (1977).
85. C.A. Naleway, M.C. Sauer, Jr., C.D. Jonah, and K.H. Schmidt. Radiat. Res. **77**, 47 (1979); M.C. Sauer, Jr., K.H. Schmidt, E.J. Hart, C.A. Naleway, and C.D. Jonah. Radiat. Res. **70**, 91 (1977).
86. M.C. Sauer, Jr., C.D. Jonah, K.H. Schmidt, and C.A. Naleway. Radiat. Res. **93**, 40 (1983).
87. B. Pastina and J.A. LaVerne. J. Phys. Chem. A **103**, 1592 (1999).
88. V. Wasselin-Trupin, G. Baldacchino, S. Bouffard, and B. Hickel. Radiat. Phys. Chem. **65**, 53 (2002).
89. H.E. Sims, C.B. Ashmore, P.K. Tait, and W.S. Walters. *In* Proceedings of JAIF (Japan Atomic Industrial Forum, Inc.) international conference on water chemistry in nuclear power plants, Kashiwazaki, Japan, October 13-16, 1998. p. 894; C.B. Ashmore, H.E. Sims, P.K. Tait, and W.S. Walters. The measurement of water radiolysis product yields at high temperature and pressure. Final report. Report AEAT-2223. U.K. Atomic Energy Authority. 1997-98.
90. M.C. Kent and H.E. Sims. *In* Proceedings of the 6th international conference on water chemistry of nuclear reactor systems. British Nuclear Energy Society, London. 1992. p. 153.
91. R.H. Schuler and A.O. Allen. J. Am. Chem. Soc. **79**, 1565 (1957).
92. A.O. Allen. Radiat. Res. Suppl. **4**, 54 (1964).
93. T.J. Hardwick. Discuss. Faraday Soc. **12**, 203 (1952); A.O. Allen. Radiat. Res. **1**, 85

(1954).

94. F.S. Dainton and H.C. Sutton. Trans. Faraday Soc. **49**, 1011 (1953).
95. K. Coatsworth, E. Collision, and F.S. Dainton. Trans. Faraday Soc. **56**, 1008 (1960); F.S. Dainton. Radiat. Res. Suppl. **1**, 1 (1959).
96. J. Bednář and J. Teplý. Collection Czechoslov. Chem. Commun. **24**, 127 (1959); J. Bednář. Chem. listy **53**, 1083 (1959).
97. G.L. Kochanny, Jr., A. Timnick, C.J. Hochanadel, and C.D. Goodman. Radiat. Res. **19**, 462 (1963).
98. T. Balkas, F.S. Dainton, J.K. Dishman, and D. Smithies. Trans. Faraday Soc. **62**, 81 (1966).
99. G. Lemaire, C. Ferradini, and J. Pucheault. J. Phys. Chem. **76**, 1542 (1972); G. Lemaire and C. Ferradini. Radiochem. Radioanal. Lett. **5**, 175 (1970).
100. E.J. Hart. Annu. Rev. Phys. Chem. **5**, 139 (1954).
101. J. Meesungnoen, J.-P. Jay-Gerin, A. Filali-Mouhim, and S. Mankhetkorn. Chem. Phys. Lett. **335**, 458 (2001).
102. J.L. Magee and A. Chatterjee. *In* Radiation chemistry: principles and applications. *Edited by* Farhataziz and M.A.J. Rodgers. VCH Publishers, New York. 1987. p. 137.
103. J.A. LaVerne and H. Yoshida. J. Phys. Chem. **97**, 10720 (1993).
104. J.-P. Jay-Gerin, N. Autsavapromporn, and J. Meesungnoen. *In* Proceedings of the 48th annual meeting of the Japanese Society of Radiation Chemistry, Osaka, Japan, October 12-14, 2005. *Edited by* S. Tagawa. Osaka University, Osaka. 2005. p. 67.
105. J.P. Keene. Radiat. Res. **22**, 14 (1964).
106. M. Běgusová and S.M. Pimblott. Radiat. Prot. Dosim. **99**, 73 (2002).
107. C.J. Hochanadel and J.A. Ghormley. J. Chem. Phys. **21**, 880 (1953).
108. R.H. Schuler and A.O. Allen. J. Chem. Phys. **24**, 56 (1956).
109. W.K. Sinclair and R.J. Shalek. Radiology **70**, 92 (1958).
110. See ref. 16, p. 13.
111. J.V. Davies, D. Greene, J.P. Keene, J. Law, and J.B. Massey. Phys. Med. Biol. **8**, 97 (1963).

112. D.M. Donaldson and N. Miller. J. Chim. Phys. **52**, 578 (1955).

113. A.O. Fregene. Radiat. Res. **31**, 256 (1967).

114. L.H. Gevantman and J.F. Pestaner. J. Chem. Phys. **31**, 1140 (1959).

115. T.J. Hardwick. Can. J. Chem. **30**, 17, 39 (1952).

116. E.J. Hart. Radiat. Res. **1**, 53 (1954); W.R. McDonell and E.J. Hart. J. Am. Chem. Soc. **76**, 2121 (1954).

117. E.J. Hart, W.J. Ramler, and S.R. Rocklin. Radiat. Res. **4**, 378 (1956); A.R. Anderson and E.J. Hart. Radiat. Res. **14**, 689 (1961).

118. J.L. Haybittle, R.D. Saunders, and A.J. Swallow. J. Chem. Phys. **25**, 1213 (1956).

119. M. Peisach and J. Steyn. Nature **187**, 58 (1960).

120. M.C. Sauer, Jr., E.J. Hart, C.A. Naleway, C.D. Jonah, and K.H. Schmidt. J. Phys. Chem. **82**, 2246 (1978).

121. N.F. Barr and R.H. Schuler. J. Phys. Chem. **63**, 808 (1959).

122. R.J. Shalek, W.K. Sinclair, and J.C. Calkins. Radiat. Res. **16**, 344 (1962).

123. J.A. LaVerne and R.H. Schuler. J. Phys. Chem. **98**, 4043 (1994).